(2)

NAVAL POSTGRADUATE SCHOOL
Monterey, California

THESIS

The Effects of Embedded Vortices on Heat Transfer in a Turbulent Boundary Layer with Film Cooling from Holes with Compound Angles

by

Stephen W. Mitchell

September 1990

Thesis Advisor: Phillip M. Ligrani

Co-Advisor: Chelakara S. Subramanian

DISCLAIMER NOTICE

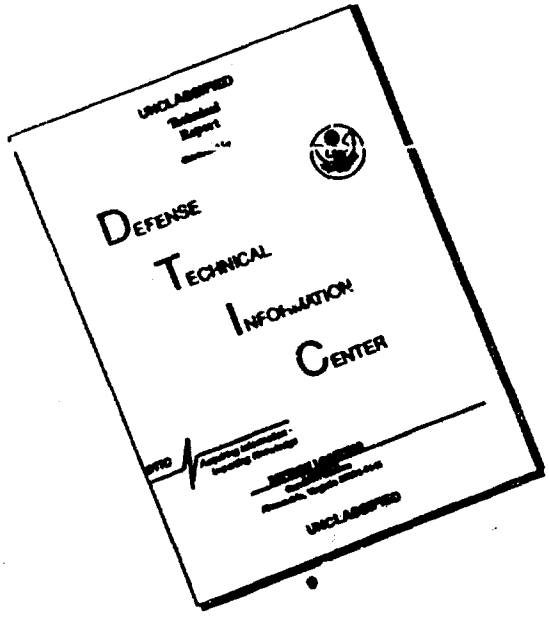

THIS DOCUMENT IS BEST QUALITY AVAILABLE. THE COPY FURNISHED TO DTIC CONTAINED A SIGNIFICANT NUMBER OF PAGES WHICH DO NOT REPRODUCE LEGIBLY.

Approved for public release; distribution is unlimited.

The Effects of Embedded Vortices on Heat Transfer in a Turbulent Boundary Layer with Film Cooling from Holes with Compound Angles

by

Stephen W. Mitchell
Lieutenant, United States Navy
B.S.E., Tulane University, 1984

Submitted in partial fulfillment of the requirements
for the degree of

MASTER OF SCIENCE IN MECHANICAL ENGINEERING

from the

NAVAL POSTGRADUATE SCHOOL
September 1990

Author: _____
Stephen W. Mitchell

Approved by: _____
Phillip M. Ligrani, Thesis Advisor

_____
Chelakara S. Subramanian, Co-Advisor

_____
Anthony J. Healey, Chairman, Department of Mechanical Engineering

Unclassified

Security Classification of this page

REPORT DOCUMENTATION PAGE

1a Report Security Classification Unclassified	1b Restrictive Markings
2a Security Classification Authority	3 Distribution Availability of Report: Approved for public release; distribution is unlimited.
2b Declassification/Downgrading Schedule	
4 Performing Organization Report Number(s)	5 Monitoring Organization Report Number(s)
6a Name of Performing Organization: Naval Postgraduate School; 6b Office Symbol (If Applicable): 34	7a Name of Monitoring Organization: Wright Aeronautical Laboratories
6c Address (city, state, and ZIP code): Monterey, CA 93943-5000	7b Address (city, state, and ZIP code): Dayton, OH 45433
8a Name of Funding/Sponsoring Organization: Wright Aeronautical Laboratories; 8b Office Symbol:	9 Procurement Instrument Identification Number (If Applicable)
8c Address (city, state, and ZIP code): Dayton, OH 45433	10 Source of Funding Numbers: MIPR FY 1455-89-N0670
	Program Element Number | Project No | Task No | Work Unit Accession No

11 Title (Include Security Classification) THE EFFECTS OF EMBEDDED VORTICES ON HEAT TRANSFER IN A TURBULENT BOUNDARY LAYER WITH FILM COOLING FROM HOLES WITH COMPOUND ANGLES

12 Personal Author(s) Stephen W. Mitchell

13a Type of Report	13b Time Covered	14 Date of Report (year, month,day)	15 Page Count
Master's Thesis	From To	September 1990	256

16 Supplementary Notation The views expressed in this thesis are those of the author and do not reflect the official policy or position of the Department of Defense or the U.S. Government.

17 Cosati Codes			18 Subject Terms (continue on reverse if necessary and identify by block number)
Field	Group	Subgroup	Compound Angle Injection, Embedded Vortex, Film-cooling, Turbulent Boundary Layer

19 Abstract (continue on reverse if necessary and identify by block number)

The effects of embedded longitudinal vortices on film cooling injectant from one row and two rows of holes with compound angles are investigated. Holes are designed such that their angle from the test surface is 30 degrees in a spanwise/normal plane projection, and 35 degrees in a streamwise/normal plane projection. A blowing ratio of 0.5, non-dimensional injection temperature parameters of 1.29 to 1.38, and freestream velocity of 10 m/s are employed. As the spanwise position of the vortex is altered, Stanton Numbers change considerably depending upon which portion of each vortex is proximate to film injection holes. These variations are vastly different depending on whether or not spanwise components of vortex secondary flows are opposed or aligned with the spanwise direction of the injectant. Mean velocity surveys, injection distribution surveys, and flow visualization results are also discussed.

20 Distribution/Availability of Abstract	21 Abstract Security Classification
[X] unclassified/unlimited [ ] same as report [ ] DTIC users	Unclassified

22a Name of Responsible Individual	22b Telephone (Include Area code)	22c Office Symbol
Phillip. M. Ligrani	(408) 646-3382	69Li

DD FORM 1473, 84 MAR 83 APR edition may be used until exhausted

All other editions are obsolete

security classification of this page Unclassified

TABLE OF CONTENTS

ABSTRACT

The effects of embedded longitudinal vortices on film cooling injectant from one row and two roles of holes with compound angles are investigated. Holes are designed such that their angle from the test surface is 30 degrees in a spanwise/normal plane projection, and 35 degrees in a streamwise/normal plane projection. A blowing ratio of 0.5, non-dimensional injection temperature parameter of 1.29 to 1.38, and freestream velocity of 10 m/s are employed. As the spanwise position of the vortex is altered, Stanton numbers change considerably depending upon which portion of each vortex is proximate to film injection holes. These variations are vastly different depending on whether or not spanwise components of the vortex secondary flows are opposed or aligned with the spanwise direction of the injectant. Mean velocity surveys, injection distribution surveys, and flow visualization results are also discussed.

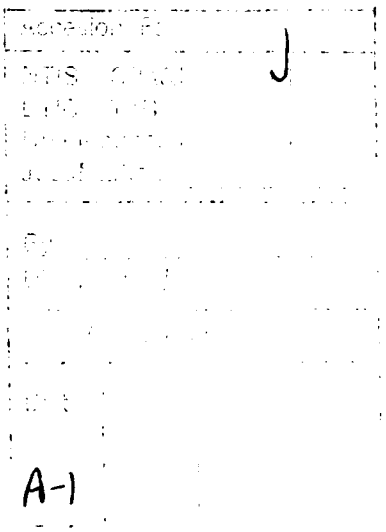

LIST OF FIGURES

the injection hole diameter

y - distance normal to the test surface

Z - spanwise distance measured from the test surface centerline

z/d - dimensionless spanwise position

Greek Symbols

α - thermal diffusivity

β_1 - complete beta function

β_{u1} - incomplete beta function

ξ - unheated starting length

η - adiabatic film cooling effectiveness

ν - kinematic viscosity

θ - non-dimensional temperature, $\frac{T_c - T_\infty}{T_w - T_\infty}$

ρ - density

Subscripts

ad - adiabatic condition

c - coolant

f - film flow

m - main flow

o - stagnation condition

w - wall

∞ - freestream

LIST OF SYMBOLS

d - injection hole diameter (0.945 cm)

h - average heat transfer coefficient

k - thermal conductivity

m - blowing ratio, $\frac{\rho_c U_c}{\rho_\infty U_\infty}$

Pr - Prandtl number

Re - Reynolds number

St - Stanton number

St_f - Iso-energetic Stanton number

St_o - Baseline Stanton number, no film cooling

T - static temperature

T_c - coolant temperature

T_{inj} - injectant temperature

T_{plenum} - plenum temperature

T_w - wall temperature

T_∞ - freestream temperature

U - mean velocity

U_∞ - freestream velocity

X - downstream distance measured from the leading edge of the boundary layer trip

x/d - dimensionless streamwise position : streamwise distance measured from the downstream edges of the injection holes divided by the

ACKNOWLEDGMENTS

This research was sponsored by Wright Aeronautical Laboratories, Wright-Patterson Air Force Base, MIPR FY 1455-89-N0670. Program monitor was Dr. Bill Troha.

Professor Phillip Ligrani was a very influential and important driving force behind the composition of this study. Dr. Chelakara Subramanian was helpful with his knowledge of computer programming and technical familiarity of all laboratory procedures employed.

I wish to thank both Professor Phillip Ligrani and Dr. Subramanian for their patience, guidance and never ending enthusiasm for this study.

I would also like to thank my wife, Susan, for helping with the typing and putting up with me during the entire thesis process.

I. INTRODUCTION

A. BACKGROUND

In an effort to increase gas turbine power output, efficiencies, and power to weight ratios, gas turbine inlet temperatures are being increased. The technology for the advanced materials required to withstand these high temperature (approaching 2000K) is somewhat limited. Consequently turbine blades are cooled using a variety of schemes which include film cooling, the injection of cool compressor air from discrete holes along blade surfaces to protect them from high temperature air flows. Many film cooling schemes involve injecting air at angles with respect to blade surfaces such that injectant emerges from the holes in the direction of the mainstream flow. This is called simple angle injection. But higher film effectiveness and better protection can often be attained by orienting film cooling holes at compound angles with respect to the freestream direction. This is called compound angle injection and is the focus of the present study.

Embedded vortices are extremely detrimental to the protection provided by film cooling. As injectant from film cooling holes spreads out over blade surfaces, significant secondary flows from vortices distort the film, leaving some areas unprotected. Such vortices are often longitudinal and embedded, and very common in the flow within turbine blade passages. These vortices are formed by one of two mechanisms. With the first of these, pressure gradients such as exist near the turbine blade leading edge and the endwall induce secondary flows

which develop into vortices. With the second mechanism, vortices develop near concave blade surfaces as a result of centrifugal instabilities.

B. RELATED STUDIES

Blair [Ref. 2] was one of the first investigators to study the effects of embedded vortices on film cooling. He found decreased film cooling effectivenesses on an endwall due to the formation of a large vortex. Using one and two rows of injection holes, Goldstein and Chen [Ref. 6 and Ref. 7] discovered a triangular region on blade surfaces where injectant was depleted by passages of vortices. Kobayashi [Ref. 13] studied formation of large vortices in a laminar boundary layer using a concave surface and suction through a permeable wall. He concluded that the laminar boundary layer tends to be stablized with suction [Ref. 14]. For the case of blowing, injection was found to have little influence on the stability of the laminar boundary layers studied. Honami and Fukagawa [Ref. 9] studied film cooling effectiveness from lateral and streamwise oriented film cooling holes on a concave surface using a blowing ratio of approximately 0.5. They concluded that the concave surface had great effect on film effectiveness when streamwise oriented cooling holes were used, but little effect when laterally oriented cooling holes were employed.

C. ONGOING RESEARCH AT THE NAVAL POSTGRADUATE SCHOOL

Research at the Naval Postgraduate School has focused on the effects of longitudinal vortices on heat transfer, film cooling distributions, and the protection normally provided by the film. Joseph [Ref. 10] studied the influences of a longitudinal vortex on injectant from one row of film cooling holes spaced

three diameters apart. He found that heat transfer is augmented and that the protection provided by the injectant is degraded on the downwash sides of vortices resulting in local "hot spots". On upwash sides of vortices, he concludes that injectant protection may be augmented by the vortices. Evans [Ref. 5] showed that injectant disturbances result mostly from vortex secondary flows. Ortiz [Ref. 18], used the same film cooling orientation, but varied the spanwise location of the vortex as well as the blowing ratio. He found that more than one peak in Stanton number ratio is present for higher blowing ratios, while for lower blowing ratios, only one peak is apparent. Williams [Ref. 22], further studied the mechanism and flow interactions present between one single film cooling jet and the vortices passing at different spanwise locations. In a later study, Craig [Ref. 3] looked at the effects of vortex circulation on injectant from a single hole and from a row of holes, when the centerline hole was located beneath vortex downwash regions. Kaisuwan [Ref. 11] studied similar configurations when the centerline injection hole was located beneath vortex upwash regions. Both of these investigations found that embeded vortices affect injectant distributions when $\Gamma/(U_c d)$ is greater than about 1.0. References 15,16 and 17 summarize the extensive research conducted by Ligrani, Subramanian, Joseph, Evans, Ortiz, Williams, Craig and Kaisuwan in this field.

D. OBJECTIVES OF THE PRESENT STUDY

The effects of embedded longitudinal vortices on heat transfer and injectant distributions downstream of one and two rows of injection holes with compound angle orientations are investigated. While a constant blowing ratio (m=0.5), constant non-dimensional injectant temperature (θ=1.35), and constant plate heat

flux are employed, the spanwise position of the vortex is varied from Z=-7.2 to Z=7.2 centimeters to provide information on the relationship between spanwise position and amounts of protection degradation caused by vortex secondary flows.

E. OUTLINE OF EXPERIMENTATION

The present study consists of four experiments:

1. Measurement of mean velocity, total pressure distributions and vorticity contours in the Y-Z planes for:

a. No film cooling, using vortex positions R0,R4,R8,L0,L4,L8 at x/d=10.2

b. Film cooling from one row of holes, using vortex positions R0-R4 and L0-L4 at x/d=45.8

c. Film cooling from two rows of holes, using vortex positions R0-R4 and L0-L4 at x/d=45.8.

2. Mean surveys of injectant distributions in the Y-Z plane for:

a. Film cooling from one row of holes, using vortex positions R0-R4 and L0-L4 at x/d=45.8

b. Film cooling from two rows of holes, using vortex positions R0-R4 and L0-L4 at x/d=45.8.

3. Stanton number ratios measured at 21 spanwise locations for:

a. Film cooling from one row of holes, using vortex positions R0-R4 and L0-L4 at x/d=45.8

b. Film cooling from two rows of holes, using vortex positions R0-R4 and L0-L4 at x/d=45.8.

4. Flow visualization for:

a. Film cooling from one row of holes, using vortex positions R0-R4 and L0-L4.

b. Film cooling from two rows of holes, using vortex positions R0-R4.

The "L" denotes vortex generator base plates placed to the left of the tunnel centerline (looking downstream). With this arrangement, secondary flows cause the counter-clockwise rotating vortices to move to the right as they convect downstream. The "R" denotes vortex generator base plates placed to the right of the tunnel centerline (looking downstream). With this arrangement, secondary flows cause the clockwise rotating vortices to move to the left as they convect downstream. Figure 4 is a schematic diagram which details this convention.

F. THESIS ORGANIZATION

Chapter II discusses the experimental apparatus and the procedures. Data and results are discussed in Chapter III. Chapter IV contains a summary and conclusions. Appendix A contains 194 figures. Appendix B contains results of an uncertainty analysis performed by Schwartz [Ref. 21]. Appendix C describes data aquisition, data processing and plotting programs employed. Finally, Appendix D contains a complete directory of the data files contained on floppy disks.

II. EXPERIMENTAL APPARATUS AND PROCEDURES

A. WIND TUNNEL AND COORDINATE SYSTEM

The experiments were conducted in an open-circuit, subsonic wind tunnel located in the laboratories of the Department of Mechanical Engineering at the Naval Postgraduate School. The same facility, without the modification for compound angle injection, was used in research by Joseph, Ortiz, Williams, Schwartz, Kaisuwan and Craig (References 10, 18, 22, 21, 11 and 3). A variable speed centrifugal blower is located at the upstream end of the facility. Ambient air from the surroundings passes through a coarse filter to the inlet of the blower and is then discharged to a diffuser. A small clearance is maintained between the blower and diffuser in order to reduce noise and vibration in the test section from the blower.

A filter located in the diffuser removes small particulates from the airstream. Four baffle vanes are also located in the diffuser to help minimize the occurrance of flow separation. A header box containing a honeycomb and three screens follows the baffle vanes to reduce spatial non-uniformities in the flow field. Downstream of the header box, the air stream encounters a 16 to 1 contraction ratio nozzle before entering the test section.

The test section is 3.05 m long and 0.61 m wide. The bottom wall contains two rows of five film cooling injection holes per row oriented at compound angles upstream of a constant flux heat transfer surface. The height of the top wall of the test section is adjustable so that a constant pressure gradient over the length of the tunnel can be maintained. In this study, a zero pressure gradient is maintained to within 0.01 inches of water differential pressure along the length

of test section. The freestream velocity is adjustable from 1 to 40 m/s. A freestream velocity of 10 m/s is used for all of the experiments in this study.

Figure 1 shows a schematic of the test section coordinate system as well as streamwise locations of test section components. Figure 2 is a top view schematic diagram of the test section. The boundary layer is tripped with a 1.5 mm high strip of tape along the entire spanwise direction at the exit of the nozzle. A vortex generator is then located 0.48 m downstream of the boundary layer trip. Downstream edges of injection holes are located 1.064 m and 1.014 m from the downstream edge of the vortex generator base plate, respectively. The leading edge of the heat transfer surface is located 1.077 m from boundary later trip, which is the unheated starting length of the test section. Streamwise locations of thermocouple rows are also shown in Figure 1.

The left hand and right hand edges of this base plate are the base edges referred to in Table 1 as location references. The left or right edge of the lexan base is used depending on whether a clockwise or counter-clockwise vortex is induced. Looking downstream, the left edge of the base is the reference for vortex generator positions R0, R1, R2, R3 and R4. Similariy, the right edge of the base plate is the reference for vortex generator positions L0, L1, L2, L3, L4. The "L" denotes vortex generator base plates placed to the left of the tunnel centerline (looking downstream). With this arrangement, secondary flows cause the counter-clockwise rotating vortices to move to the right as they convect downstream. The "R" denotes vortex generator base plates placed to the right of the tunnel centerline (looking downstream). With this arrangement, secondary flows cause the clockwise rotating vortices to move to the left as they convect downstream. Figure 4 shows details of these reconfigurations in greater detail.

B. VORTEX GENERATOR

The vortex generator consists of a half-delta wing which is attached to the test section at an angle of 18 degrees with respect to the streamwise direction. The design is similar to those employed by Williams [Ref.23] and Craig [Ref.4]. Figure 3 shows that the height of the wing is 3.2 cm and the length is 7.6 cm. The wing is attached to a Lexan mounting plate which acts as a base. This base is 4.2 cm wide and 9.2 cm long and is attached to the test section at various positions in the spanwise direction at a streamwise location which is 0.48 m downstream from the boundary layer trip. Lines for angles of 18, 15, 12, 8.4 and 0 degrees with respect to the streamwise direction of the base are scribed into the plate. The plate may be used for clockwise or counter-clockwise vortices depending on the orientation of the delta wing on the base plate. In this study, vortices are formed using the delta wing at an 18 degree orientation, with the generator apex pointing upstream (see Figure 3). The labels used for the different spanwise vortex positions are given in Table 1, along with corresponding distances of the base edge to the wind tunnel centerline.

TABLE I. SPANWISE COORDINATE OF VORTEX POSITION

VORTEX POSITION NOMENCLATURE	SPANWISE COORDINATE IN CM	VORTEX POSITION AT X/D=10.2 IN CM
R0	0.0	-3.05
R1	1.8	
R2	3.6	
R3	5.4	
R4	7.2	4.06
L0	0.0	2.54
L1	-1.8	
L2	-3.6	
L3	-5.4	
L4	-7.2	-5.08

C. INJECTION HOLE CONFIGURATION

The injection hole configuration consists of two rows of five holes per row. The hole diameter used is 0.945 cm and the holes are 7.8 d apart in the spanwise direction and 5.2d apart in the streamwise direction. The injection holes are oriented at compound angles such that the plane of each hole is angled at 50.5 degrees with respect to the streamwise/normal (X-Y) plane. Within the plane of each hole, each is angled at 24 degrees with the X-Z plane of the test surface. This arrangement amounts to a spanwise/normal projection of 30 degrees with respect to the test surface and a streamwise/normal projection of 35 with respect

to the test surface. The centerline of the middle hole in the row nearest the heat transfer surface is located at the test surface centerline. A schematic of the test surface with this configuration is shown in Figure 5.

D. INJECTION SYSTEM

Injection air originates in a 1.5 hp, single stage, Rotron blower. The injectant continues through a valve, a rotometer, a small diffuser and into a plenum chamber. In the plenum chamber are two heating pads to heat the injectant to a temperature above ambient. With this arrangement, injectant temperatures as high as 100 degrees Celsius above ambient air temperature may be achieved.

The film coolant is injected from the two rows of holes into the boundary layer which is developing along the test section. Downstream edges of the injection holes which are furthest downstream are 1.064 m from the boundary layer trip, 0.584 m from the leading edge of the vortex generator and 0.013 m upstream from the constant heat flux surface. Additional details of these streamwise locations are found in Figures 1 and 2.

Qualification of the injection system includes determination of the discharge coefficient variation with Reynolds number. These data agree with earlier injection system results presented by Williams [Ref. 22] .

Variations of temperatures at the exits of injection holes T_{inj} with injection plenum temperature T_{plenum} were also measured by Bishop [Ref. 1]. This reference shows that T_{inj} has a linear dependence on T_{plenum} for blowing ratios from 0 to 1.5 and injection temperatures from 20 to 100 degrees Celsius. Blowing ratios m of 1.3 and 0.5 were used in the present study. The 0.5 blowing

ratio was used with one row of holes and two rows of holes. When one row was used, the upstream row of holes was plugged and covered with cellophane tape.

E. HEAT TRANSFER SURFACE

The heat transfer surface is designed to provide a constant heat flux over its area. The constant heat flux plate is located at the bottom of the wind tunnel just downstream of the film cooling holes. The uppermost surface is adjacent to the air stream and is maintained level with the test surface by using height adjustment screws located in the support frame. Closest to the airstream is a 1.3 m by 0.476 m by 0.20 mm stainless steel sheet of foil painted with seven layers of liquid crystals. The foil is arranged so that heat is dissipated uniformly throughout the heater. Just under the foil are 126 Copper-Constantan thermocouples arranged in six rows. Each row consists of 21 thermocouples with a spanwise spacing of 1.27 cm to provide adequate spanwise spatial resolution of surface temperature distributions. The lead wires of the thermocouples are placed in grooves cut into a triple sheet of 0.254 mm thick double sided tape. These grooves are then filled with RTV epoxy. Underneath them is the 6.0 mm by 1.118 m by 0.438 m etched foil heater, which is attached to the double sided tape with Electrofilm electroband epoxy. The heater is rated at 120 Volts and 1500 Watts. An ammeter and a voltmeter are used to measure heater power levels which are adjusted using a type 3000B Standard Electric Company Variac. The insulation beneath the heater consists of a 12.7 mm thick Lexan sheet, a 25.4 mm thich layer of foam insulation, an 82.55 mm thick layer of styrofoam , three sheets of 0.254 mm thick Lexan and a 9.53 mm thick sheet

of balsa wood. The heat transfer test surface is enclosed in a plexiglass support frame which is mounted onto the underside of the wind tunnel.

Conductive heat losses amount to 1.5 to 2.5 per cent of the total power of the heater, and are determined using an equation given by Ortiz [Ref. 18] based on an energy balance. Radiation losses are determined using an equation given by Joseph [Ref. 10] and average about 8.5 per cent of the total power. Thermocouple contact resistances are determined using equations given by Ortiz [Ref. 18] and Williams [Ref. 22].

Local Stanton number values with film cooling are often normalized using Stanton number baseline values. Baseline Stanton numbers are ones measured when no film cooling and no vortex are present. These results are compared to the empirical relationship from Kays and Crawford [Ref. 12] for a constant heat flux surface downstream of an unheated starting length in Figure 7. The empirical equation is given by:

$$St\,Pr^{0.4} = 0.03\,Re^{-0.2} \times \frac{\beta_1(1/9, 10/9)}{\beta_{u1}(1/9, 10/9)} \qquad \text{(Equation 2.1)}$$

where u1 is defined by:

$$u1 = 1 - \left(\frac{\xi_1}{x}\right)^{\frac{9}{10}} \qquad \text{(Equation 2.2)}$$

Figure 7 shows that experimental baseline data correspond well with the empirical correlation with a maximum devariation of 3 per cent for Reynolds numbers greater than 8×10^5.

F. TEMPERATURE MEASUREMENTS

Calibrated copper-constantan thermocouples are used to measure all temperatures, including heat transfer surface temperatures, the injection plenum temperature, the local boundary layer temperature, and the free stream temperature. The calibration equation for the freestream thermocouple is given by Williams [Ref. 22] and the calibration equation for the 126 thermocouples used to measure the surface temperatures of the heat transfer plate is given by Ortiz [Ref. 18]. The equation used to convert voltage to temperature for the thermocouples located in the injection plenum chamber and at local positions in the boundary layer is given as:

$$T_{inj}\ (^{o}C) = 2.2907 + 0.85948 * T_{plenum}\ (^{o}C) \qquad \text{(Equation 2.3)}$$

Calibration of these thermocouples was performed using a temperature bath which is controlled and regulated with electric heaters, and a platinum resistance thermometer for a temperature reference ($\pm$.01° C). The new thermocouples employed in the plenum chamber are connected to channels 148, 149 and 150. The thermocouple used to measure local boundary layer temperature is connected to channel 153.

Local boundary layer temperature measurements, made to determine injectant distributions in Y-Z planes, were performed using one of the newly calibrated thermocouples. For these surveys, the freestream temperature remains at a.nbient conditions with the injectant heated to 50 degrees Celsius and

no power applied to the heat transfer surface. Local temperatures are taken at 800 locations in the Y-Z plane corresponding to an overall plane of 12 cm X 22 cm at a streamwise distance of x/d = 45.8 cm. Twenty points are taken in the vertical direction and forty point are taken in the horizontal direction in each measurement plane. The spacing between points in the Y and Z directions is 0.2 inches. The thermocouple probe is mounted in a traversing device consisting of two traversing blocks which allows for two degrees of freedom. The blocks are each mounted separately. Each is guided by two steel, case hardened support shafts and driven by a 20 thread per inch pitch driving screw. Superior Electric Company M092-FD310 type stepping motors are used to drive each of the two shafts. The motors are controlled by a two-axis Superior Electric company MITAS, controller, which is able to store 2K bytes of information and is equipped with a MC6800 16 bit microprocessor assembly. The MITAS is operated by a Hewlett-Packard Series 200, Model 9836S computer, which also controlls a Hewlett-Packard 3497A Data Acquisition/Control unit and 3498A extender used to acquisition voltages from thermocouples.

G. MEAN VELOCITY MEASUREMENTS

A United Sensors and Control Corporation DC-250-24CD five hole pressure probe is used to measure the three components of mean velocity. The probe has a conical tip of diameter 6.35 mm. Calibration characteristics of the five hole pressure probe are given by Williams [Ref. 23] for yaw and pitch angles ranging from -20 degrees to +20 degrees. During measurements, it is mounted in a traversing device similar to the one used used for the injectant surveys. Each of the five ports of the pressure probe is connected to a Celesco LCVR differential

pressure transducer with a full scale range of 0-2.0 cm of water. These, in turn, are connected to five Celesco CD-10D carrier demodulators which convert the output signal of the transducer to a D.C. voltage. The D.C. voltages are then acquisitioned by the Hewlett-Packard 3497A Data Acquisition Unit. Velocities are determined from pressure coefficients using software contained in the Hewlett-Packard 9836S computer.

H. FLOW VISUALIZATION

The injectant is visualized by contaminating it with theatrical fog in the plenum chamber before it enters the injection holes and then passes along the test surface. A model 1500 Rosco Fog/Smoke Machine is used to supply the fog. The machine uses a fluid which contains a mixture of low molecular weight glycols. During fog production, the fog fluid is first heated to a state condition near vaporization. Atomized vapor is then produced as the fog fluid expands through an orifice. During flow visualization tests, the injectant flow pressure is maintained entirely by the fog machine, requiring adjustment of the freestream velocity of the wind tunnel to create desired blowing ratios.

A Dage-MTI video camera, model number CCD 72, is used for photography of visualized flow patterns. A tripod is used to hold the camera stationary as the photographs are taken. Both the camera and tripod are positioned 50.8 cm above the transparent top of the wind tunnel as Tungsten lamp spotlights are used to provide illumination of flow patterns. The video image is monitored on an MTI HR 1000 video screen and the resulting hard copy images are produced by a Mitsubishi P65U video copy processor.

III. EXPERIMENTAL RESULTS

A. BASELINE HEAT TRANSFER DATA

Dimensional spanwise-averaged Stanton numbers are presented in Figure 5 along with baseline data from Bishop [Ref. 1] and the empirical relationship given by Kays and Crawford [Ref. 12] for a turbulent boundary layer developing along a constant heat flux surface downstream of an unheated starting length (see Equations 2.1 and 2.2). Both experimental baseline data sets agree with the empirical correlation within five percent, for Reynolds numbers greater than 8 x 10^5. The baseline data set from the present study is used to normalize Stanton numbers presented in Section D.

B. FILM COOLING HEAT TRANSFER DATA WITH NO VORTEX AND FILM COOLING, M=1.3

Data taken with film cooling but no vortex present are now presented. A constant blowing ratio of 1.3 (to within $\pm$0.005) was employed from one row of compound angle injection holes. Values of the non-dimensional temperature (θ) employed were approximately 1.3, 1.0, 0.5, and 0. Adiabatic effectiveness values and iso-energetic Stanton numbers were determined using the linear superposition technique described by Bishop [Ref. 1].

Figure 6 shows adiabatic film cooling effectiveness (η) plotted versus non-dimensional streamwise distance (x/d). Included in this figure are results from Bishop [Ref.1] for blowing ratios of 0.5 and 1.0 . When compared to results for a blowing ratio of 1.3, these results show that the film cooling effectiveness (η) value is lowest for the highest blowing ratio (m=1.3). In addition, data are

essentially invariant with x/d for x/d greater than 30. Figure 8 shows the variation of the iso-energetic Stanton number ratio (St_f / St_0) with x/d. This ratio varies only slightly over the entire length of the test surface for x/d up to about 100 .

Figures 9,10 and 11 show three-dimensional plots of the Stanton number ratio (St/St_0), iso-energetic Stanton number ratio (St_f/St_0) and film cooling effectiveness as functions of x/d and z/d. Data are given for six different streamwise locations, x/d = 6.7, 17.2, 33.1, 54.3 and 96.6. All three types of data show spanwise periodic distributions over most of the x/d range studied. Such spanwise variations of St/St_0 , St_f /St_0 and η correspond to spanwise accumulations and deficits of injectant.

Figures 12-26 contain plots of Stanton number ratio (St/St_0) versus non-dimensional temperature (θ) for three different spanwise locations, z=0.0, 6.35, and -6.35 and six different streamwise locations. With the exception of one or two data points in Figures 16 and 21, each graph shows a linear relationship between St/St_0 and θ, where St/St_0 values generally increase with decreasing θ.

C. HEAT TRANSFER DATA FOR VORTEX POSITIONS R0, L0 WITH NO FILM COOLING

Figures 27 shows St/St_0 values versus spanwise coordinate (Z) obtained with an 18 degree vortex at generator position R0. Similarly Figure 28 shows results obtained with the vortex generator at position L0. Some scatter is present for X=1.15 m in both plots, however, in general, data correspond well to similar results presented by Craig [Ref. 3]. In Figure 27, maximum St/St_0 values shift to larger Z as streamwise distance increases for position R0. In Figure 28, St/St_0 values shift to smaller Z with streamwise distance for position

L0. Away from the test section centerline, where spanwise variations are small, St/St_0 values approach 1.0, as expected.

D. HEAT TRANSFER DATA WITH FILM COOLING AND EMBEDDED VORTICES

Heat transfer results are presented in six parts. These are: One row of film cooling holes, no vortex ; one row of film cooling holes, vortex positions R0-R4; one row of film cooling holes, vortex positions L0-L4; two rows of film cooling holes, no vortex; two rows of film cooling holes, vortex positions R0-R4; and two rows of film cooling holes, vortex positions L0-L4.

1. One row of film cooling holes, no vortex with m=0.5

St_f/St_0 data versus spanwise distance (Z) are presented in Figure 29 for injection from one row of film cooling holes with m=0.5 and no vortex present for x=1.4m. This figure shows a spanwise periodic variation of St_f/St_0 due to accumulations and deficits of film cooling across the test section span. These are shifted in the spanwise direction from hole locations due to the compound angle nature of the holes. This shift is approximately 2-3 cm, and increases with streamwise distance.

2. One row of film cooling holes, Vortex positions R0-R4, with m=0.5

Figures 30 and 31 show St/St_0 variations with Z for X=1.4 m for vortex positions R0-R4. Figure 30 shows that St/St_0 variations for positions R0 and R4 are quantitavely similar (accounting for the spanwise shift of the vortex generator) because positions R0 and R4 are similarly oriented with respect to film cooling holes (R4 is positioned one hole over from R0). For Z larger than 9-10 cm and Z less than -7 to -8 cm, St/St_0 data in Figure 30 approach

distributions which exist when no vortex is present. The influence of the vortex is most important between these regions. Maxima St/St_0 for vortices R0-R4 are at different locations and have different magnitudes in Figure 31. Of these vortices, the ones with downwash regions farther to the right have lower maxima.

Figures 32-36 show the streamwise development of St/St_0 and St_f/St_0 variations. These figures show how vortex secondary flows become more detrimental as well as how the protection offered by the film cooling diminishes locally with streamwise development.

3. One row of film cooling holes, Vortex positions L0-L4, with m=0.5

Data obtained using one row of film cooling holes, vortex positions L0-L4, with m=0.5 are presented in Figures 37 and 38 for x=1.4 m. The first of these figures shows that St/St_0 data for vortex positions L0 and L4 are quite similar, only shifted in the spanwise direction with respect to each other.

Figure 38 shows that maximum St/St_0 shift to the left as vortices are moved to the left in the spanwise direction. Vortex L2 has the highest local maximum and vortex L3 has the lowest local maximum.

Figures 39-43 provide information on the streamwise variation of St/St_0 and St_f/St_0 data for vortices L0 -L4. As for vortices R0-R4, the most significant Stanton number ratios with respect to ratios with film cooling only occur farther downstream at X of 1.6 m, 1.8 m, and 2.0 m . A comparison of these results with data in Figures 32-36 shows that maxima St/St_0 are generally smaller for vortices L0-L4.

4. Two rows of film cooling holes, no vortex with m=0.5

Figure 43 shows the spanwise variation of St_f/St_0 for x=1.4 m. Comparison of these data to results in Figure 29 indicates a more spanwise uniform, less spanwise periodic, distribution of St_f/St_0 with Z.

5. Two rows of film cooling holes, Vortex positions R0-R4, with m=0.5

Figures 45 and 46 show variations of St/St_0 with z for x=1.4 m for vortices R0-R4. Figure 45 shows that magnitudes of St/St_0 for vortices R0 and R4 are similar in shape. Figure 46 shows that the minimum St/St_0 occurs for vortex R0 and that the maximum St/St_0 occurs for vortex R2. The vortex providing the largest local St/St_0 maximum is R2.

Figures 47-51 show a comparison of St/St_0 to St_f/St_0. Again, as the fluid moves downstream, the vortices dominate local heat transfer behavior, and the film cooling no longer provides adequate protection at these locations.

6. Two rows of film cooling holes, Vortex positions L0-L4, with m=0.5

Figures 52 and 53 show St/St_0 variations at x=1.4 for vortices L0-L4. Shapes and magnitudes of St/St_0 are similar for vortices L0 and L4. Figure 53 shows that the maximum St/St_0 corresponds to vortex L2. The vortex providing the largest local St/St_0 maximum is L2.

Figures 54-58 show a comparison of St/St_0 to St_f/St_0. As for earlier results, vortex effects dominate local St/St_0 behavior farther downstream. Comparison of these results to ones in Figures 46-50 for vortices R0-R4 shows that maxima St/St_0 are much smaller in magnitude for vortices L0-L4.

E. FIVE HOLE PRESSURE PROBE SURVEYS

In the discussion of results obtained using the five hole pressure probe, streamwise vorticity contours are presented first. This is followed by discussion of secondary flow vectors, streamwise velocity distributions, and total pressue distributions. Surveys are presented for two different streamwise locations: position A where x/d=10.2, and position B where x/d=45.8.

1. Streamwise vorticity contours

a. Probe position x/d=10.2, no film cooling

Figures 59-64 show vorticity contours determined from measurements taken at position A, x/d=10.2, with no film cooling. Data are given for vortices L0, L4, L8, R0, R4 and R8. In each of these figures, the vortex core is approximately circular in shape. Vorticity and circulation levels are approximately constant for the different vortices. Here, L8 and R8 refer to vortex generator base plates, placed 10.8 cm from the left or right of the tunnel centerline (looking downstream). The average distance between core centers is 7.3 cm which corresponds well to 7.2 cm, the value used for spanwise positioning of the vortex generator.

b. Probe position x/d=45.8, 1 row film cooling holes, m=0.5

Figures 83-90 show vorticity contours taken at position B, x/d=45.8, with one row of film cooling holes, m=0.5, and vortices R0-R3 and L0-L3. The cores are again circular in shape. The average maximum vorticity is 616 rads/s. The average spanwise distance between cores is 1.7 cm, which corresponds well to 1.8 cm, the spanwise distance between vortex generator positions. The

deviations from this spacing result because of slight repositioning of the vortices by the film cooling.

c. Probe position x/d=45.8, 2 rows of film cooling holes, m=0.5

Figures 91-98 show vorticity contours taken at position B, x/d=45.8, with two rows of holes used for film cooling. A blowing ratio of 0.5 is used with all vortices. The average vorticity of vortices R0-R4 is 675 rads/s (± 5%) which varies significantly from the value for vortices L0-L4, which is 476 rads/s. This difference is due to the fact that the injectant flow opposes vortex secondary flows near the wall for vortices L0-L4. Vortex cores are spaced an average of 1.6 cm apart.

2. Secondary flow vectors, streamwise velocity and total pressure distributions

a. Probe position x/d=10.2, no film cooling

Figures 65-82 give the secondary flow vectors, streamwise velocity distributions and total pressure distributions at probe position A, x/d=10.2, for verticesR0, R4, R8, L0, L4 and L8. Vortices in these figures are evidenced by clockwise directed secondary flow vectors (for vortices R0-R4) or counter-clockwise directed secondary flow vectors (for vortices L0-L4) when viewed looking downstream. The size and shape of each vortex are consistent with vorticity contours presented in Figures 59-64. Spanwise positions of vortices R0, R4, and R8 are about 7.2 cm apart. Similar spacing is evident for vortices L0, L4 and L8.

b. Probe position x/d=45.8, 1 row of film cooling holes, m=0.5

Figures 99-122 show secondary flow vectors, streamwise velocity distributions and total pressure distributions for vortices R0-R4 and L0-L4 as measured at x/d=45.8. These data are consistent with similar data given by Williams [Ref. 22] and Craig [Ref. 3]. Each plot shows a region of low velocity or low pressure corresponding to injectant locations. These locations are well correlated to regions of injectant depletion shown in Figures 163-170.

c. Probe position x/d=45.8, 2 rows of film cooling holes, m=0.5

Figures 122-145 show plots of secondary flow vectors, velocity distributions and total pressure distributions measured downstream of two rows of film cooling when vortices R0-R4 and L0-L4 are present. Sizes and shapes of different vortices are similar. As for data taken downstream of one row of holes, velocity and pressure deficits are evident at locations where injectant accumulates.

F. INJECTANT DISTRIBUTION SURVEYS

In this section, the results of injectant distribution surveys are presented as measured downstream of one row of holes and two rows of holes using a blowing ratio of 0.5. They are presented for x/d=45.8.

1. Injectant distributions, one row of film cooling holes, m=0.5

Injectant distributions for vortices R0-R4 and L0-L4 are found in Figures 147-154 and 163-190. Each plot contains two of three regions of injectant

injectant concentration as well as regions where injectant is depleted near vortex downwash regions and beneath vortex cores.

2. Injectant distribution, two rows of film cooling holes, m=0.5

Figures 155-162 and 171-178 show injectant distribution surveys measured downstream of two staggered rows of injection holes for vortices R0-R4 and L0-L4. These results are qualitatively similar to ones measured downstream of one row of holes. One important difference is evident near walls, where injectant accumulations are more frequent in number across the channel span.

G. FLOW VISUALIZATION RESULTS

Flow visualization data are found as Figures 179-194. Figure 179 shows visualized film coolant downstream of two rows of holes with no vortex present. Figures 180-184 for vortices R0-R4 downstream of two rows of holes show that vortex R2 provides the most significant rearrangement of injectant. In contrast, the phototgraphs in Figures 185-189 for vortices L0-L4 downstream of one row of holes show that vortex L4 causes the most disturbance to the injectant. For vortices R0-R4 downstream of one row of film cooling holes, vortices R0 and R4 are most detrimental.

IV. SUMMARY AND CONCLUSIONS

Experimental results are presented which document the effects of embedded longitudinal vortices on film cooling injection from one and two rows of holes with compound angle orientations. Holes are designed such that their angles with respect to the test surface are 30 degrees in a spanwise/normal plane projection, and 35 degrees in a streamwise/normal plane projection. A blowing ratio of 0.5, non-dimensional injection temperature parameter of 1.29 to 1.38, and freestream velocity of 10 m/s are employed. Results show that injectant distributions are affected by the longitudinal embedded vortices, their directions of rotation, their spanwise positions with respect to film injection holes, as well as the number of rows of film cooling holes. Maximum Stanton number ratios are smaller in magnitude for counter-clockwise vortices (viewed when looking downstream). These heat transfer results are further substantiated by surveys of streamwise mean velocity, secondary flow vectors, total pressure, streamwise mean vorticity and injectant distributions.

APPENDIX A

FIGURES

Appendix A contains all of the figures generated for this thesis. These figures include test set-up, hole configurations, plots of Stanton numbers versus Reynolds numbers and spanwise plots of velocity, pressure and temperature for all configurations used. Flow visualization pictures are also included for some configurations.

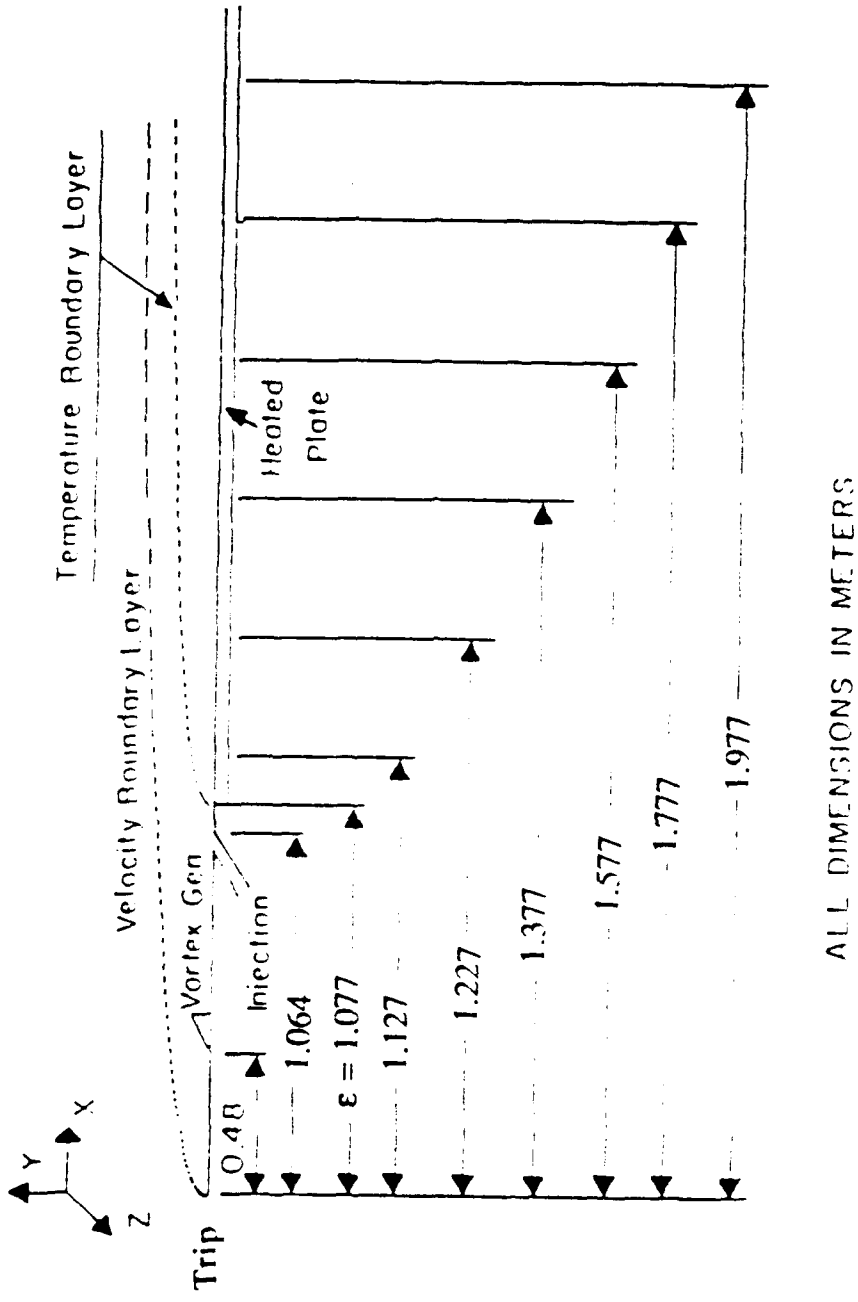

Figure 1. Test Section Coordinate System

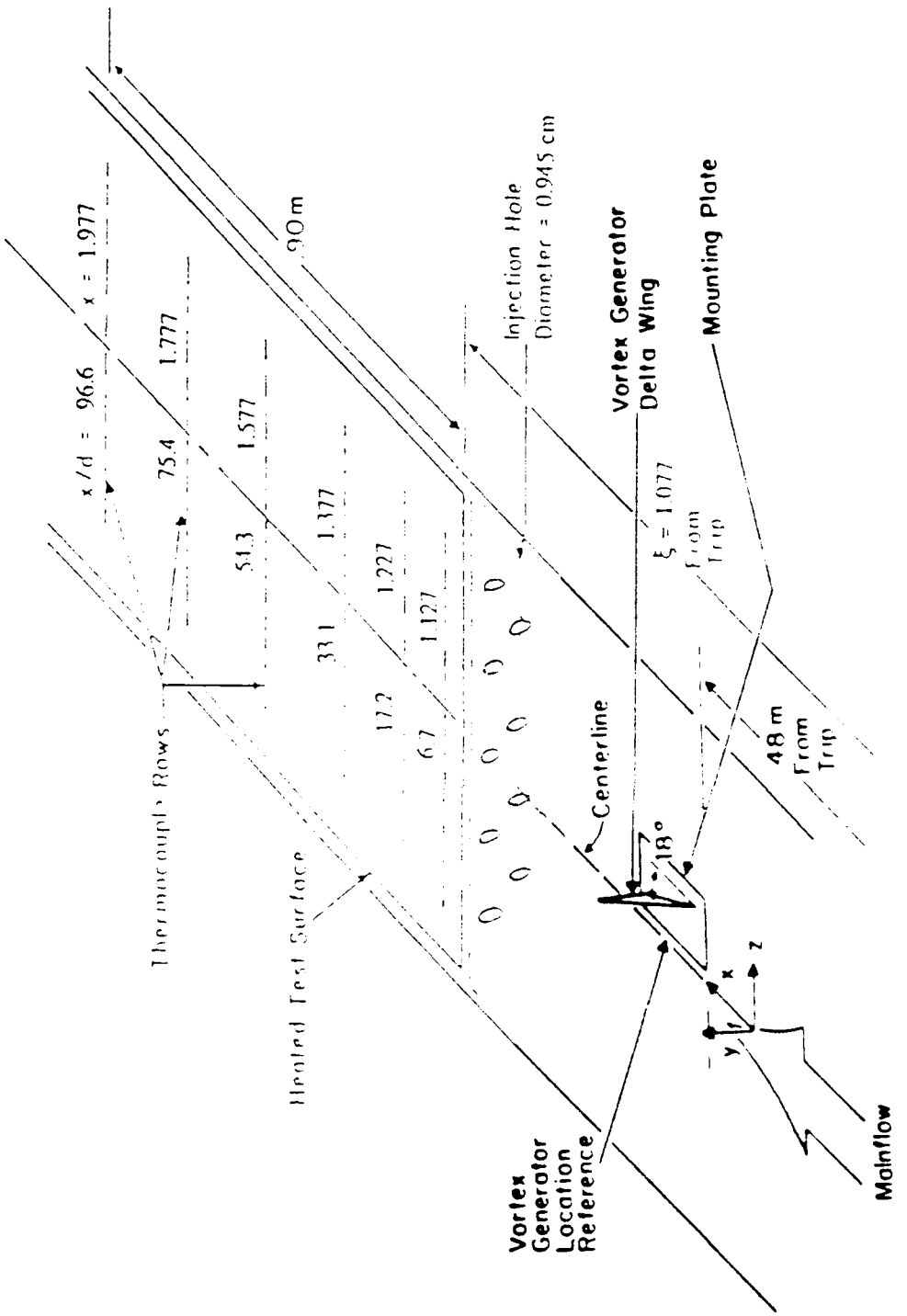

Figure 2. Top View Schematic of Wind Tunnel Test Section

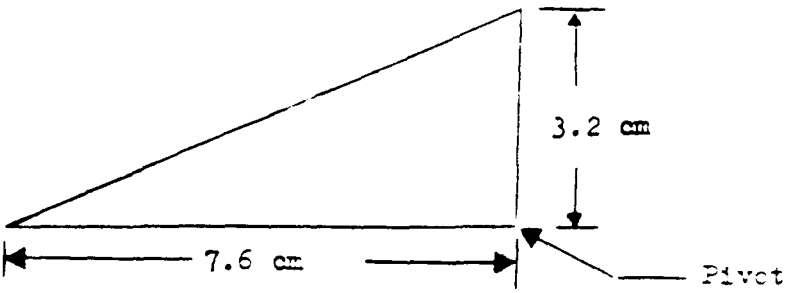

Half Delta Wing

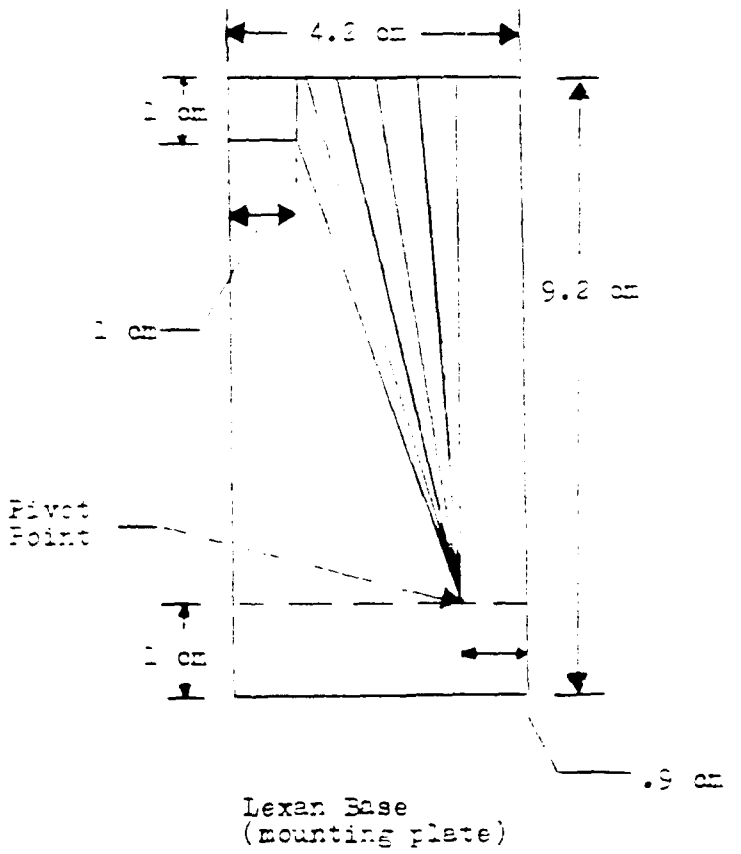

Lexan Base
(mounting plate)

Figure 3. Vortex Generator Details

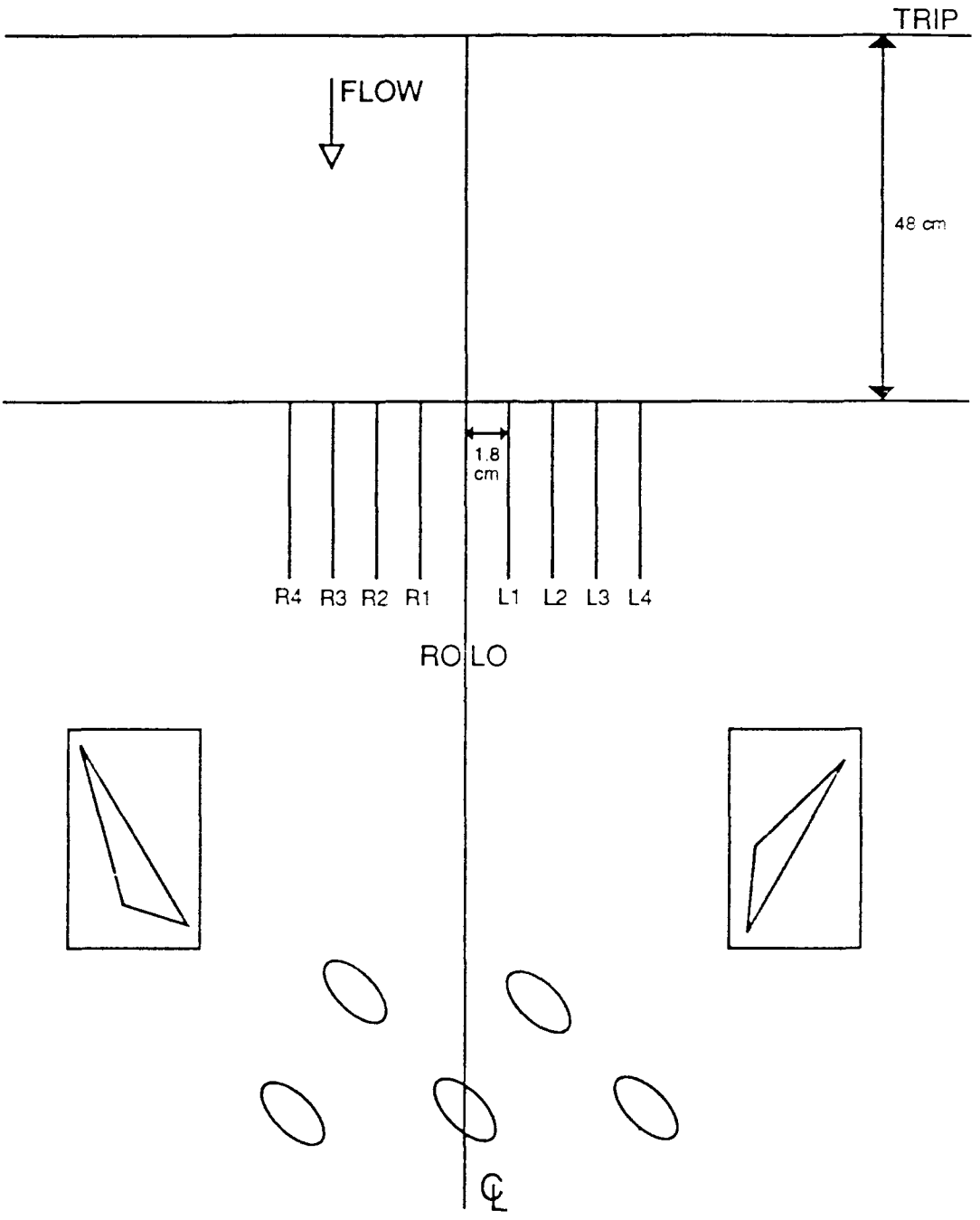

Figure 4. Vortex Position Schematic

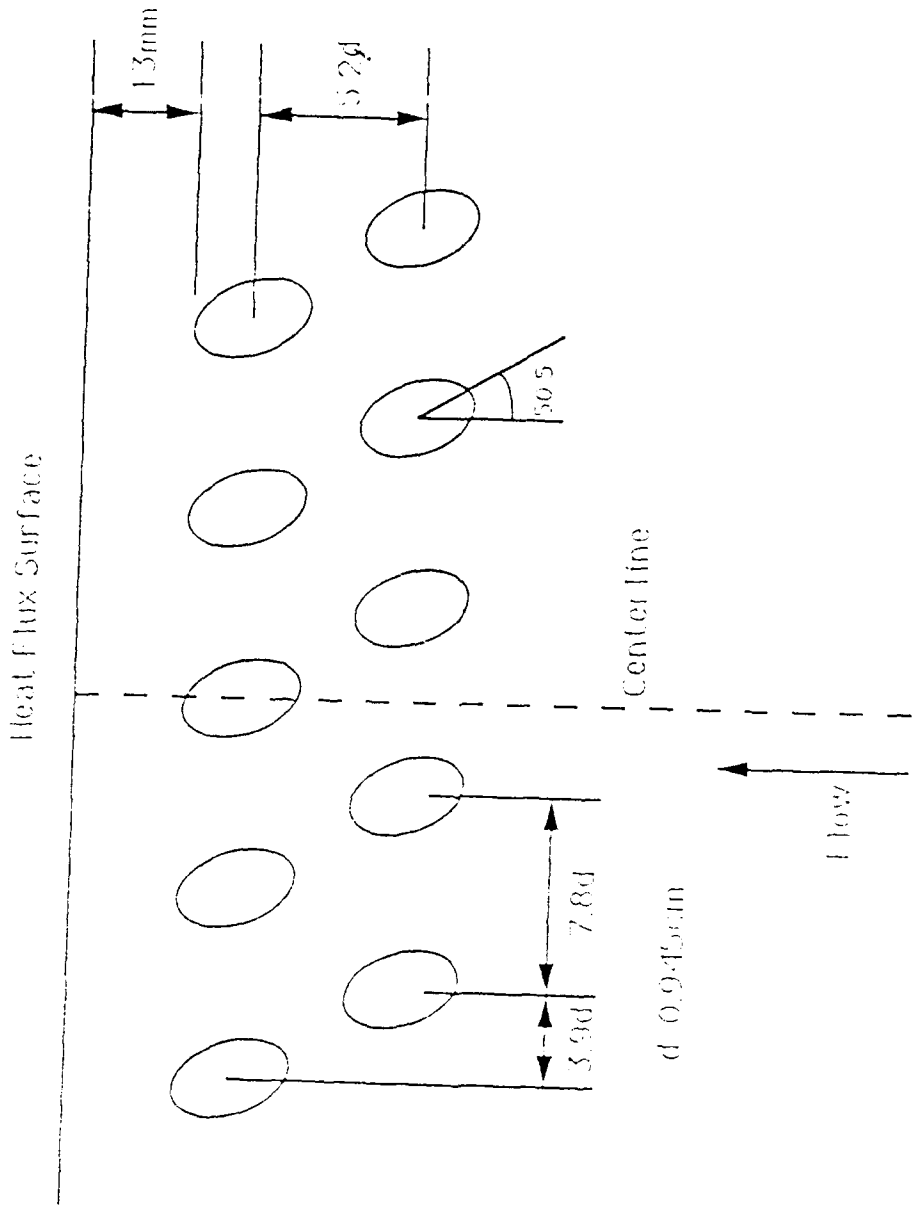

Figure 5. Injection Hole Configuration

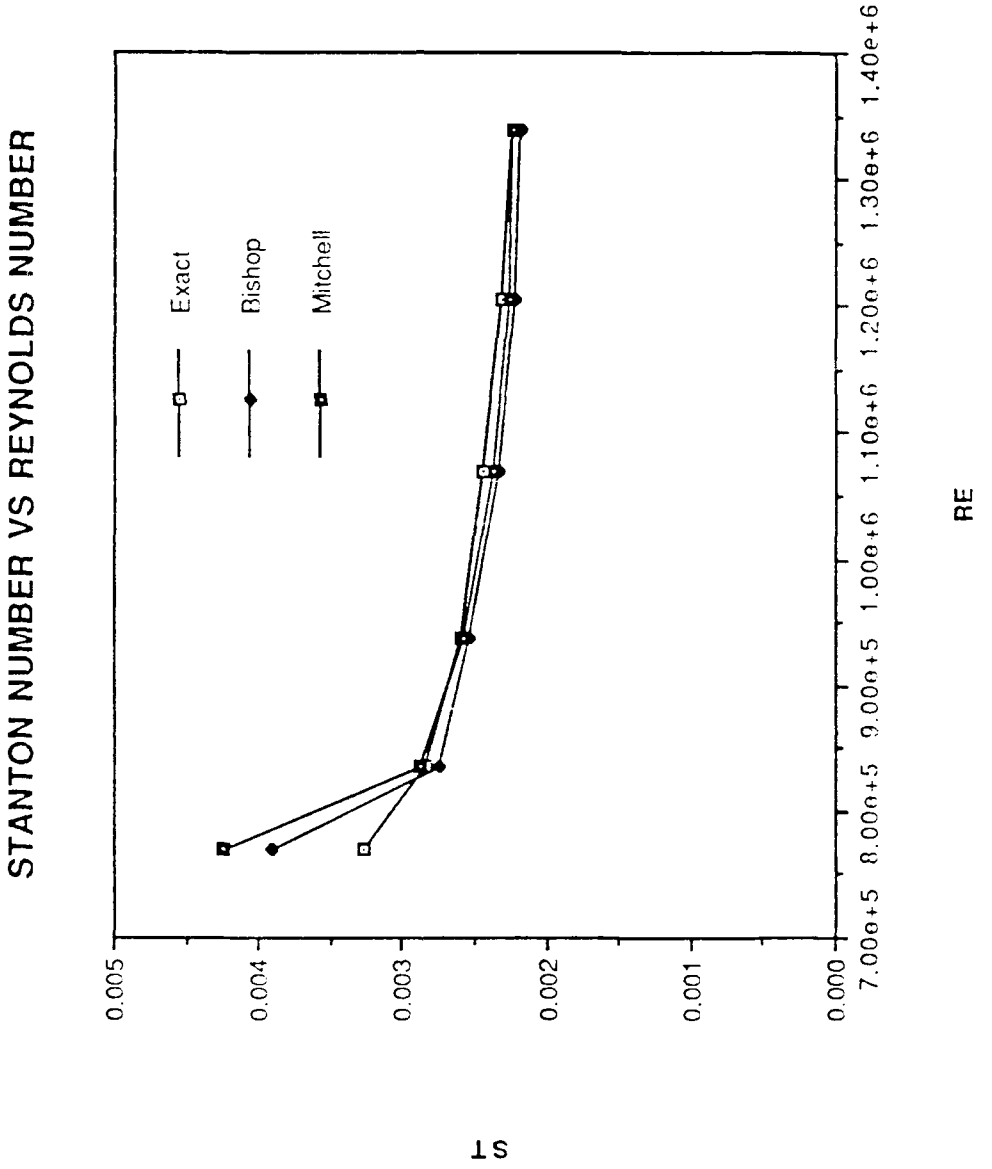

Figure 6. Stanton Number Comparison Between Exact Solution and Experimental Measurements

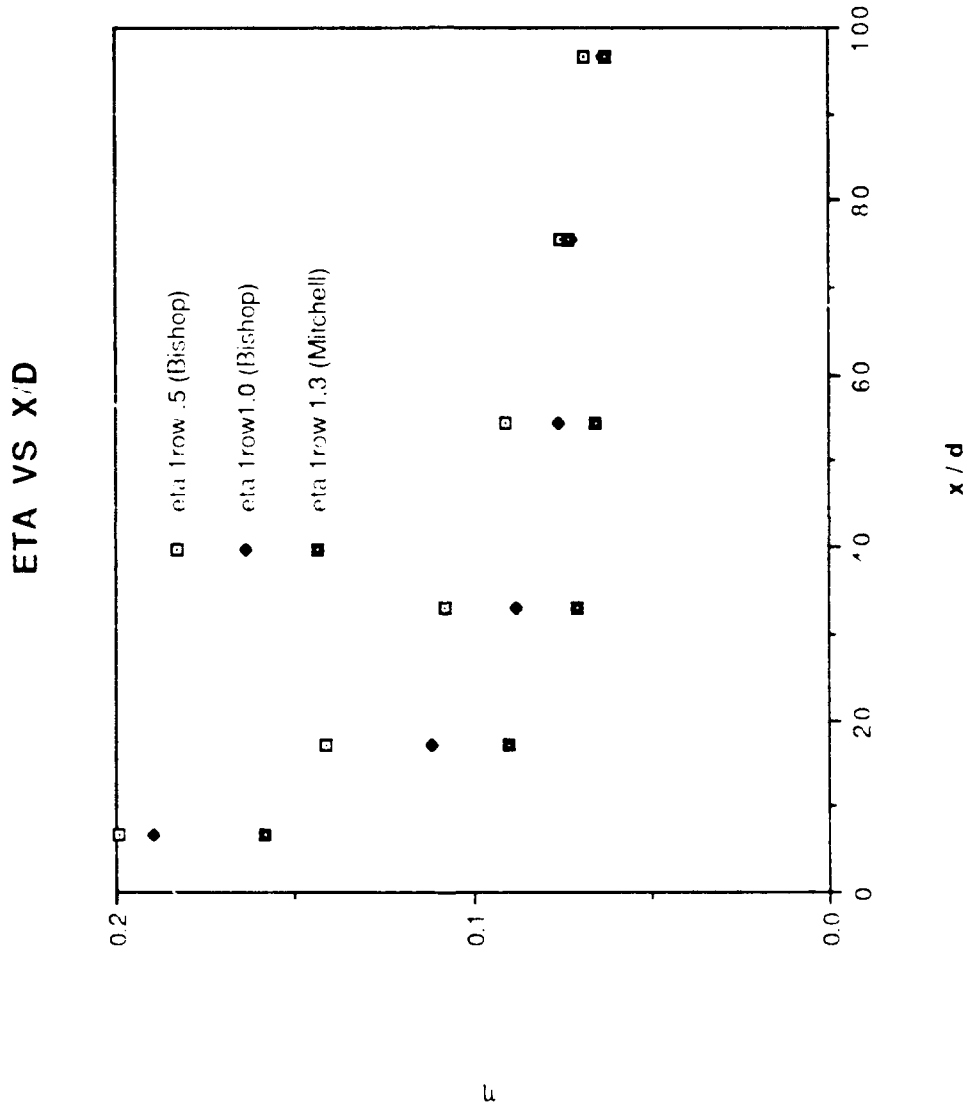

Figure 7. Film Cooling Effectiveness Versus x/d for θ =1.3

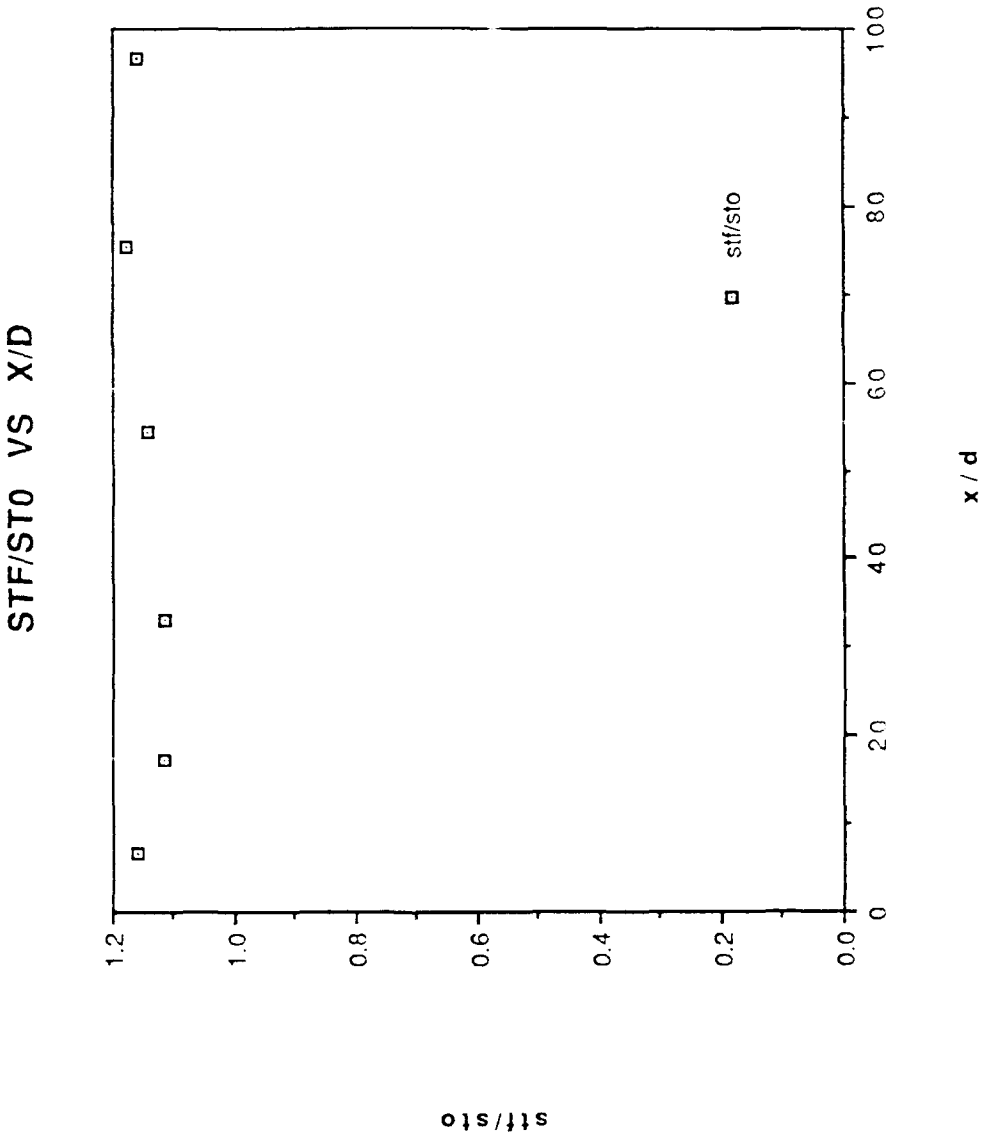

Figure 8. Local Stanton Number Ratio, St/St_0 Versus Streamwise Location, x/d, with Film Cooling, m=1.3, One Row of Injection Holes

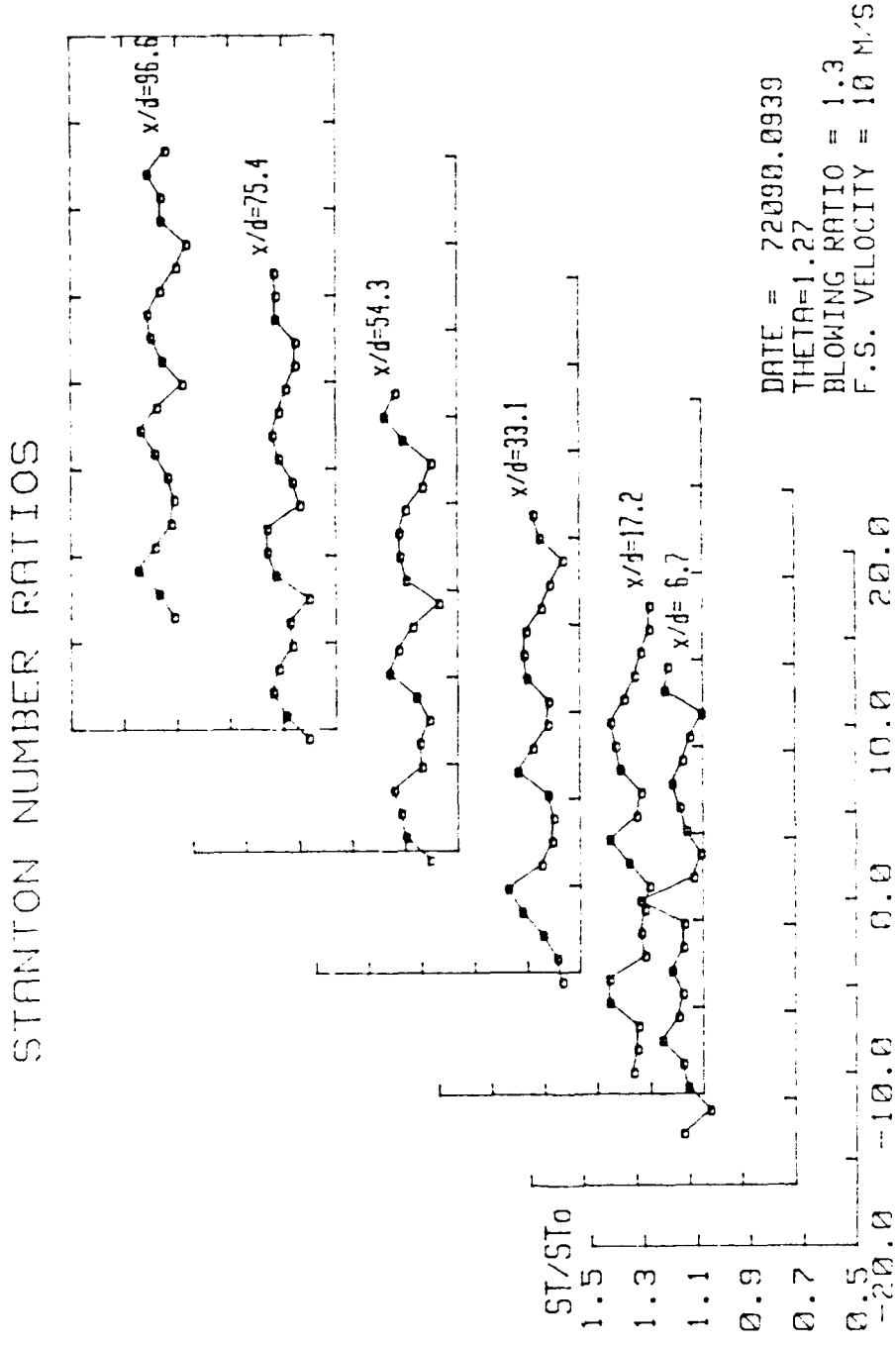

Figure 9. Spanwise Variation of St/St_0 Ratios, m=1.3,θ =1.27, One Row of Holes, No Vortex

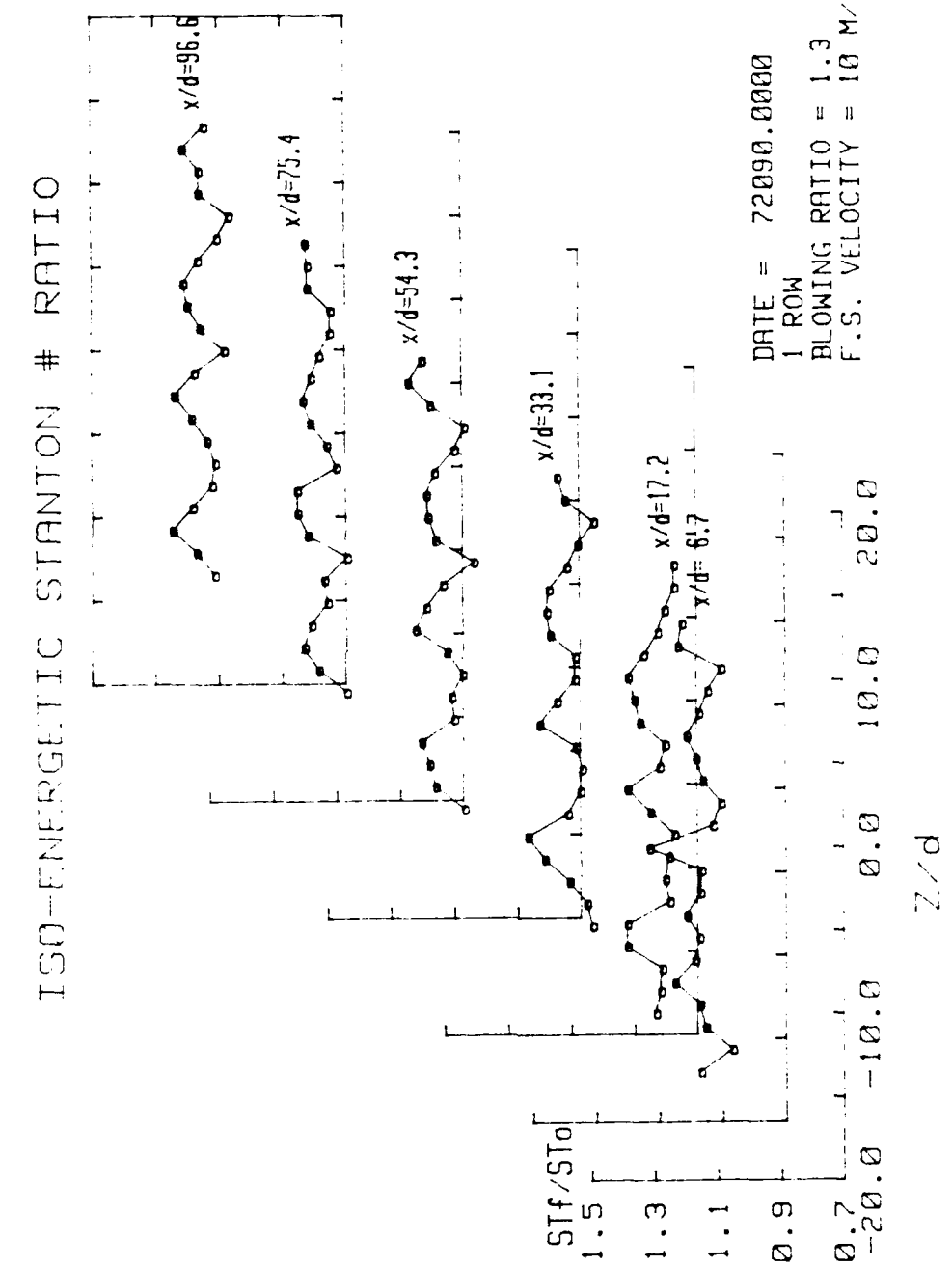

Figure 10. Spanwise Variation of Iso-Energetic St_f/St_0 Ratio, m=1.3, One Row of Holes, No vortex

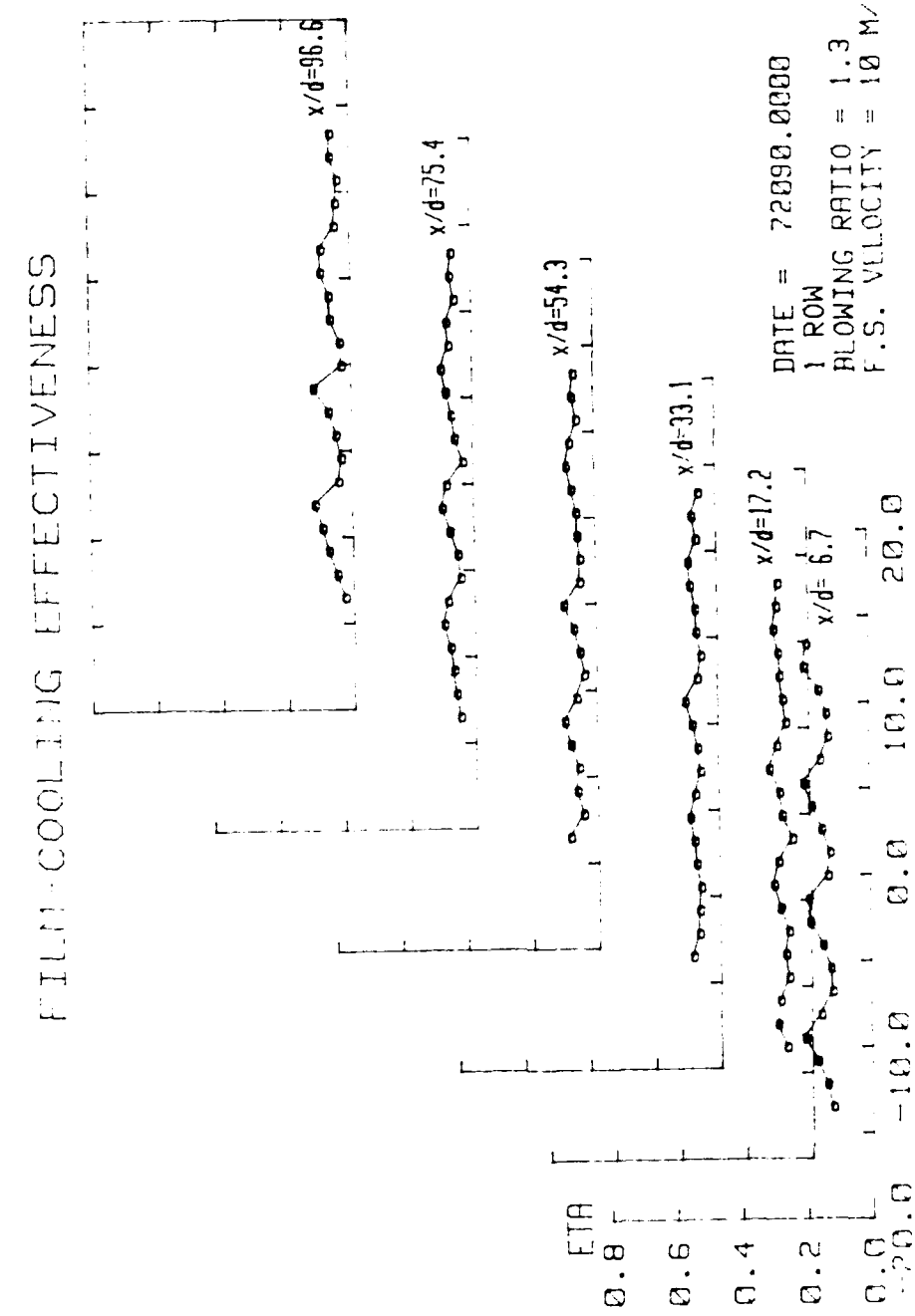

Figure 11. Spanwise Variation of Film Cooling Effectiveness, m=1.3

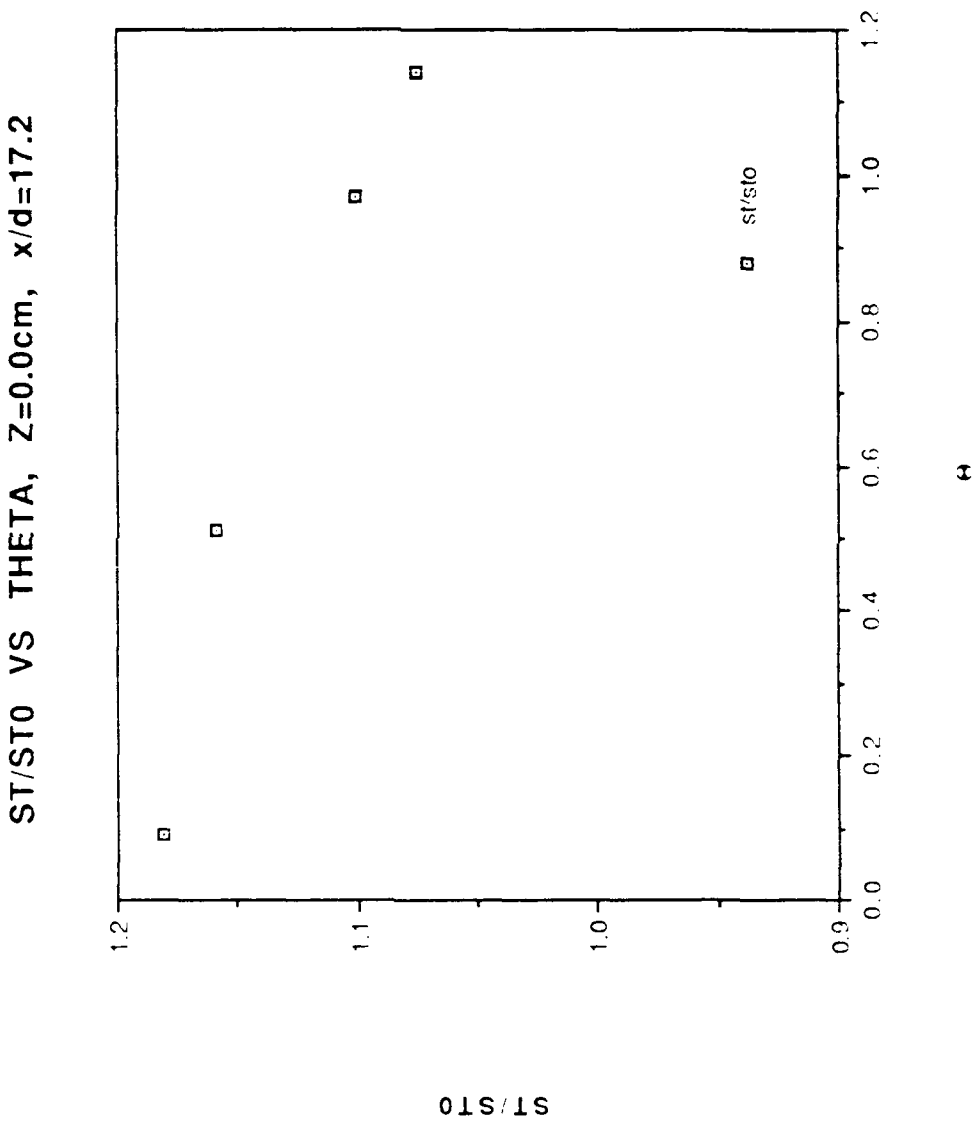

Figure 12. St/St_0 Versus θ , z=0.0 cm, x/d=17.2

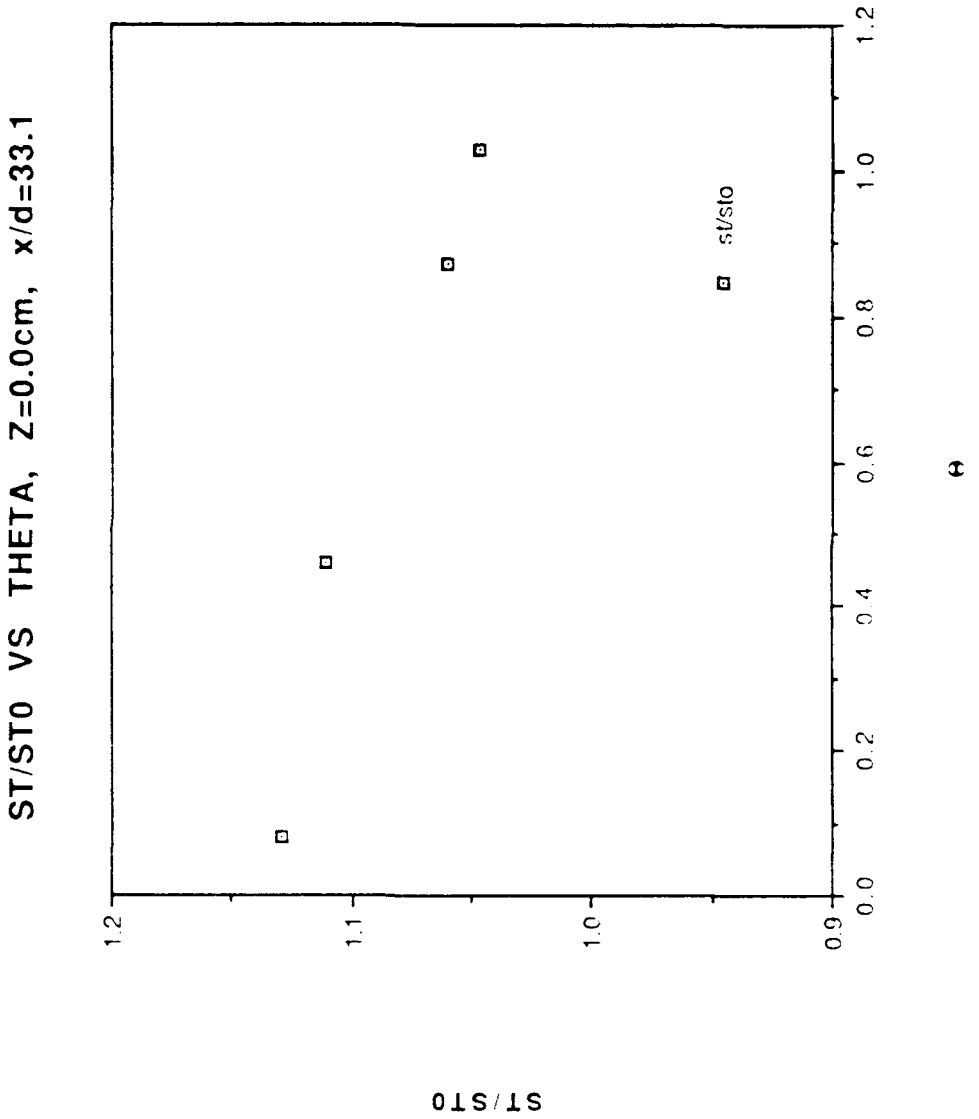

Figure 13. St/St_0 Versus θ , z=0.0 cm, x/d=33.1

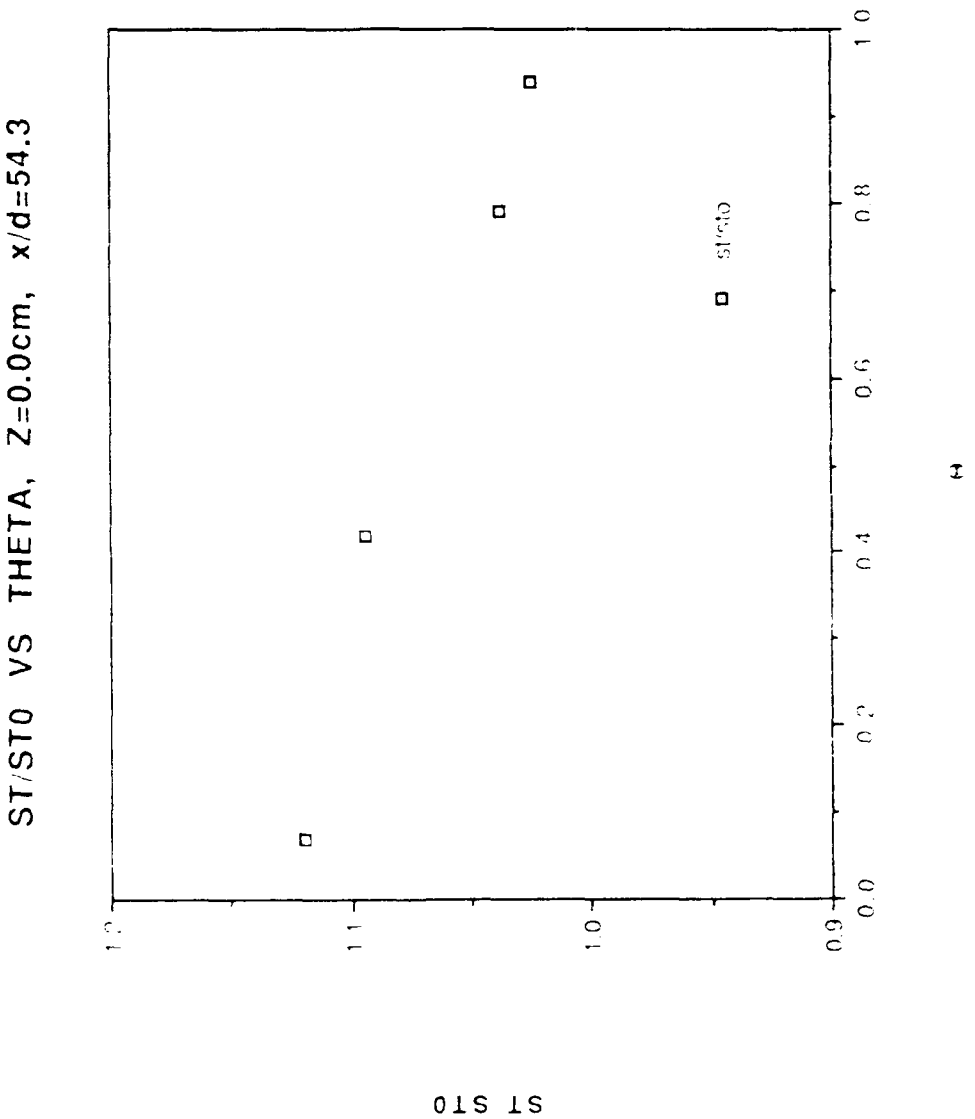

Figure 14. St/St_0 Versus θ , z=0.0 cm, x/d=54.3

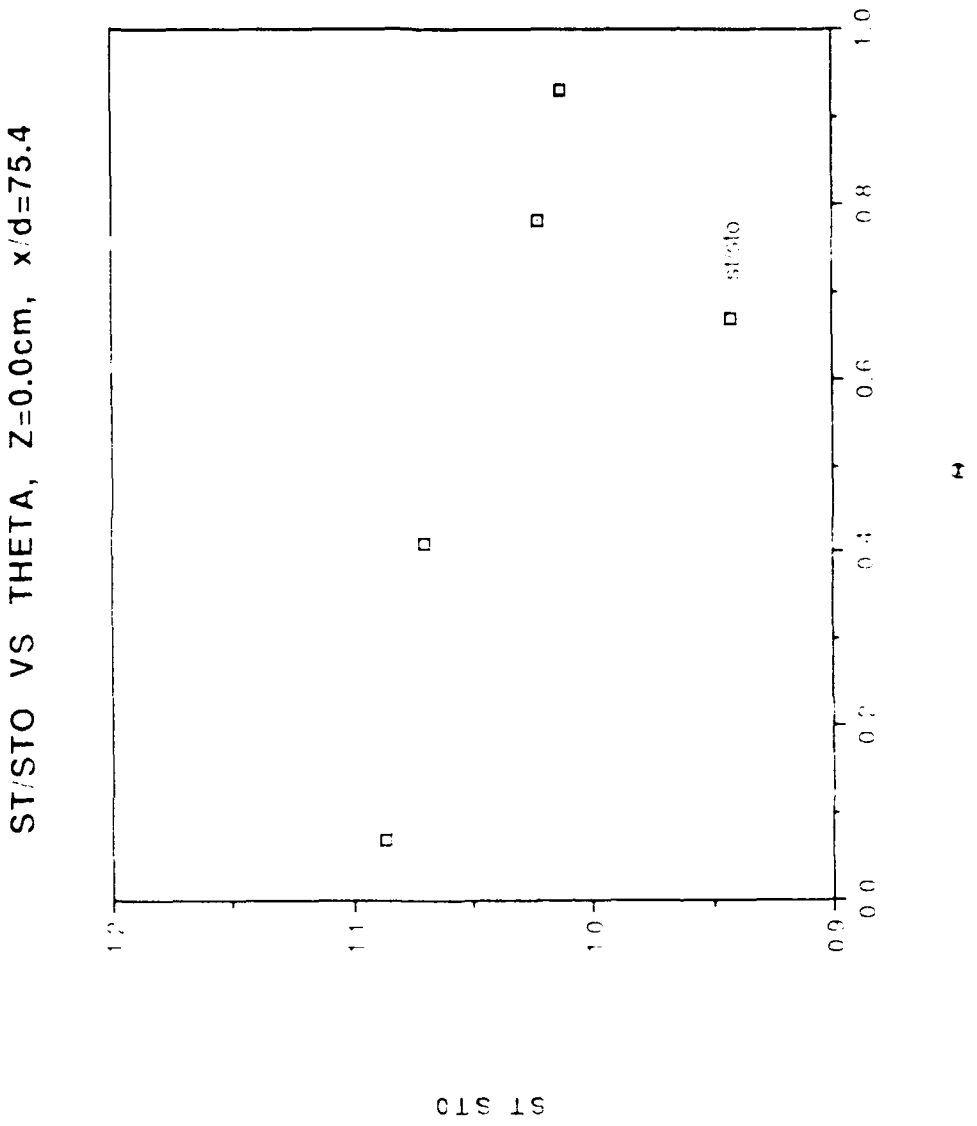

Figure 15. St/St_0 Versus θ , z=0.0 cm, x/d=75.4

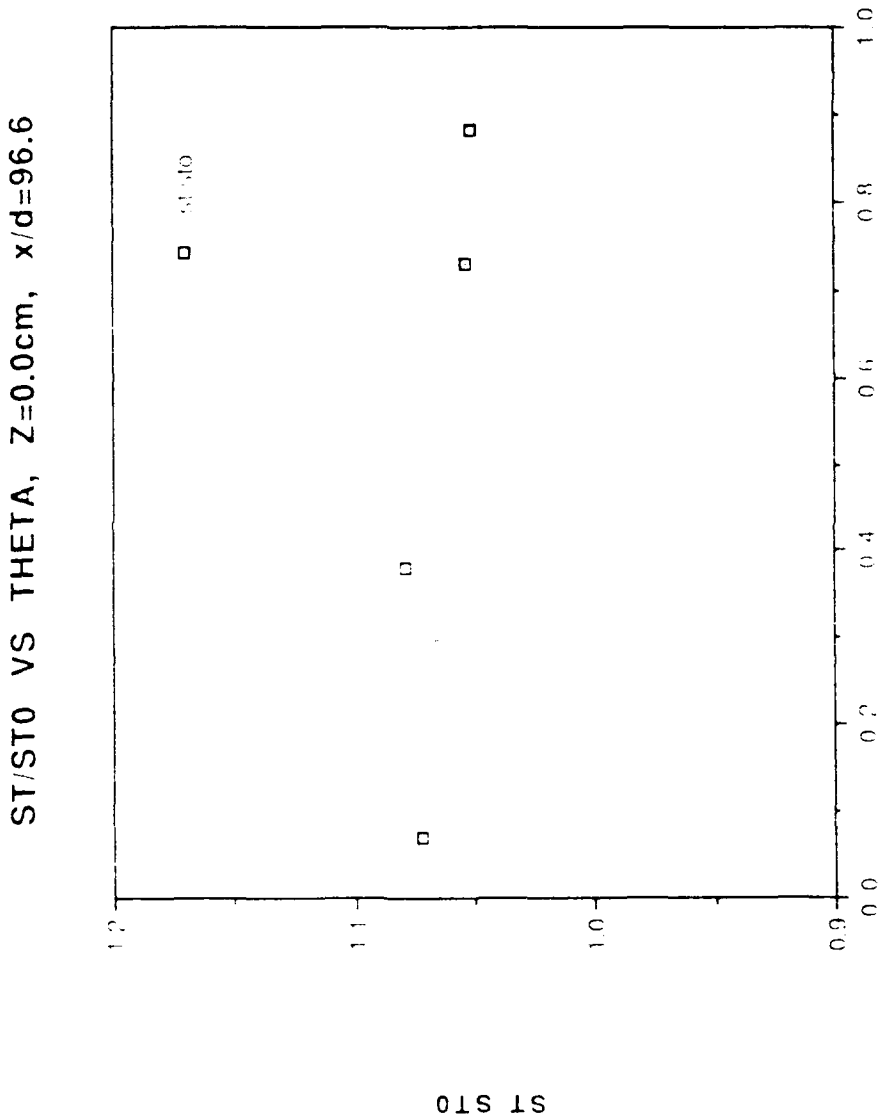

Figure 16. St/St_0 Versus θ , z=0.0 cm, x/d=96.6

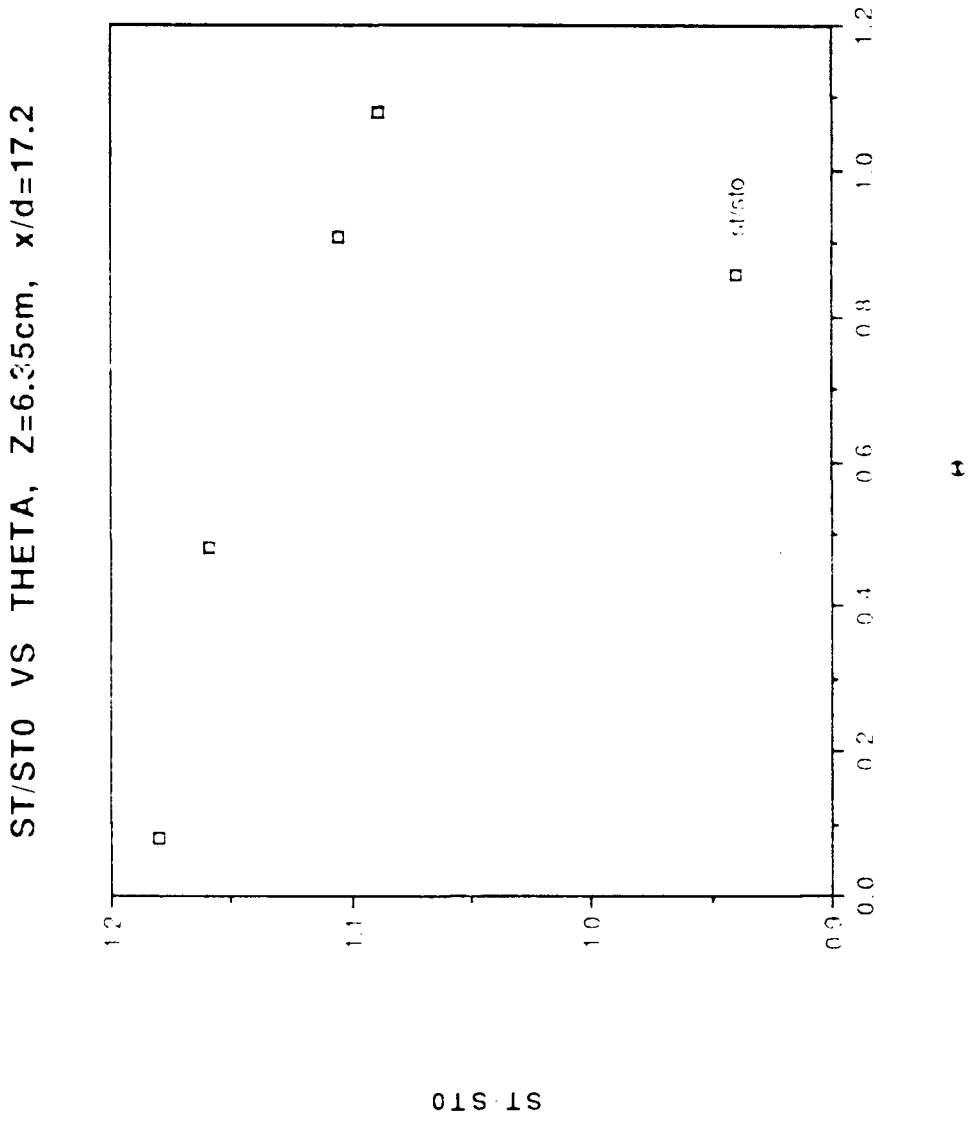

Figure 17. St/St_0 Versus θ , z=6.35 cm, x/d=17.2

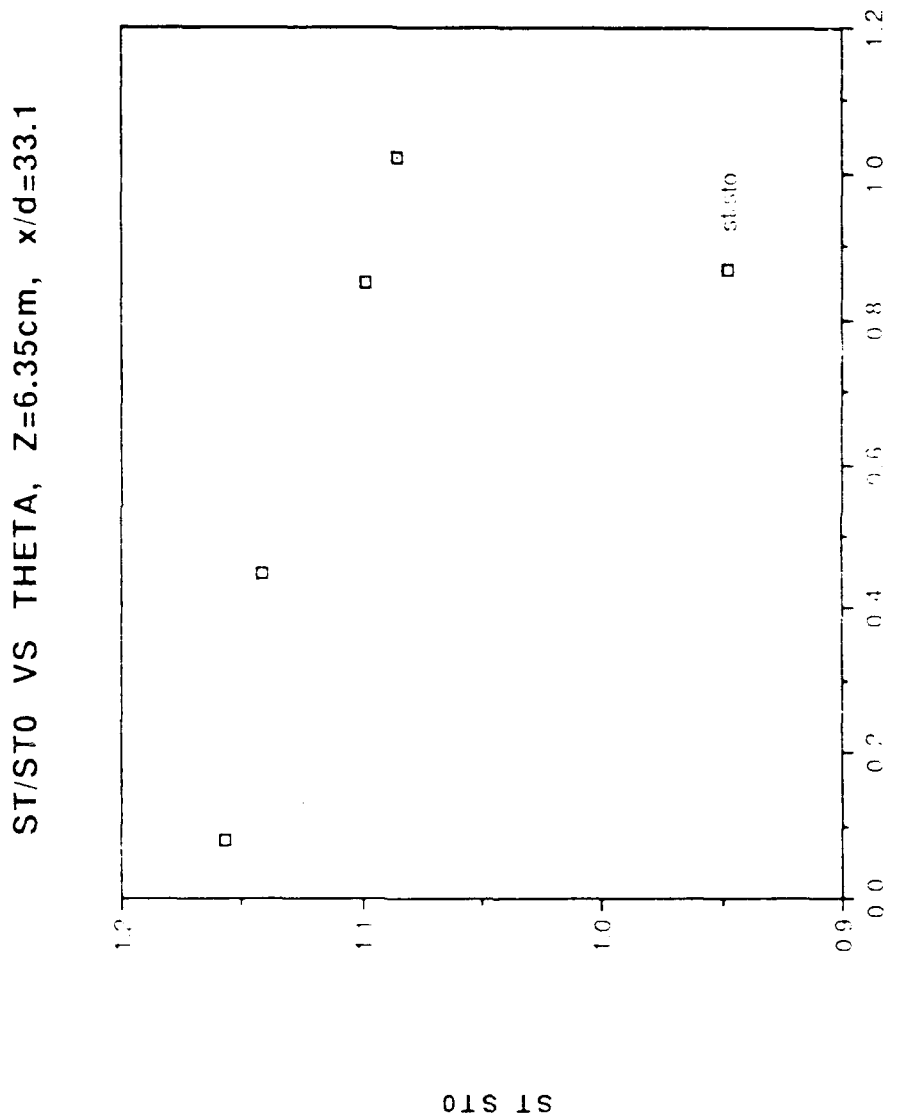

Figure 18. St/St_0 Versus θ , z=6.35 cm, x/d=33.1

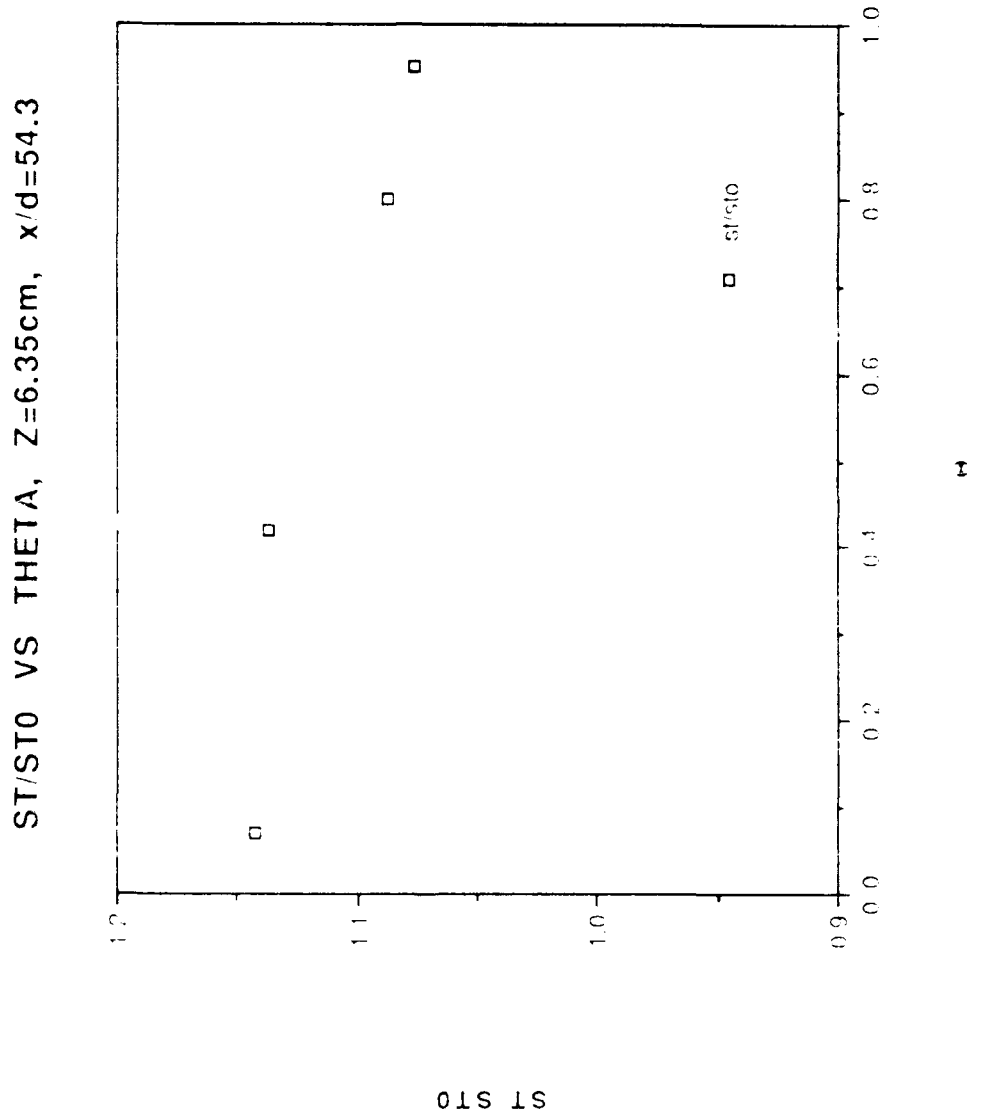

Figure 19. St/St_0 Versus θ , z=6.35 cm, x/d=54.3

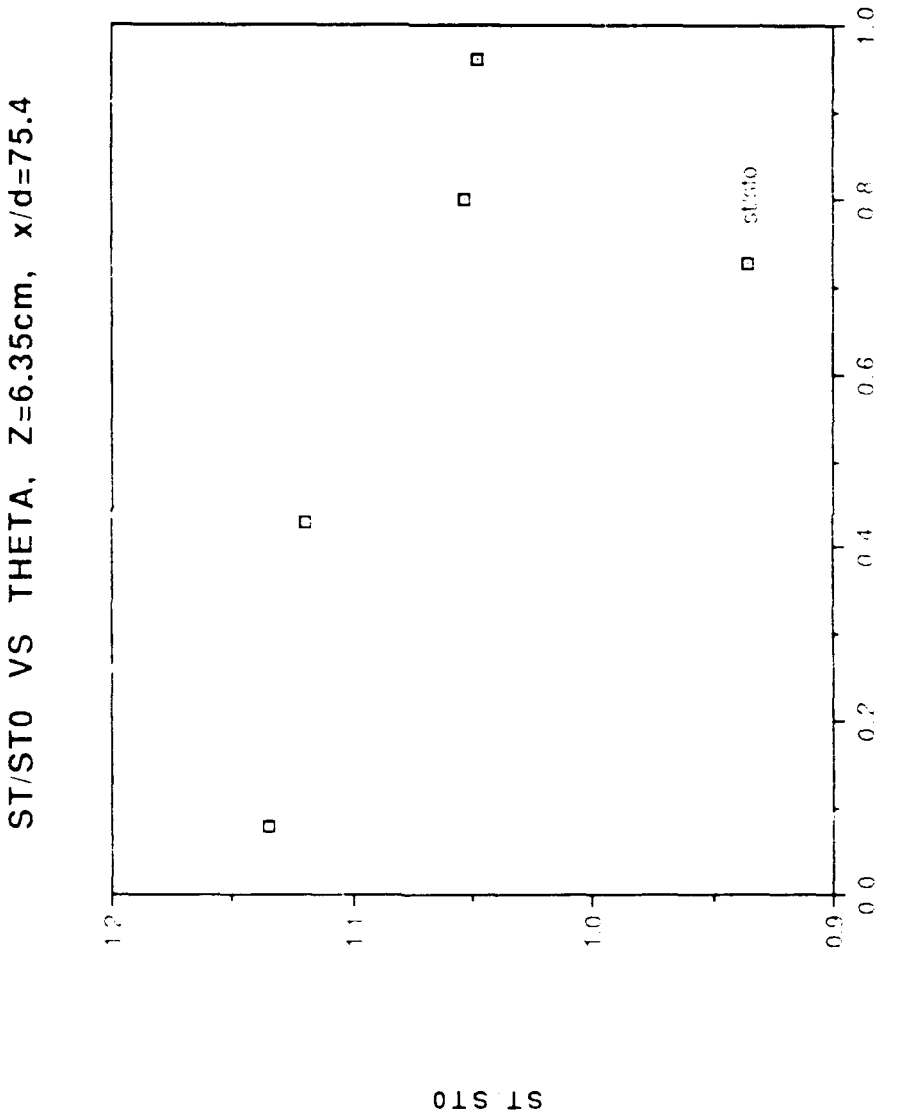

Figure 20. St/St_0 Versus θ , z=6.35 cm, x/d=75.4

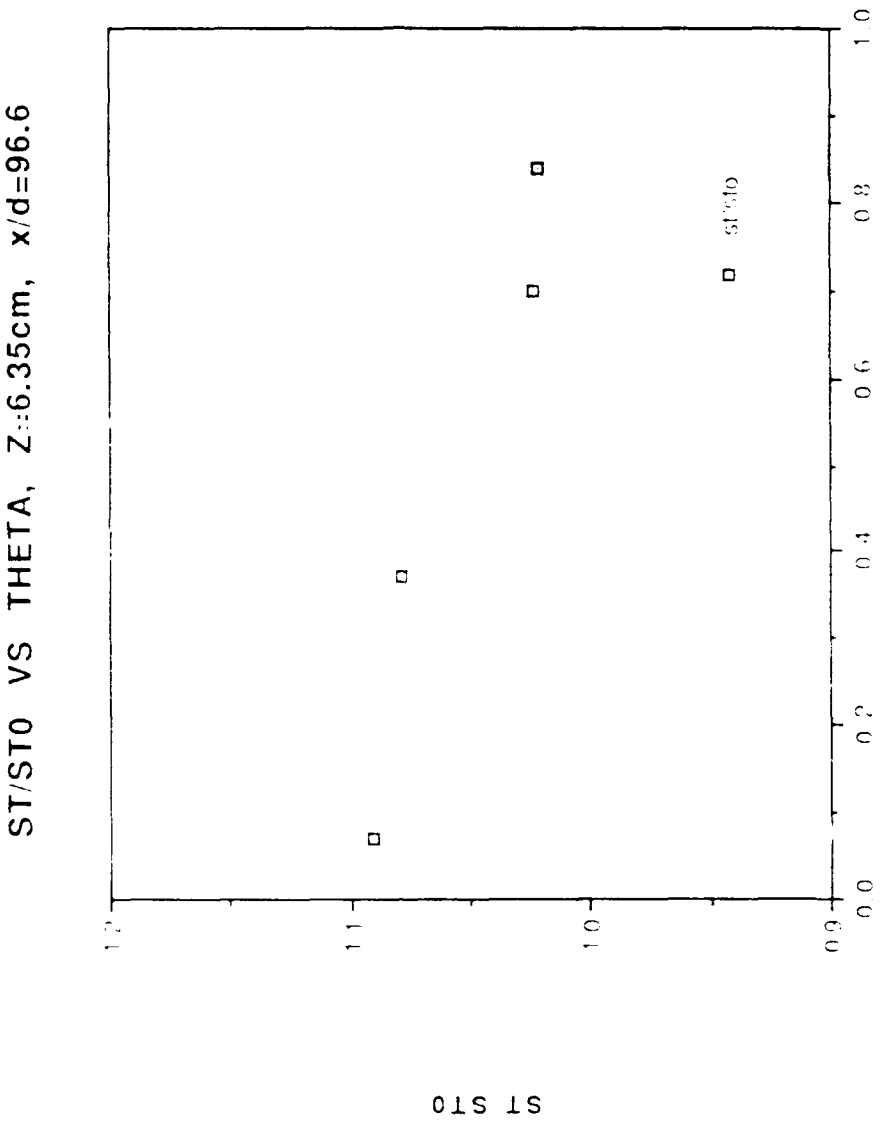

Figure 21. St/St_0 Versus θ , z=6.35 cm, x/d=96.6

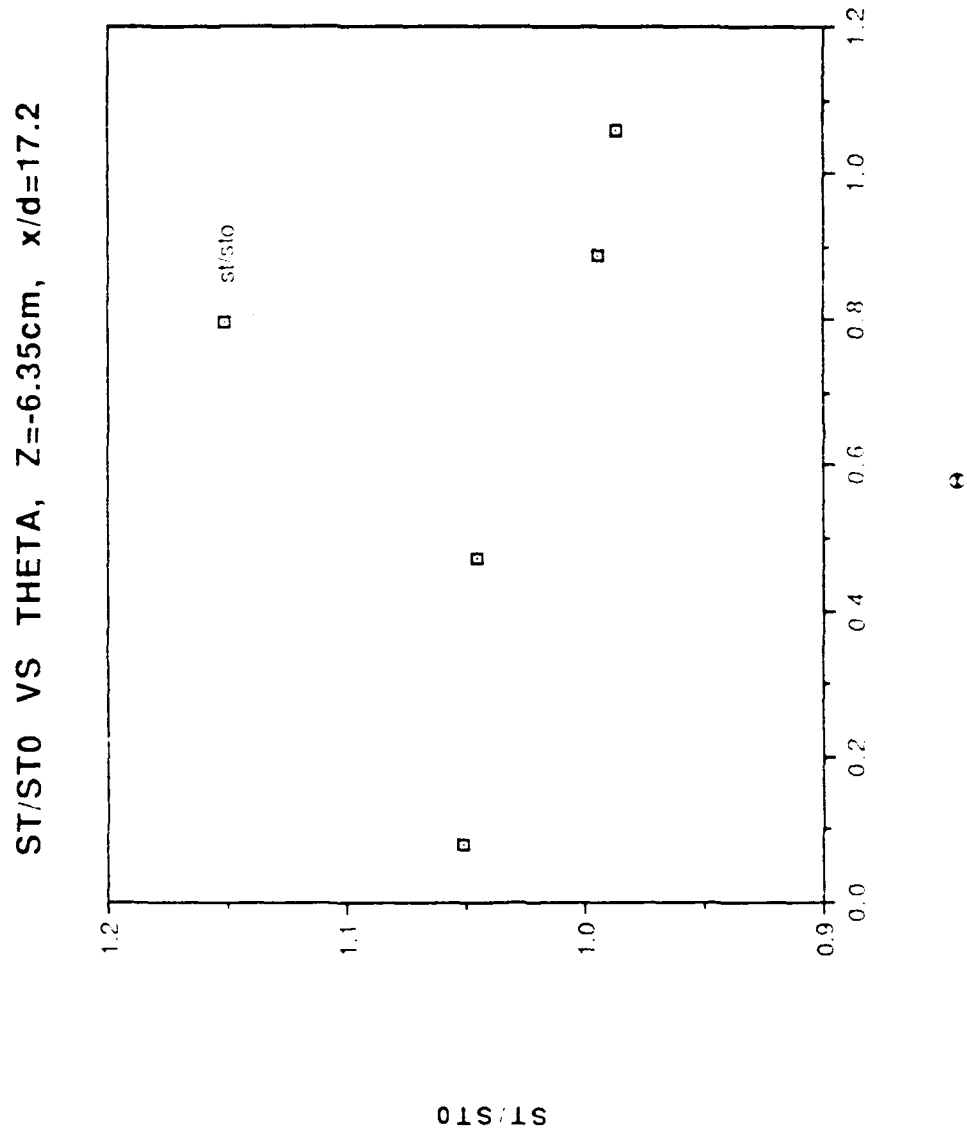

Figure 22. St/St_0 Versus θ , z=-6.35 cm, x/d=17.2

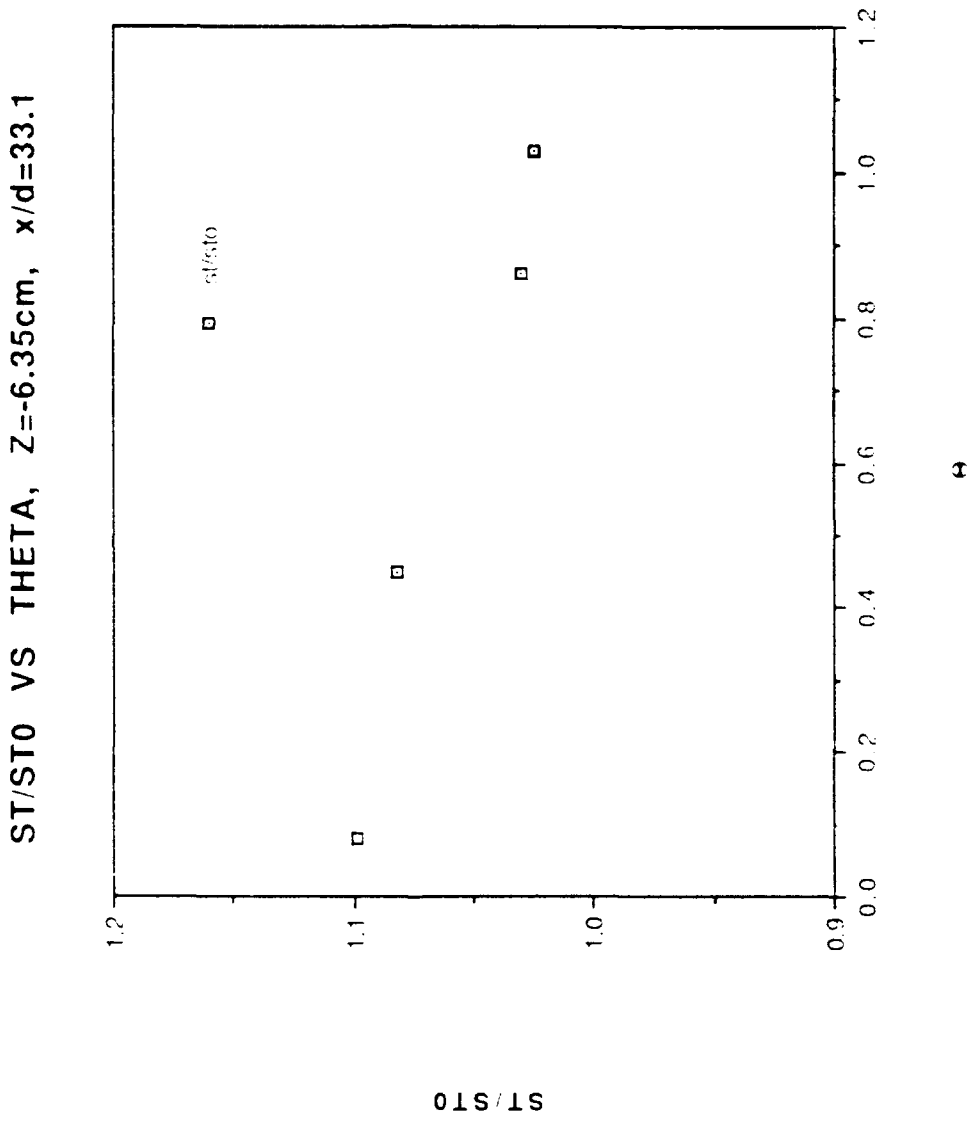

Figure 23. St/St_0 Versus θ , z=-6.35 cm, x/d=33.1

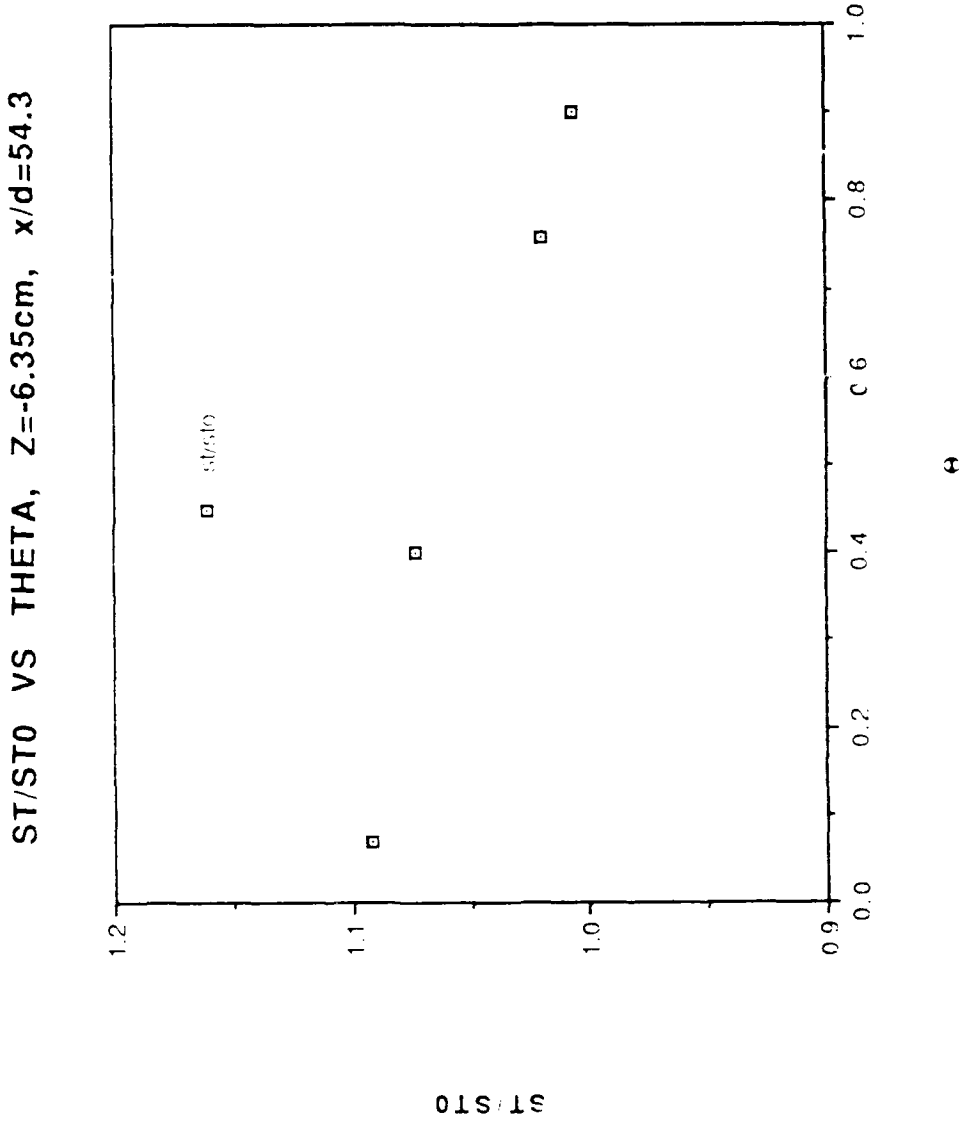

Figure 24. St/St_0 Versus θ z=-6.35 cm, x/d=54.3

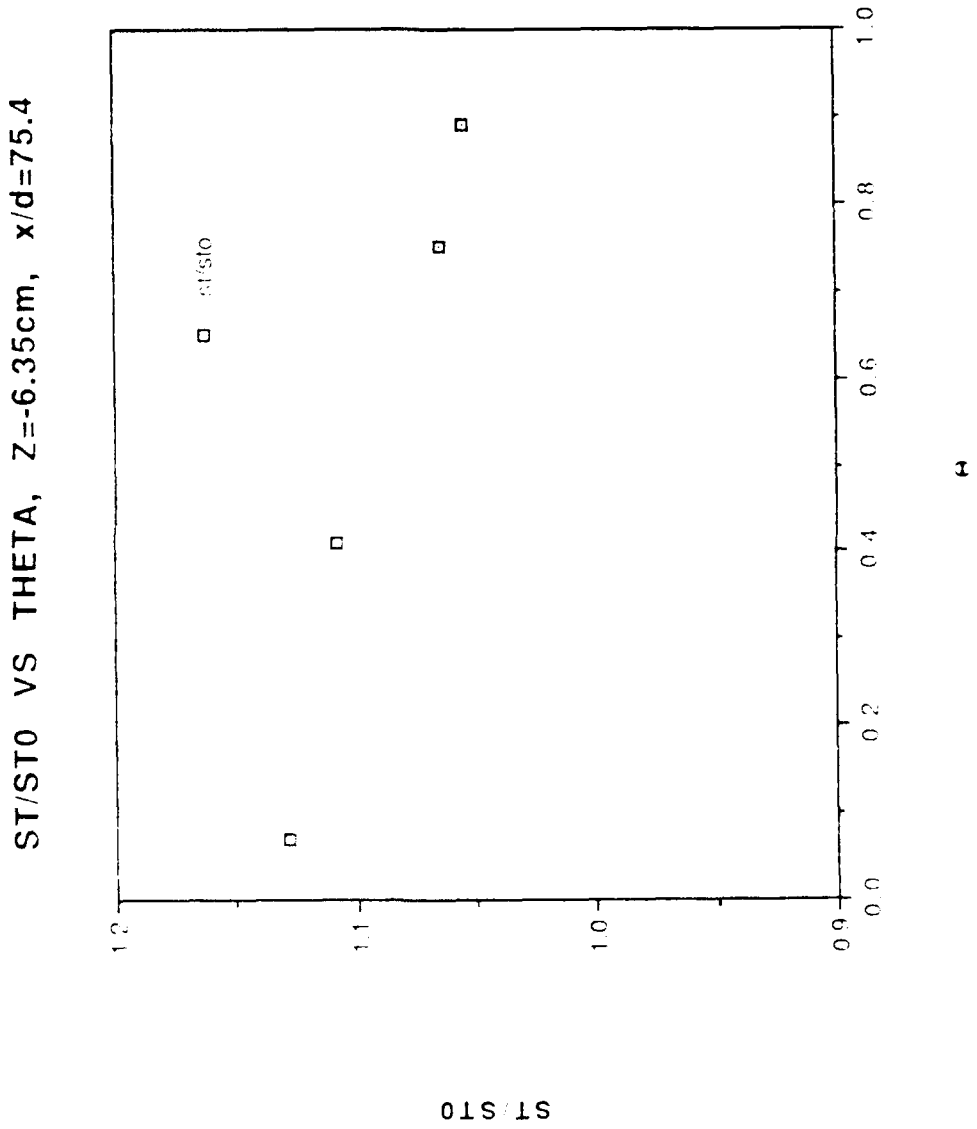

Figure 25. St/St_0 Versus θ , z=-6.35 cm, x/d=75.4

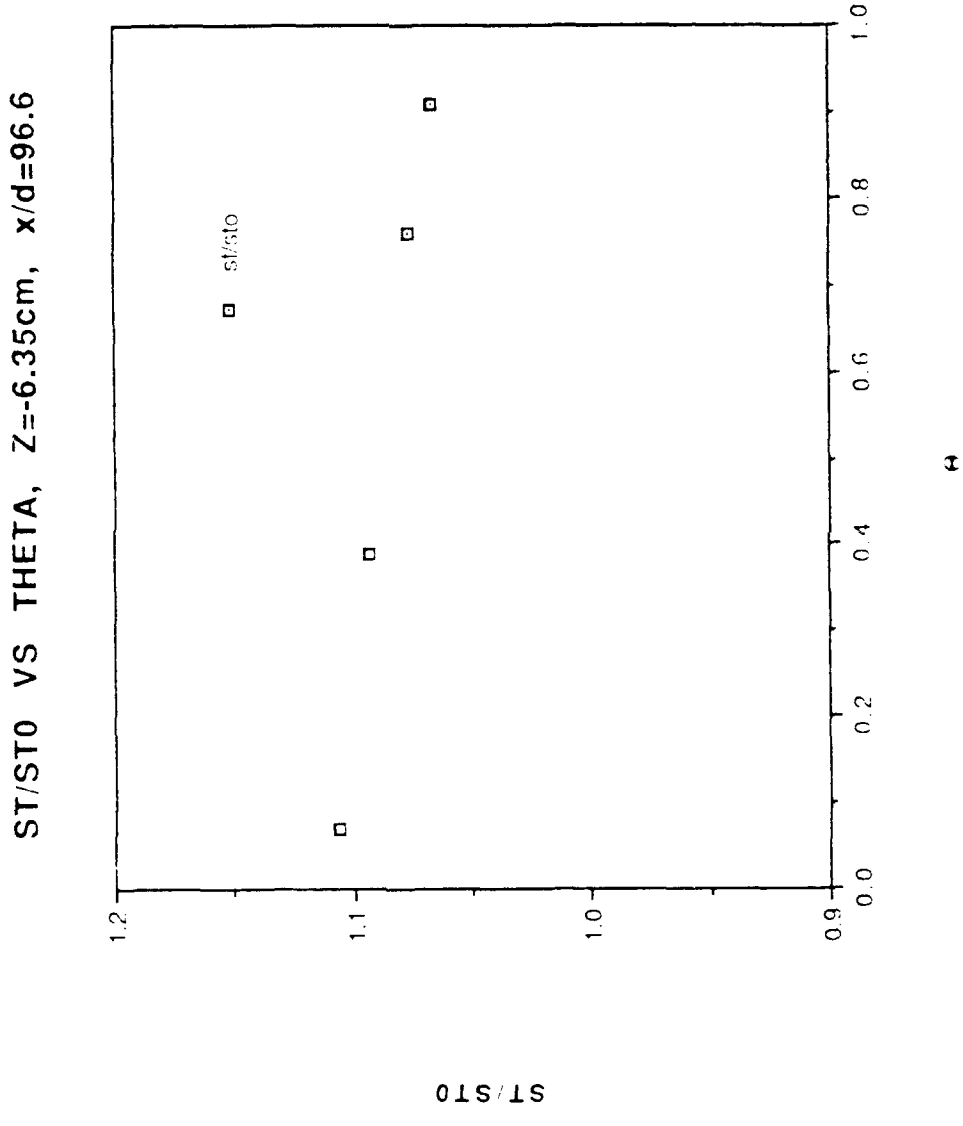

Figure 26. St/St_0 Versus θ , z=-6.35 cm, x/d=96.6

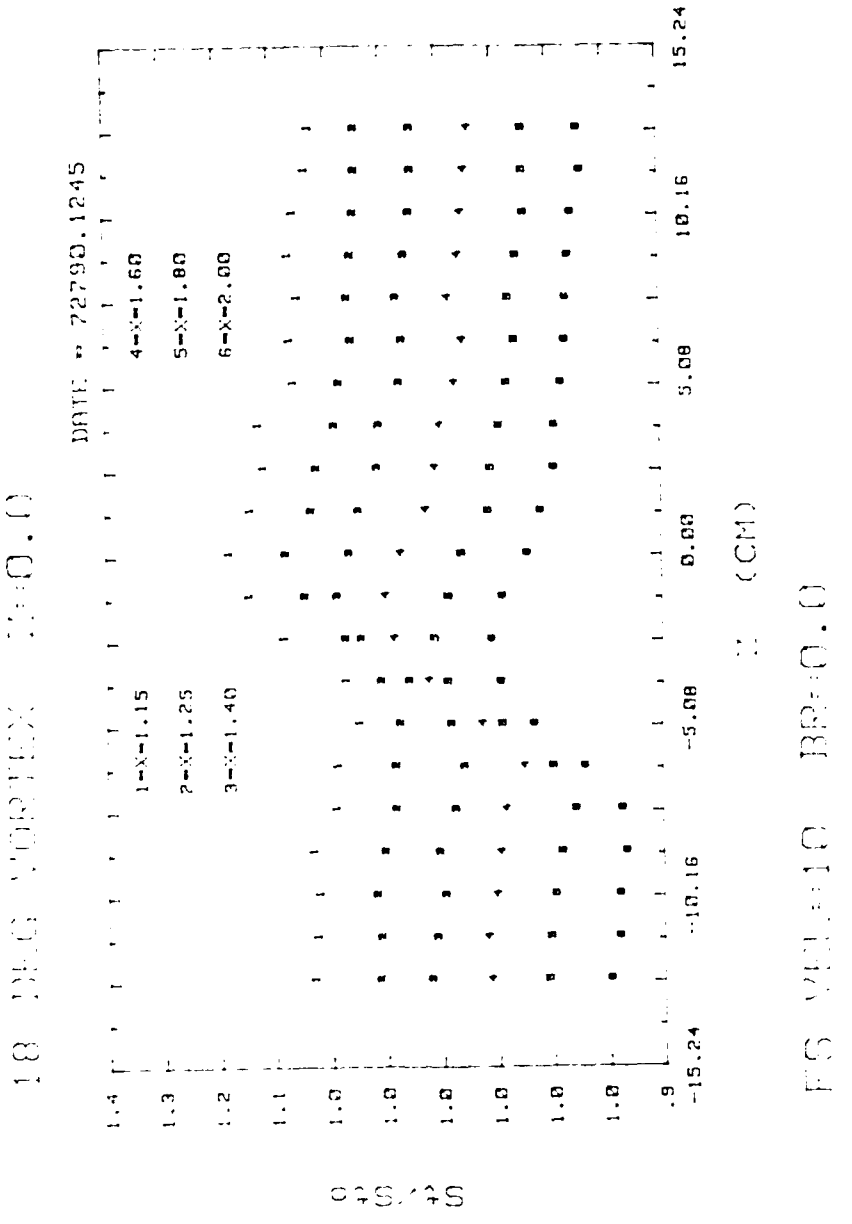

Figure 27. Local St/St_0 Distribution with No Film Cooling, Vortex R0

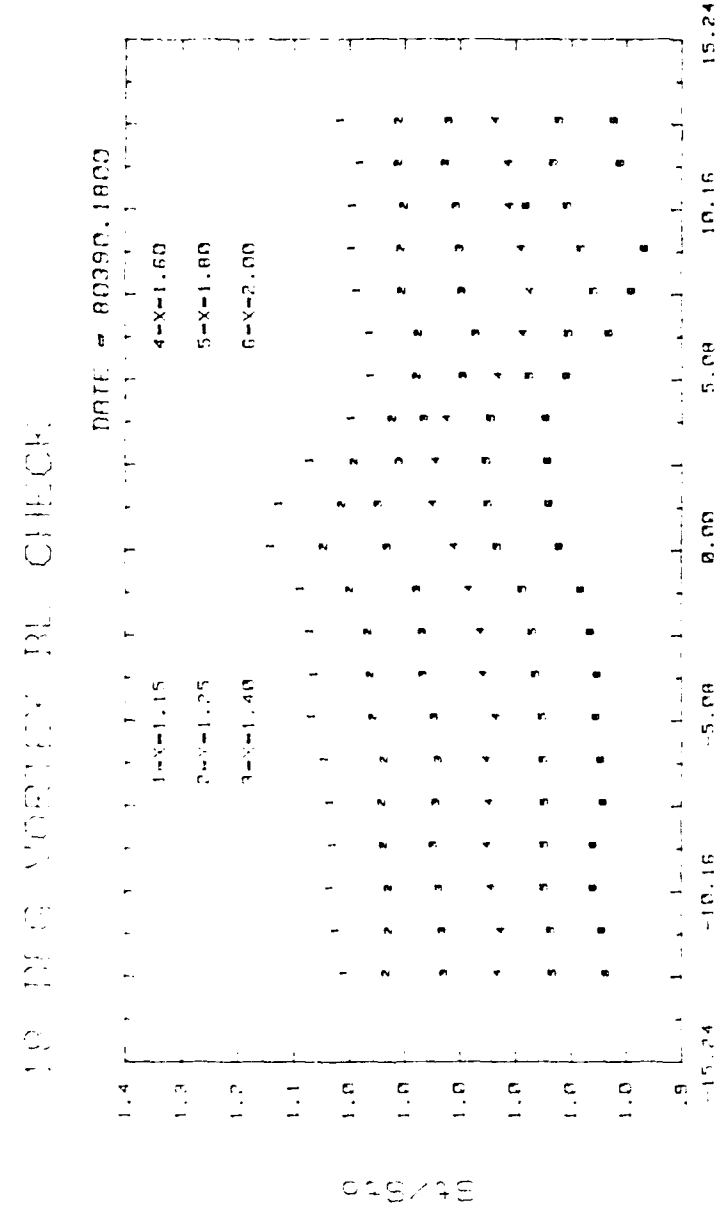

Figure 28. Local St/St_0 Distribution with No Film Cooling, Vortex L0

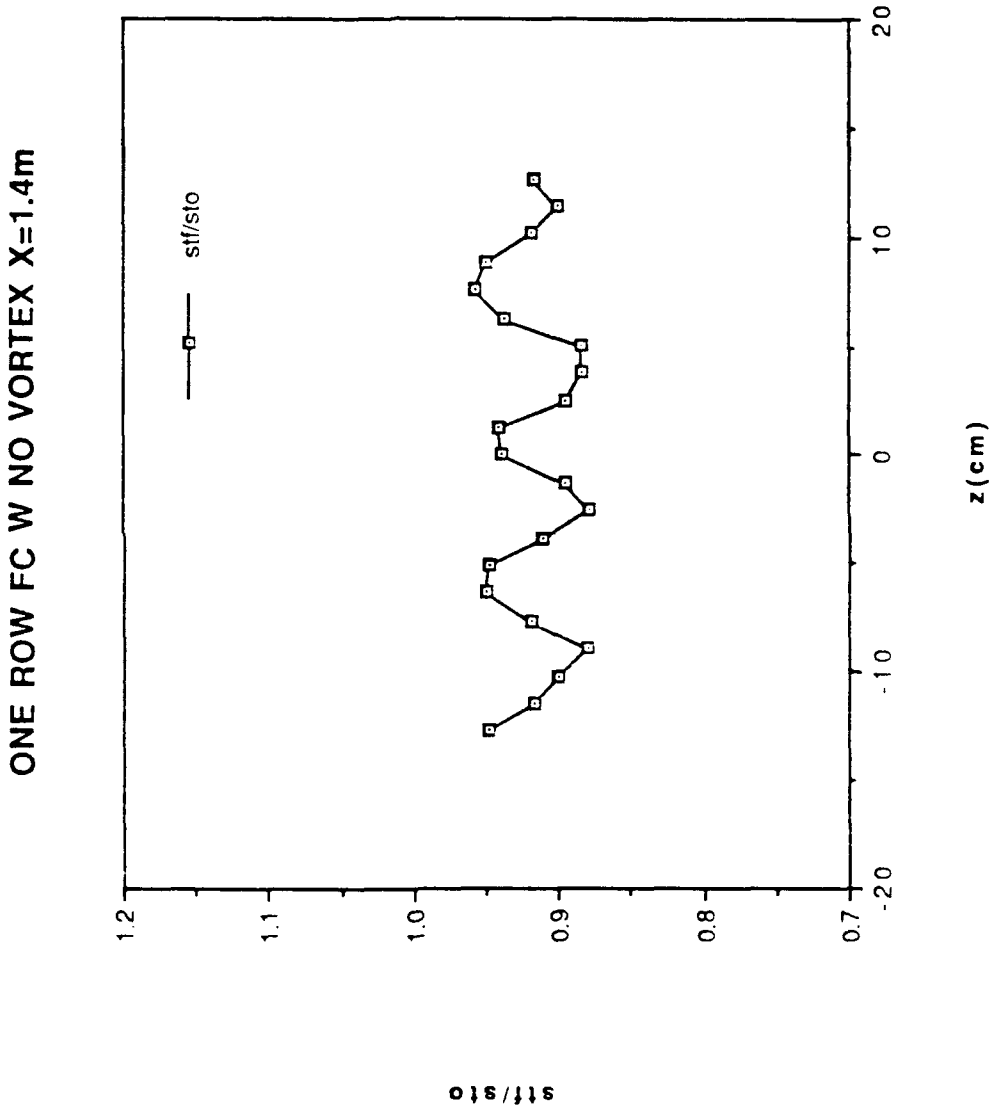

Figure 29. Spanwise Variation of St/St_0 Ratios, m=0.5, One Row of Holes, No Vortex, X=1.4m

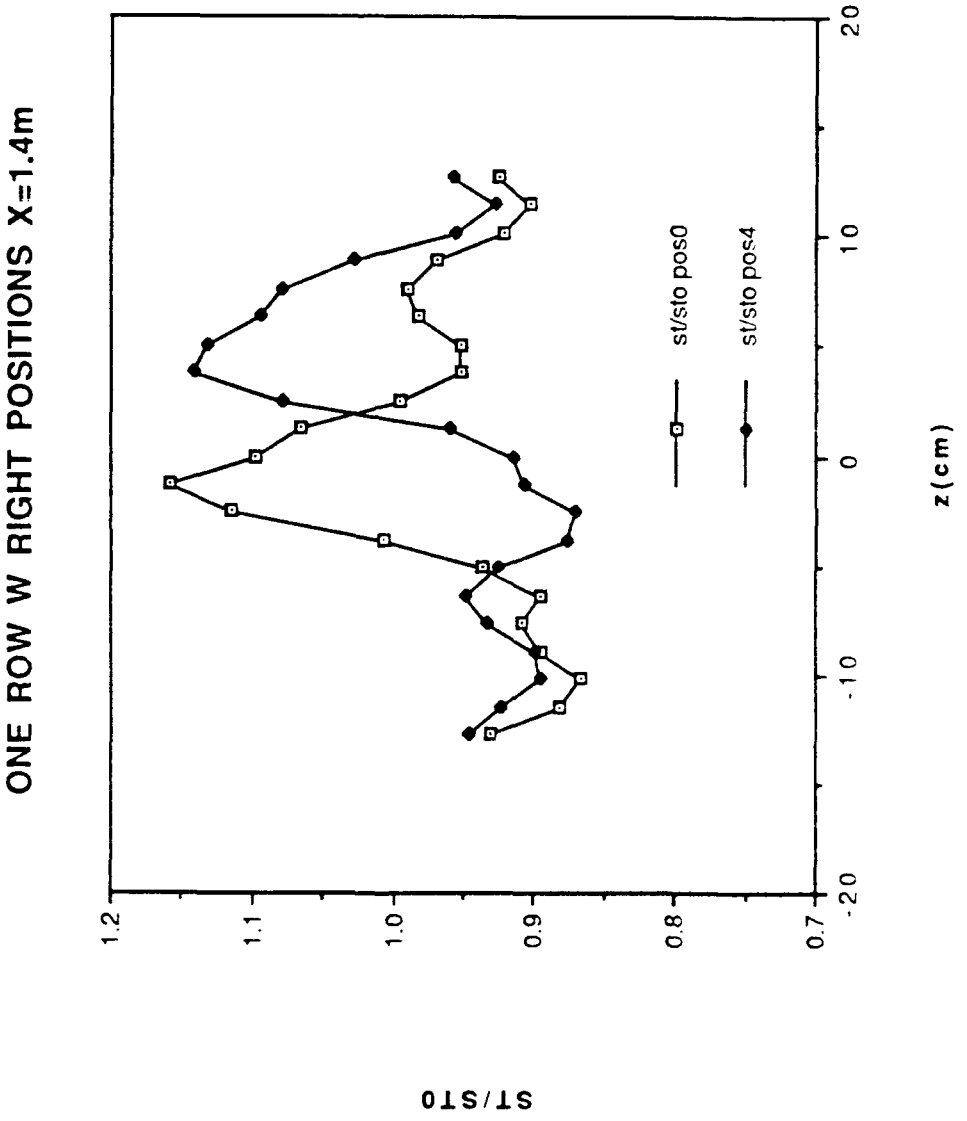

Figure 30. Spanwise Variation of St/St_0 Ratios, m=0.5, One Row of Holes, Vortex Positions R0 and R4, X=1.4m

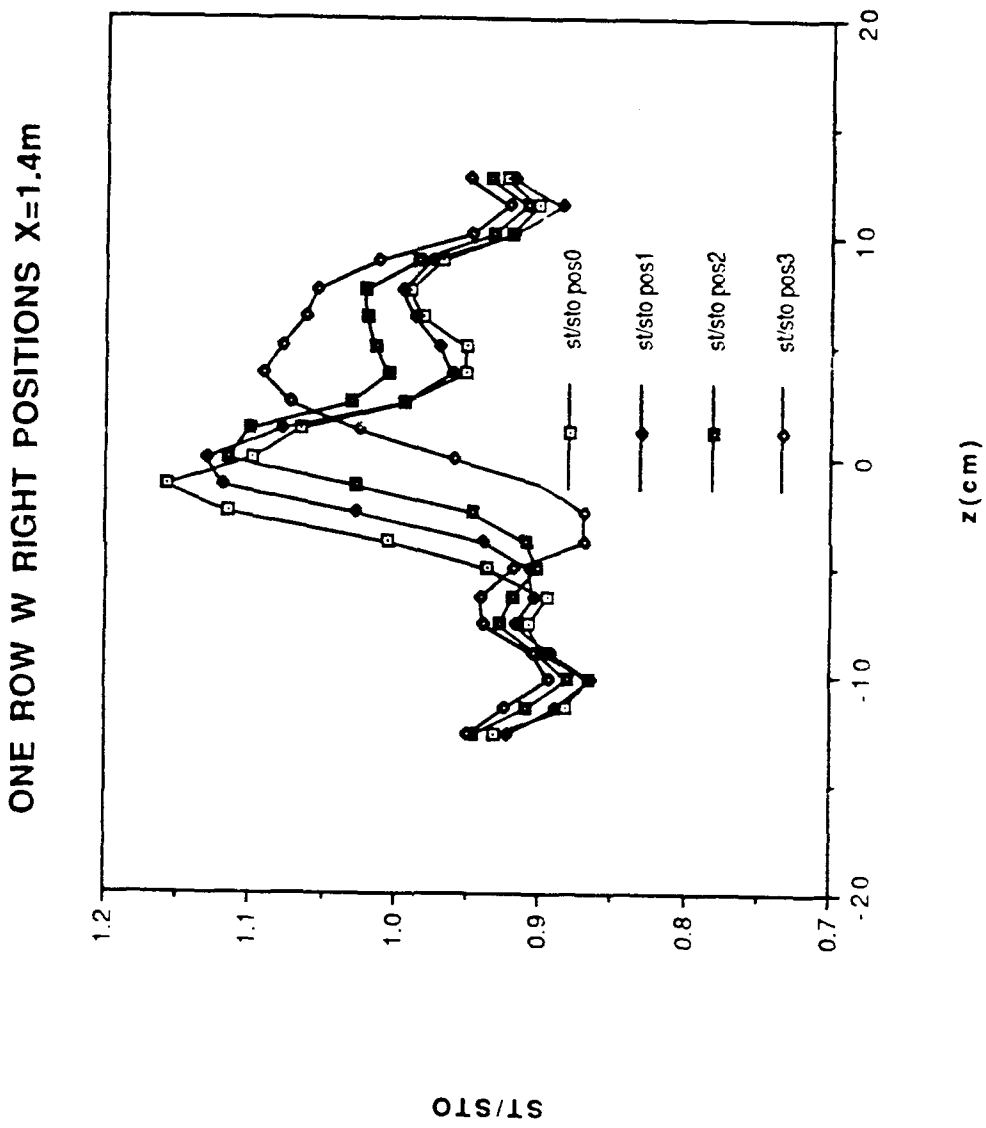

Figure 31. Spanwise Variation of St/St_0 Ratios, m=0.5, One Row of Holes, Vortex Positions R0 through R3, X=1.4m

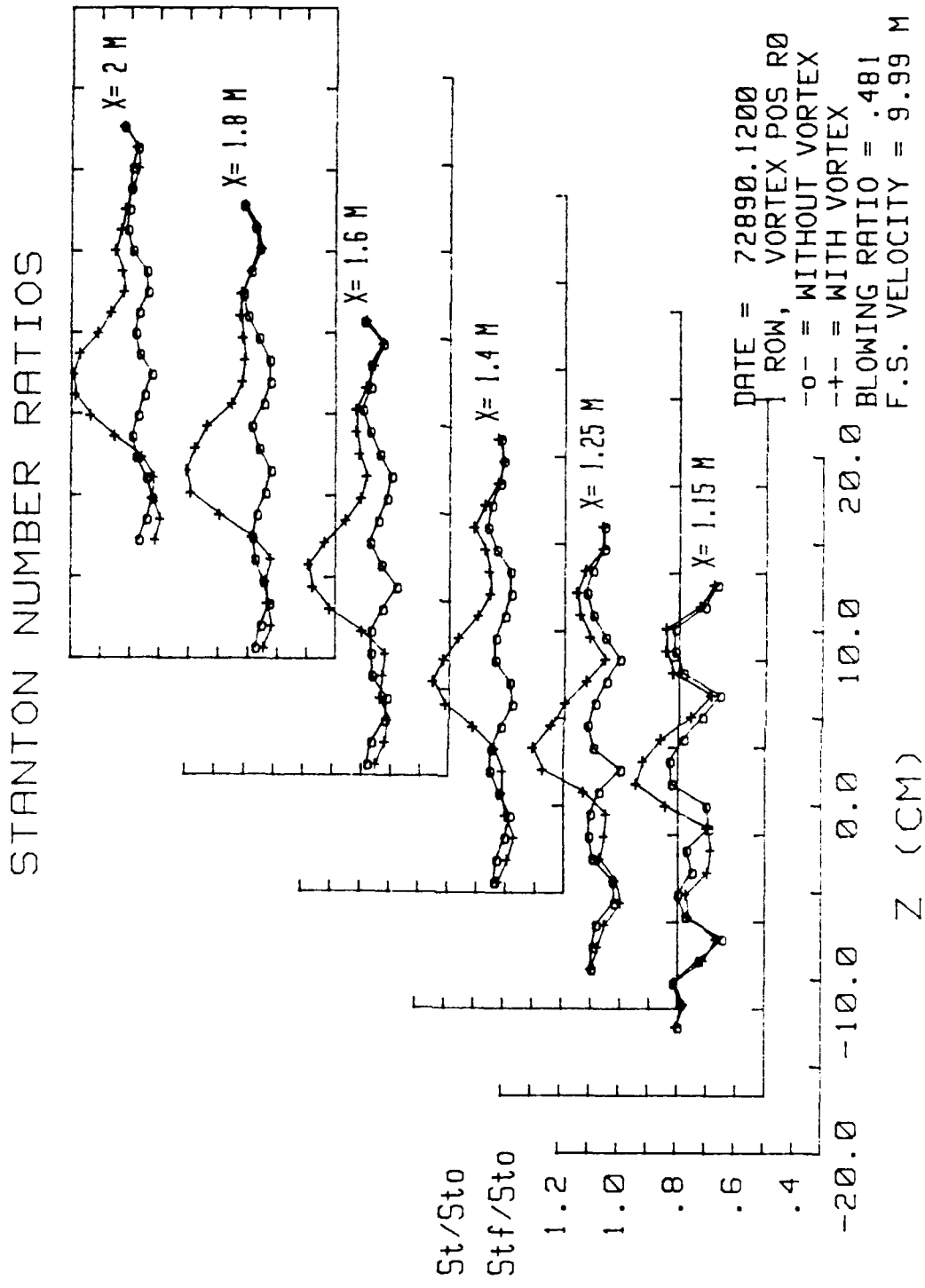

Figure 32. Spanwise Variation of St/St_0 and St_f/St_0 Ratios, m=0.5, One Row of Holes, Vortex Position R0

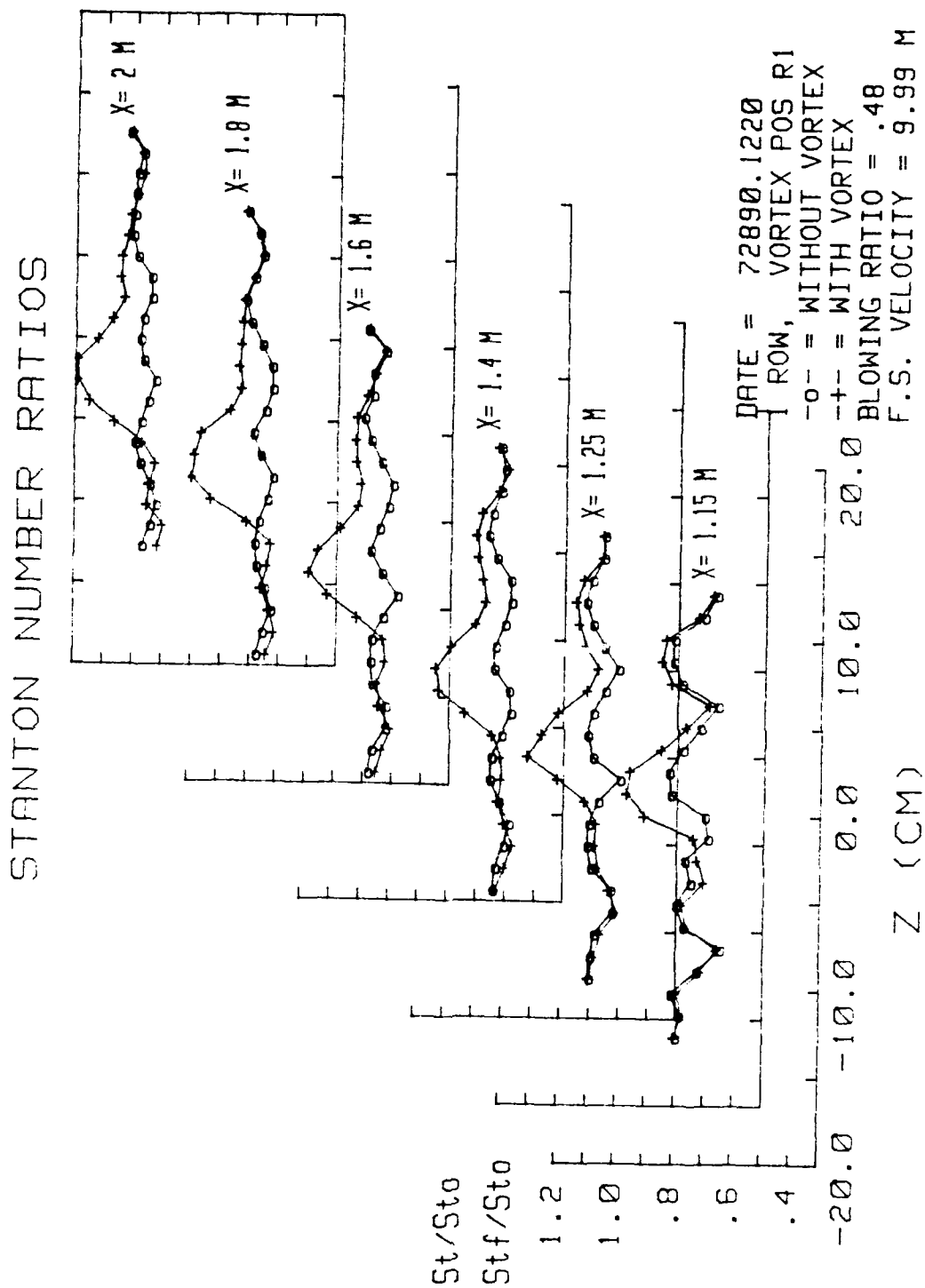

Figure 33. Spanwise Variation of St/St_0 and St_f/St_0 Ratios, m=0.5, One Row of Holes, Vortex Position R1

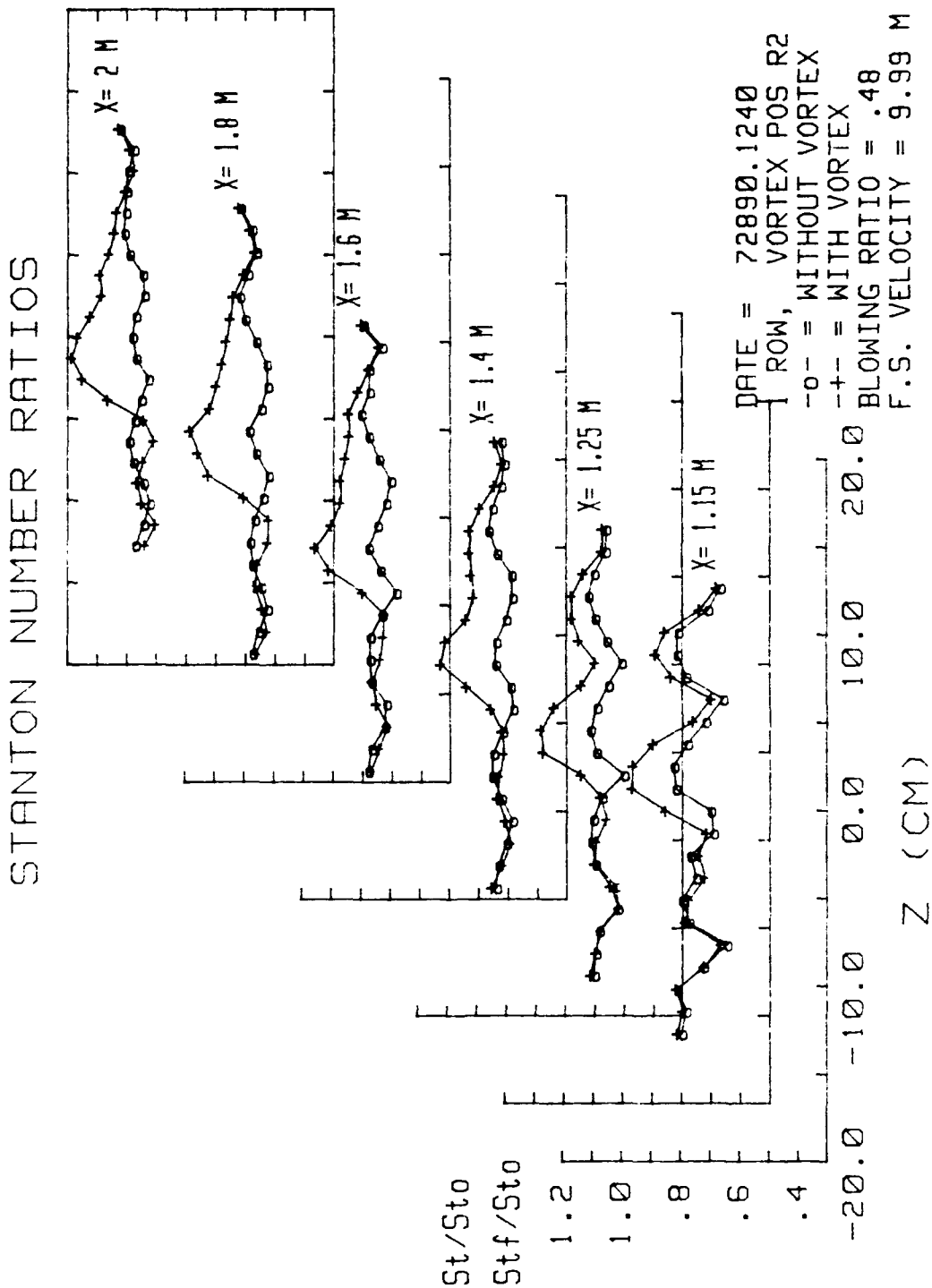

Figure 34. Spanwise Variation of St/St_0 and St_f/St_0 Ratios, m=0.5, One Row of Holes, Vortex Position R2

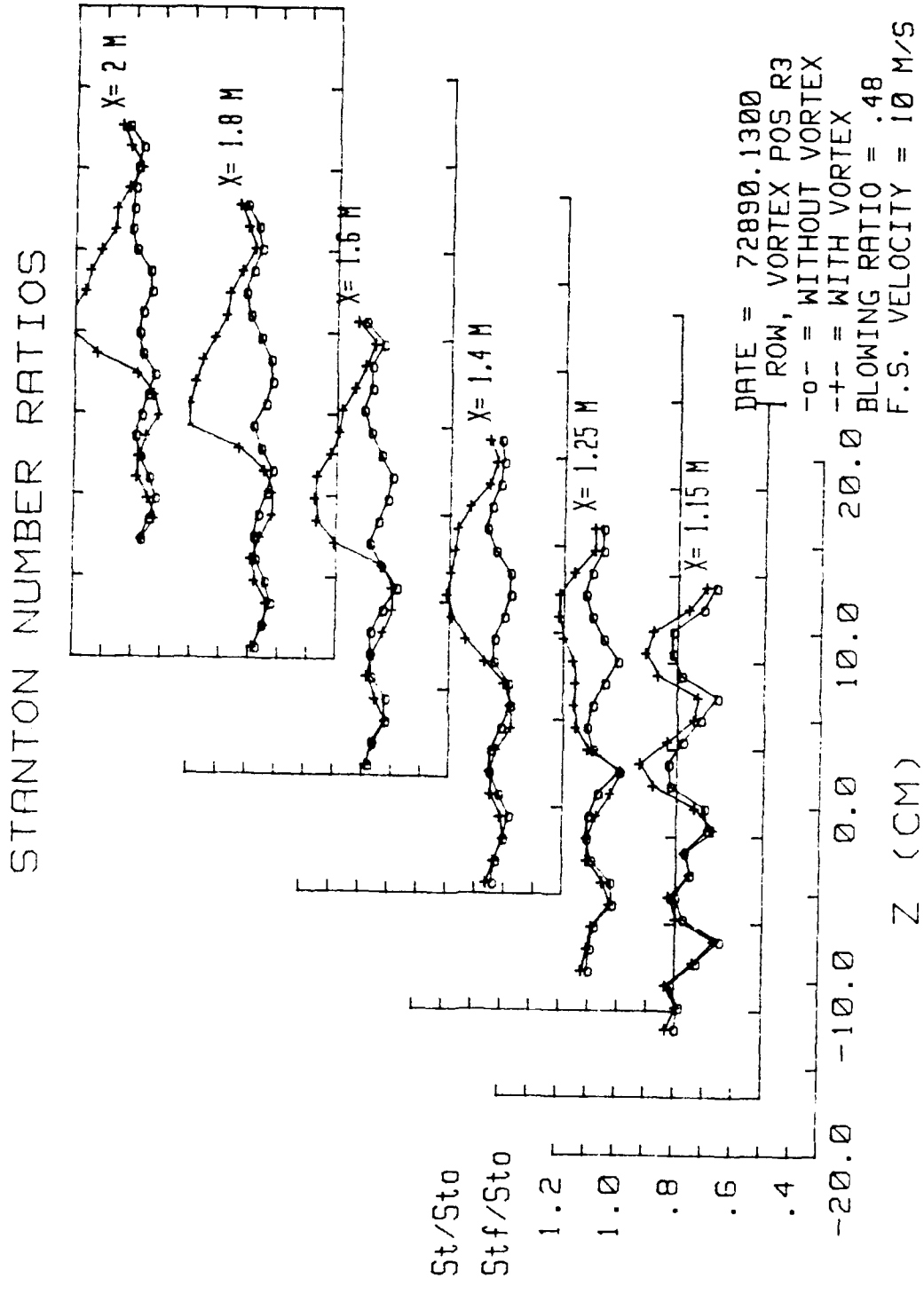

Figure 35. Spanwise Variation of St/St_0 and St_f/St_0 Ratios, m=0.5, One Row of Holes, Vortex Position R3

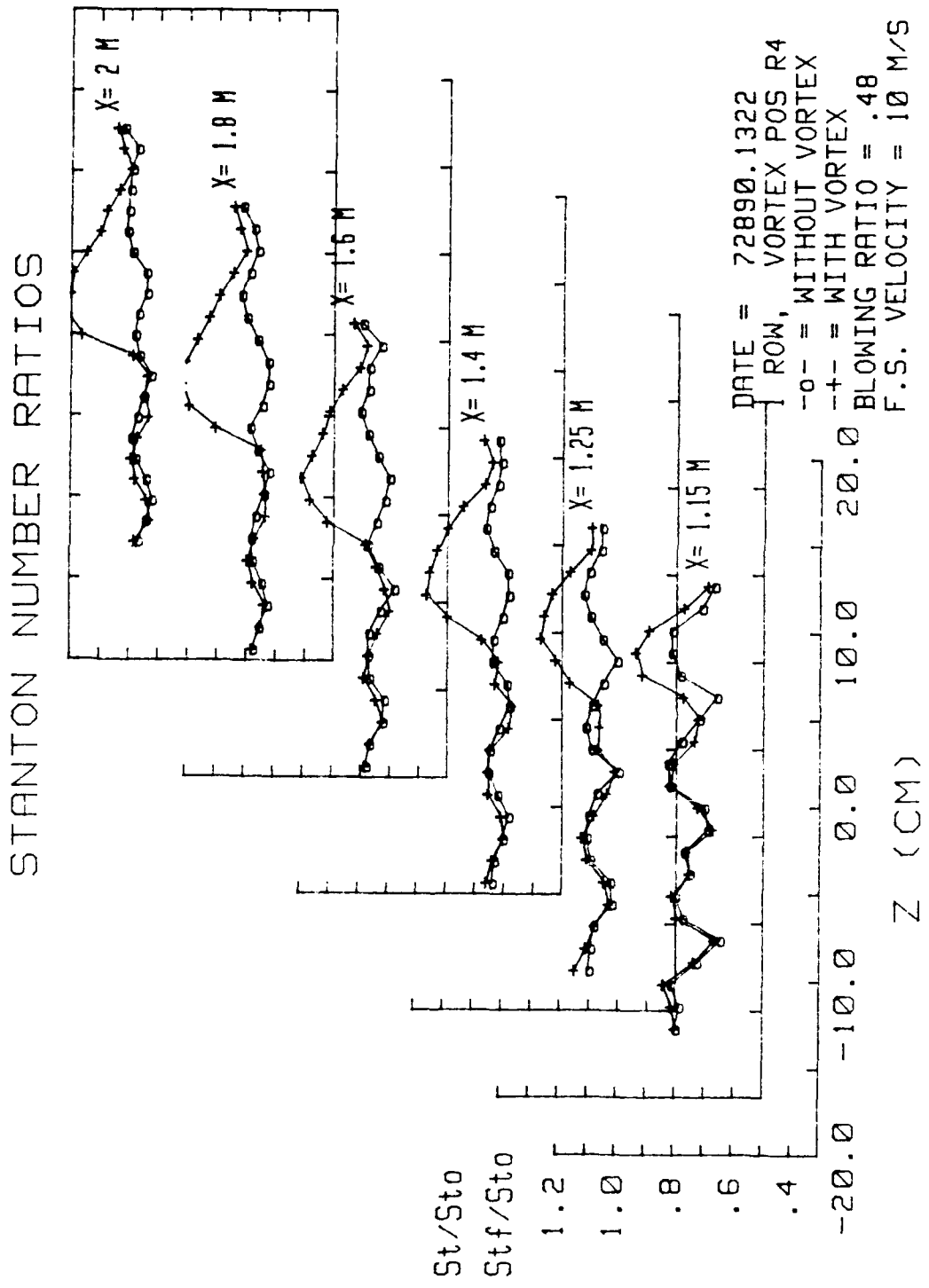

Figure 36. Spanwise Variation of St/St_0 and St_f/St_0 Ratios, m=0.5, One Row of Holes, Vortex Position R4

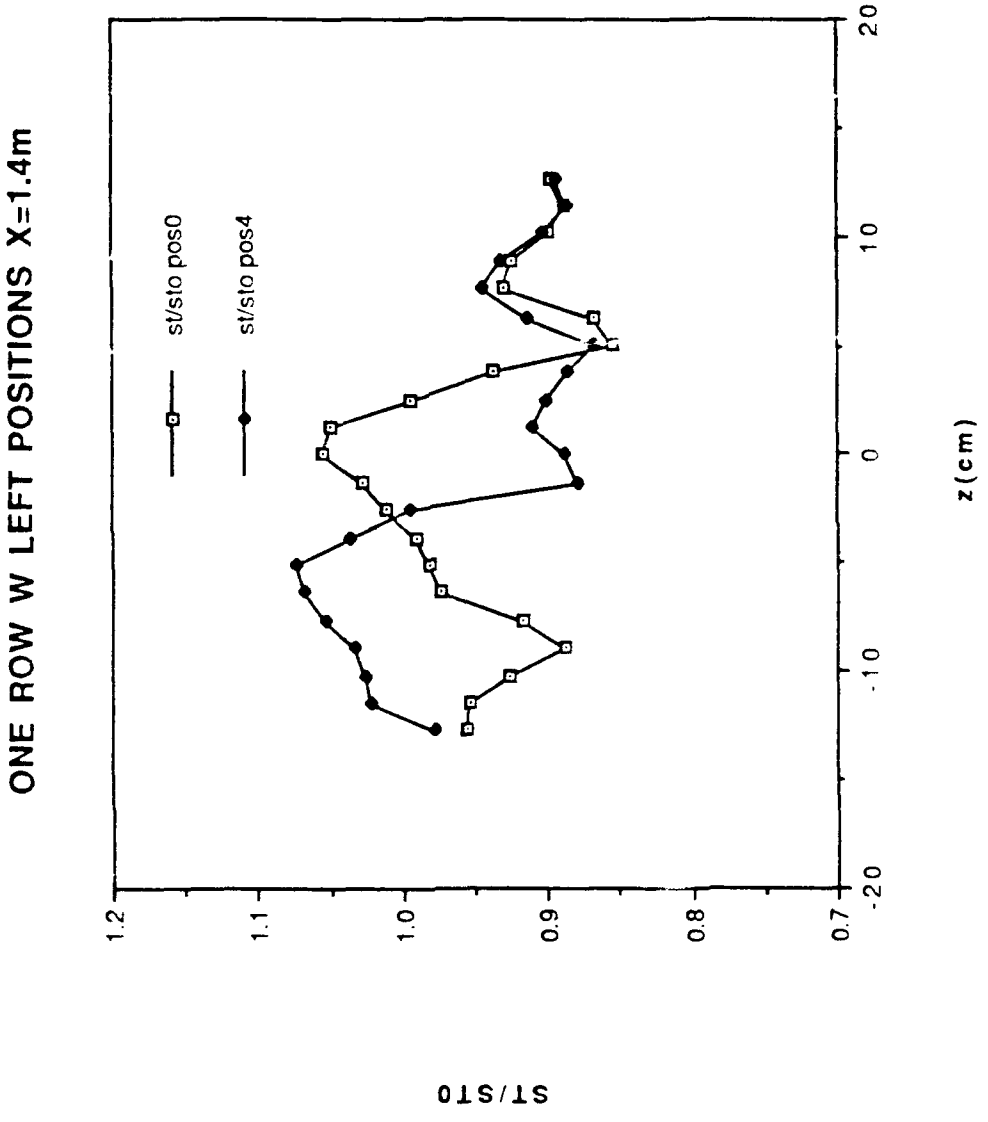

Figure 37. Spanwise Variation of St/St_0 Ratios, m=0.5, One Row of Holes, Vortex Positions L0 and L4, X=1.4m

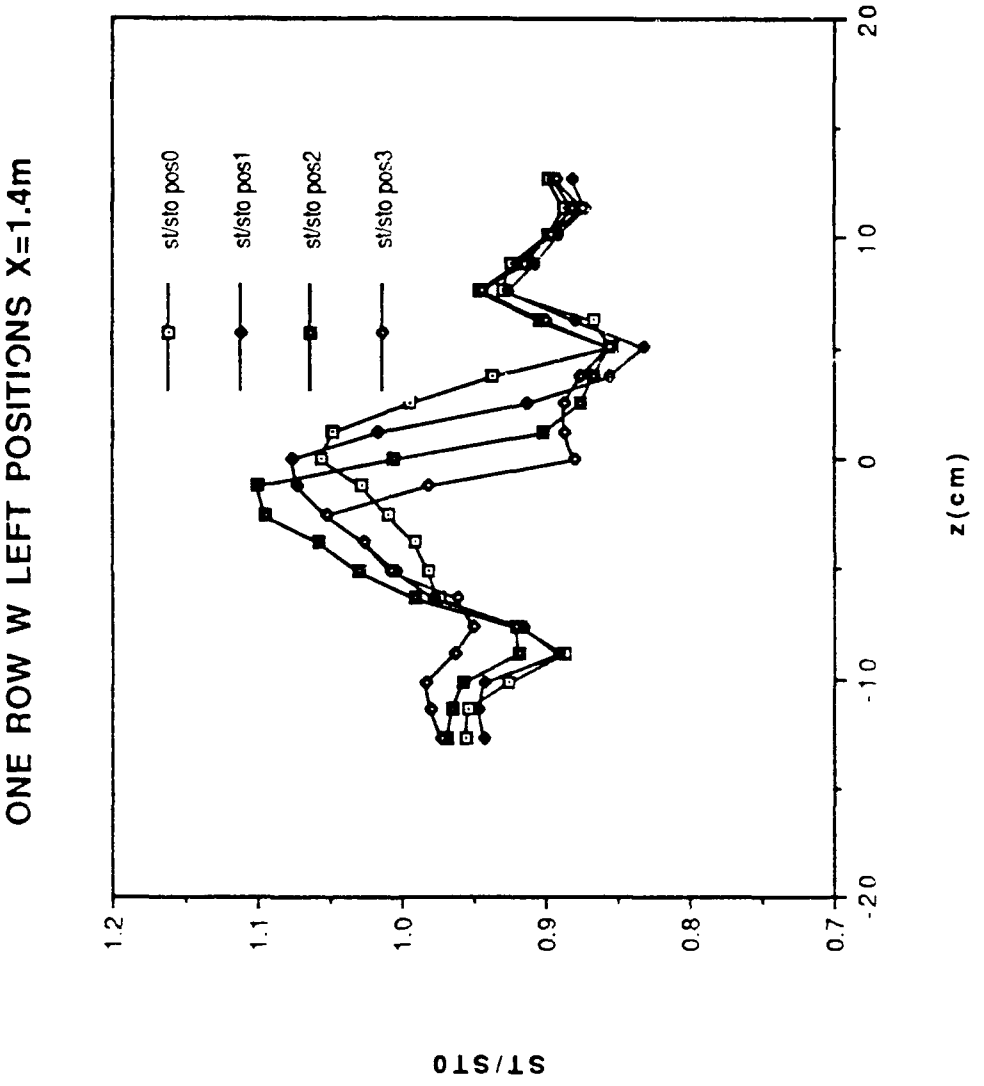

Figure 38. Spanwise Variation of St/St_0 Ratios, m=0.5, One Row of Holes, Vortex Positions L0 through L3

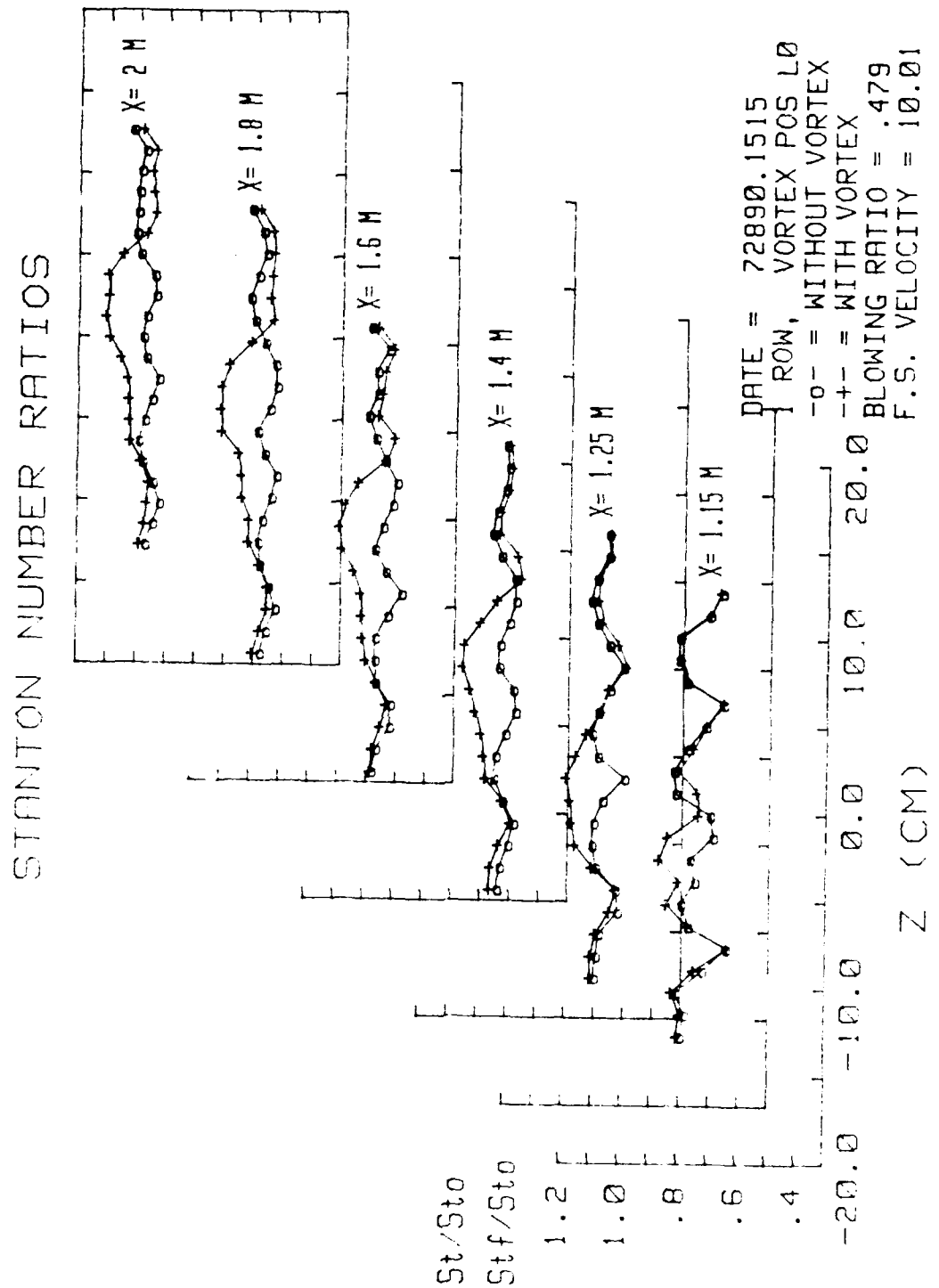

Figure 39. Spanwise Variation of St/St_o and St_f/St_o Ratios, m=0.5, One Row of Holes, Vortex Position L0

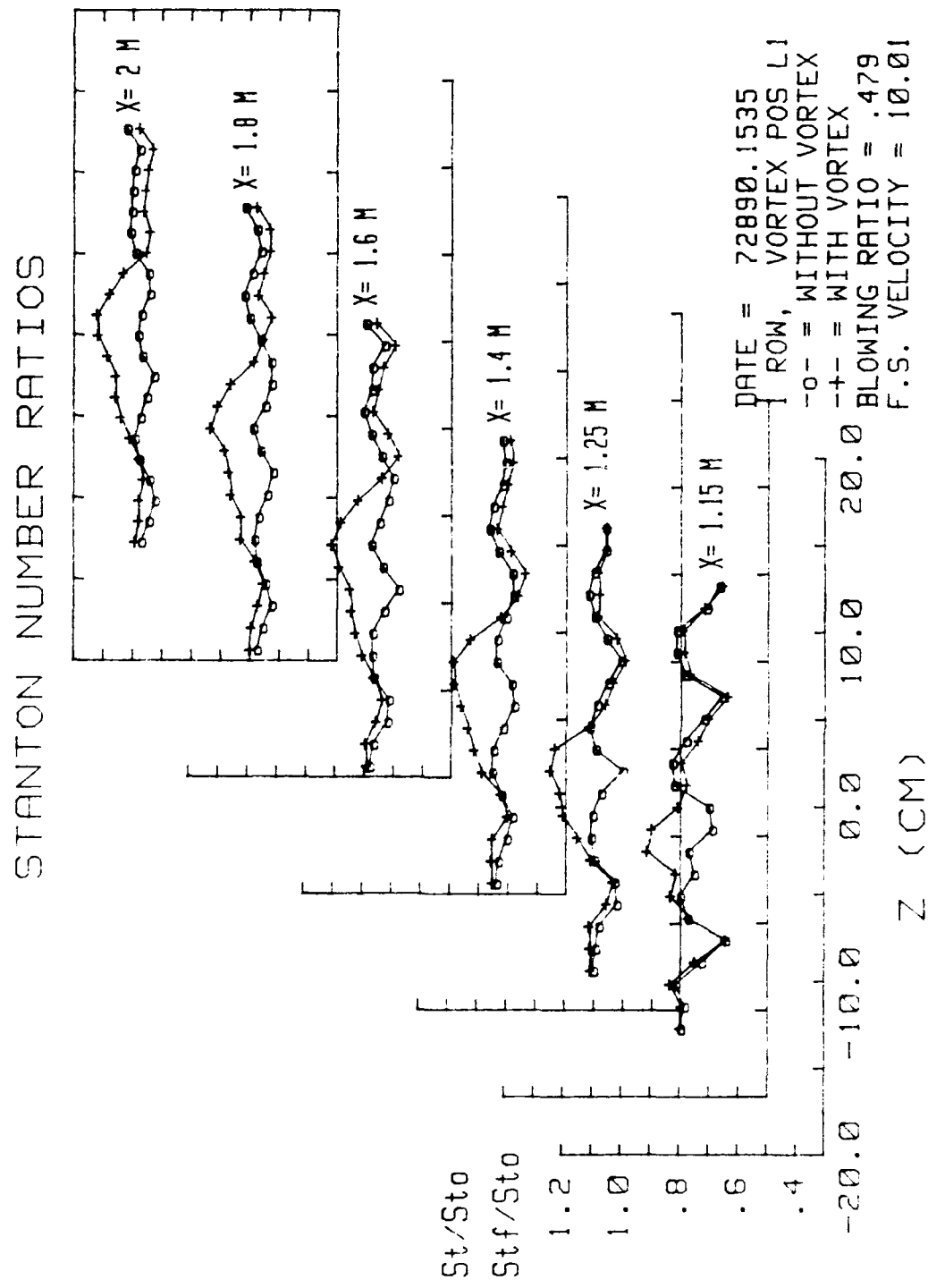

Figure 40. Spanwise Variation of St/St_0 and St_f/St_0 Ratios, m=0.5, One Row of Holes, Vortex Position L1

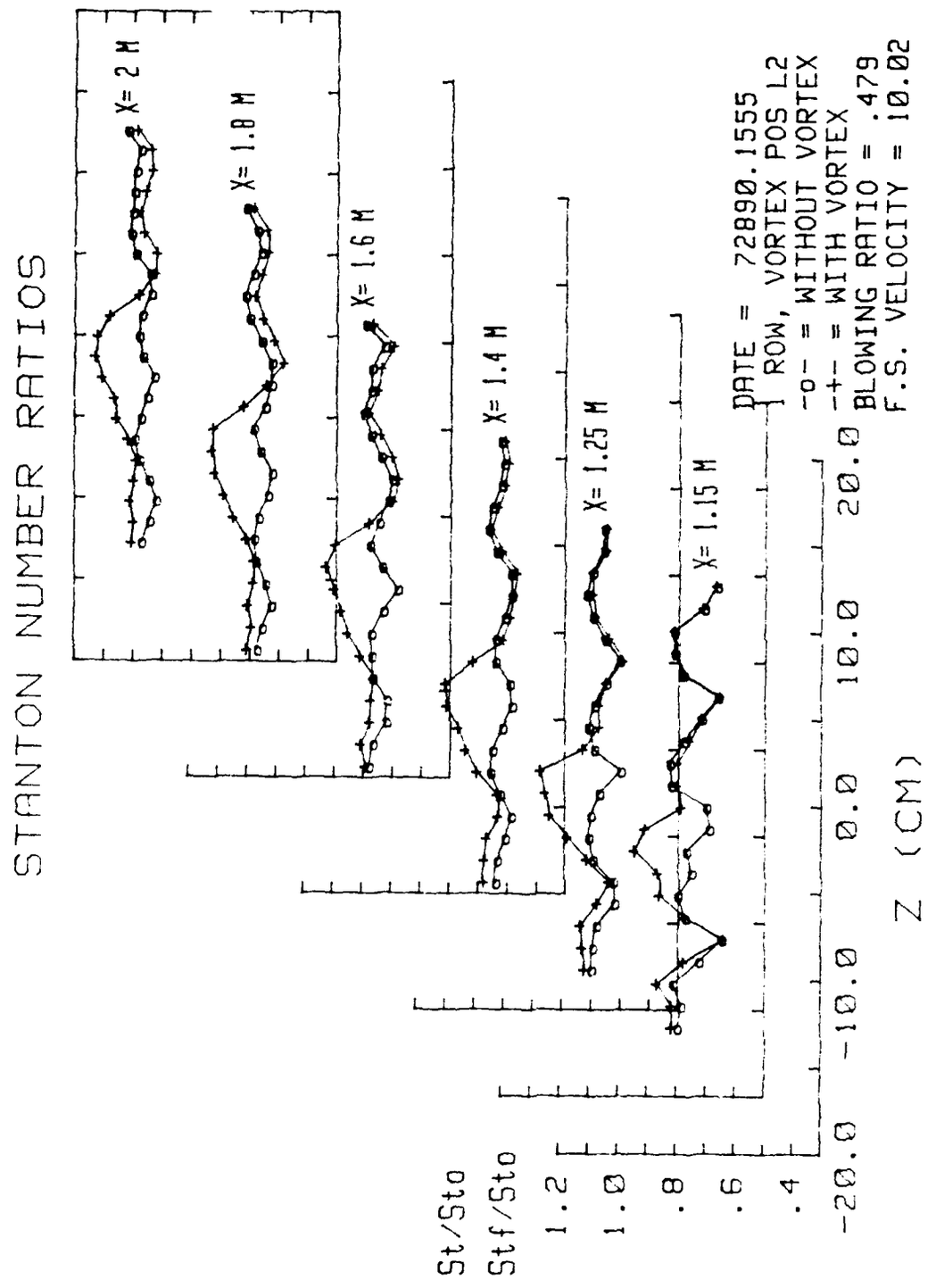

Figure 41. Spanwise Variation of St/St_0 and St_f/St_0 Ratios, m=0.5, One Row of Holes, Vortex Position L2

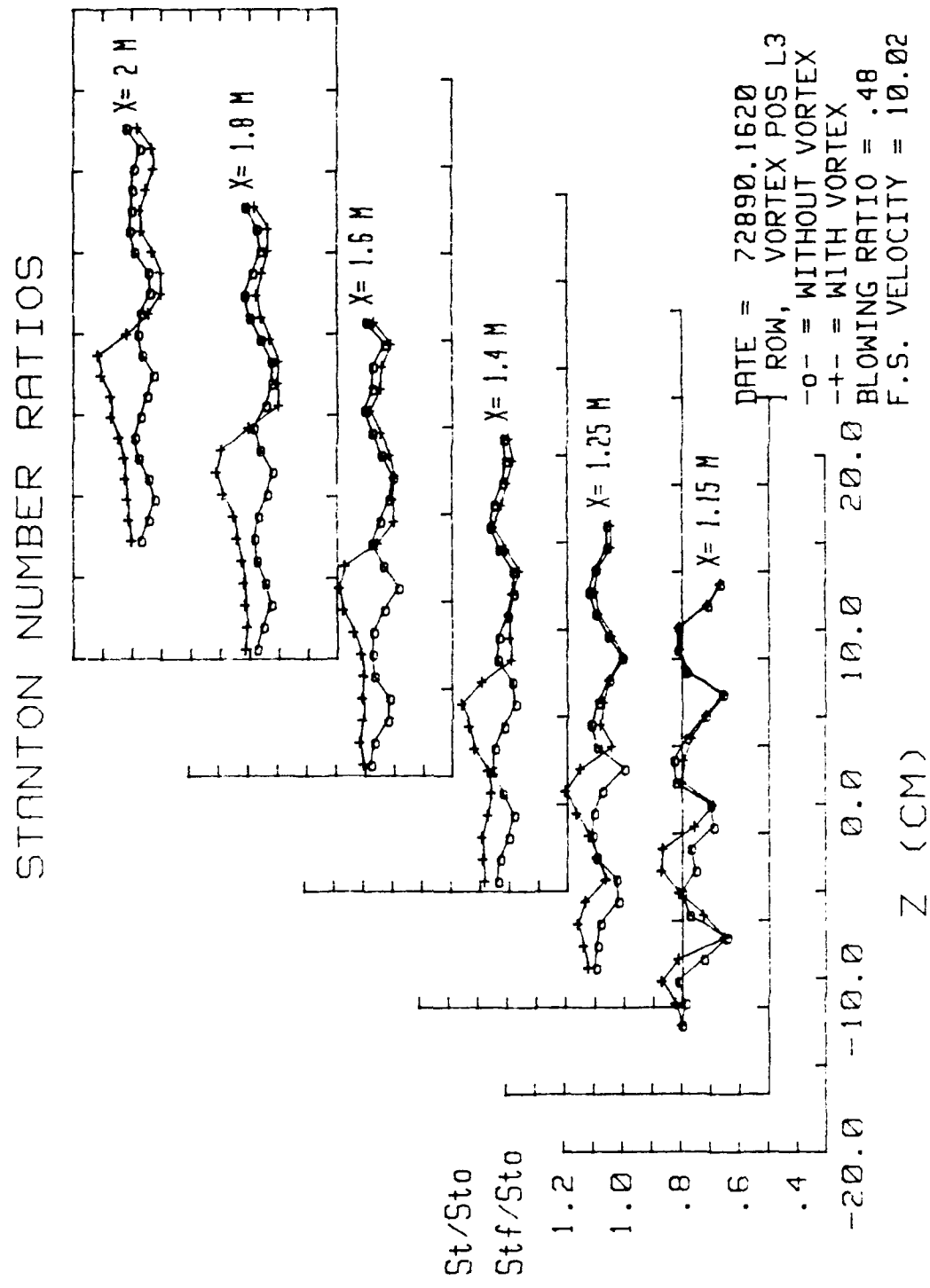

Figure 42. Spanwise Variation of St/St_0 and St_f/St_0 Ratios, m=0.5, One Row of Holes, Vortex Position L3

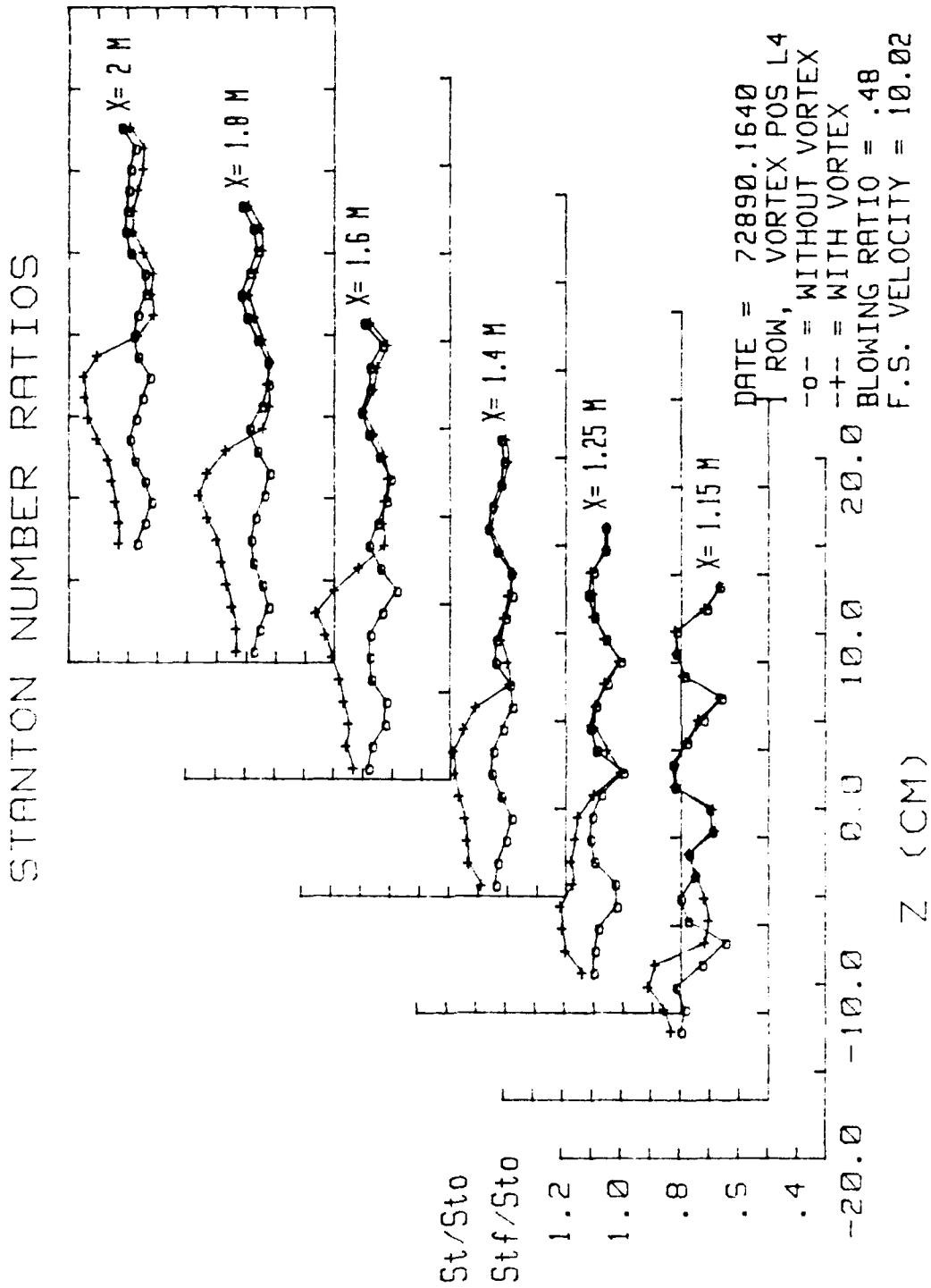

Figure 43. Spanwise Variation of St/St_0 and St_f/St_0 Ratios, m=0.5, One Row of Holes, Vortex Position L4

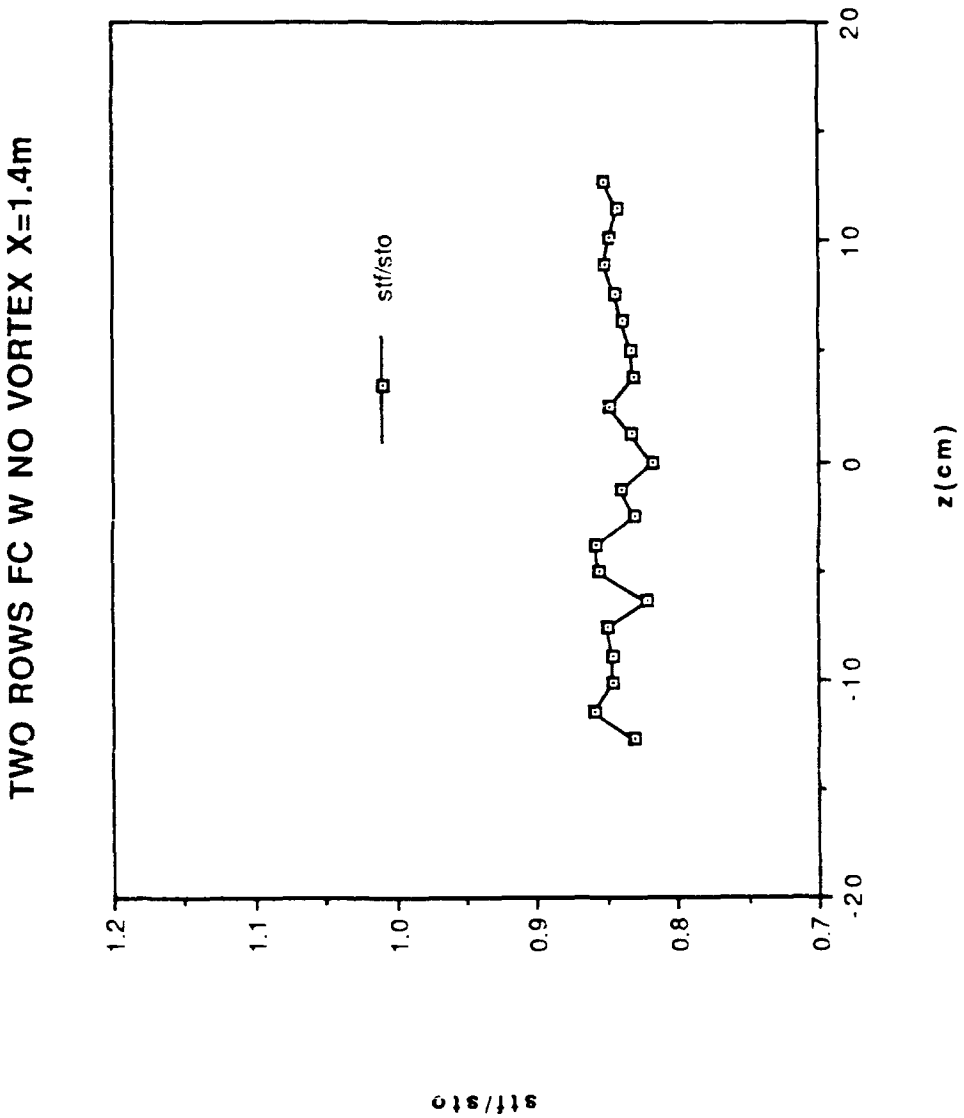

Figure 44. Spanwise Variation of St/St_0 Ratios, m=0.5, Two Rows of Holes, No Vortex , X=1.4m

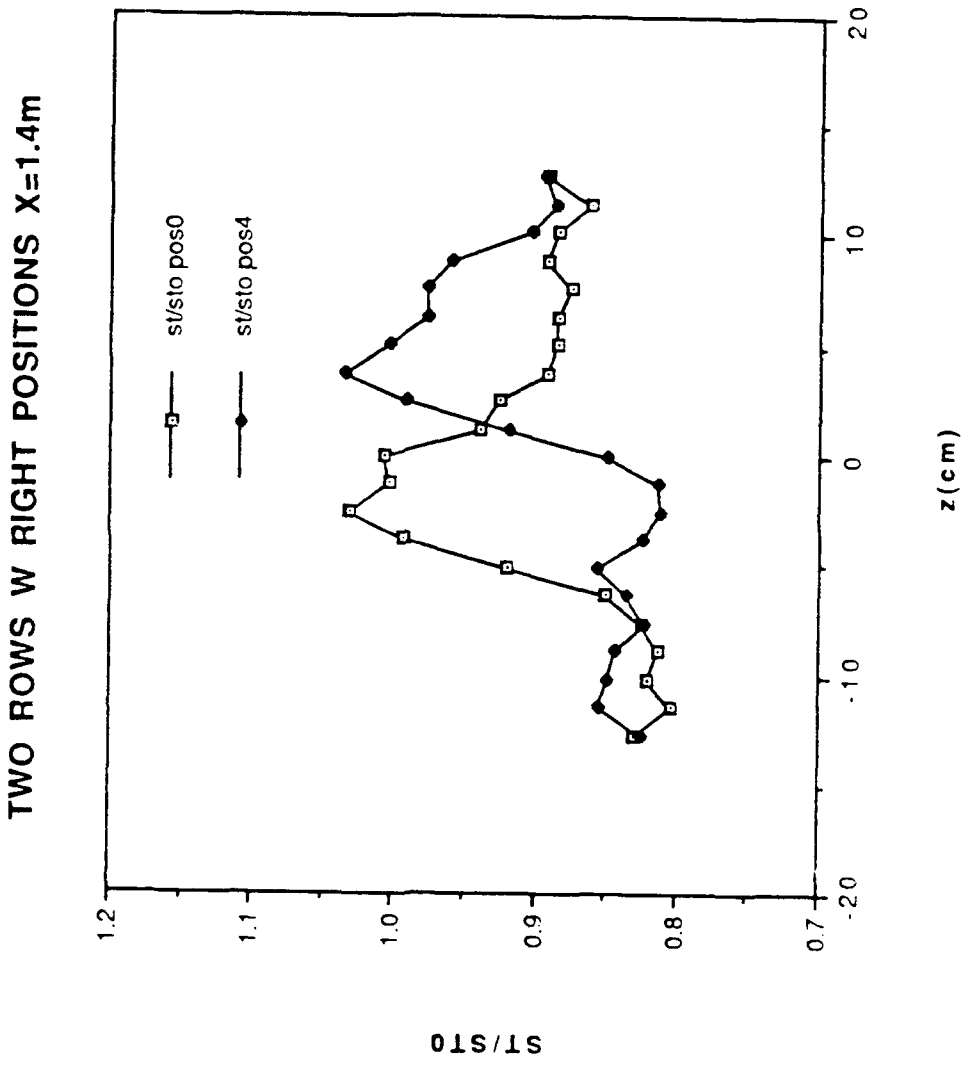

Figure 45. Spanwise Variation of St/St_0 Ratios, m=0.5, Two Rows of Holes, Vortex Positions R0 and R4, X=1.4m

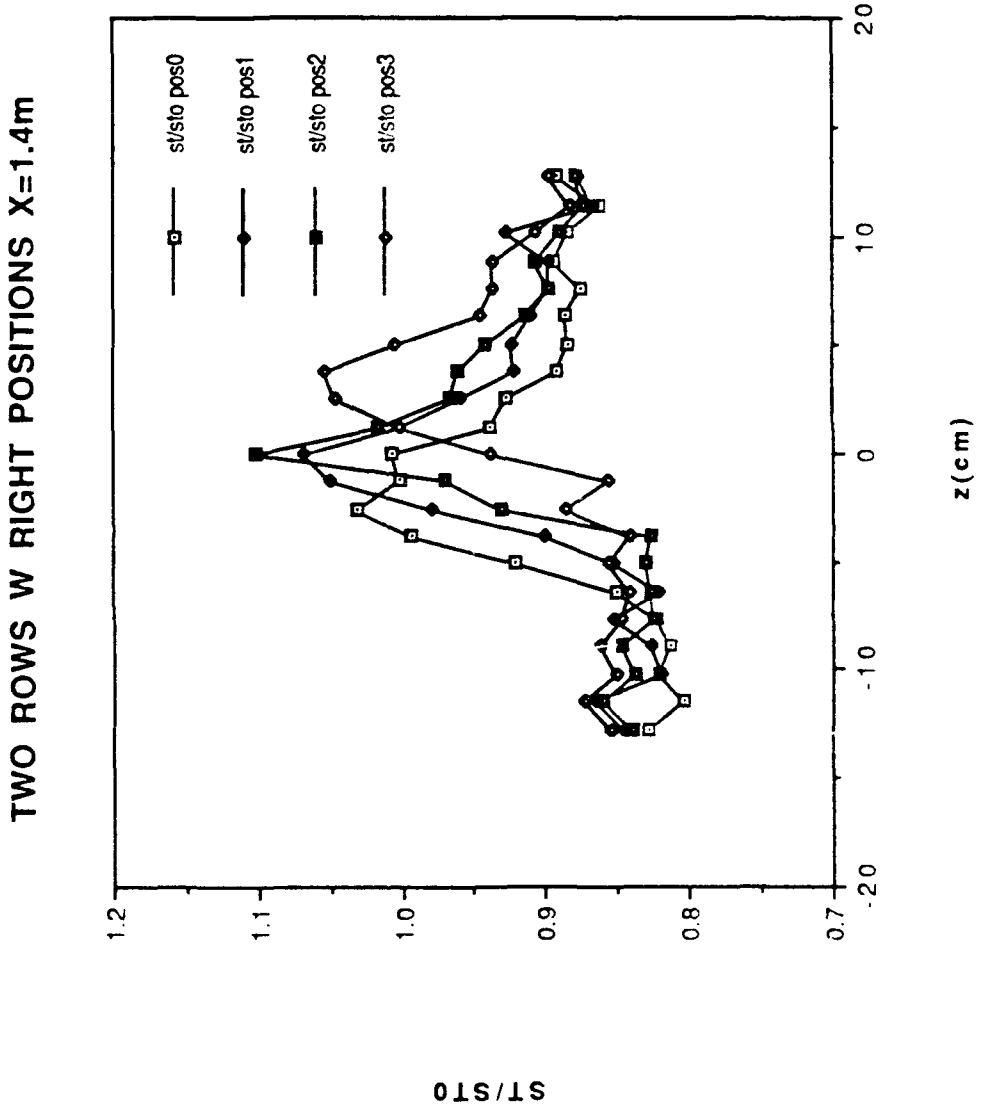

Figure 46. Spanwise Variation of St/St_0 Ratios, m=0.5, Two Rows of Holes, Vortex Positions R0 through R3, X=1.3m

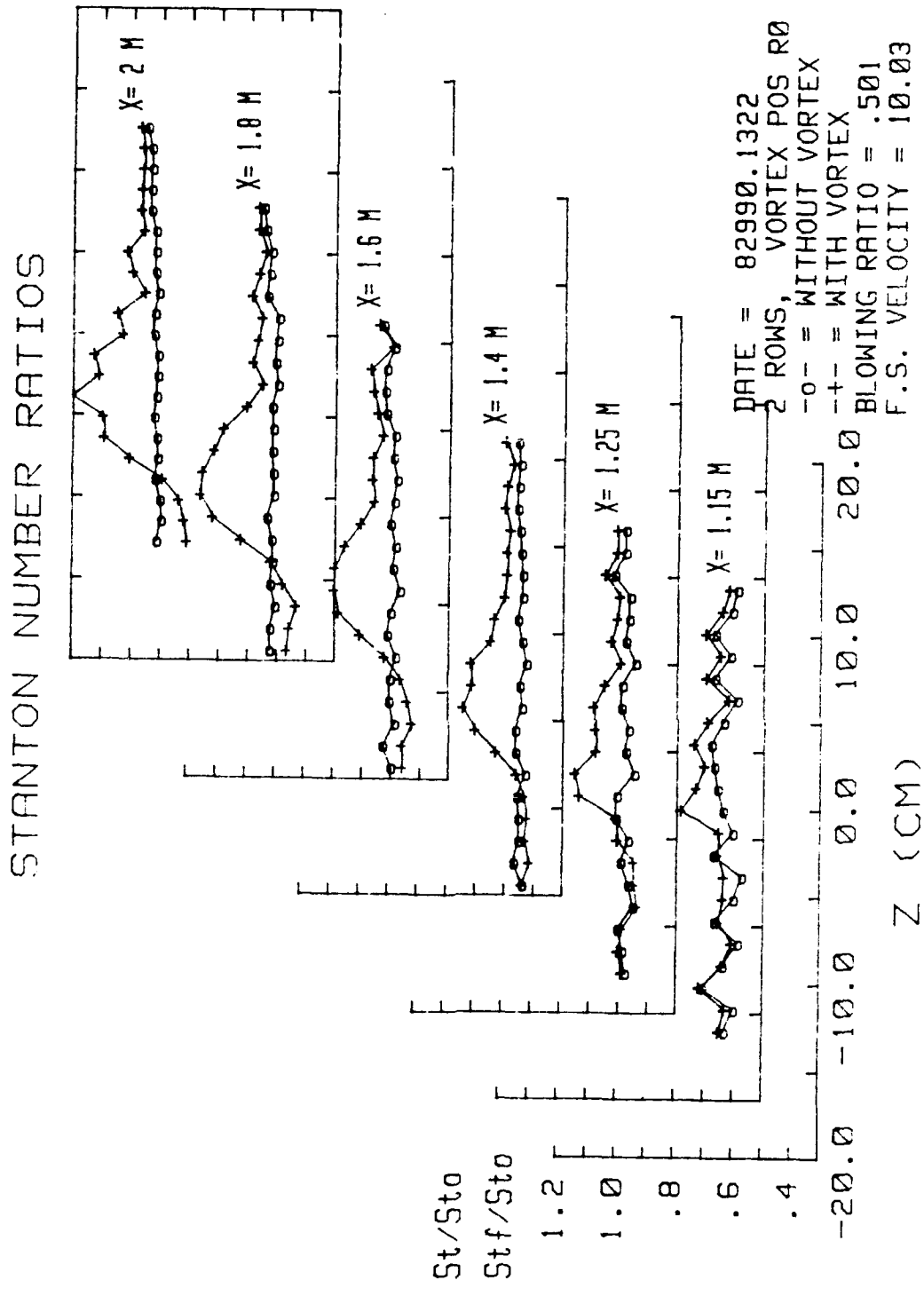

Figure 47. Spanwise Variation of St/St_0 and St_f/St_0 Ratios, m=0.5, Two Rows of Holes, Vortex Position R0

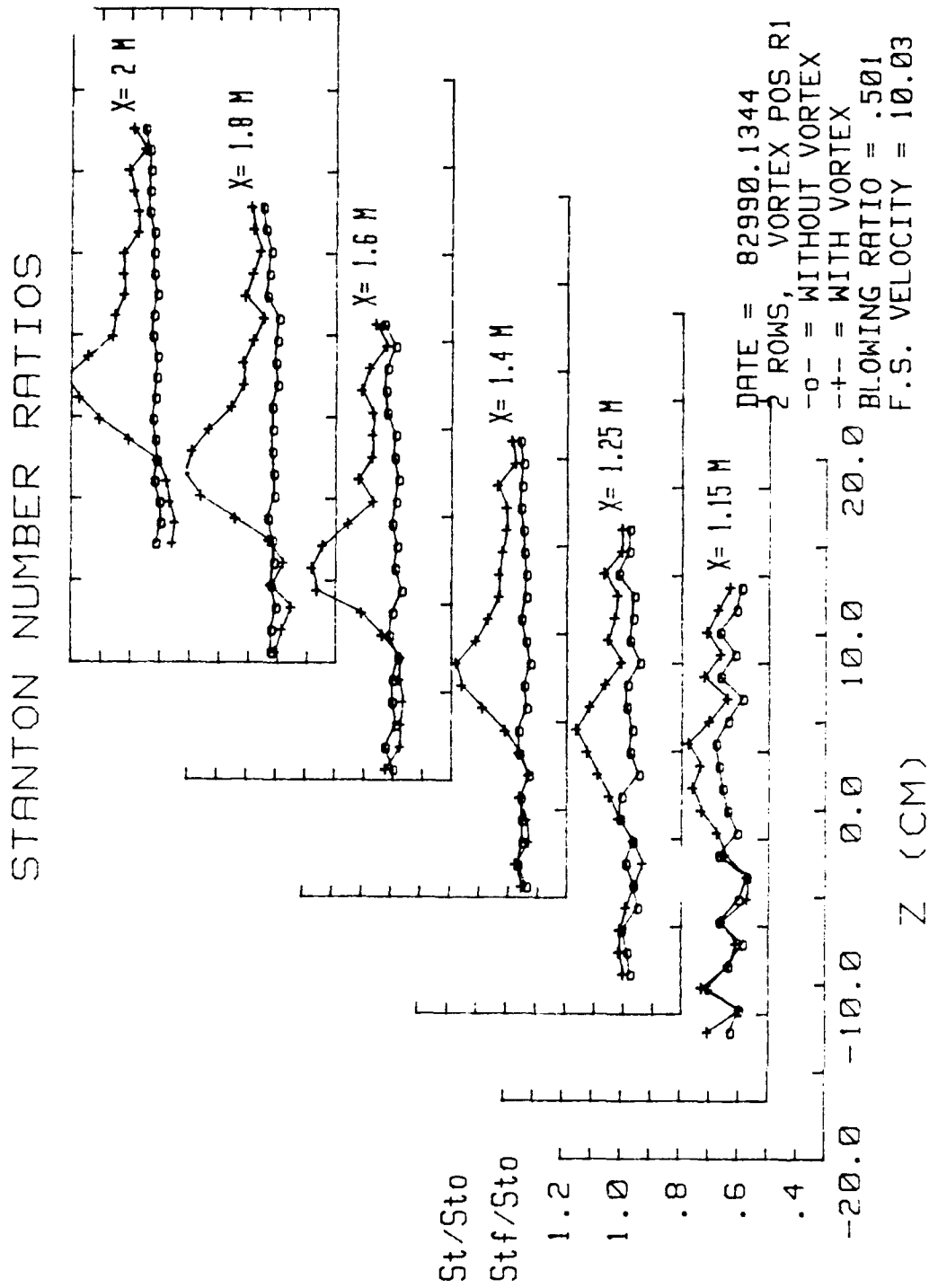

Figure 48. Spanwise Variation of St/St_0 and St_f/St_0 Ratios, m=0.5, Two Rows of Holes, Vortex Position R1

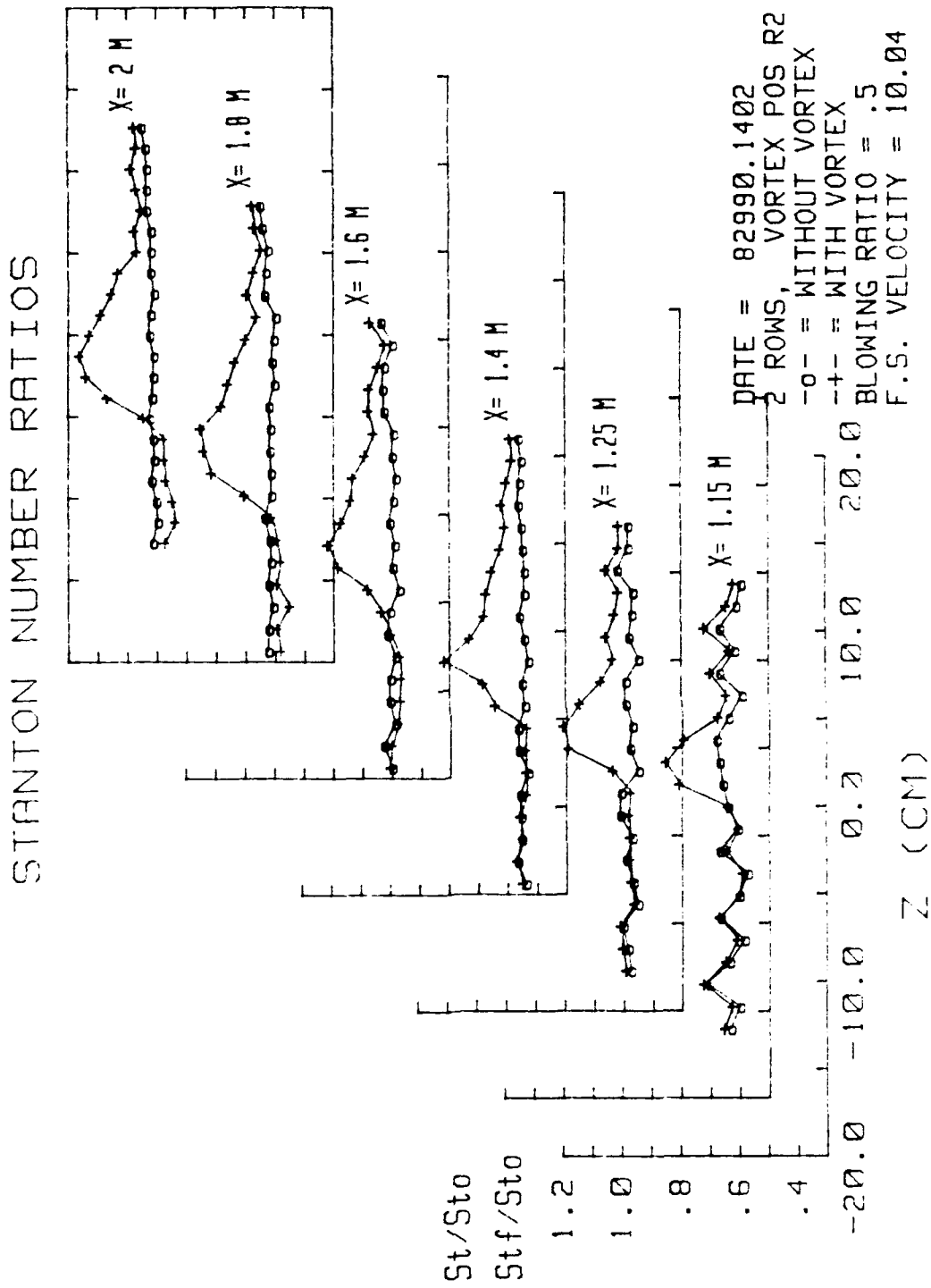

Figure 49. Spanwise Variation of St/St_0 and St_f/St_0 Ratios, m=0.5, Two Rows of Holes, Vortex Position R2

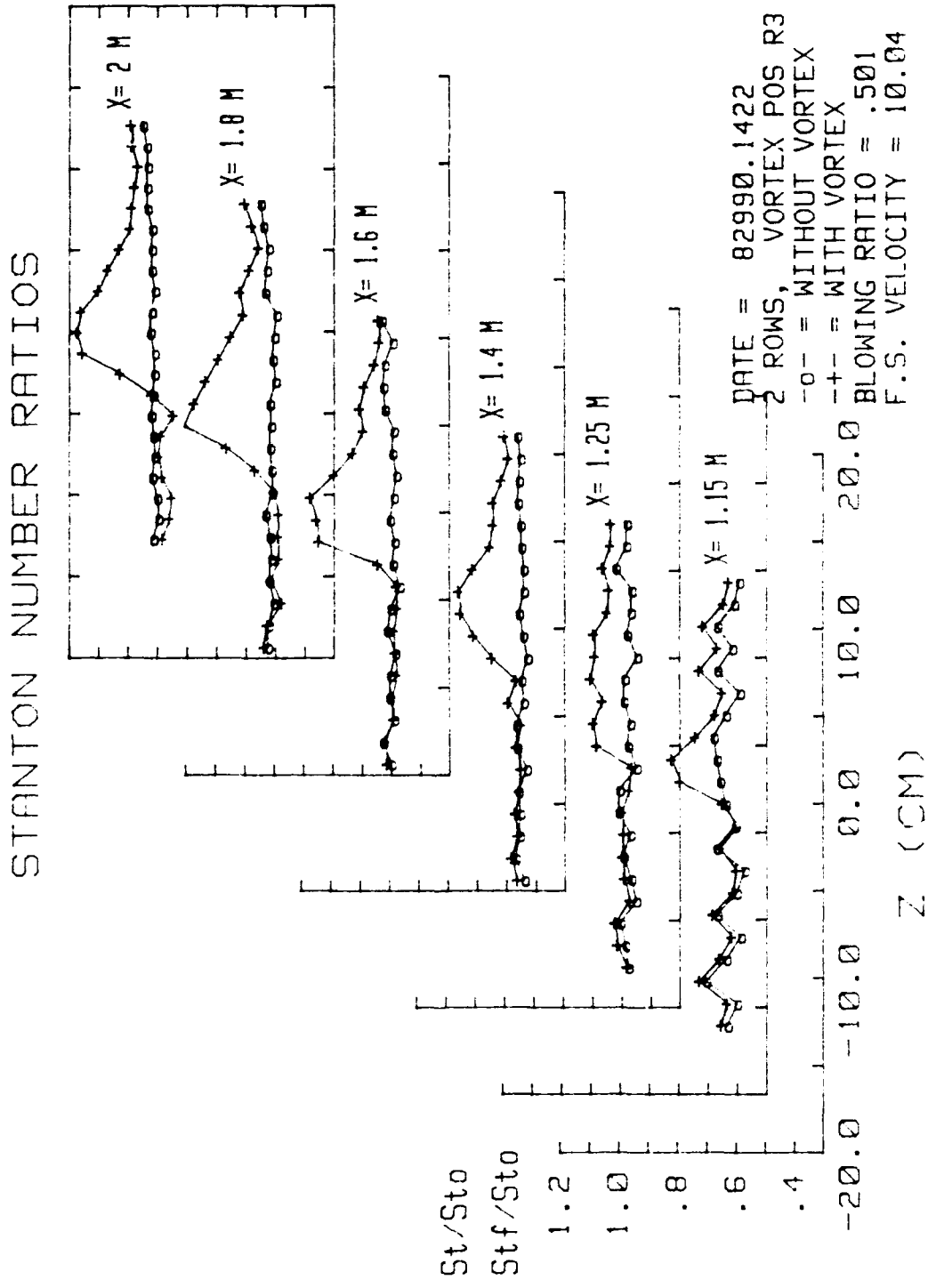

Figure 50. Spanwise Variation of St/St_0 and St_f/St_0 Ratios, m=0.5,Two Rows of Holes, Vortex Position R3

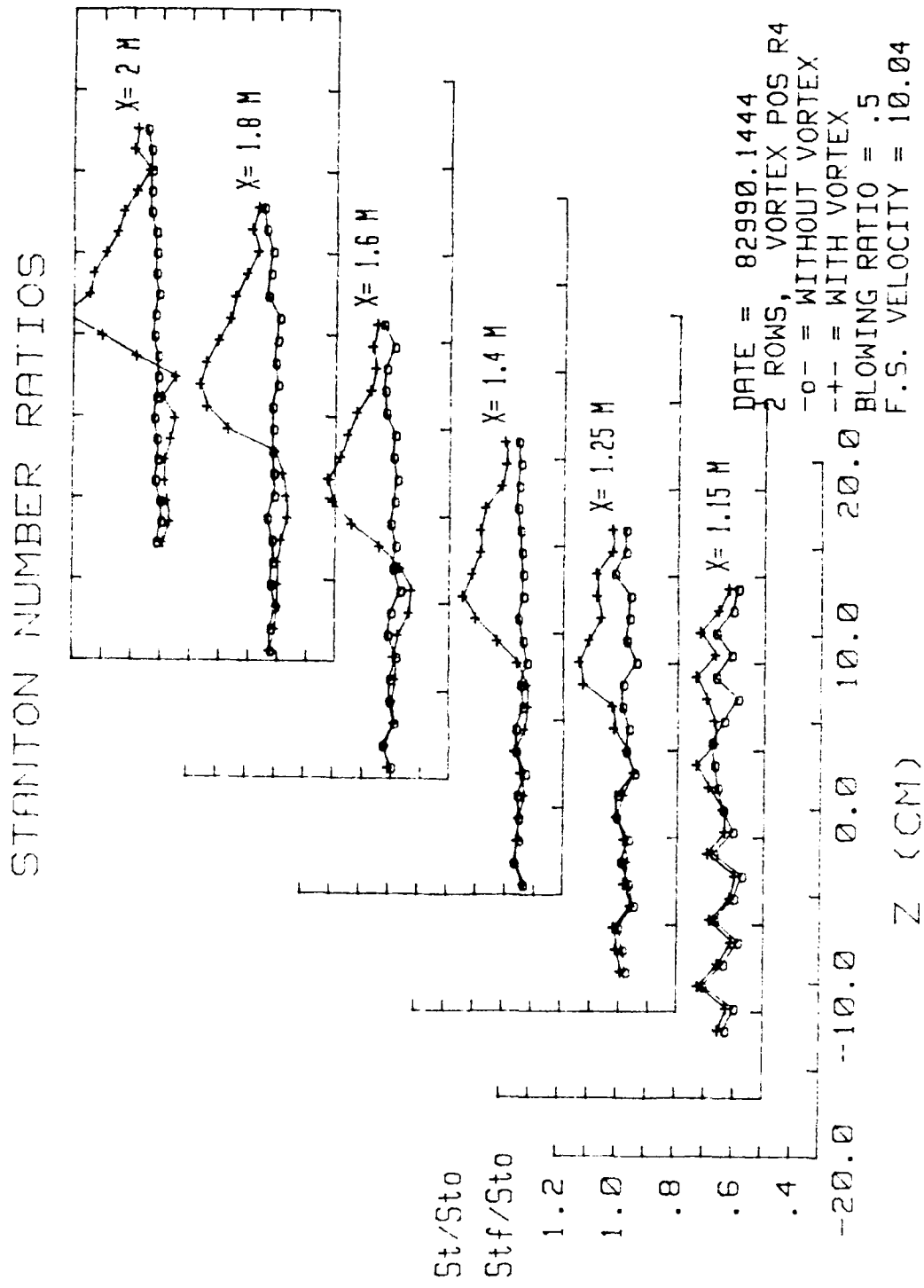

Figure 51. Spanwise Variation of St/St_0 and St_f/St_0 Ratios, m=0.5,Two Rows of Holes, Vortex Position R4

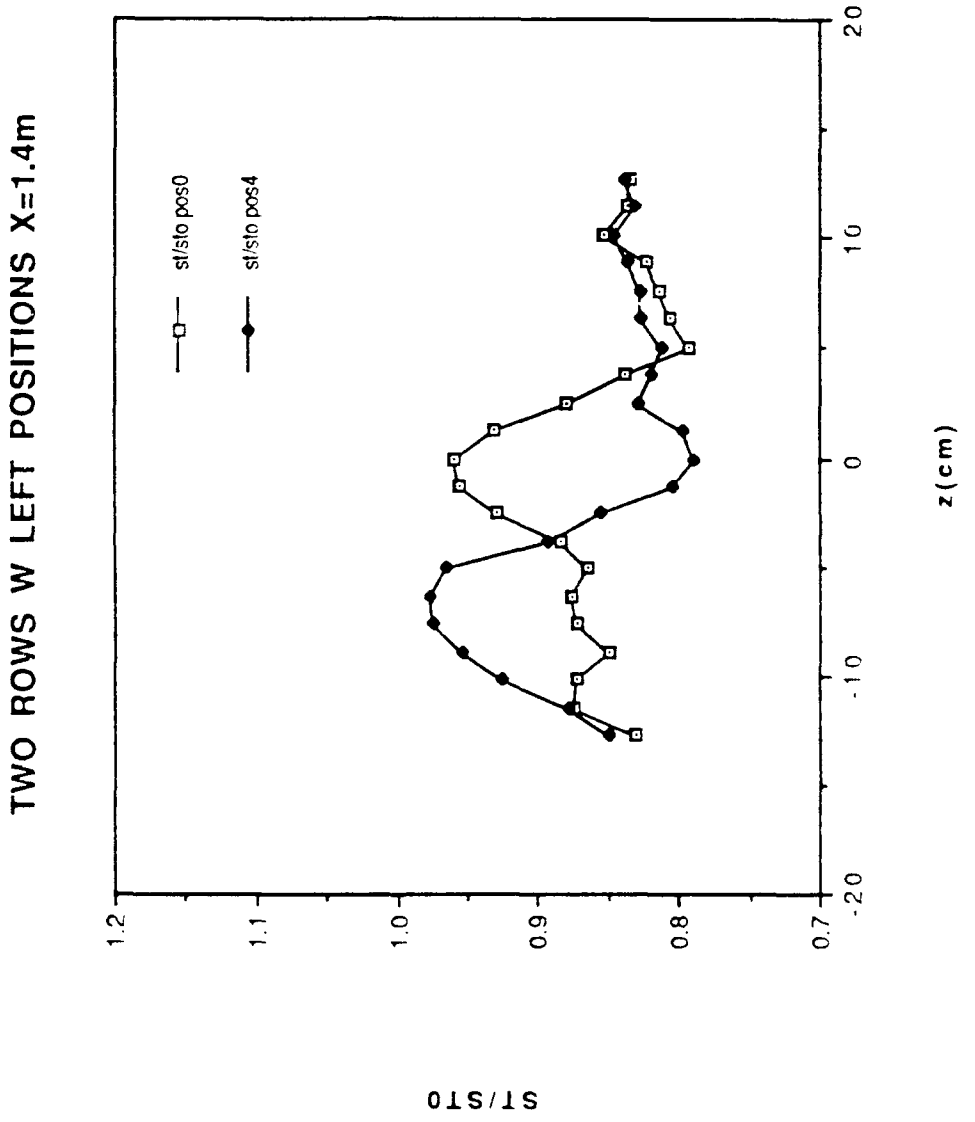

Figure 52. Spanwise Variation of St/St_0 Ratios, m=0.5, Two Rows of Holes, Vortex Positions L0 and L4, X=1.4m

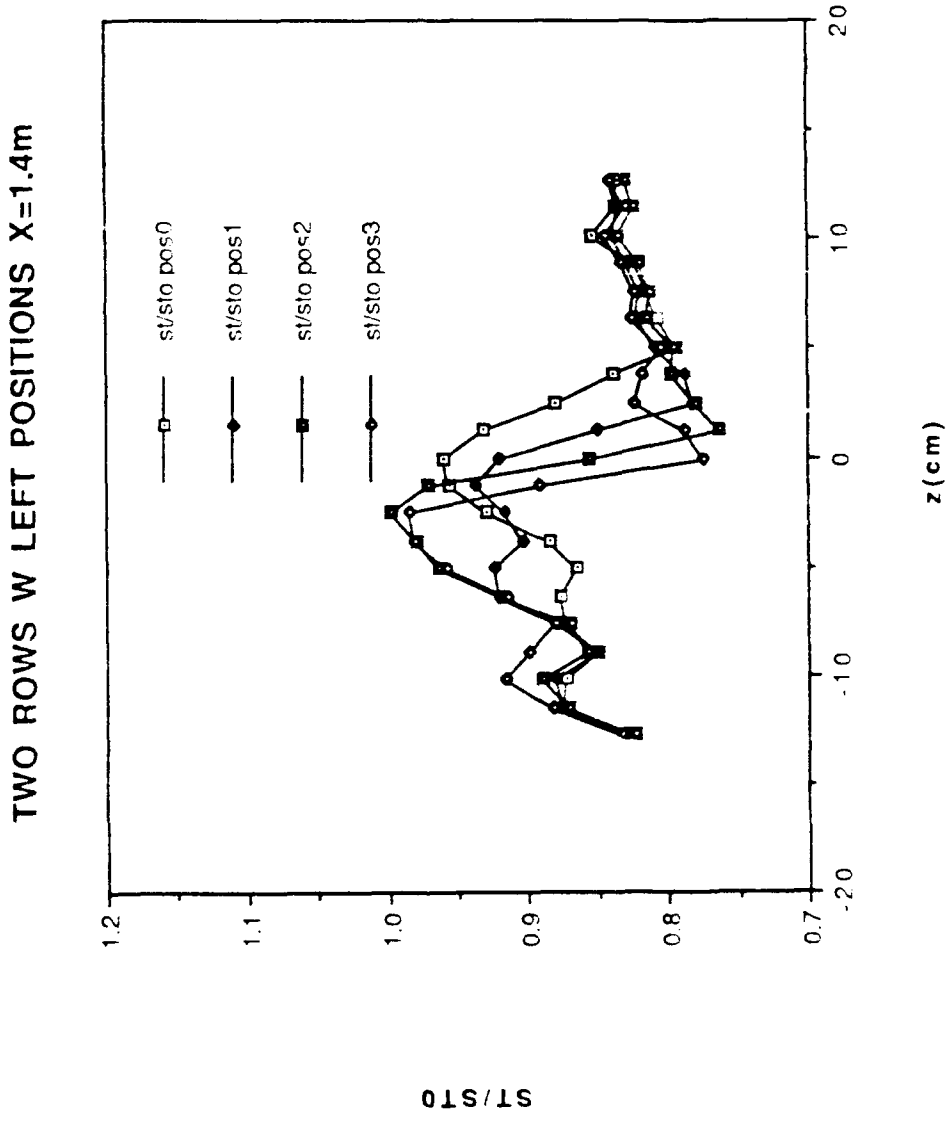

Figure 53. Spanwise Variation of St/St_0 Ratios, m=0.5, Two Rows of Holes, Vortex Positions L0 through L3

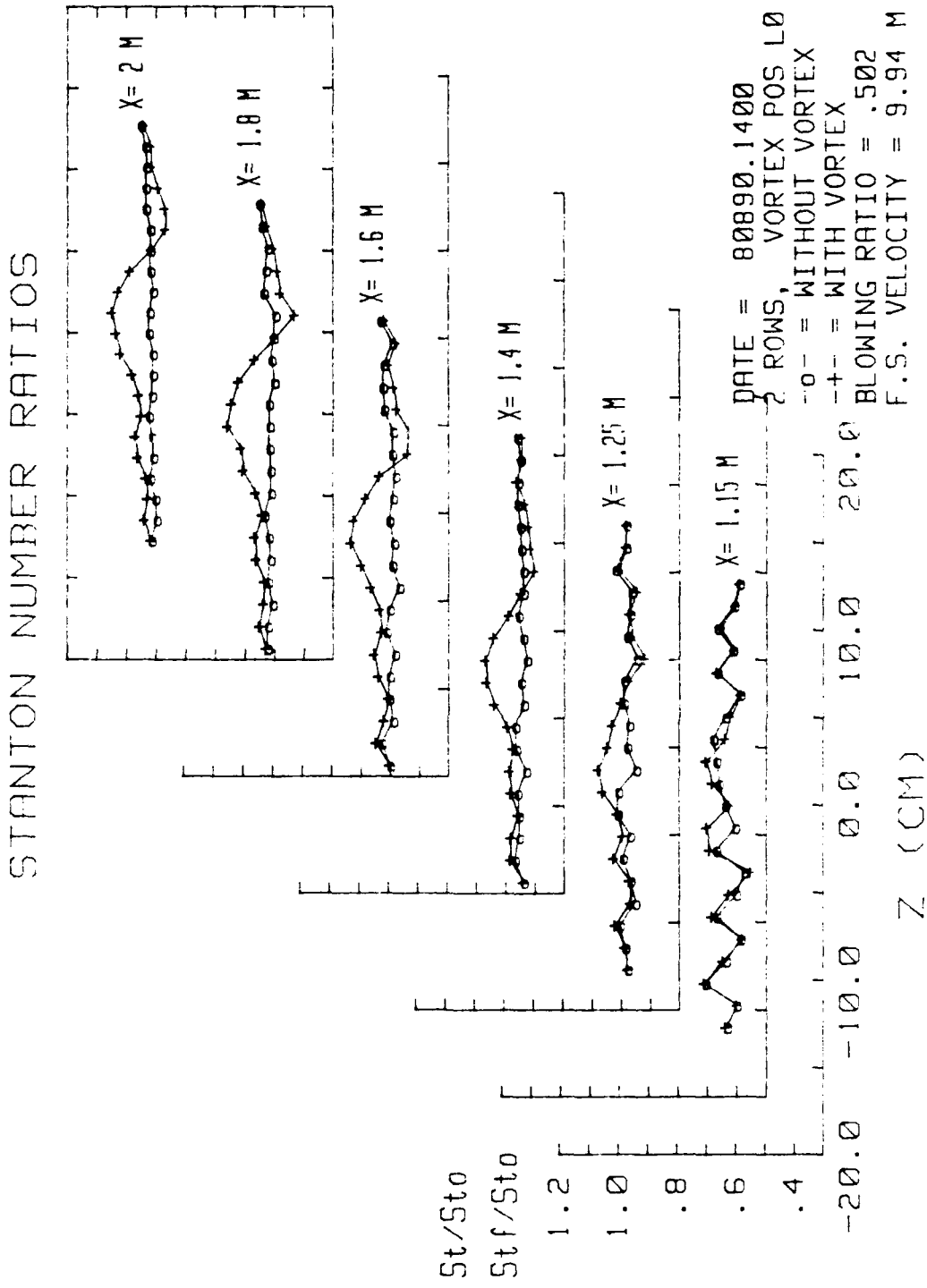

Figure 54. Spanwise Variation of St/St_0 and St_f/St_0 Ratios, m=0.5, Two Rows of Holes, Vortex Position L0

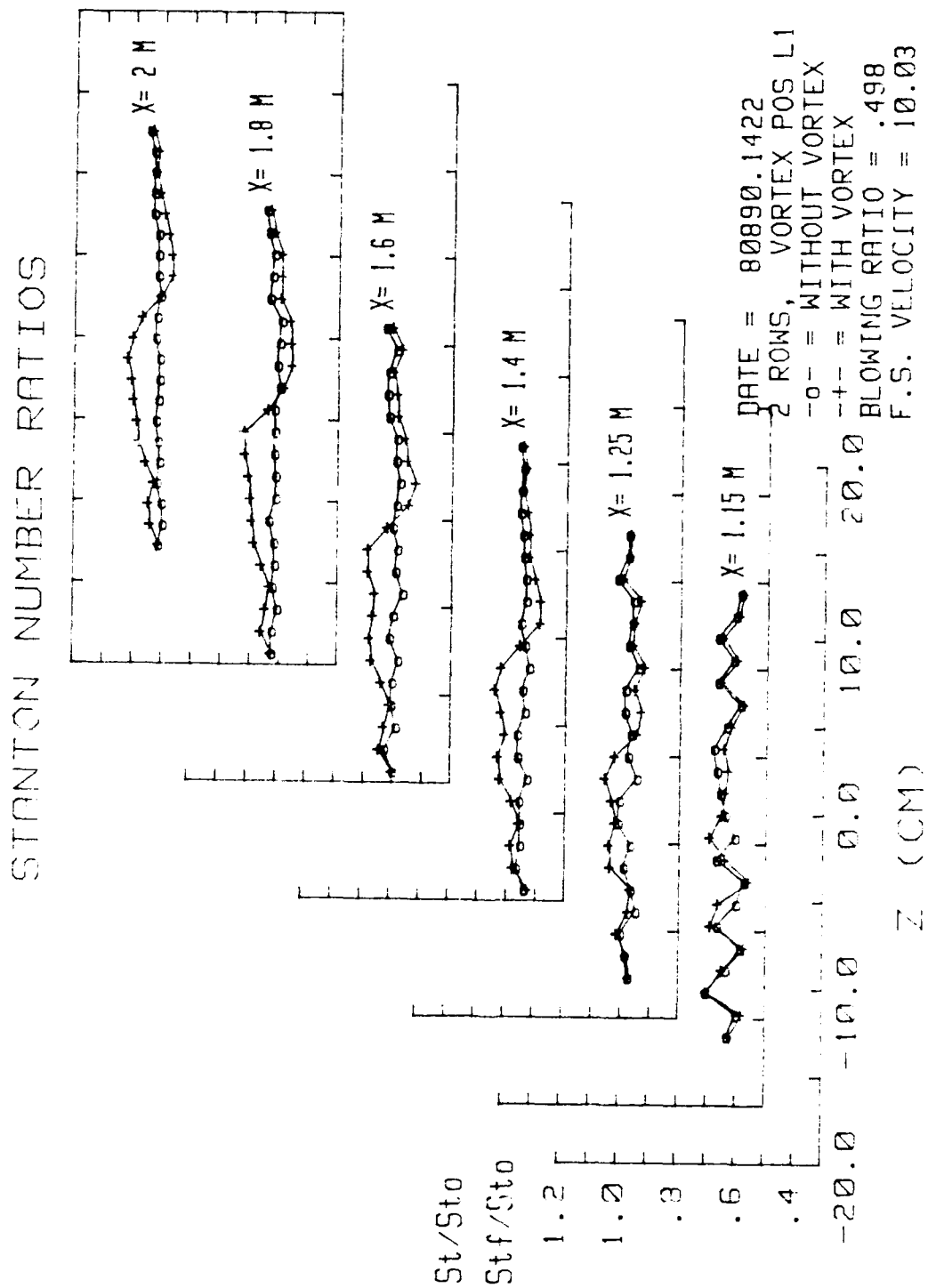

Figure 55. Spanwise Variation of St/St_0 and St_f/St_0 Ratios, m=0.5, Two Rows of Holes, Vortex Position L1

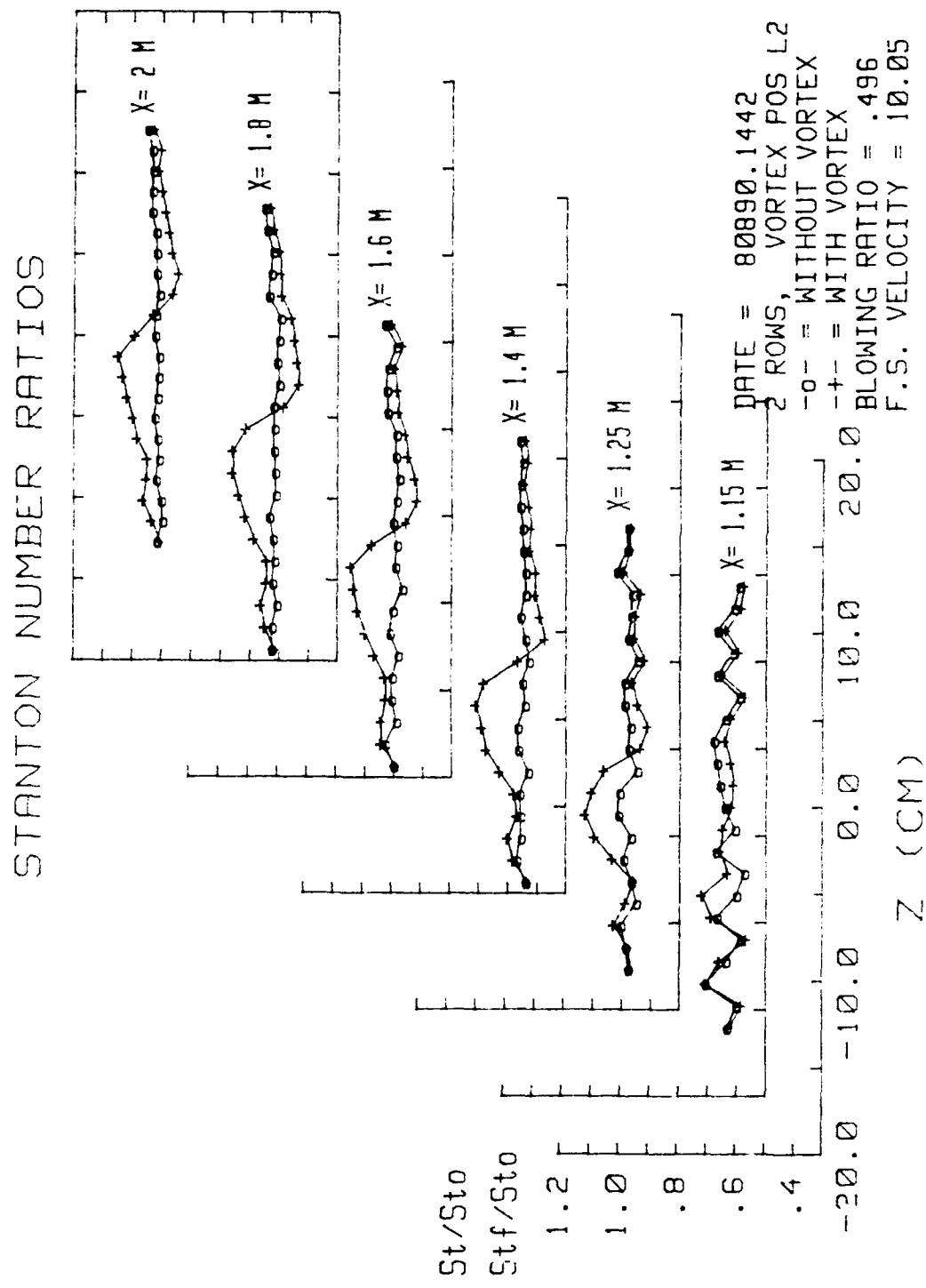

Figure 56. Spanwise Variation of St/St_0 and St_f/St_0 Ratios, m=0.5, Two Rows of Holes, Vortex Position L2

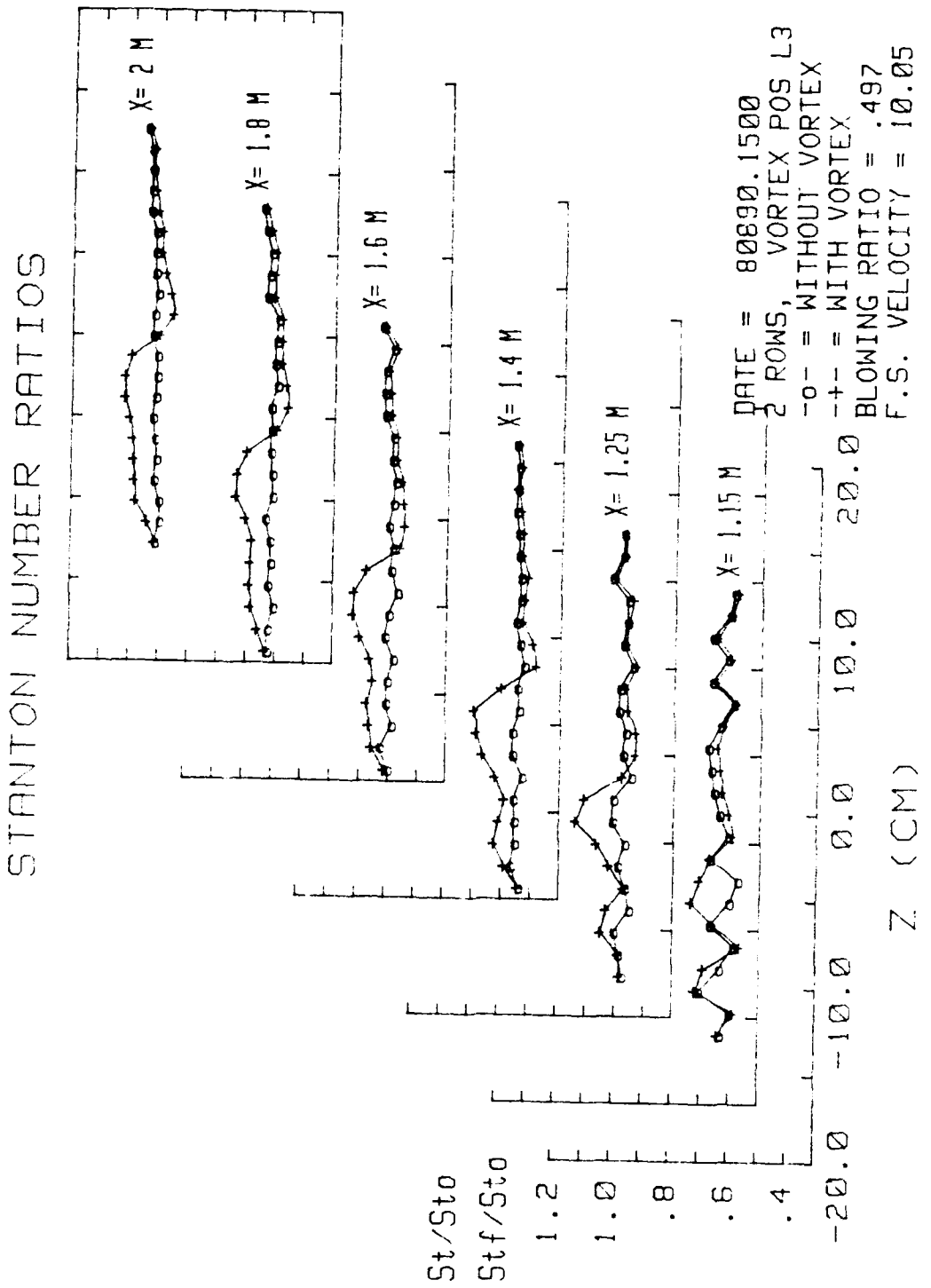

Figure 57. Spanwise Variation of St/St_0 and St_f/St_0 Ratios, m=0.5, Two Rows of Holes, Vortex Position L3

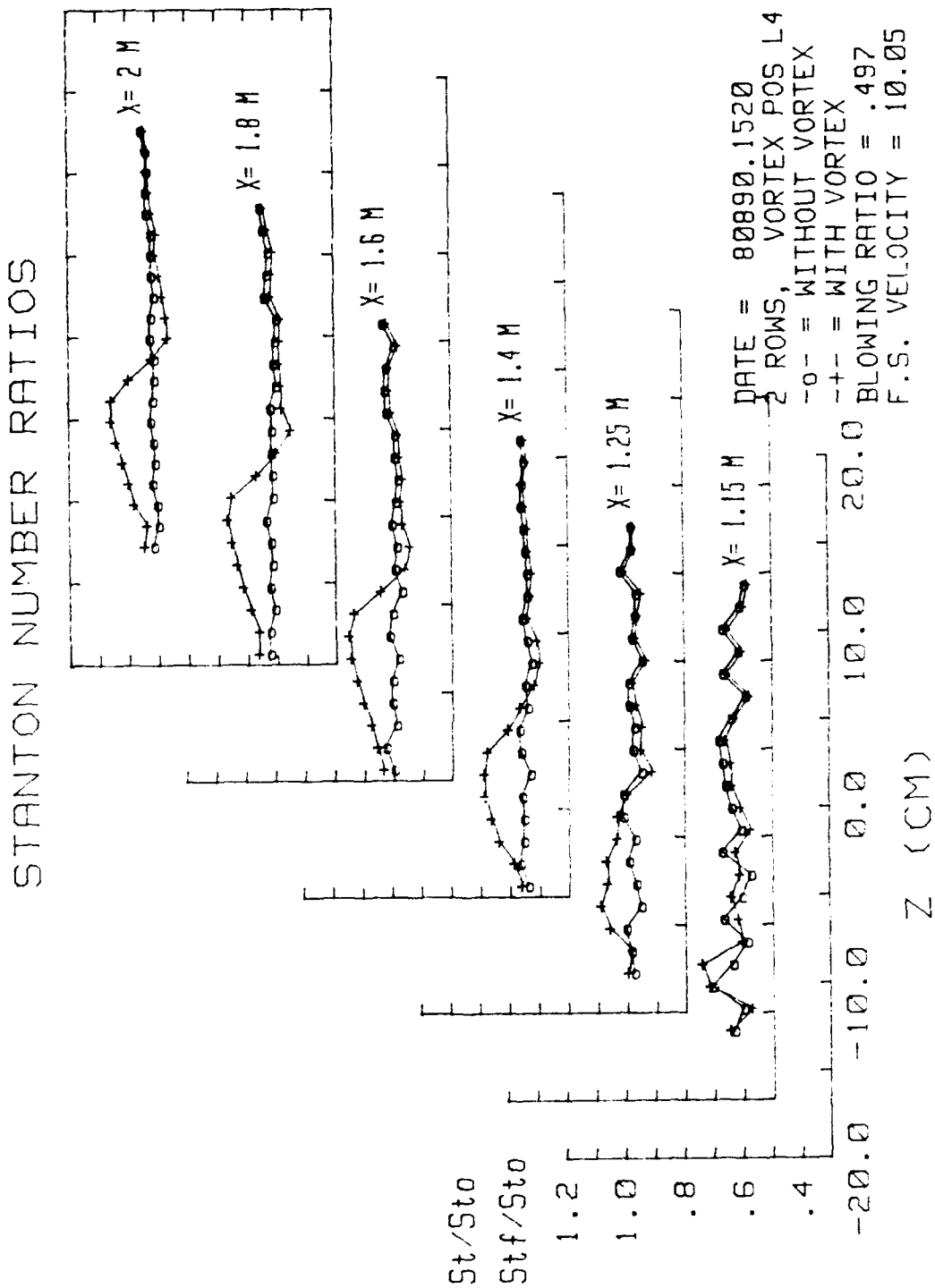

Figure 58. Spanwise Variation of St/St_0 Ratios, m=0.5, Two Rows of Holes, Vortex Position L4

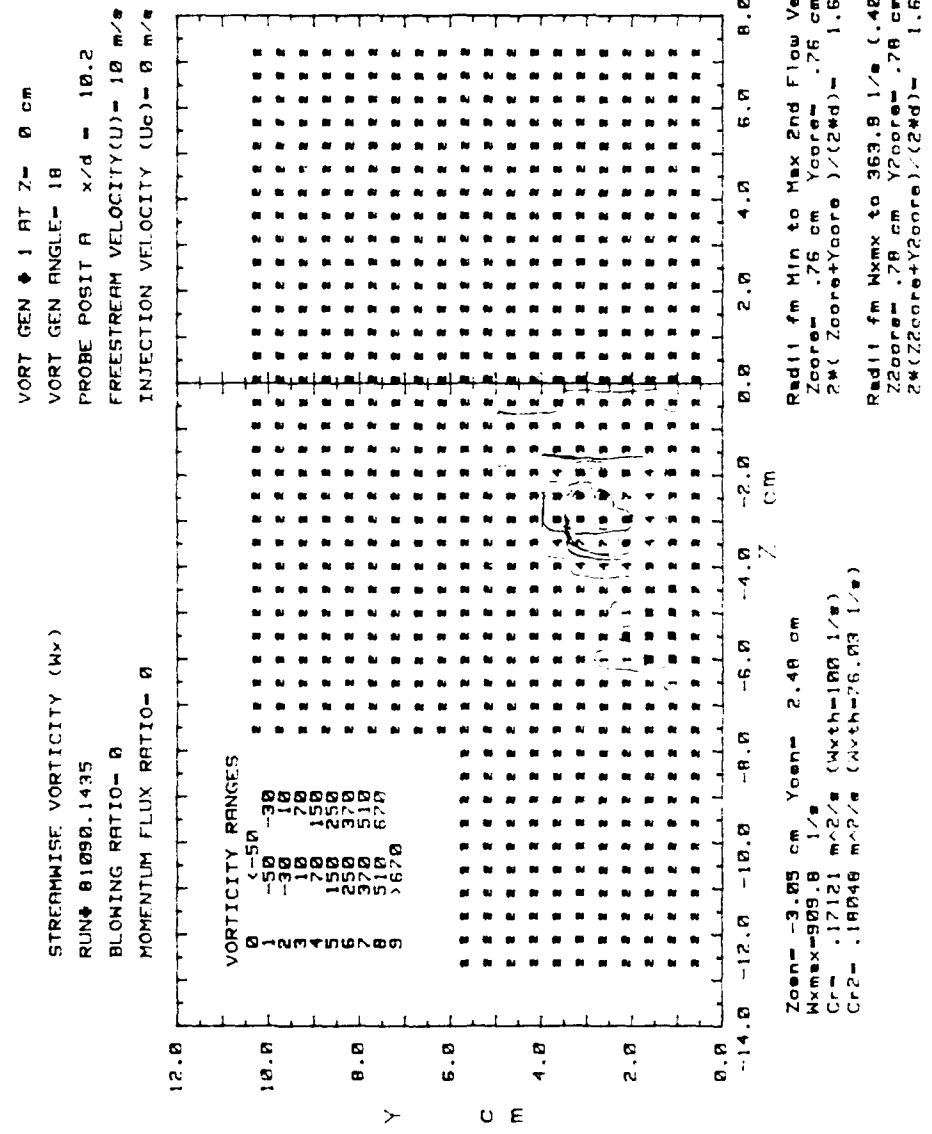

Figure 59. Streamwise Vorticity Contours, x/d=10.2, No Film Cooling, Vortex R0

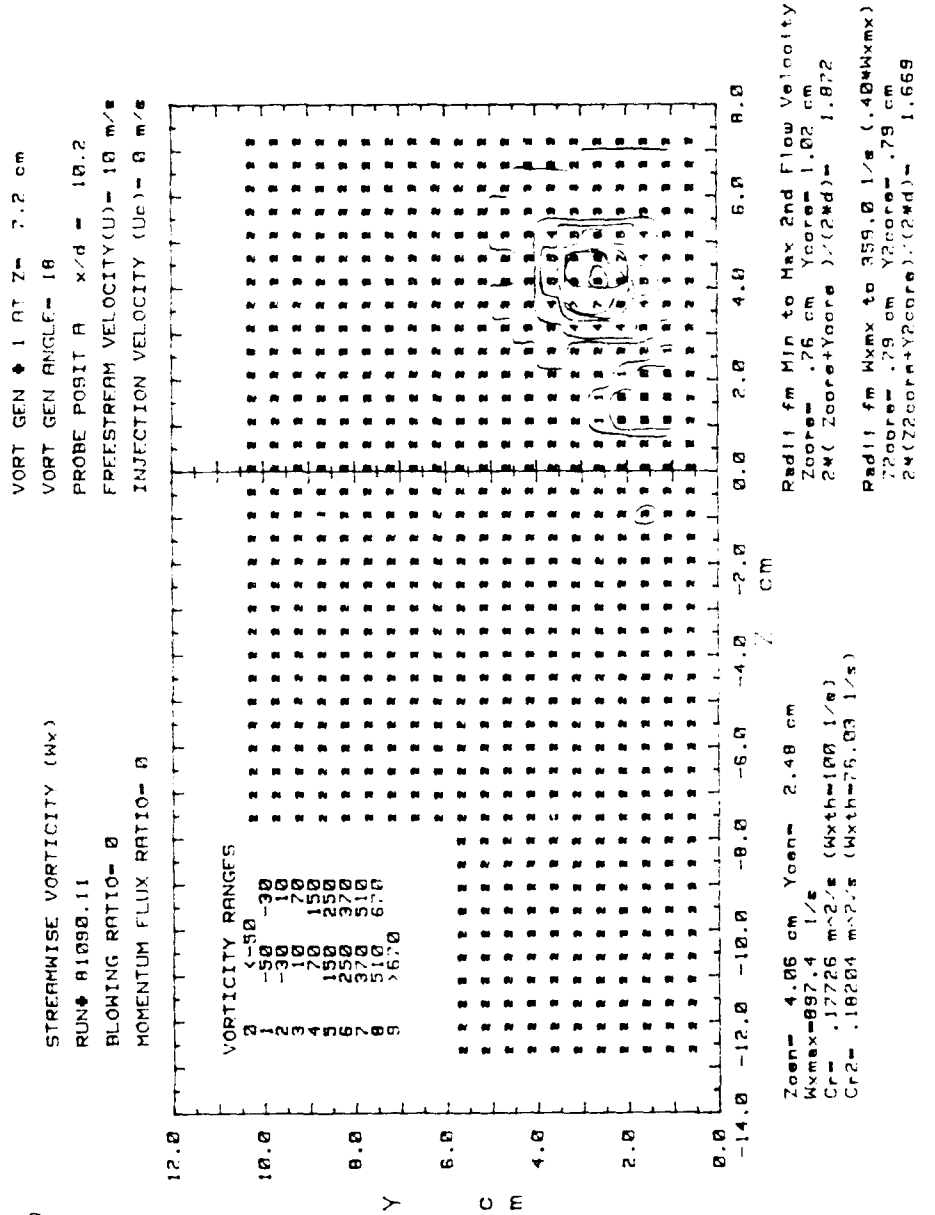

Figure 60. Streamwise Vorticity Contours, x/d=10.2, No Film Cooling, Vortex R4

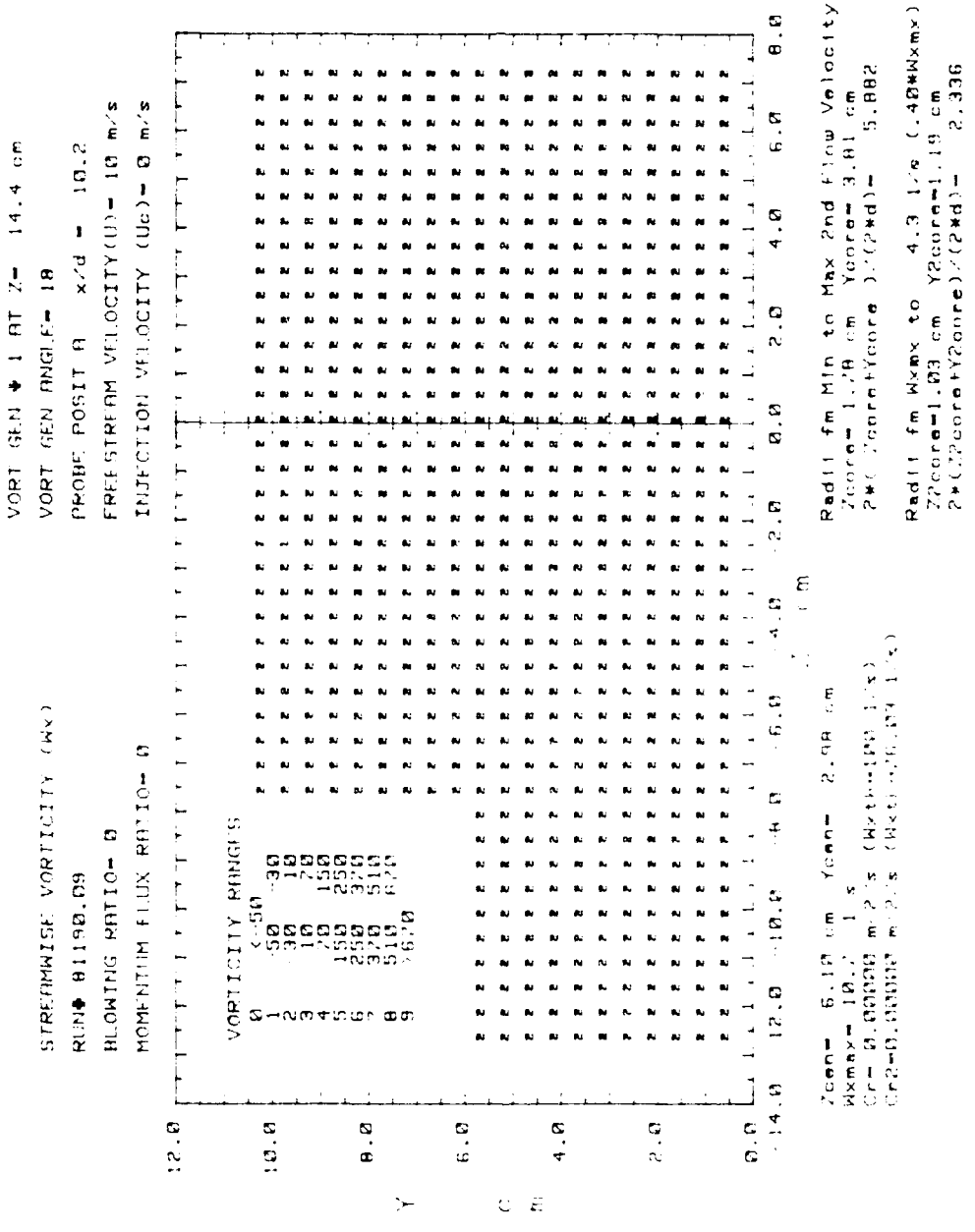

Figure 61. Streamwise Vorticity Contours, x/d=10.2, No Film Cooling, Vortex R8

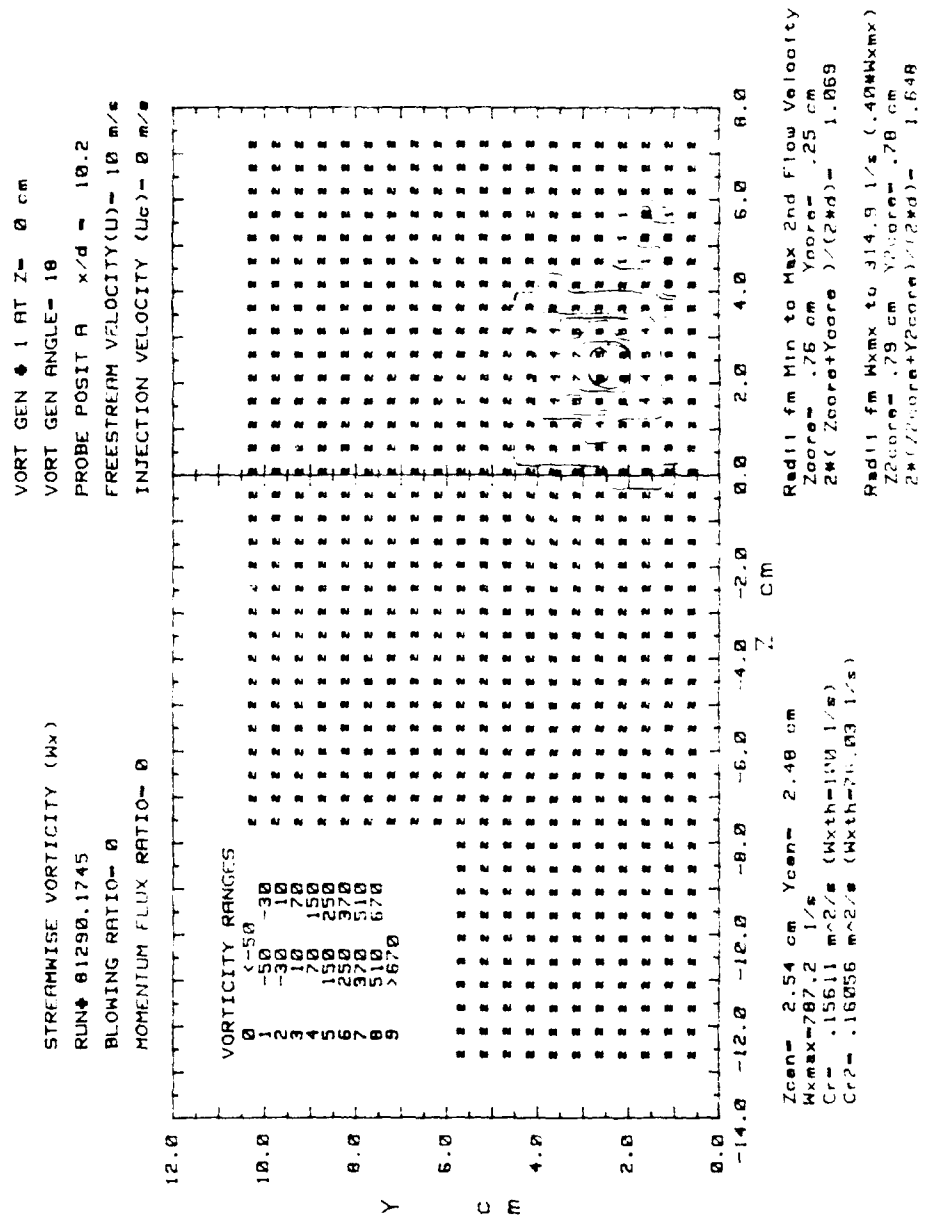

Figure 62. Streamwise Vorticity Contours, x/d=10.2, No Film Cooling, Vortex L0

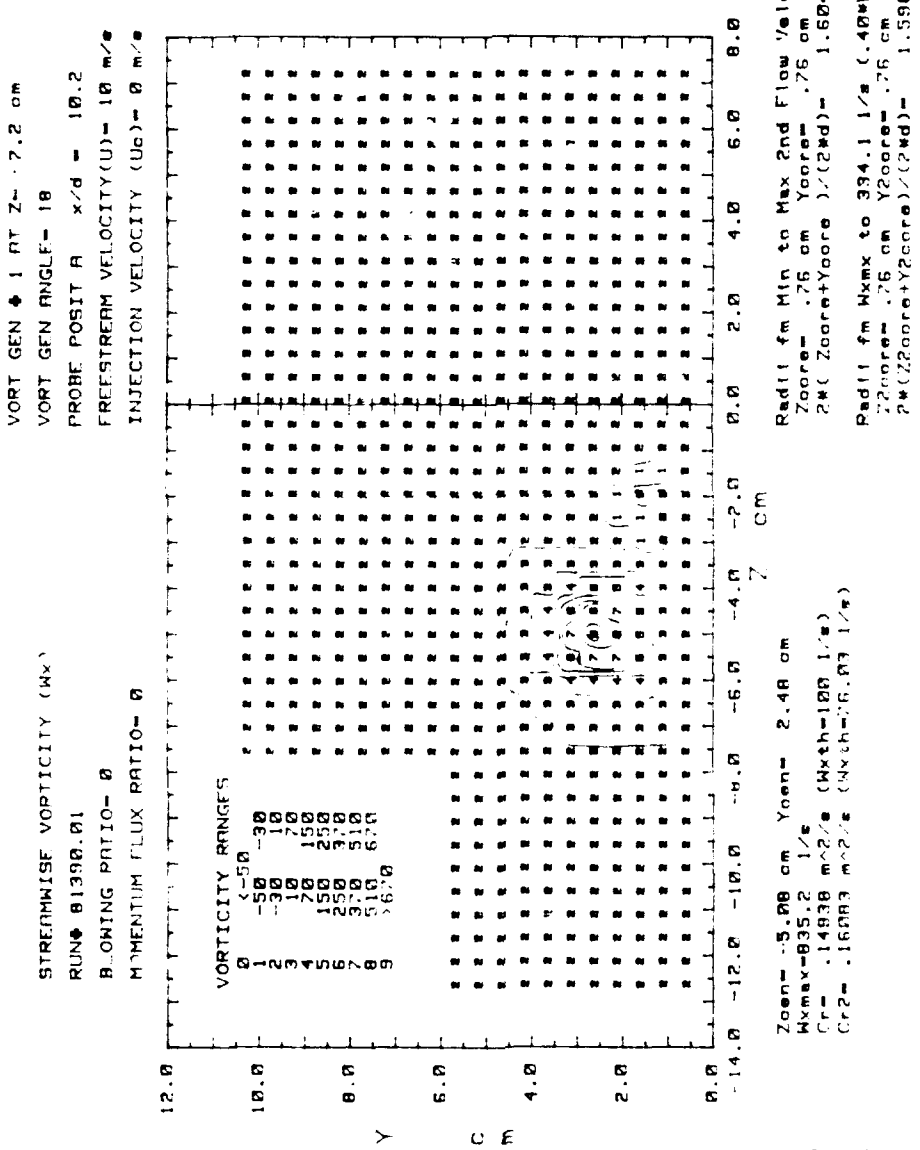

Figure 63. Streamwise Vorticity Contours, x/d=10.2, No Film Cooling, Vortex L4

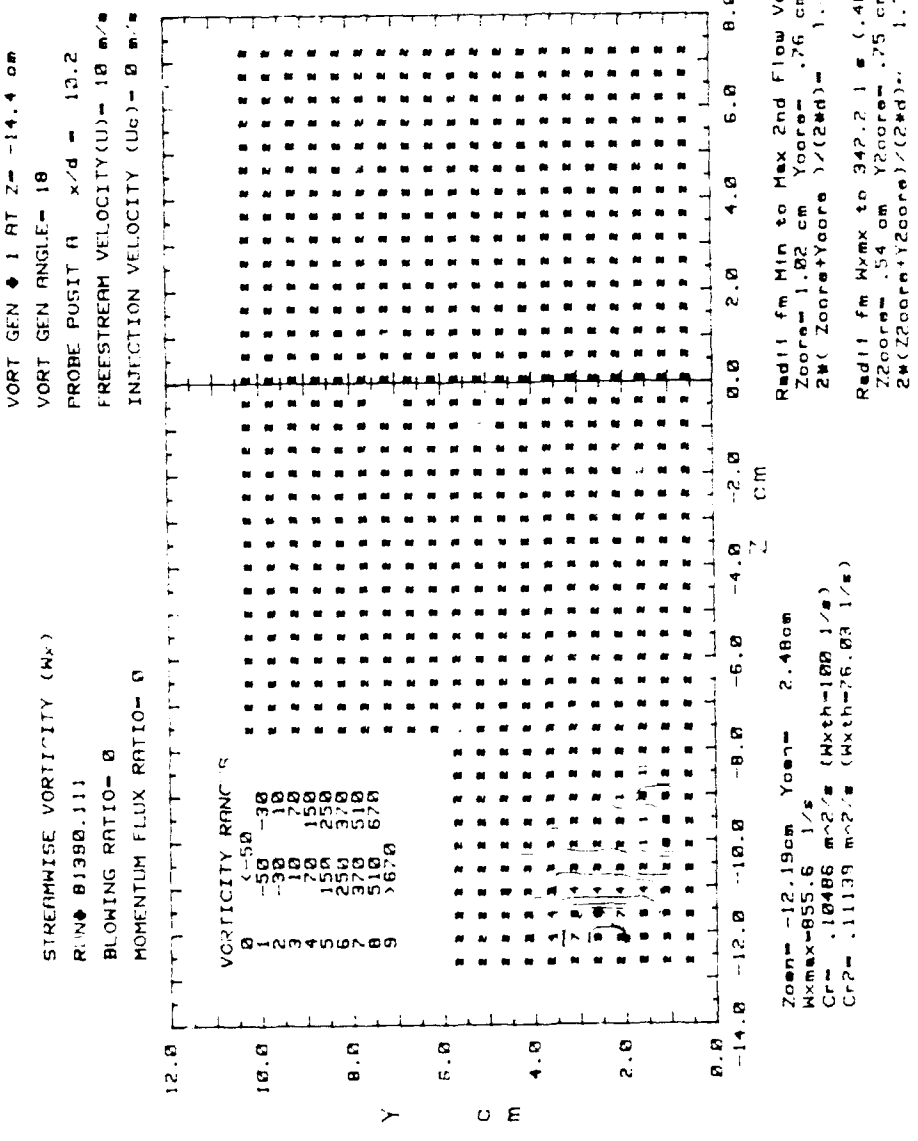

Figure 64. Streamwise Vorticity Contours, x/d=10.2, No Film Cooling, Vortex L8

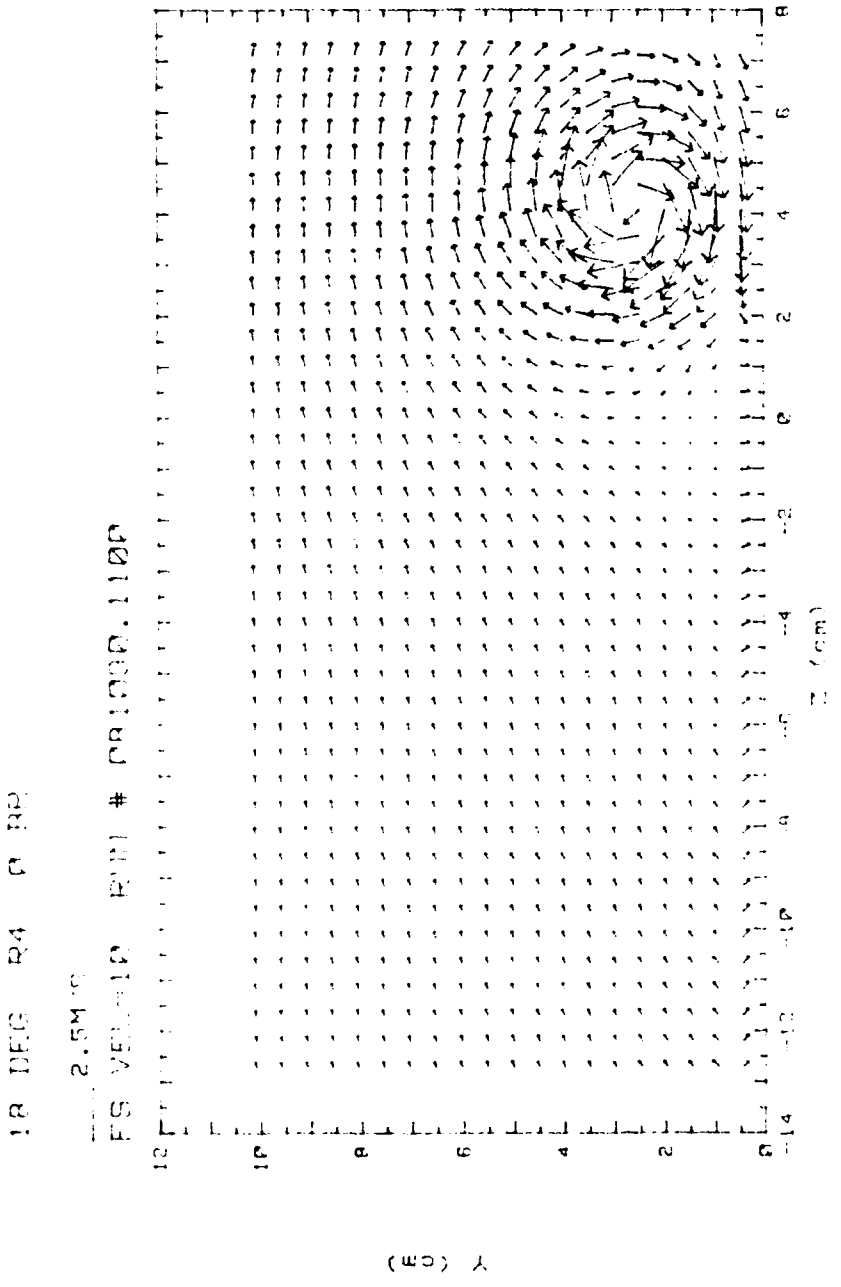

Figure 65. Secondary Flow Vectors, x/d=10.2, No Film Cooling, Vortex R0

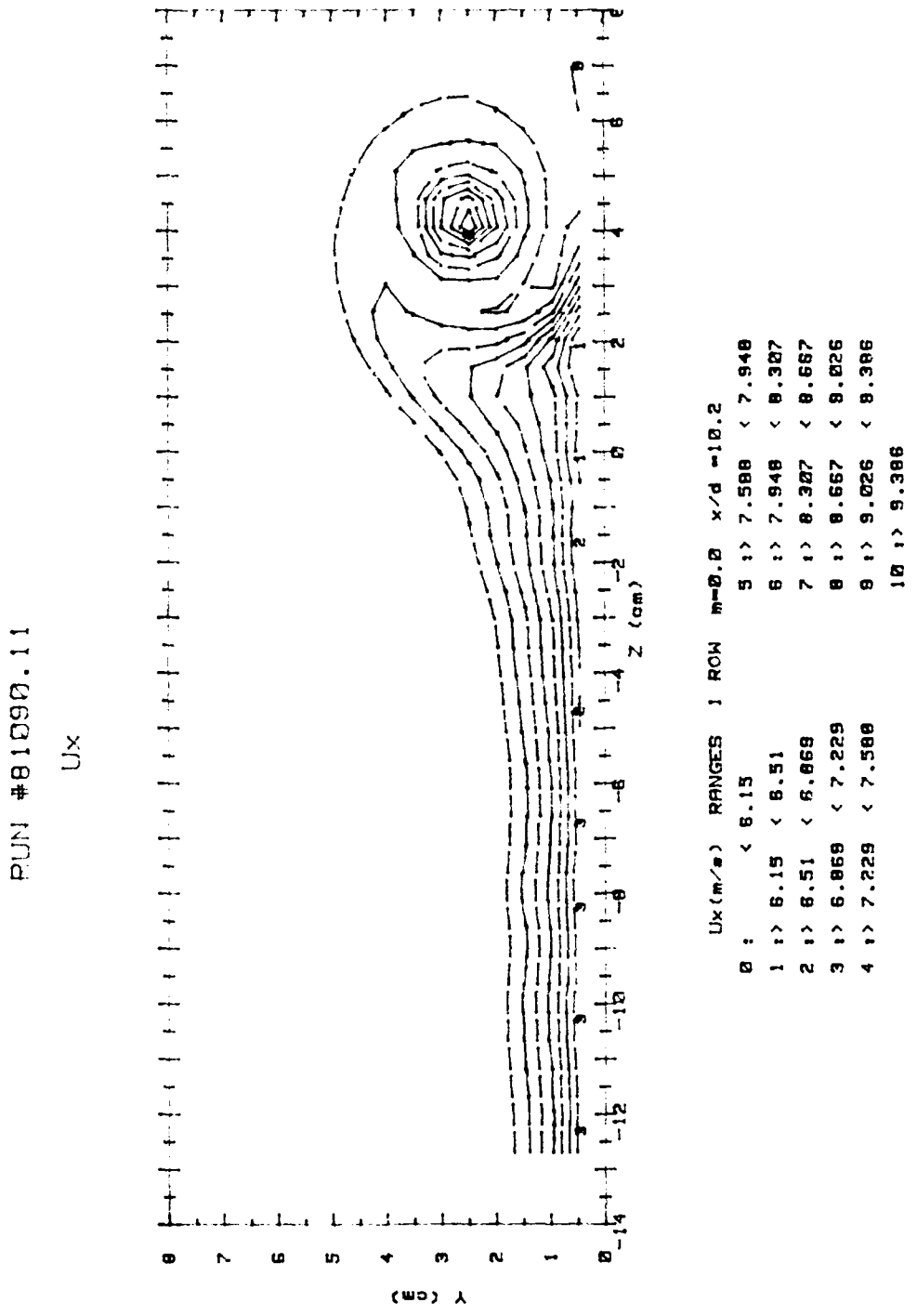

Figure 66. Streamwise Velocity Field, x/d=10.2, No Film Cooling, Vortex R0

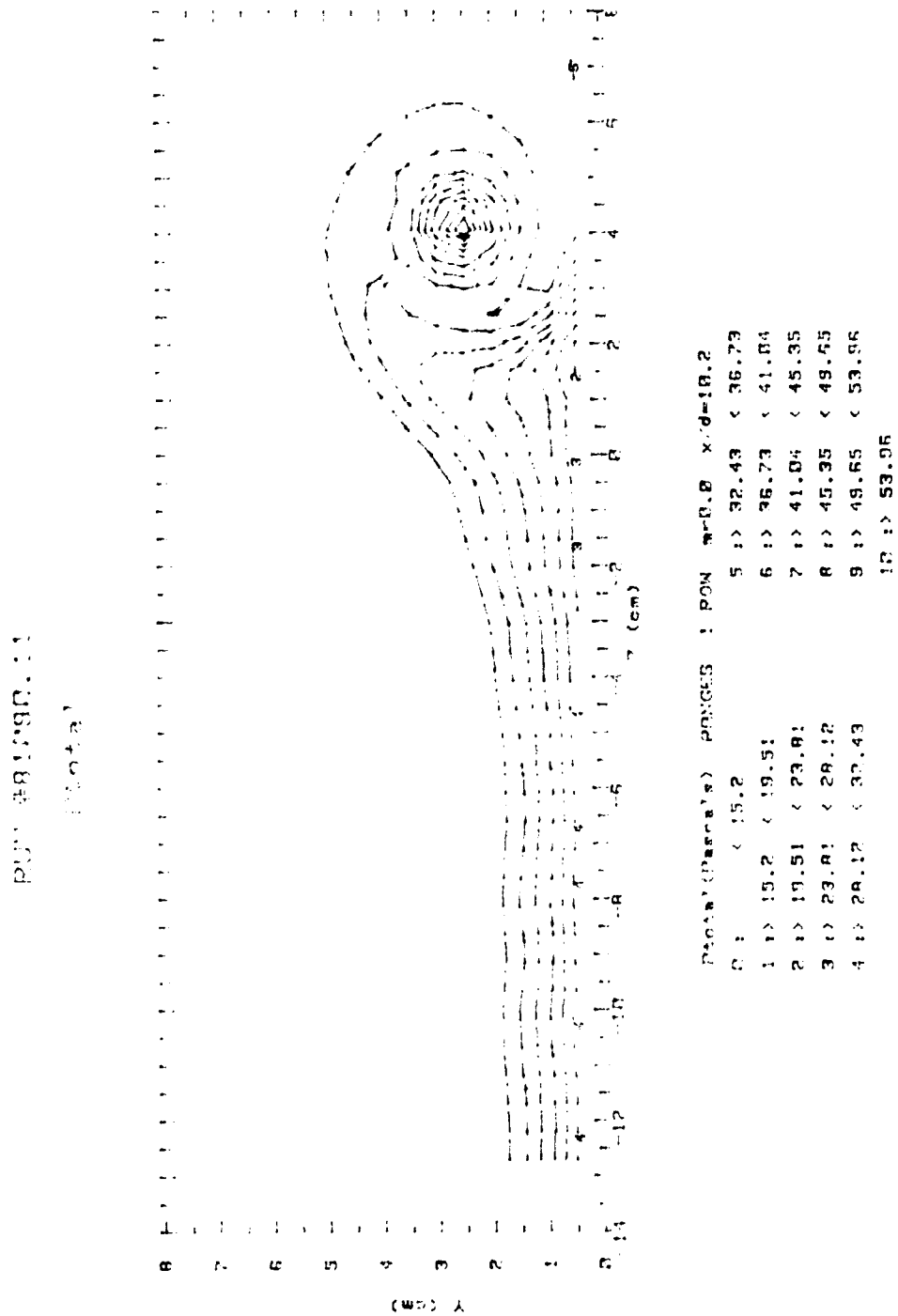

Figure 67. Total Pressure Field, x/d=10.2, No Film Cooling, Vortex R0

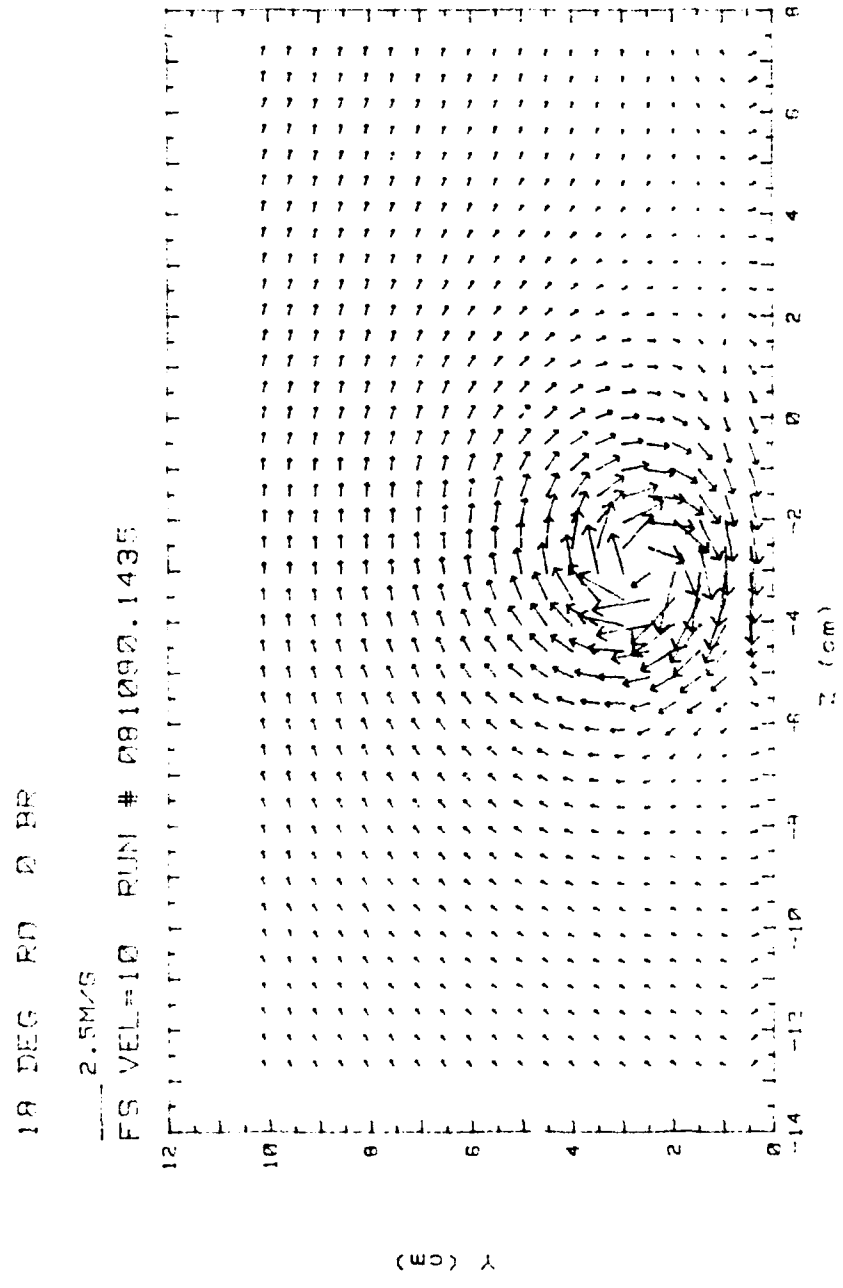

Figure 68. Secondary Flow Vectors, x/d=10.2, No Film Cooling, Vortex R4

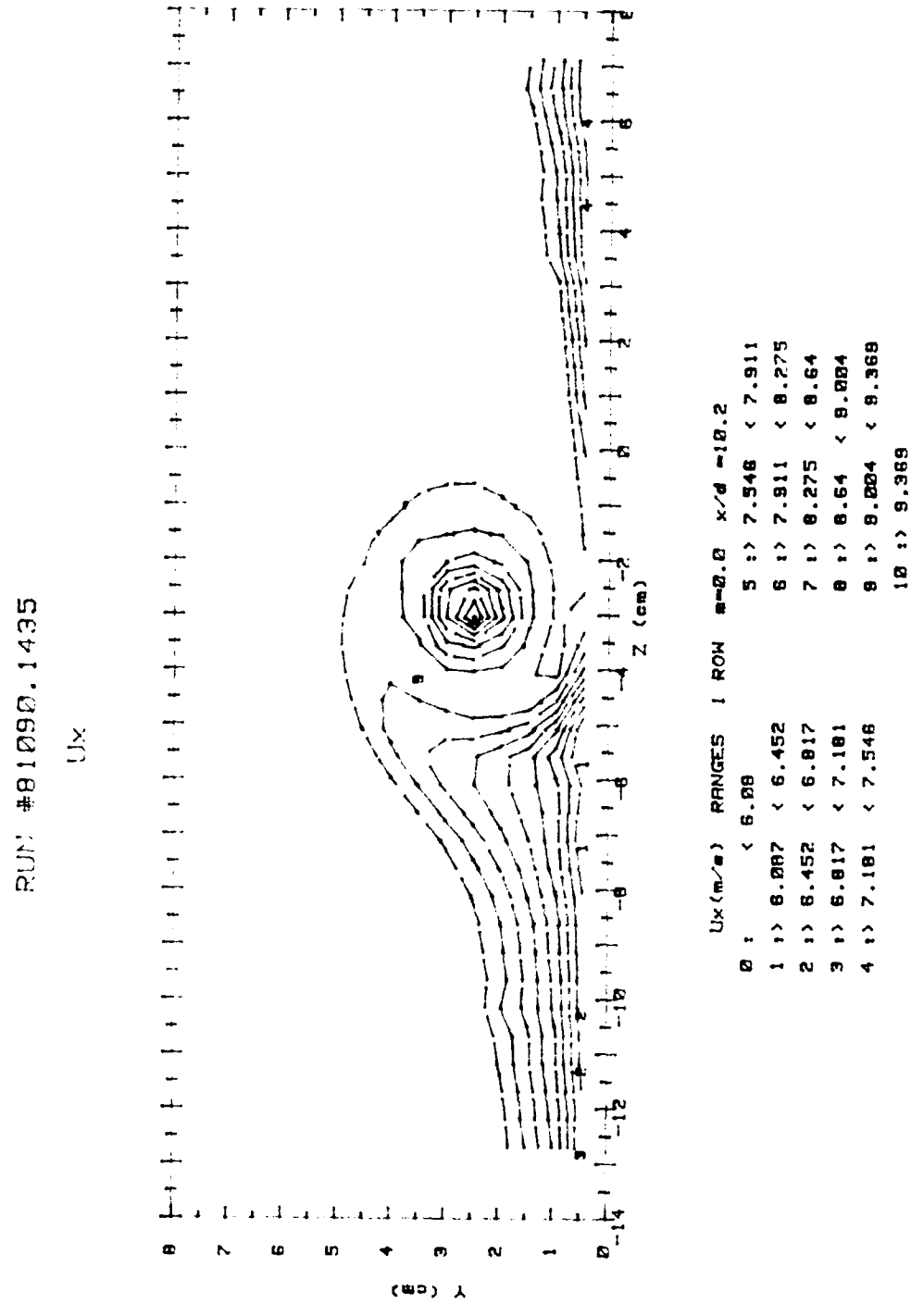

Figure 69. Streamwise Velocity Field, x/d=10.2, No Film Cooling, Vortex R4

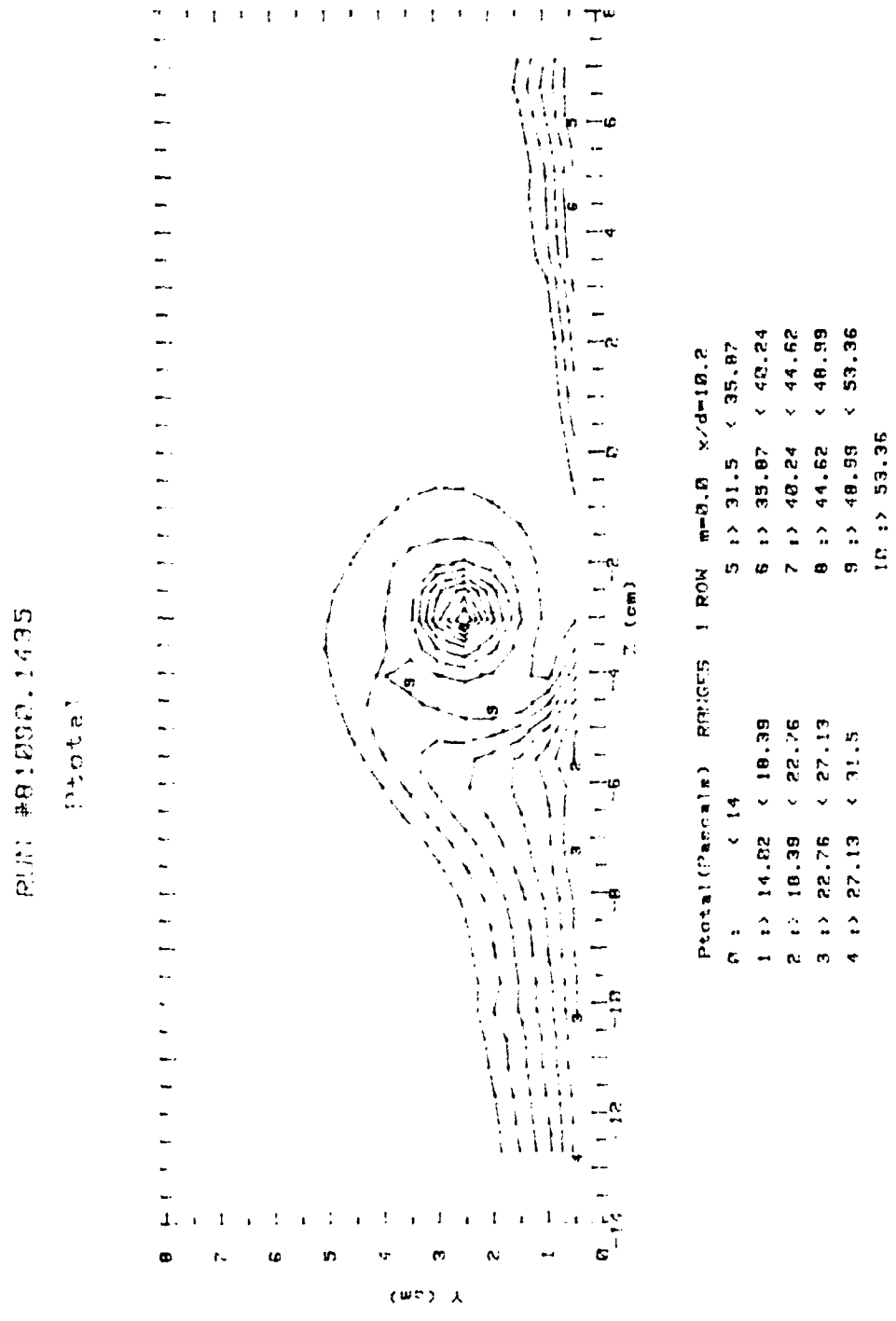

Figure 70. Total Pressure Field, x/d=10.2, No Film Cooling, Vortex R4

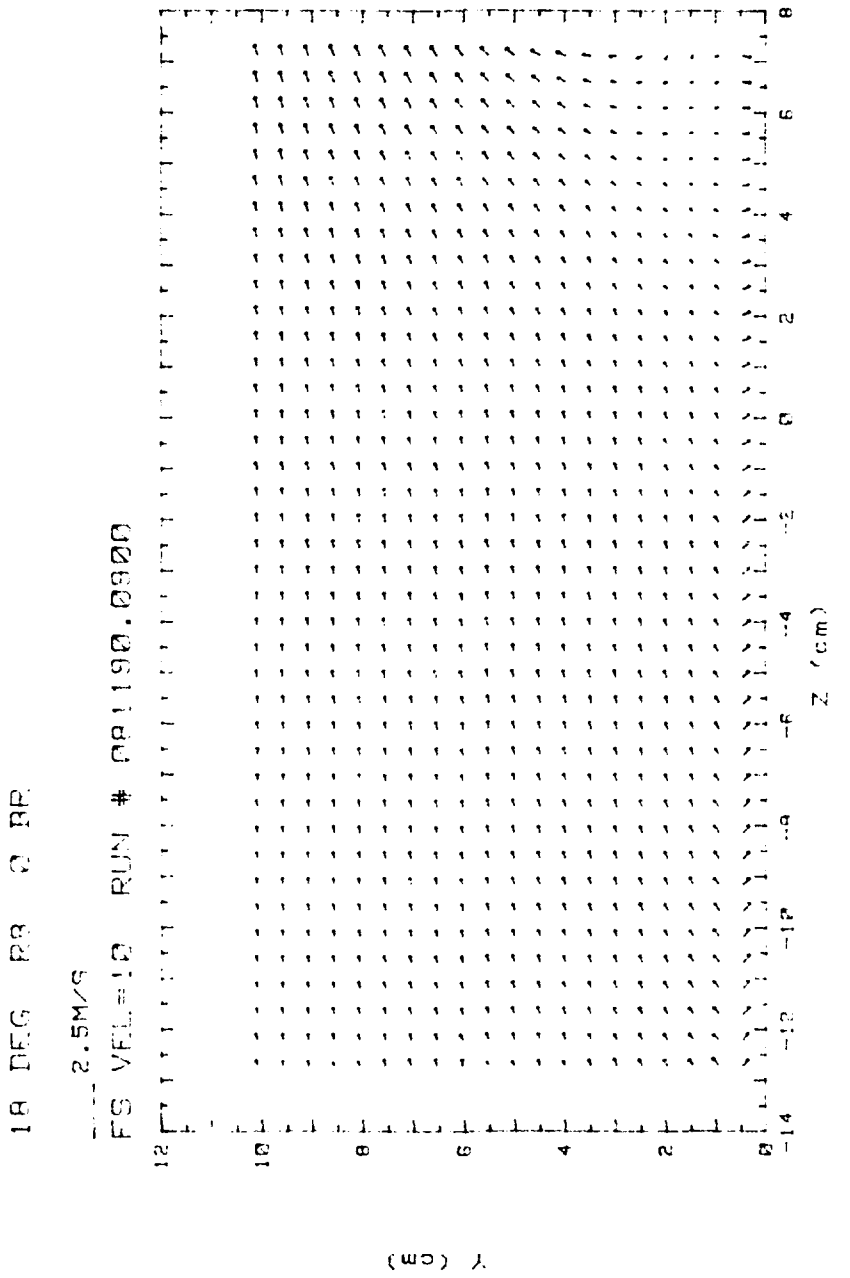

Figure 71. Secondary Flow Vectors, x/d=10.2, No Film Cooling, Vortex R8

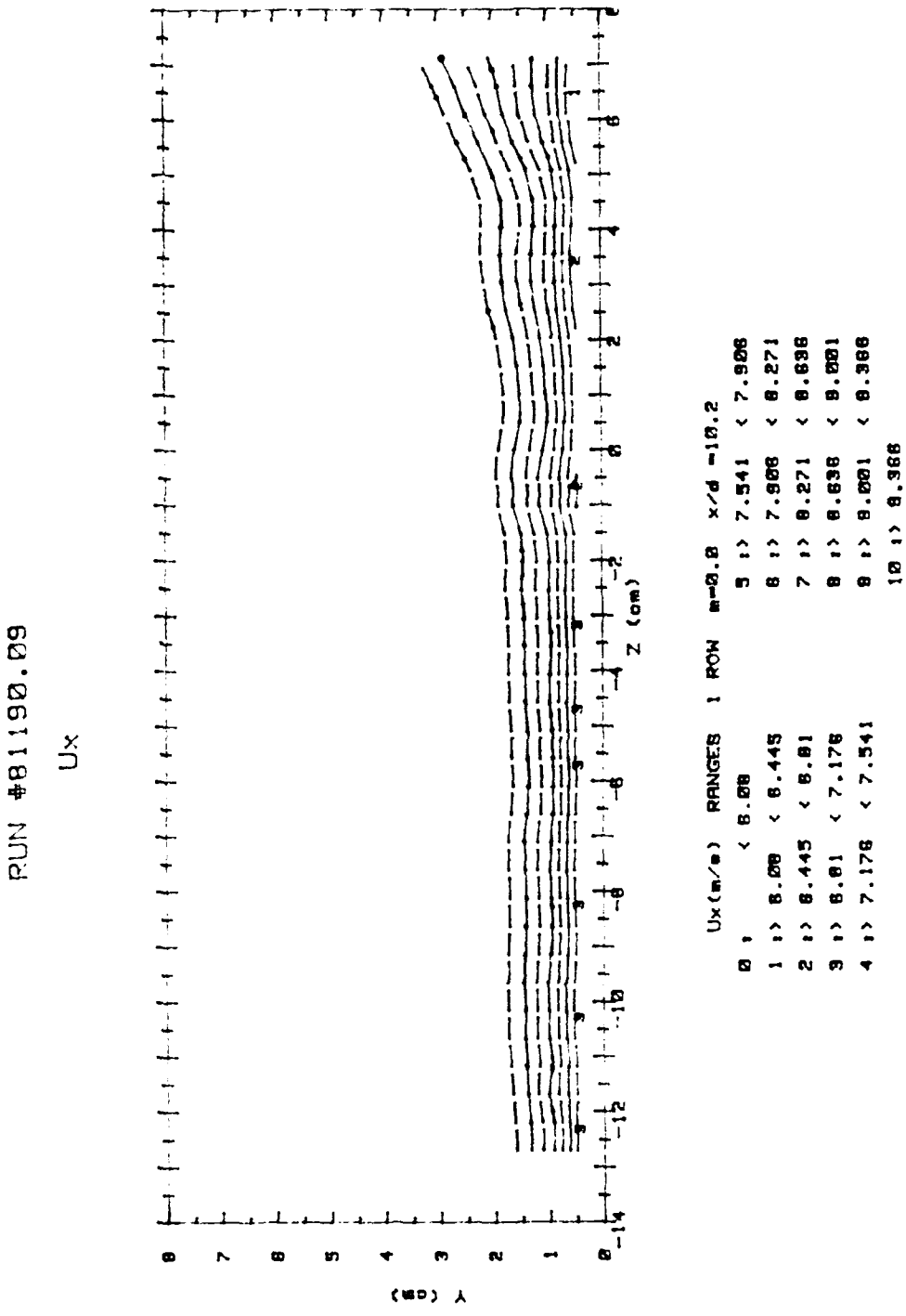

Figure 72. Streamwise Velocity Field, x/d=10.2, No Film Cooling. Vortex R8

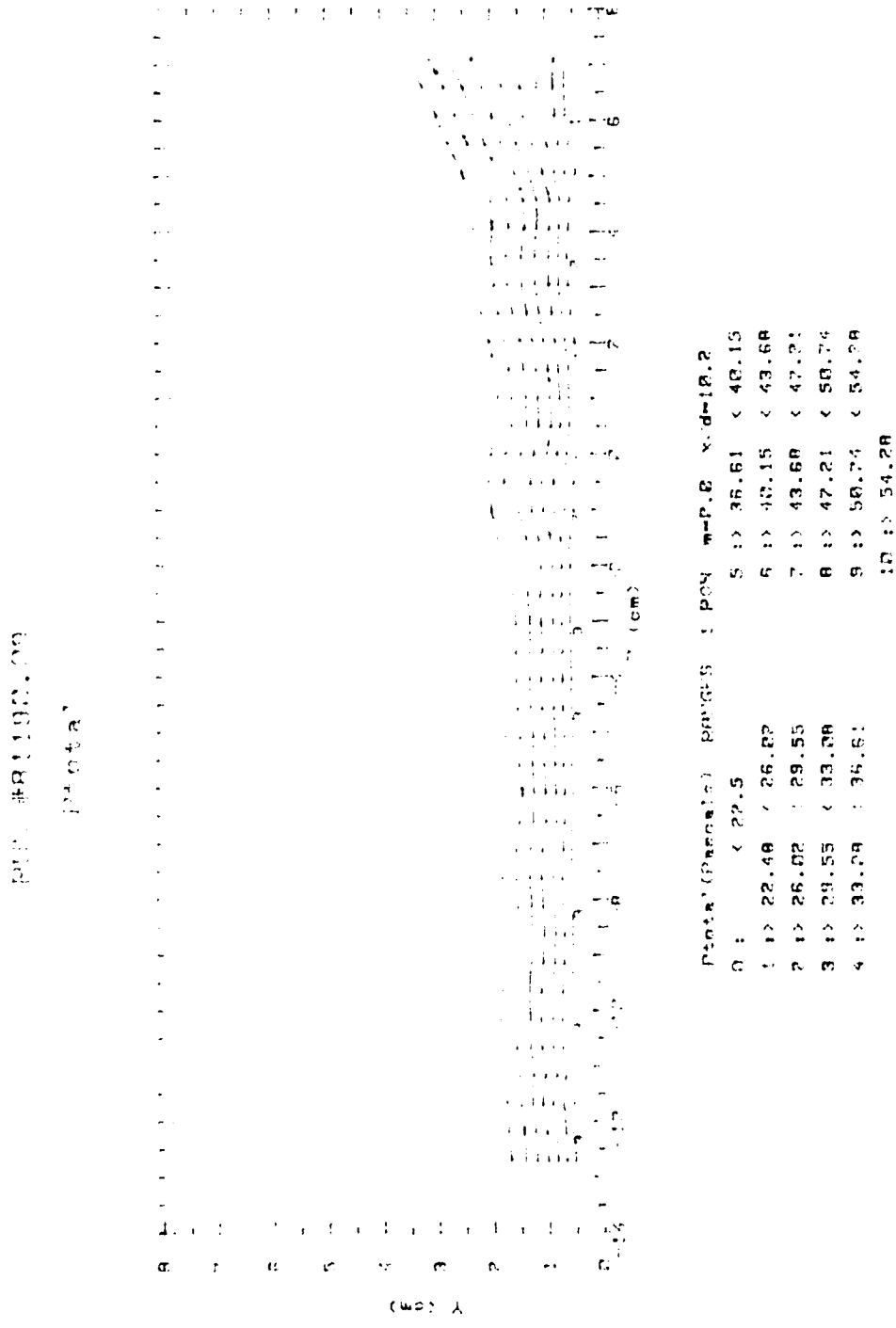

Figure 73. Total Pressure Field, x/d=10.2, No Film Cooling. Vortex R8

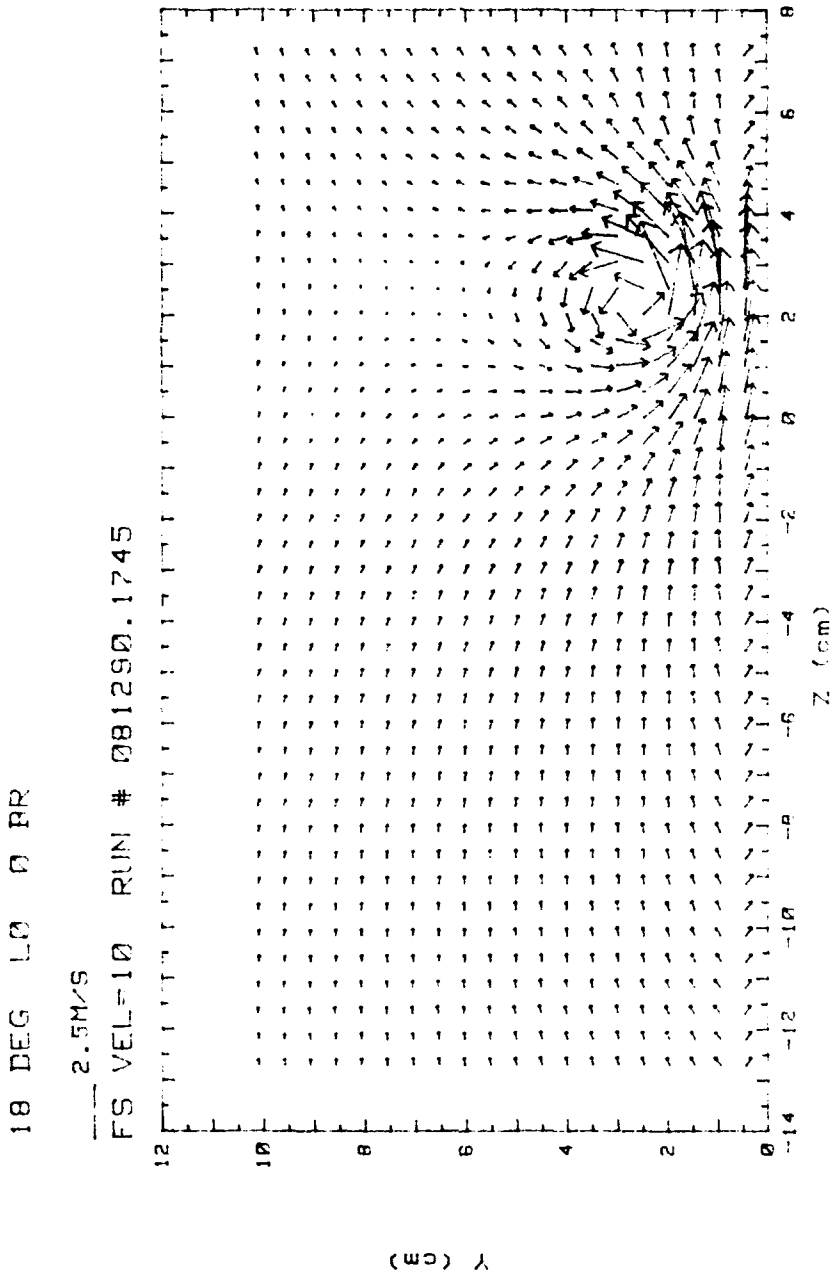

Figure 74. Secondary Flow Vectors, x/d=10.2, No Film Cooling, Vortex L0

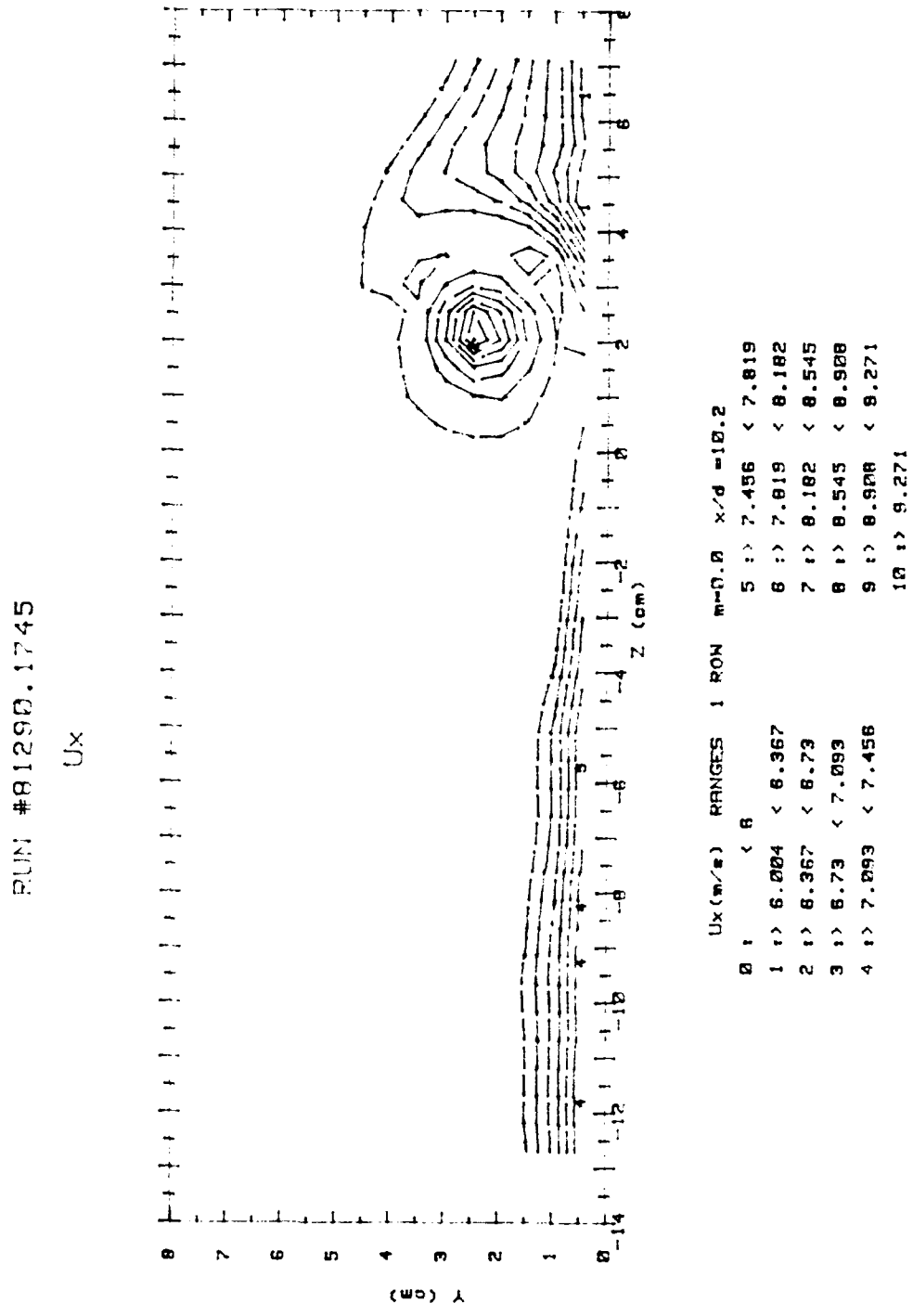

Figure 75. Streamwise Velocity Field, x/d=10.2, No Film Cooling, Vortex L0

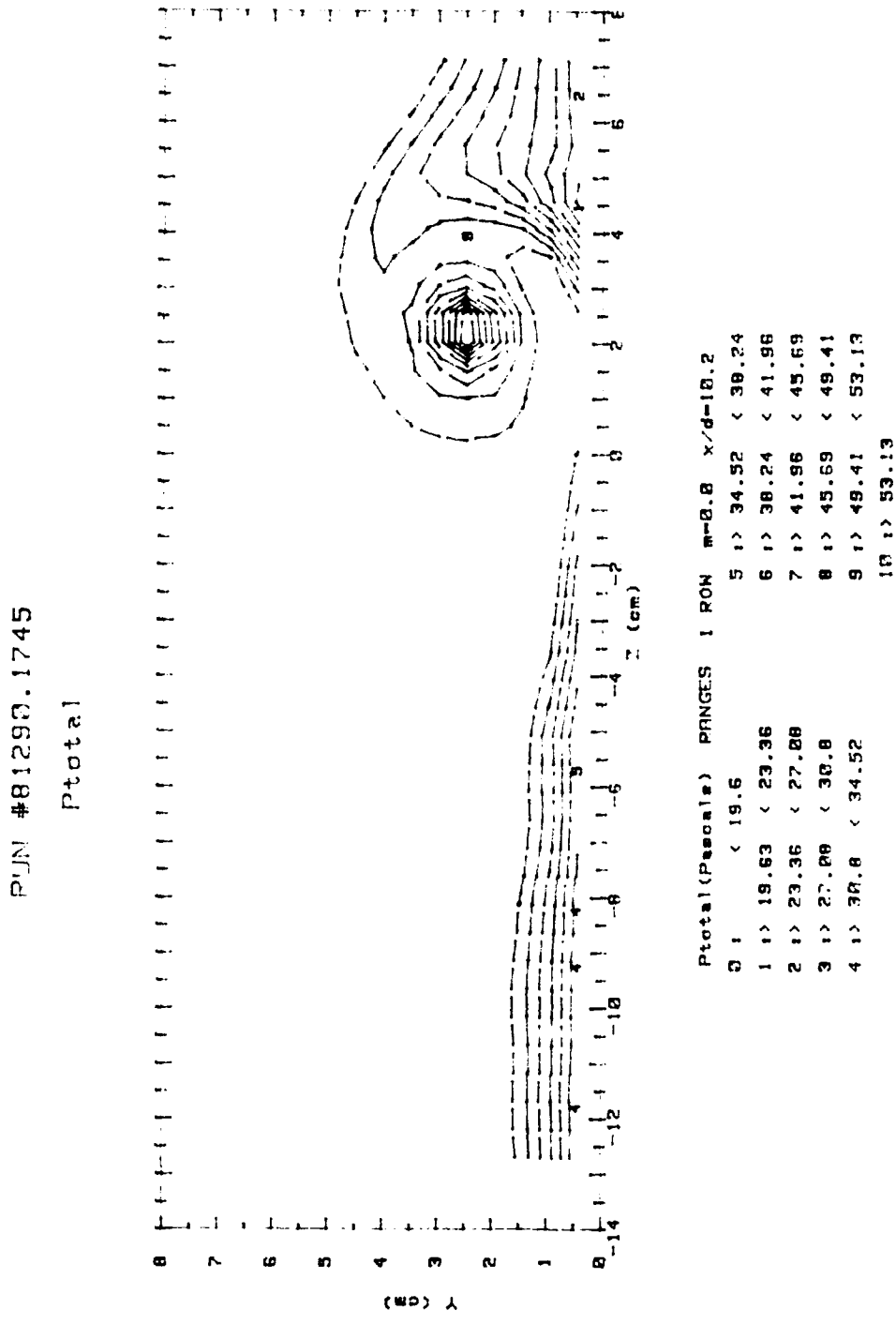

Figure 76. Total Pressure Field, x/d=10.2, No Film Cooling, Vortex L0

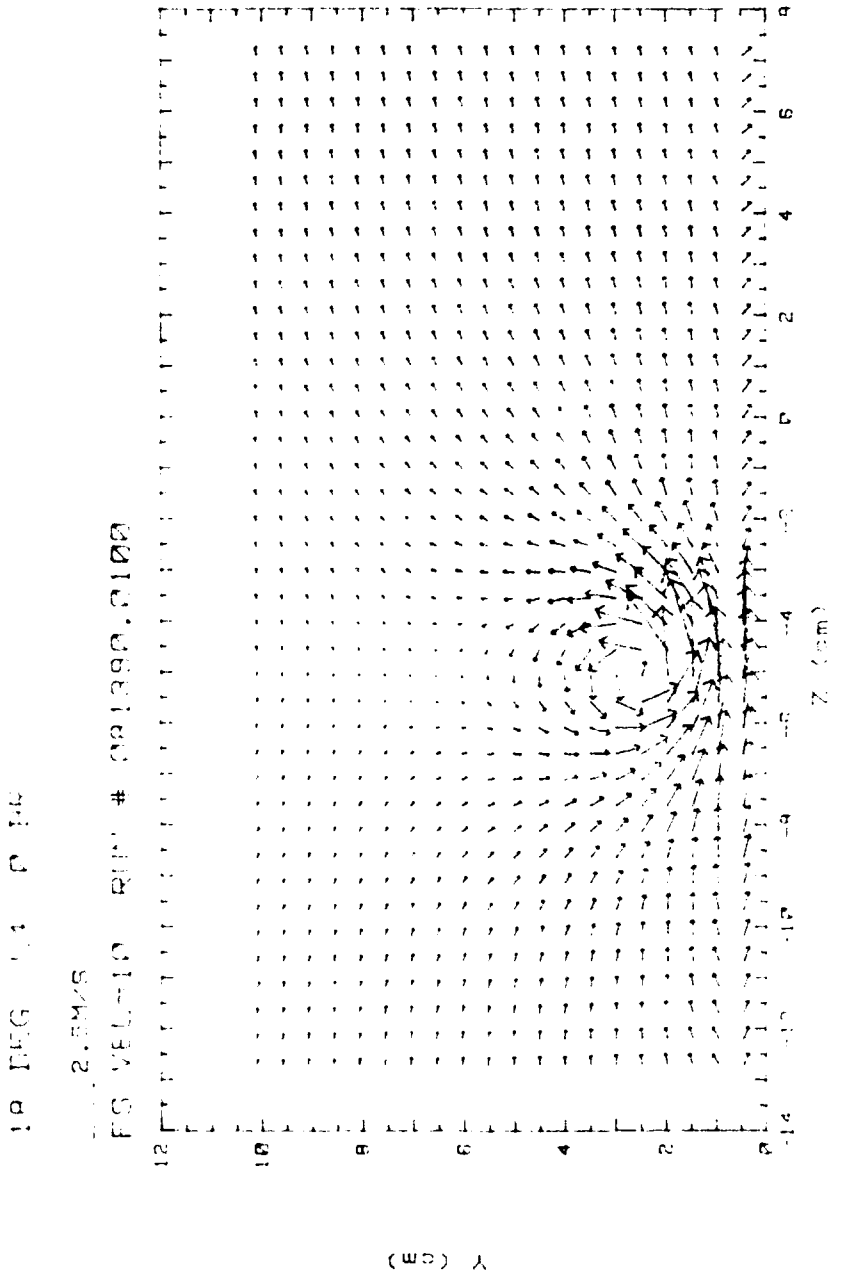

Figure 77. Secondary Flow Vectors, x/d=10.2, No Film Cooling, Vortex L4

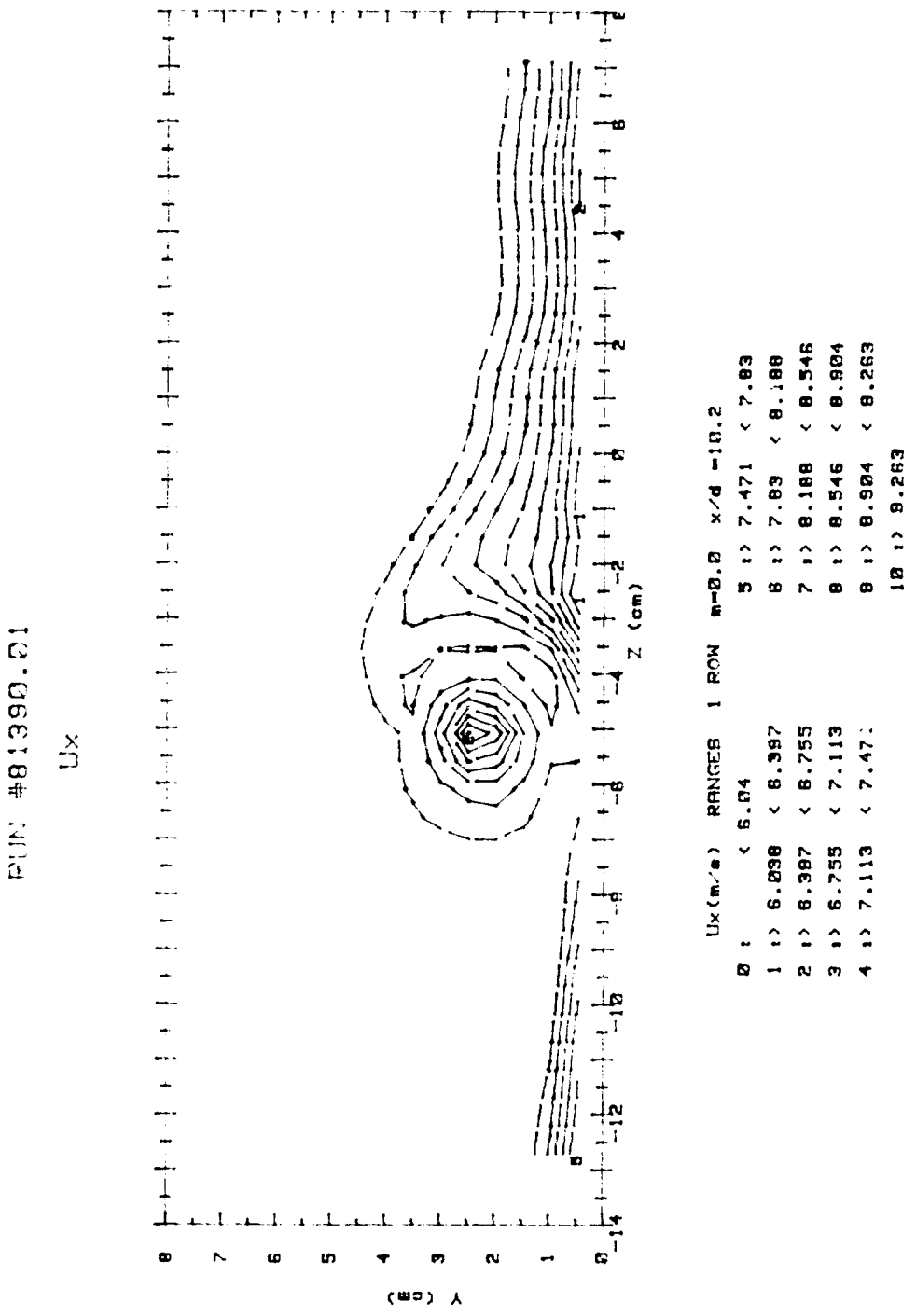

Figure 78. Streamwise Velocity Field, x/d=10.2, No Film Cooling, Vortex L4

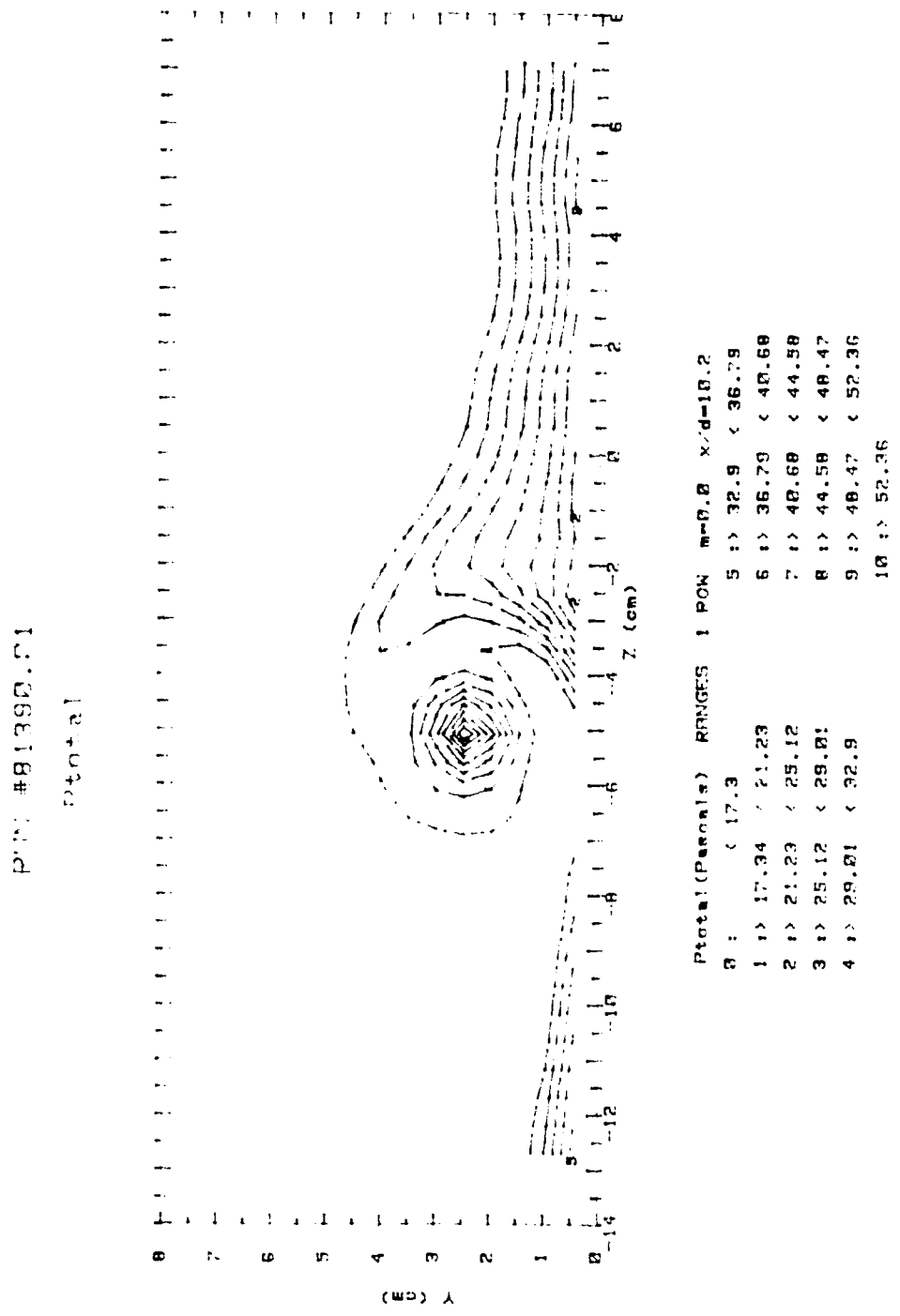

Figure 79. Total Pressure Field, x/d=10.2, No Film Cooling, Vortex L4

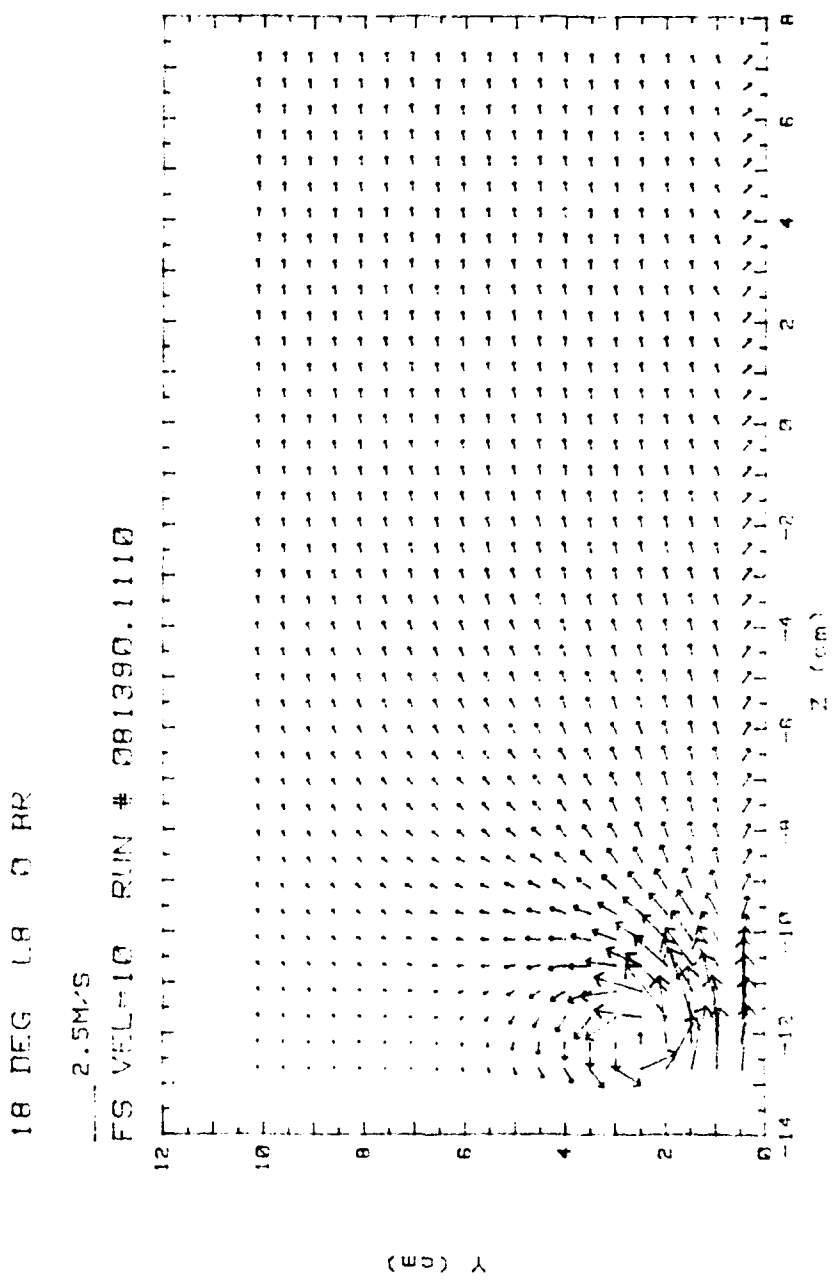

Figure 80. Secondary Flow Vectors, x/d=10.2, No Film Cooling. Vortex L8

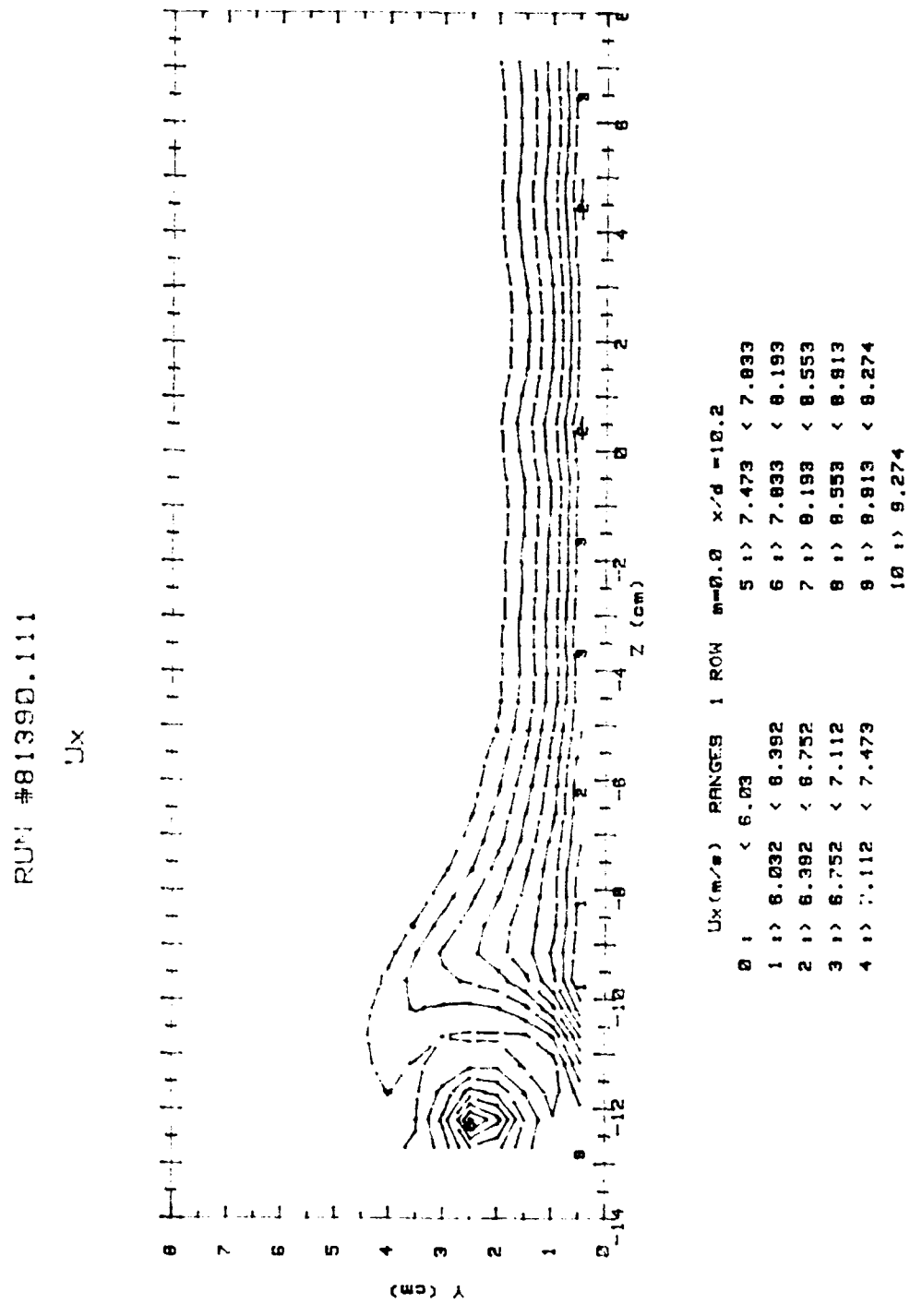

Figure 81. Streamwise Velocity Field, x/d=10.2, No Film Cooling, Vortex L8

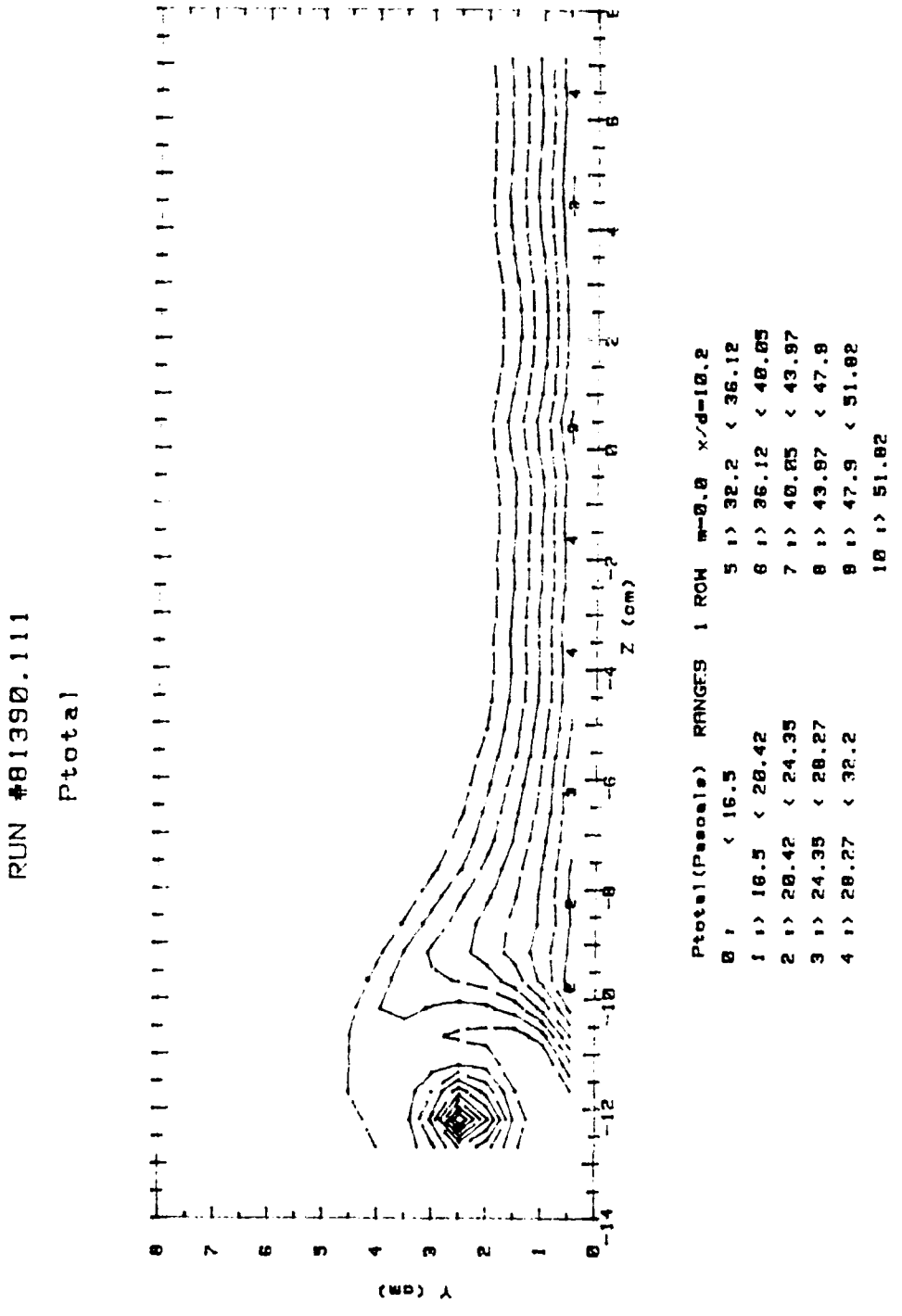

Figure 82. Total Pressure Field, x/d=10.2, No Film Cooling, Vortex L8

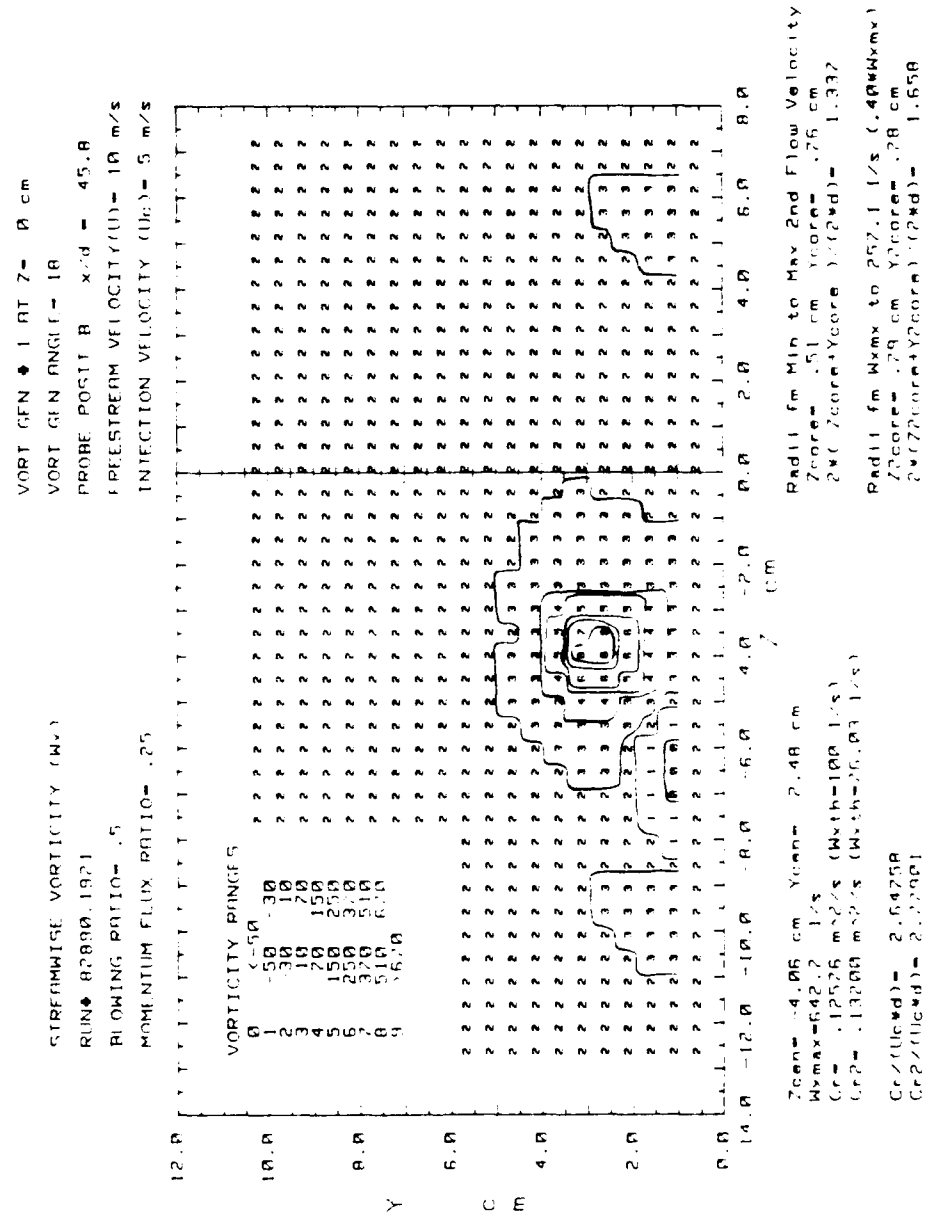

Figure 83. Streamwise Vorticity Contours, x/d=45.8, One Row Film Cooling, Vortex R0

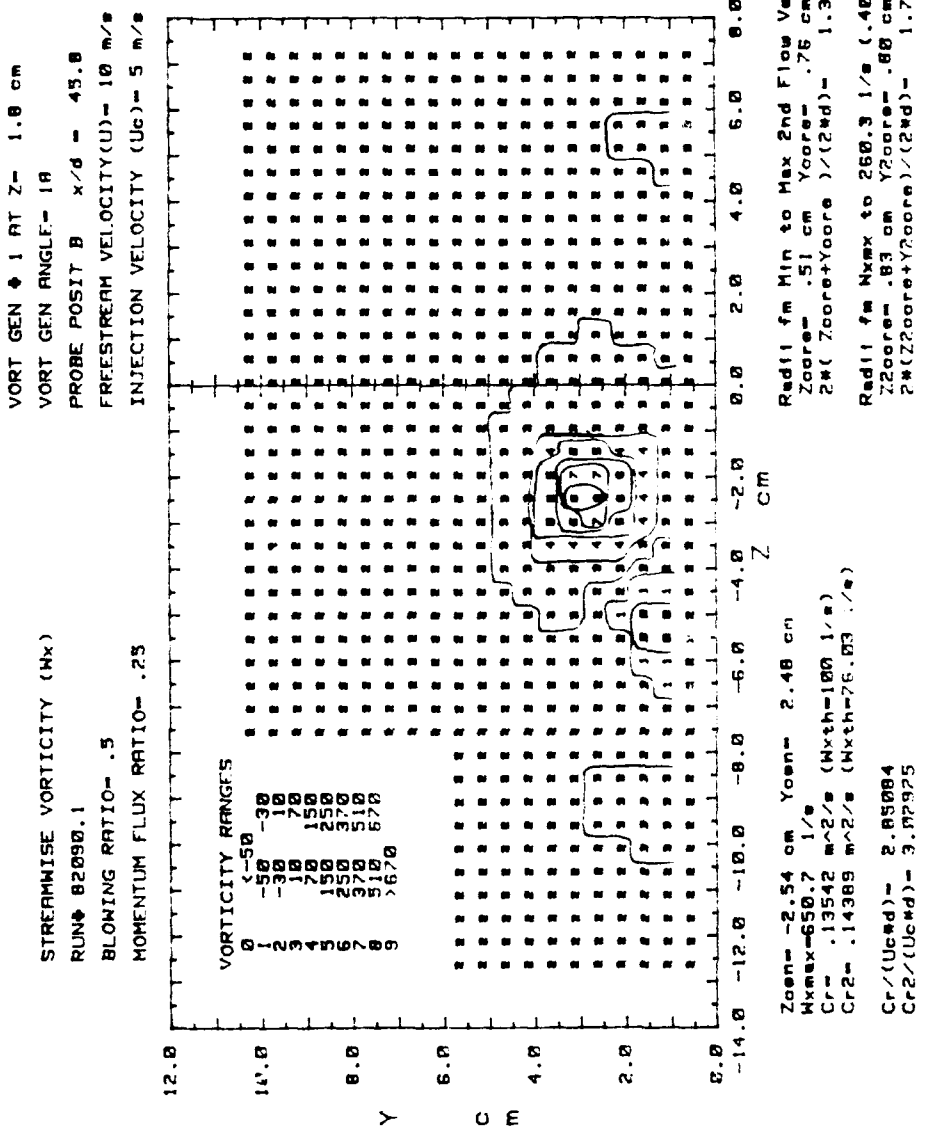

Figure 84. Streamwise Vorticity Contours, x/d=45.8, One Row Film Cooling, Vortex R1

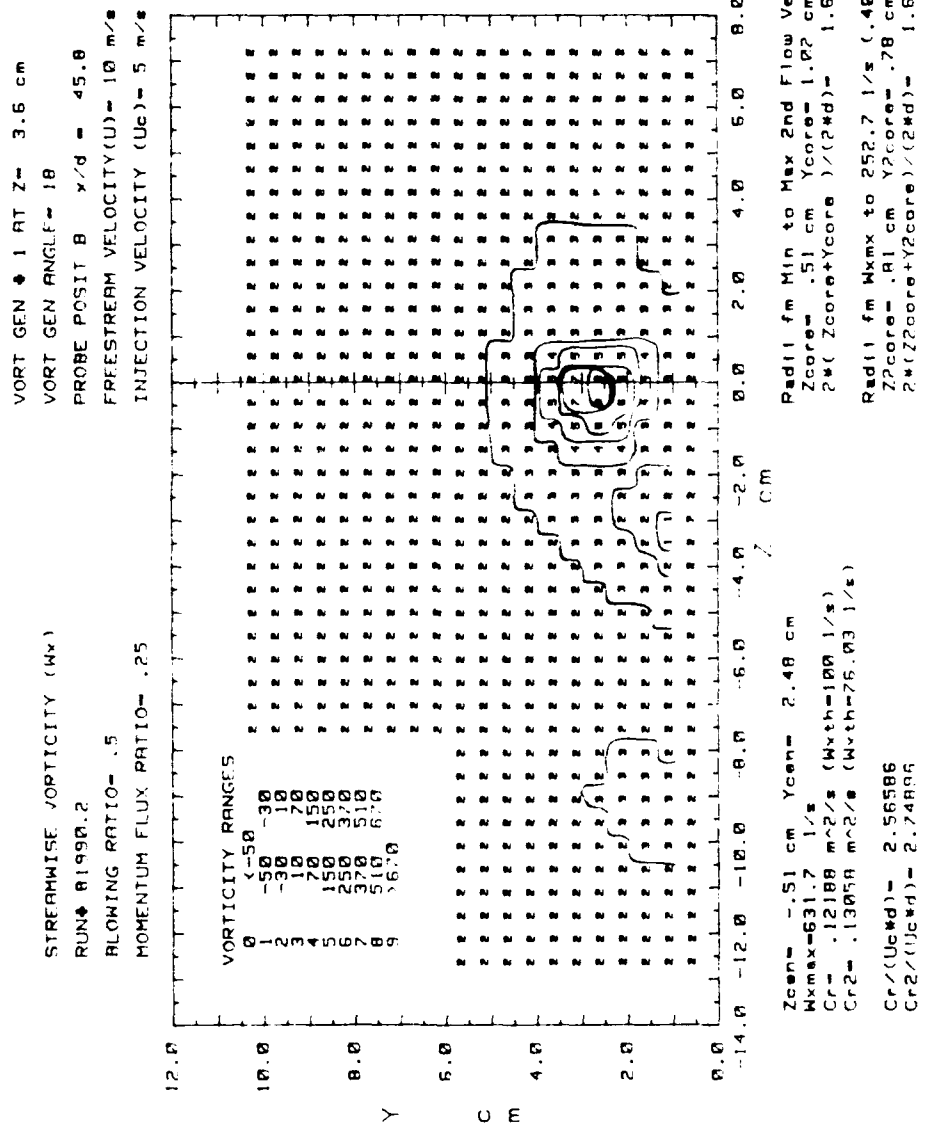

Figure 85. Streamwise Vorticity Contours, x/d=45.8, One Row Film Cooling, Vortex R2

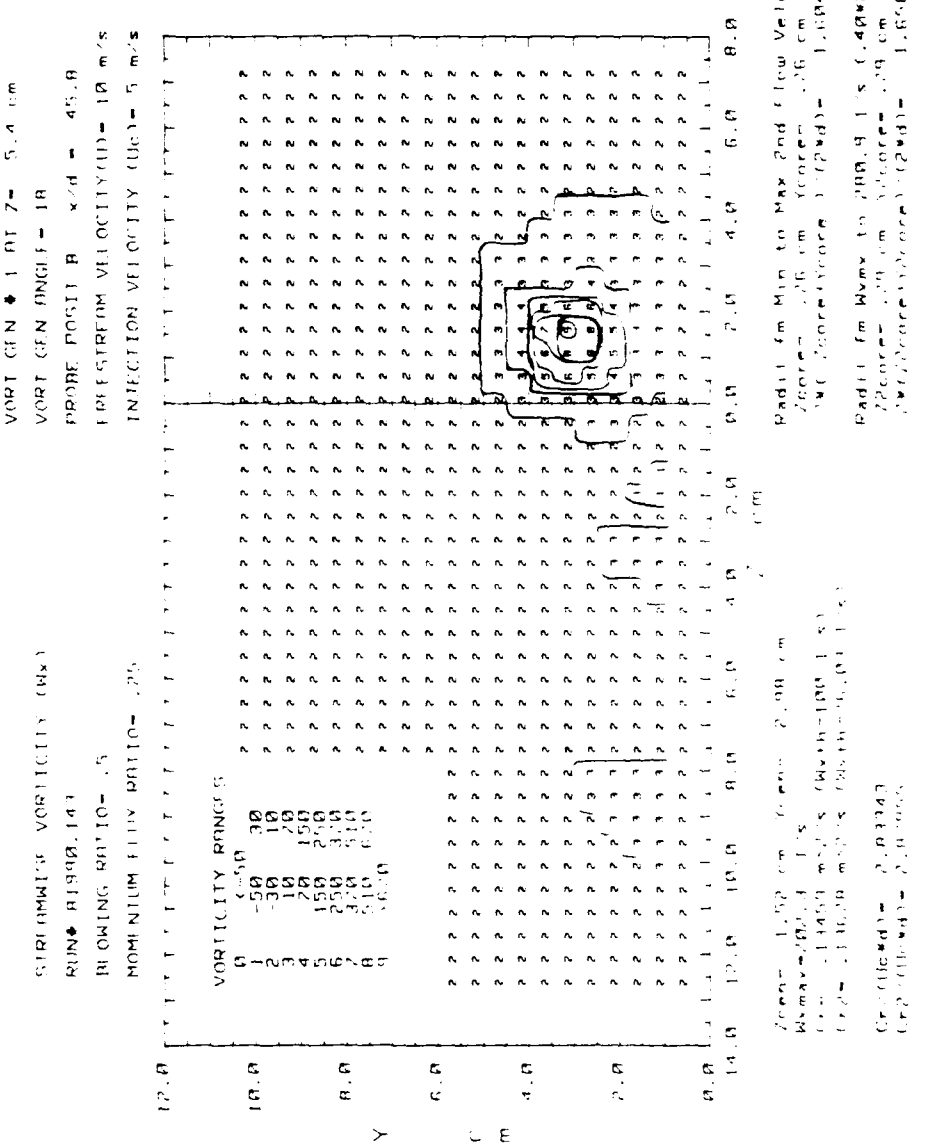

Figure 86. Streamwise Vorticity Contours, x/d=45.8, One Row Film Cooling, Vortex R3

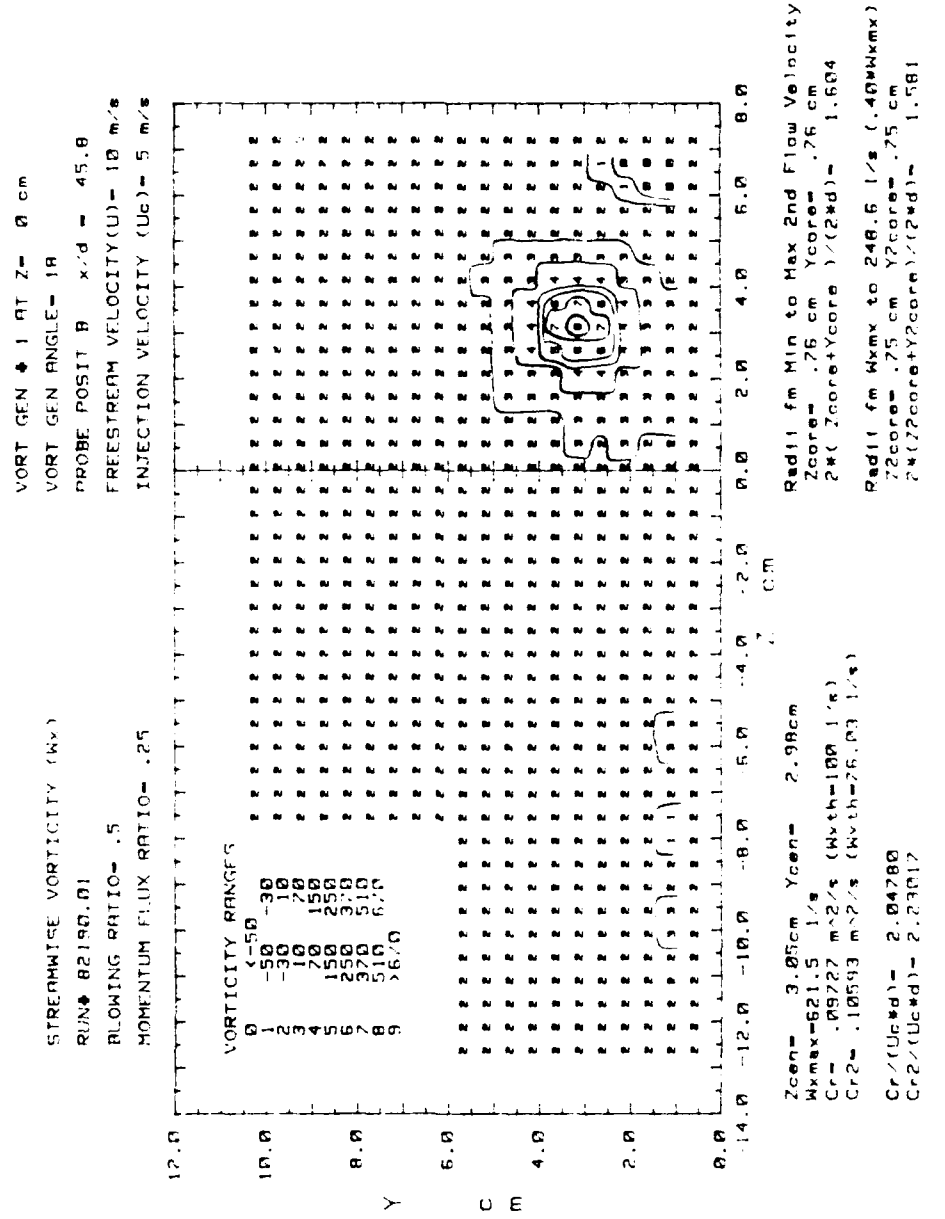

Figure 87. Streamwise Vorticity Contours, x/d=45.8, One Row Film Cooling, Vortex L0

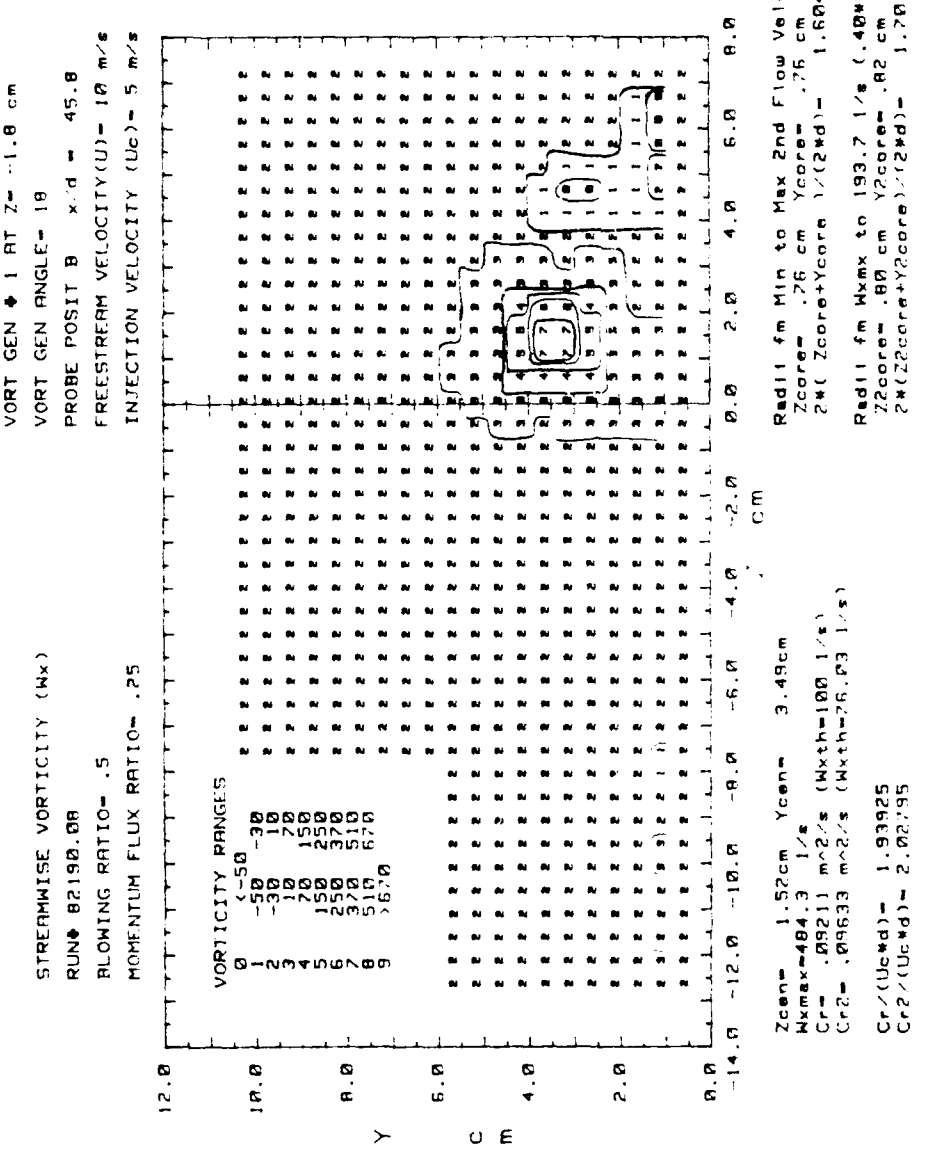

Figure 88. Streamwise Vorticity Contours, x/d=45.8, One Row Film Cooling, Vortex L1

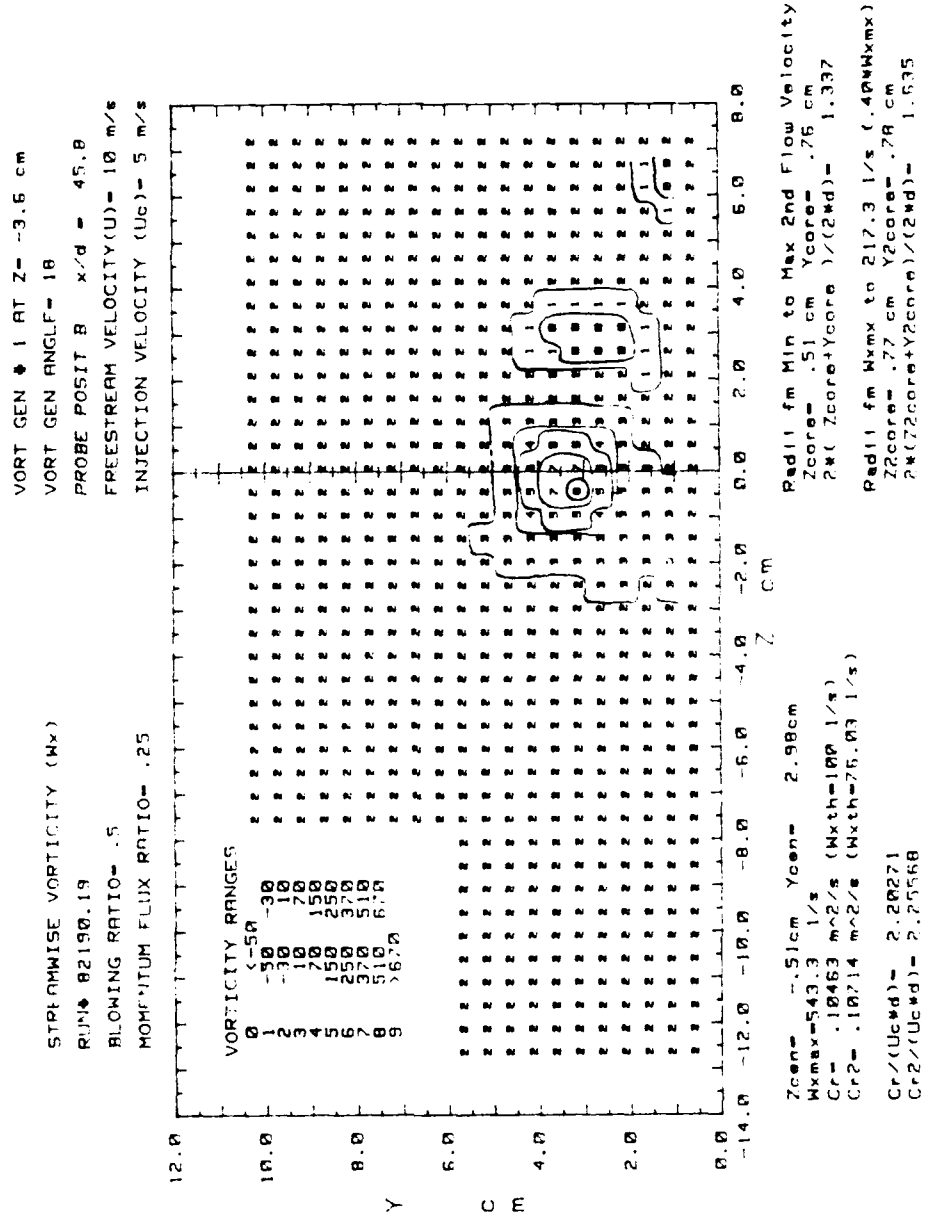

Figure 89. Streamwise Vorticity Contours, x/d=45.8, One Row Film Cooling, Vortex L2

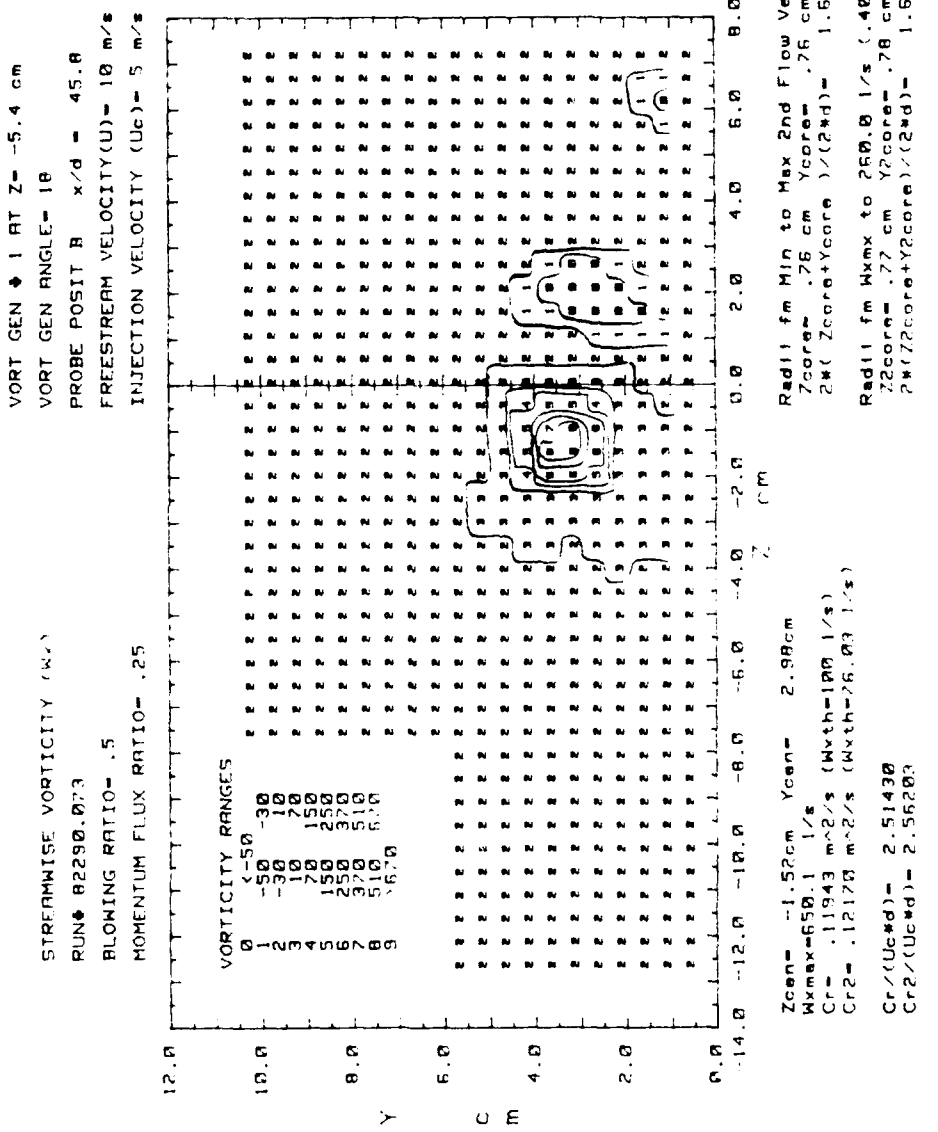

Figure 90. Streamwise Vorticity Contours, x/d=45.8, One Row Film Cooling, Vortex L3

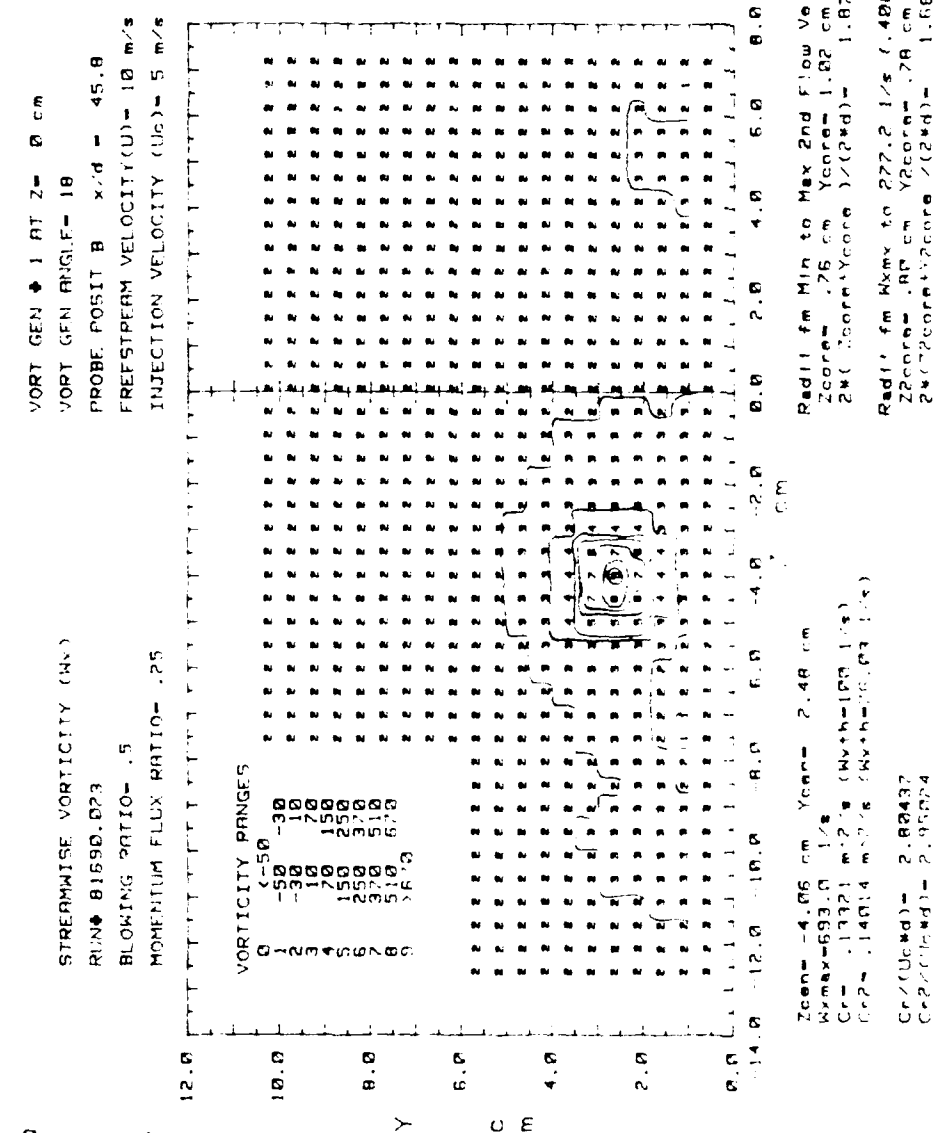

Figure 91. Streamwise Vorticity Contours, x/d=45.8, Two Rows Film Cooling, Vortex R0

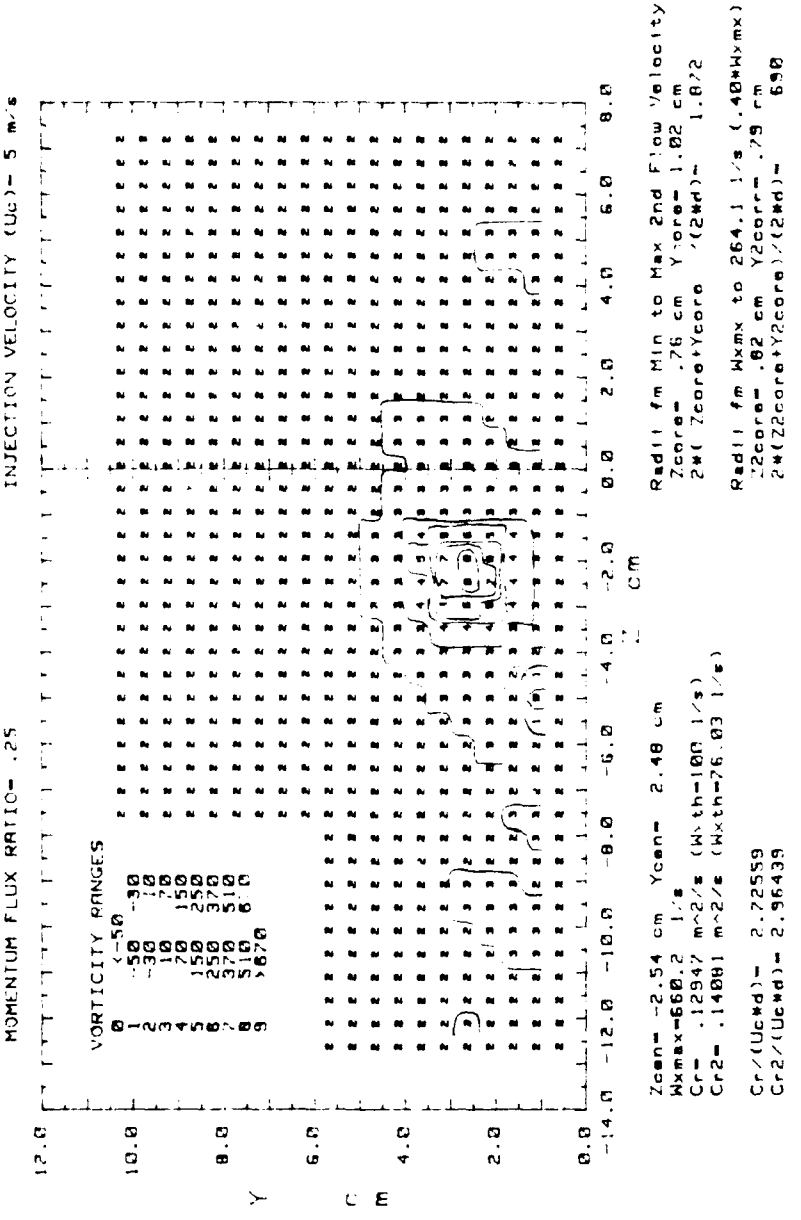

Figure 92. Streamwise Vorticity Contours, x/d=45.8, Two Rows Film Cooling, Vortex R1

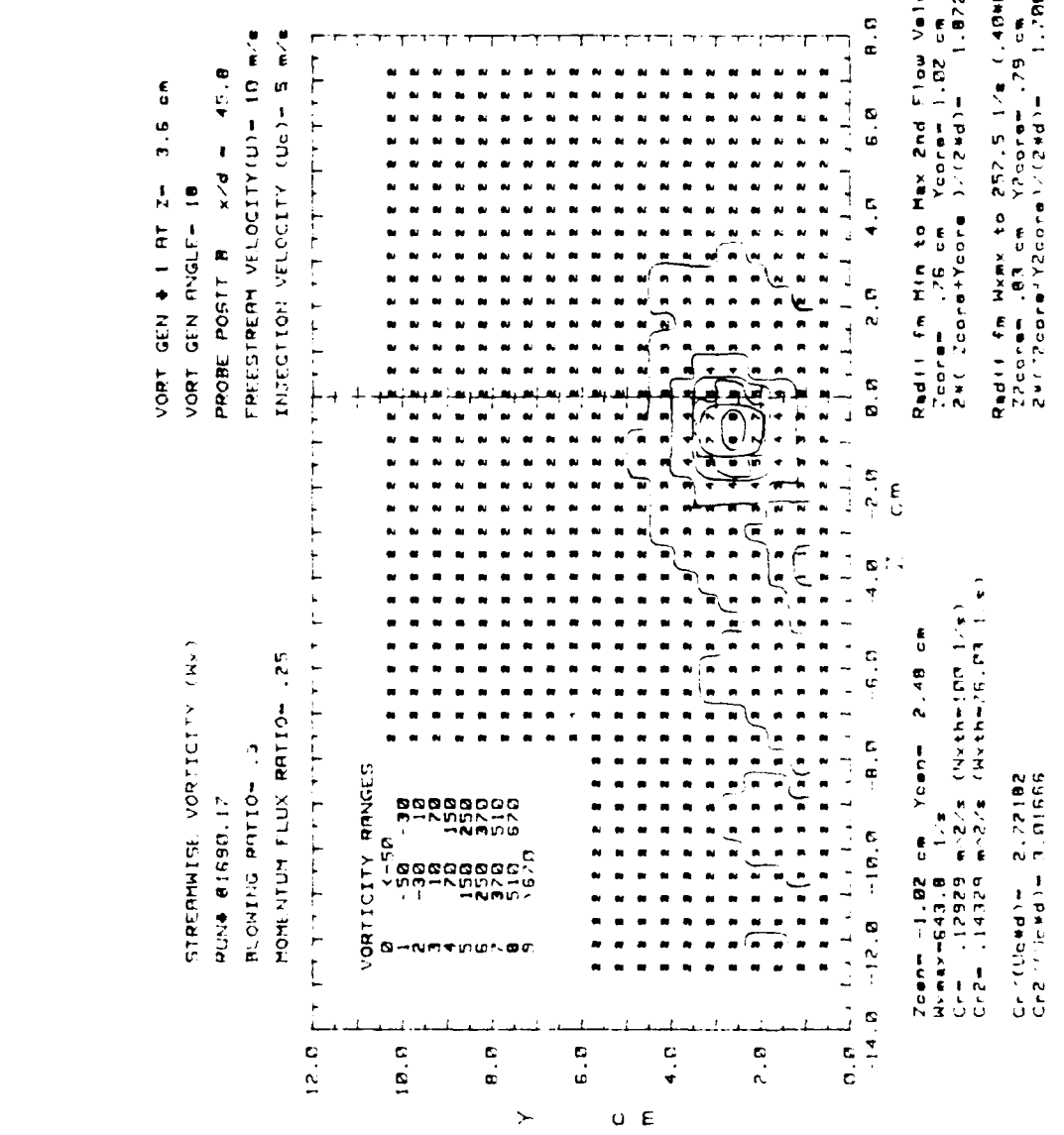

Figure 93. Streamwise Vorticity Contours, x/d=45.8, Two Rows Film Cooling, Vortex R2

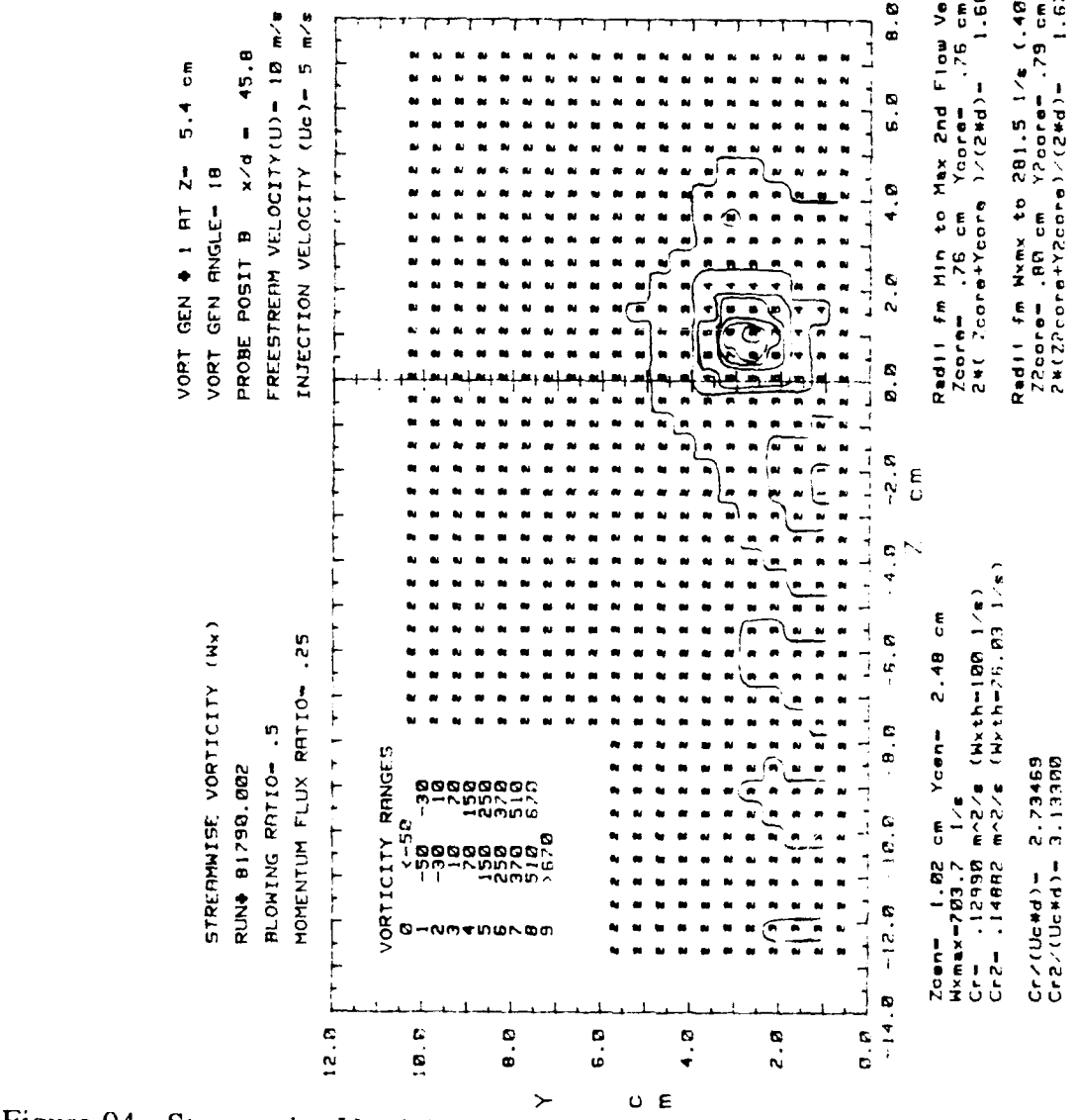

Figure 94. Streamwise Vorticity Contours, x/d=45.8, Two Rows Film Cooling, Vortex R3

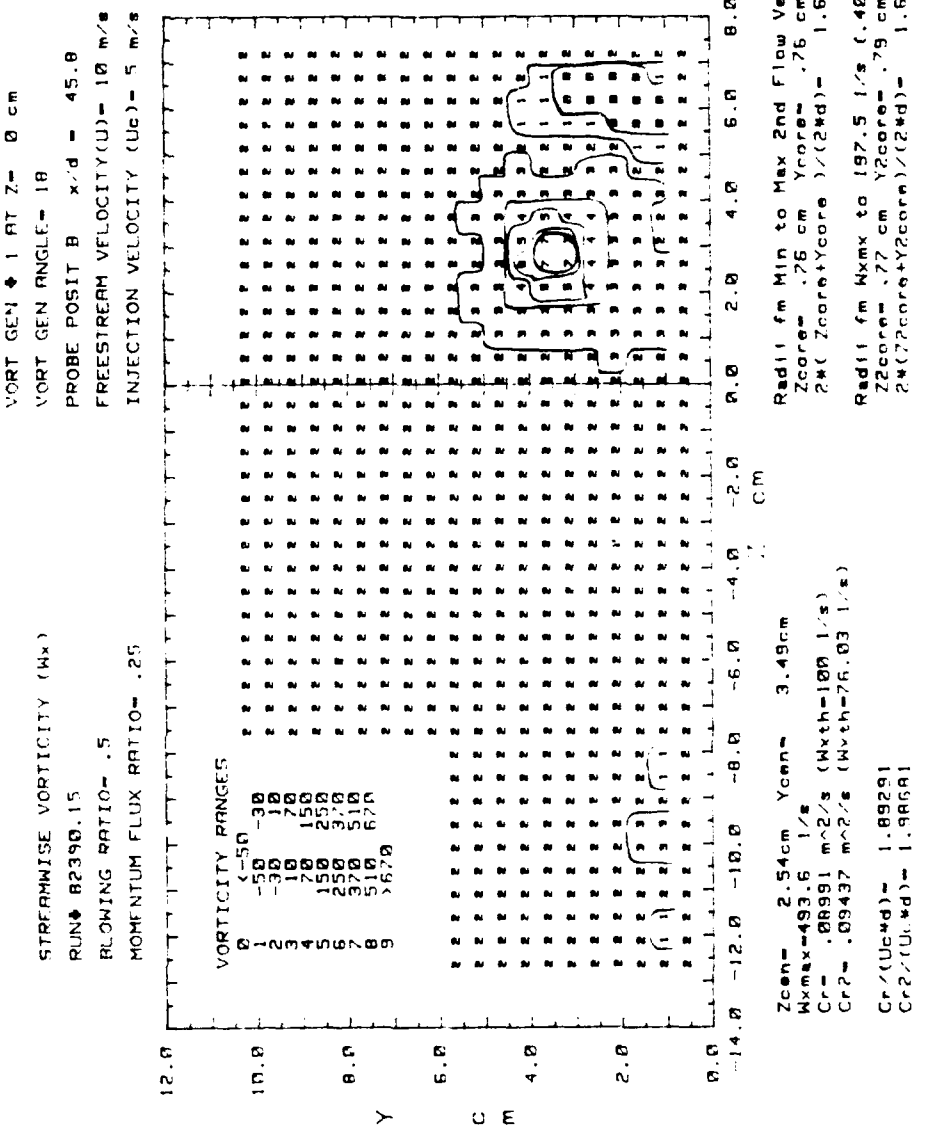

Figure 95. Streamwise Vorticity Contours, x/d=45.8, Two Rows Film Cooling, Vortex L0

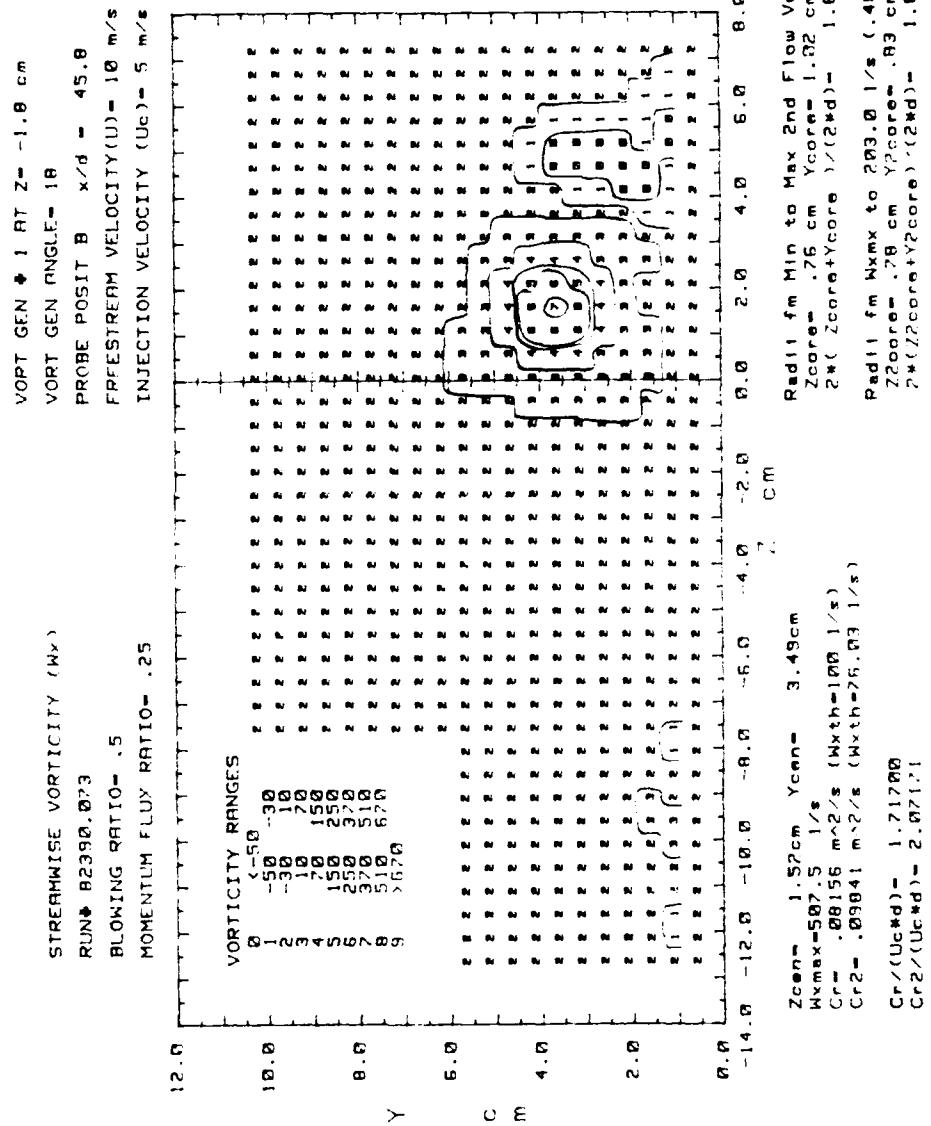

Figure 96. Streamwise Vorticity Contours, x/d=45.8, Two Rows Film Cooling, Vortex L1

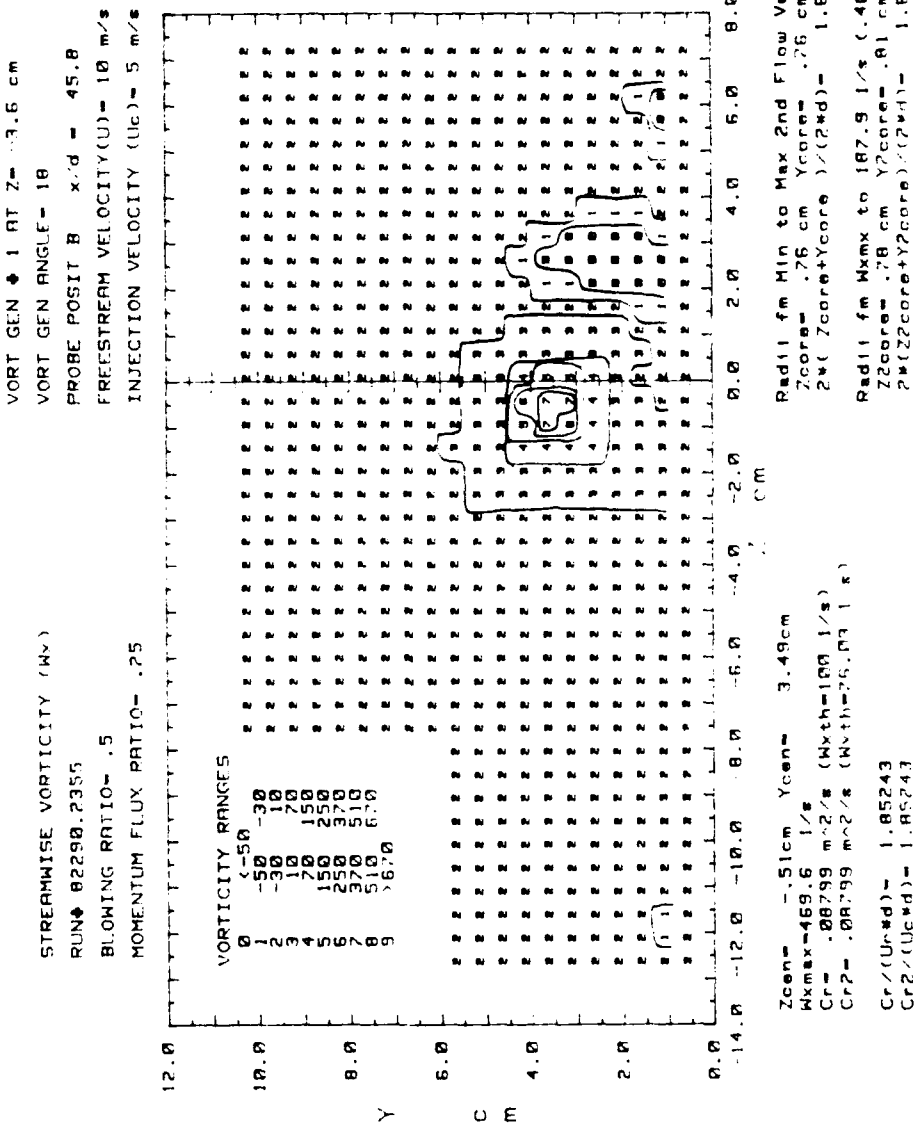

Figure 97. Streamwise Vorticity Contours, x/d=45.8, Two Rows Film Cooling, Vortex L2

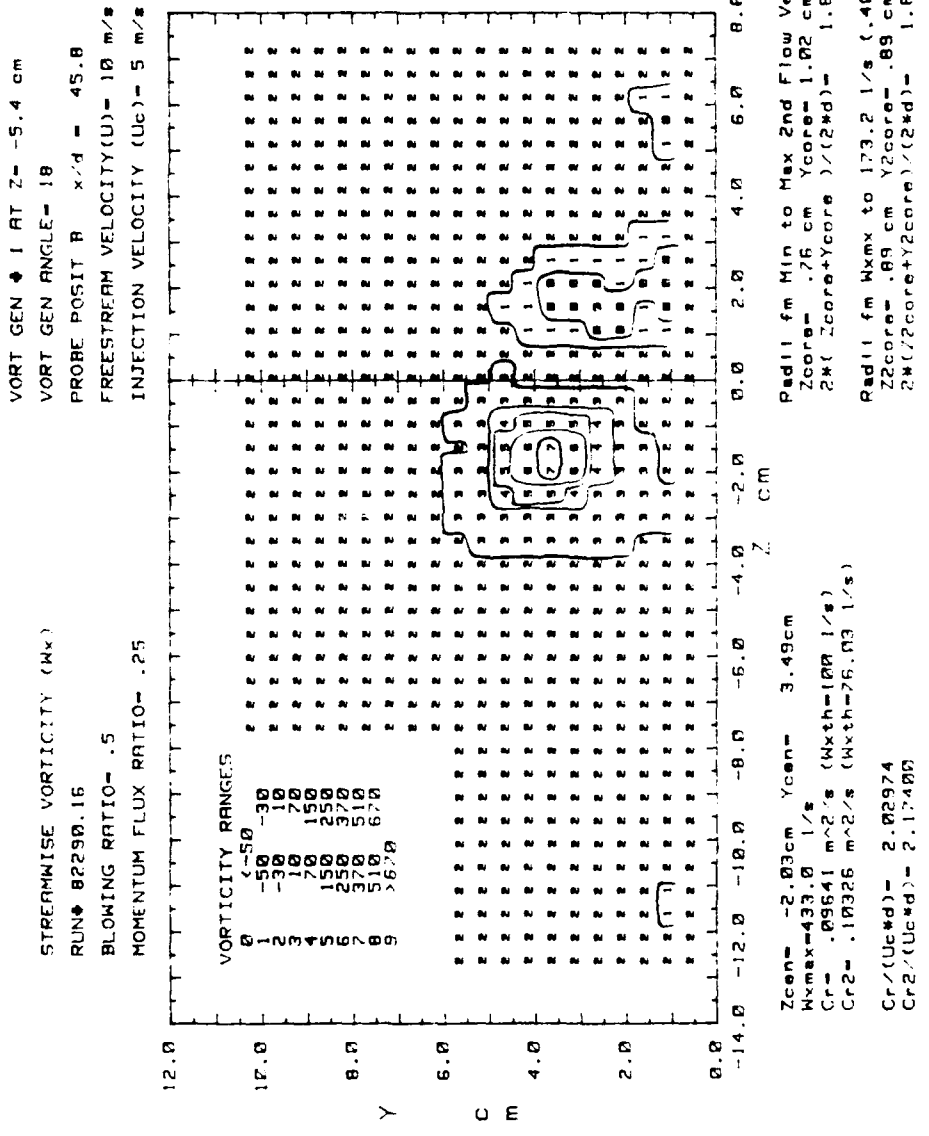

Figure 98. Streamwise Vorticity Contours, x/d=45.8, Two Rows Film Cooling, Vortex L3

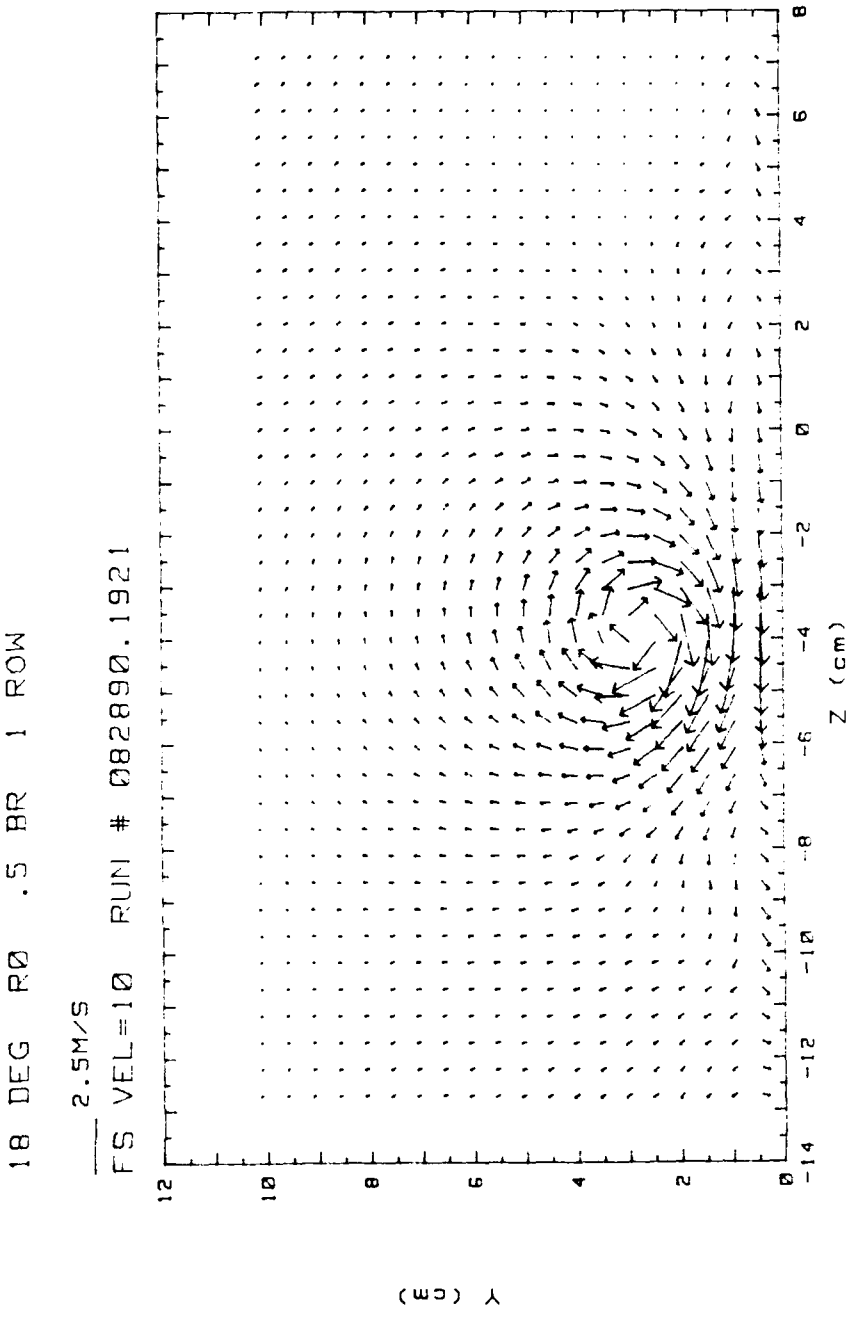

Figure 99. Secondary Flow Vectors, x/d=45.8, 1 Row, Vortex R0

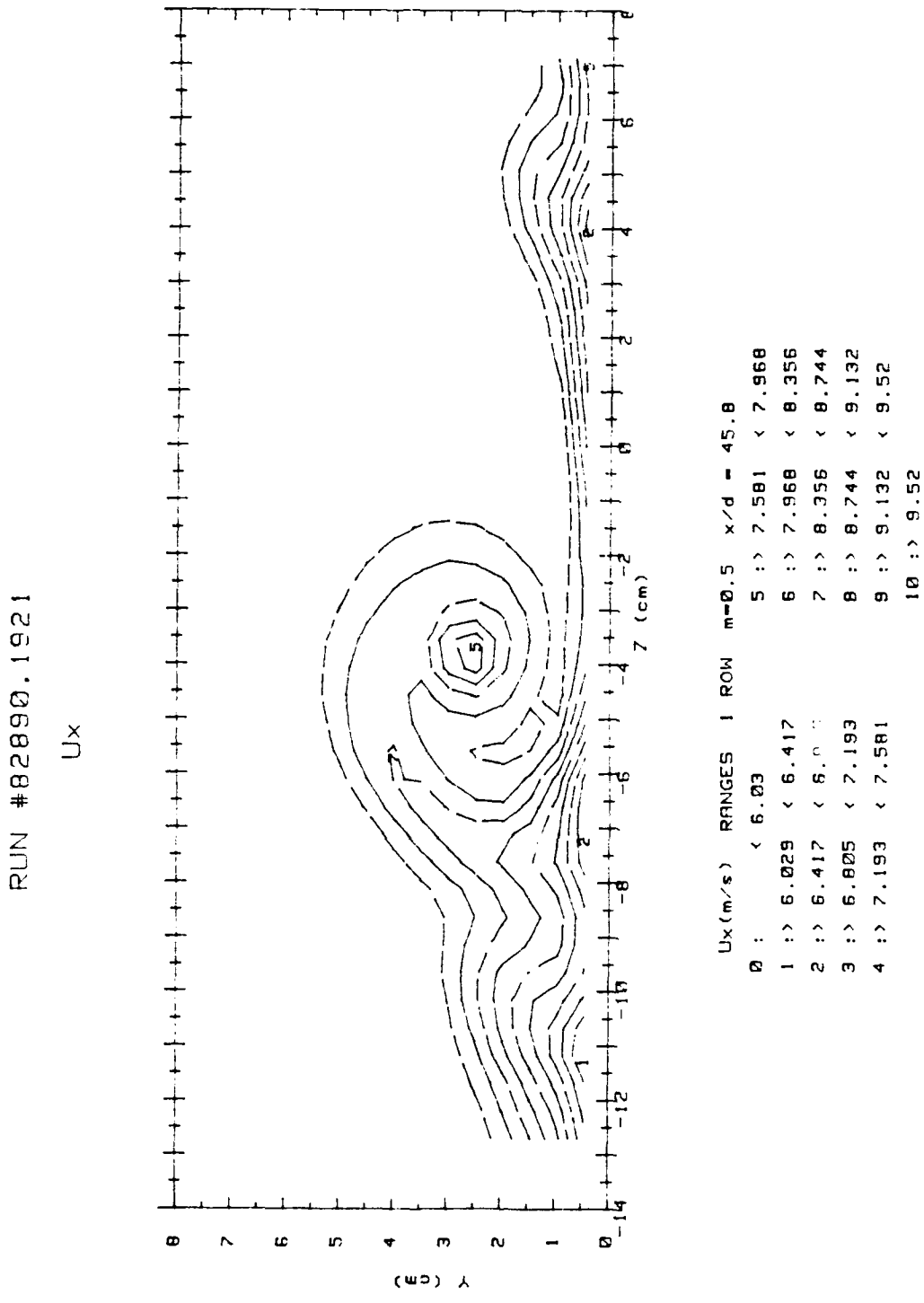

Figure 100. Streamwise Velocity Field, x/d=45.8, 1 Row, Vortex R0

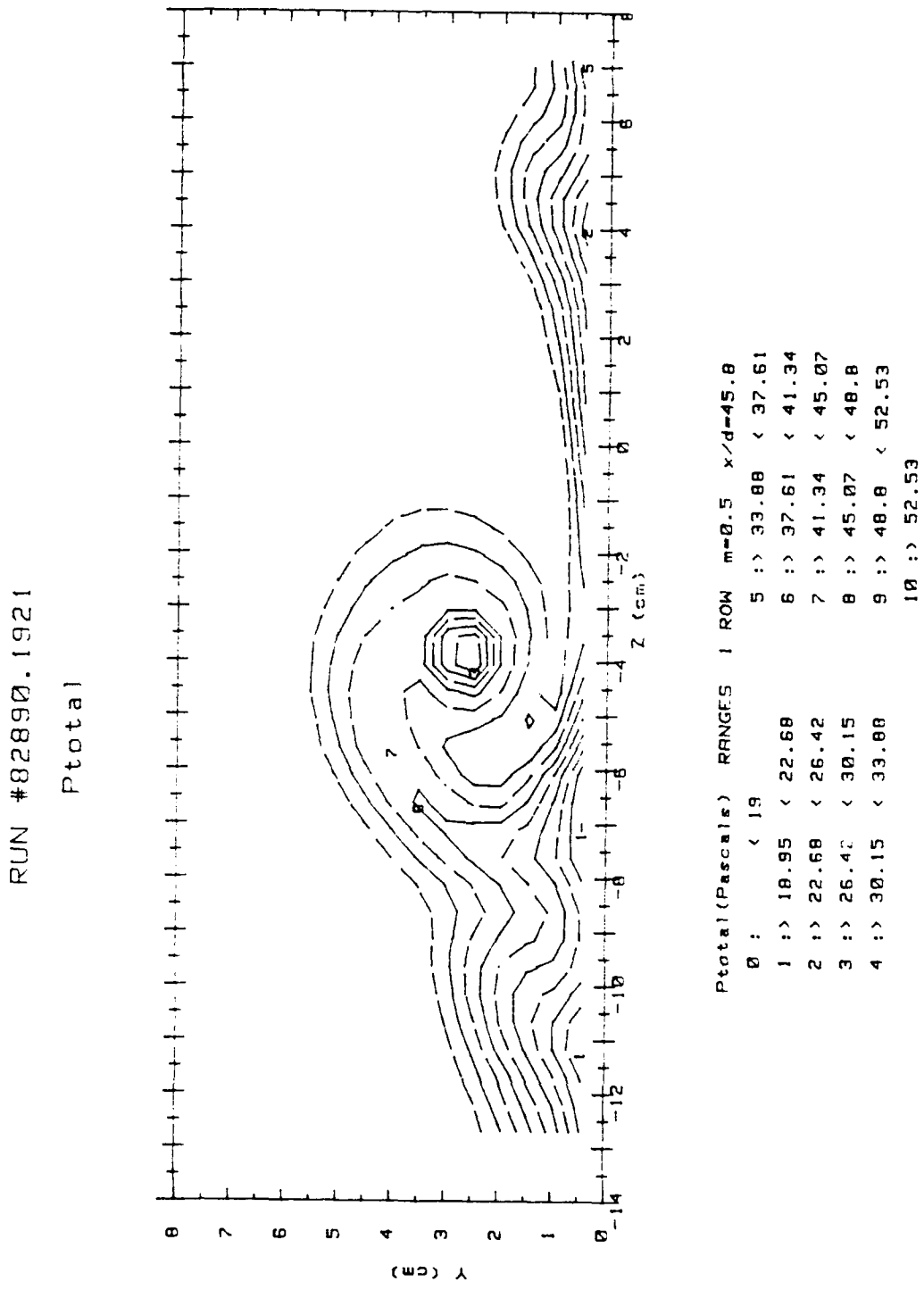

Figure 101. Total Pressure Field, x/d=45.8, 1 Row, Vortex R0

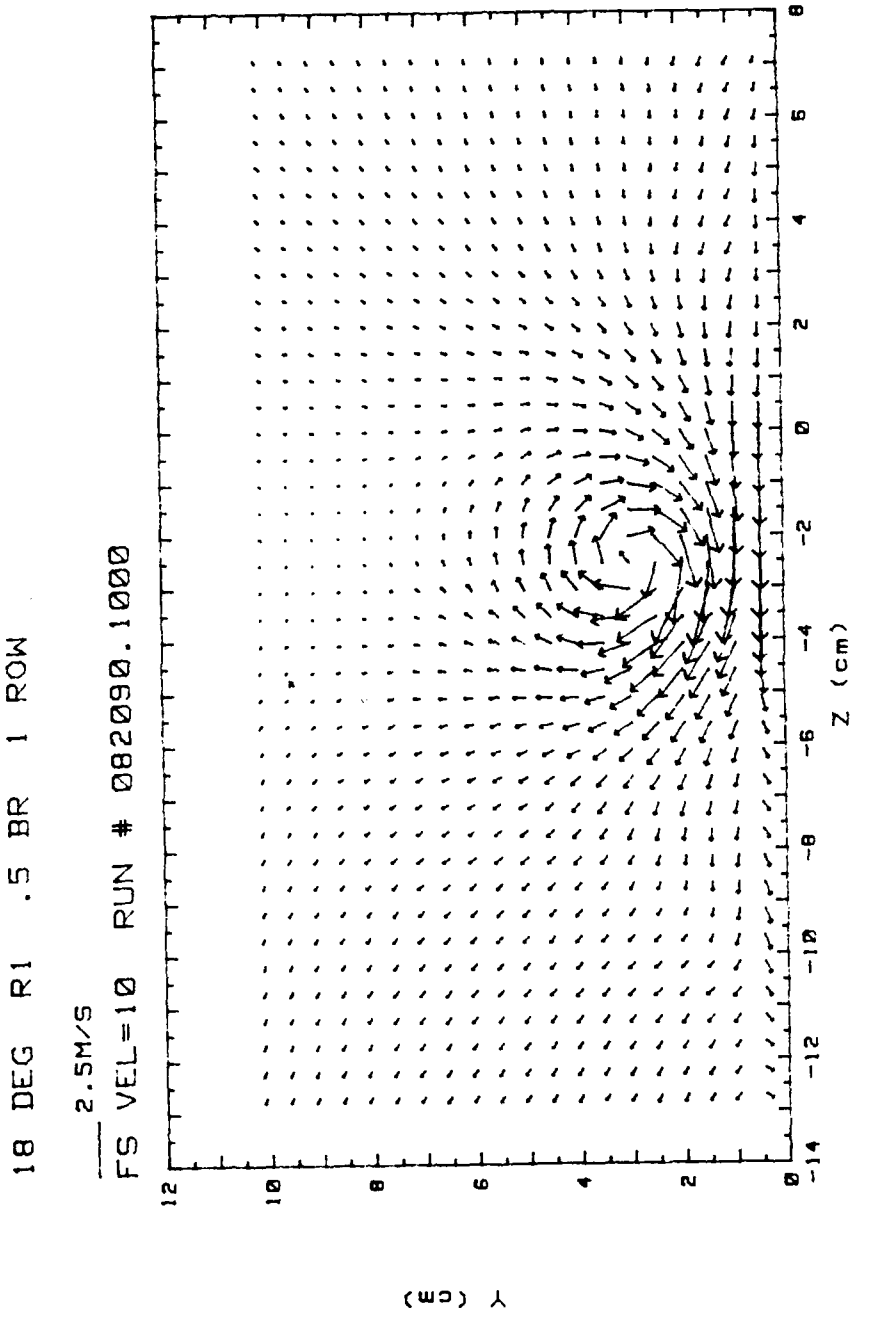

Figure 102. Secondary Flow Vectors, x/d=45.8, 1 Row, Vortex R1

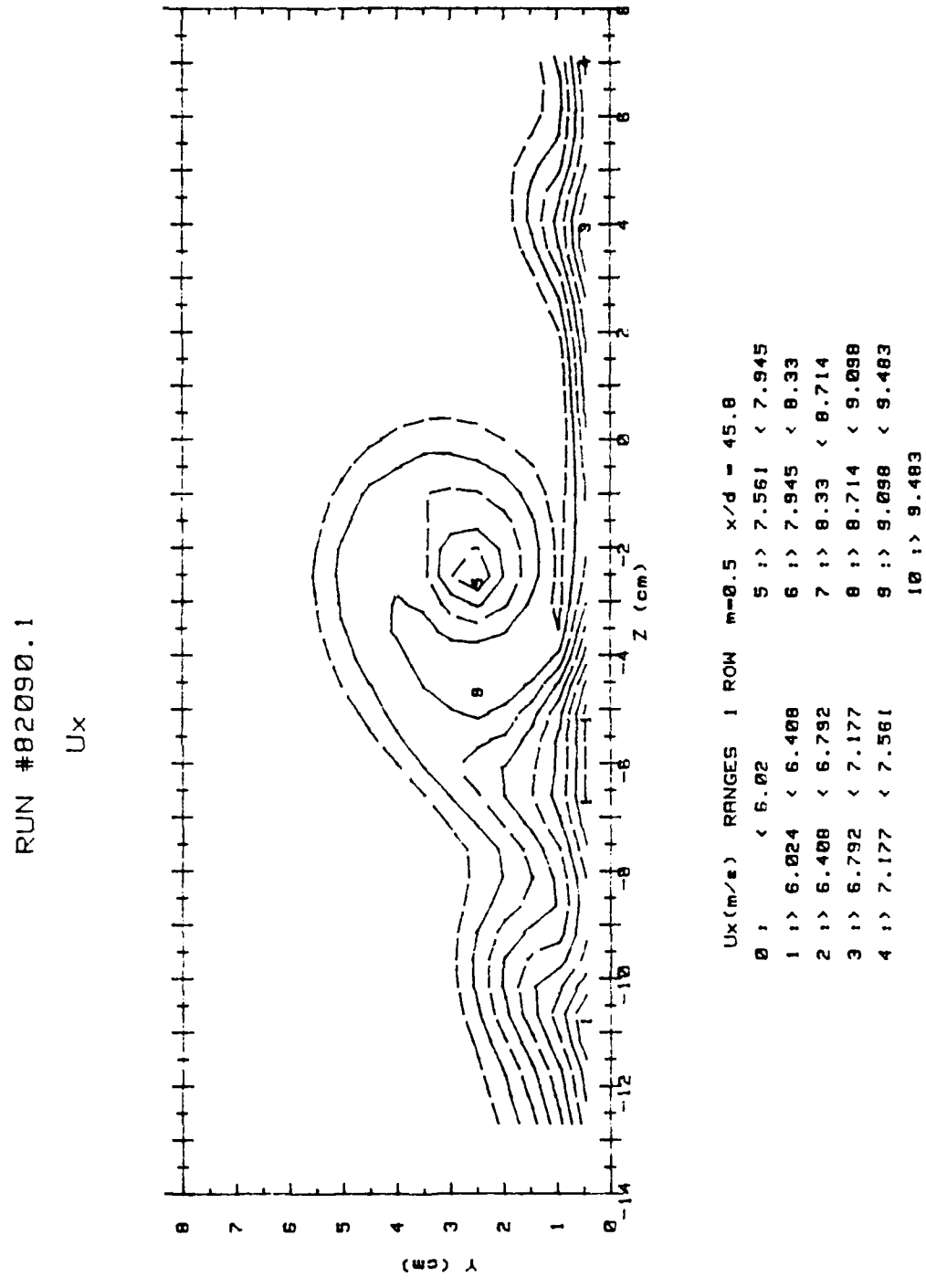

Figure 103. Streamwise Velocity Field, x/d=45.8, 1 Row, Vortex R1

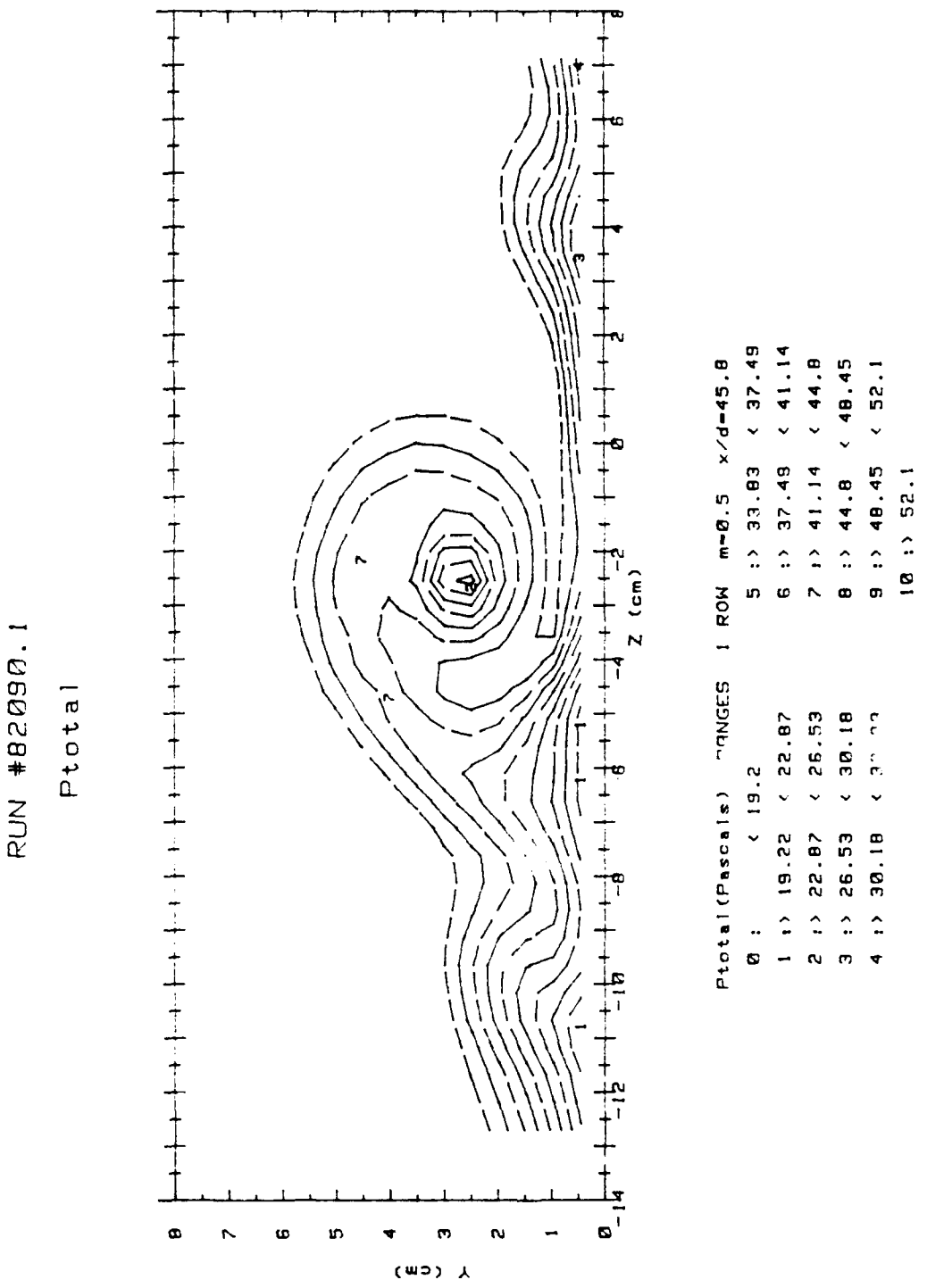

Figure 104. Total Pressure Field, x/d=45.8, 1 Row, Vortex R1

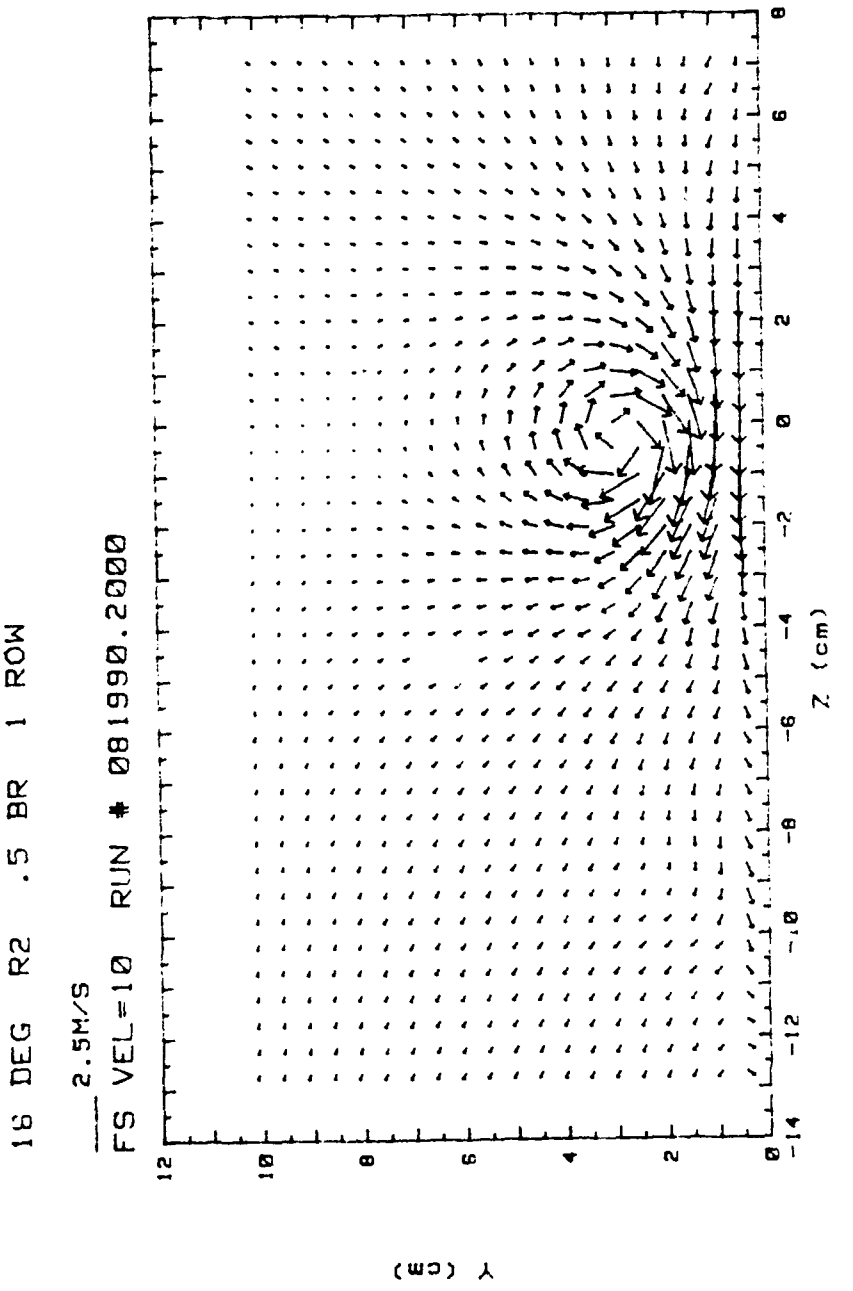

Figure 105. Secondary Flow Vectors, x/d=45.8, 1 Row, Vortex R2

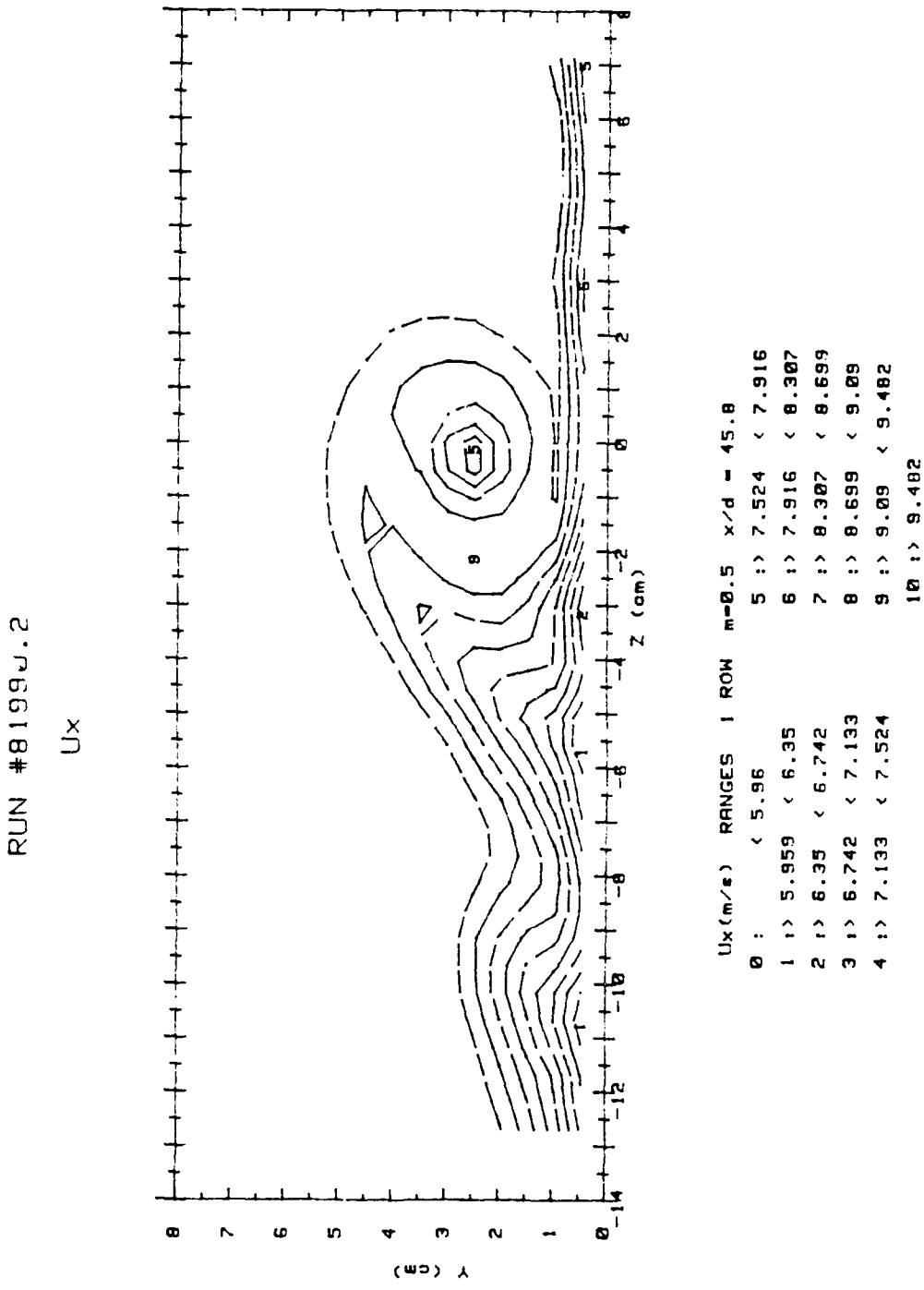

Figure 106. Streamwise Velocity Field, x/d=45.8, 1 Row, Vortex R2

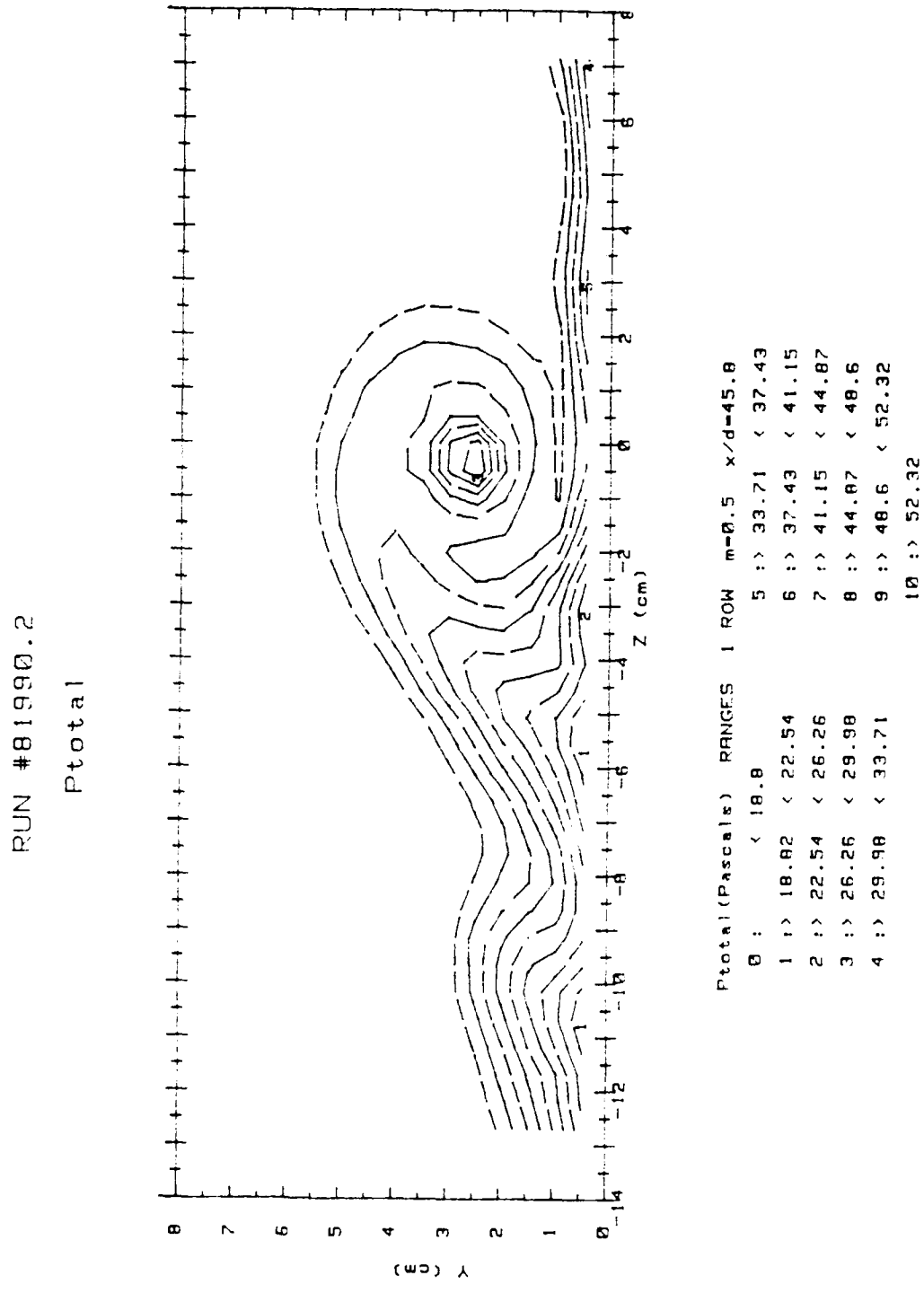

Figure 107. Total Pressure Field, x/d=45.8, 1 Row, Vortex R2

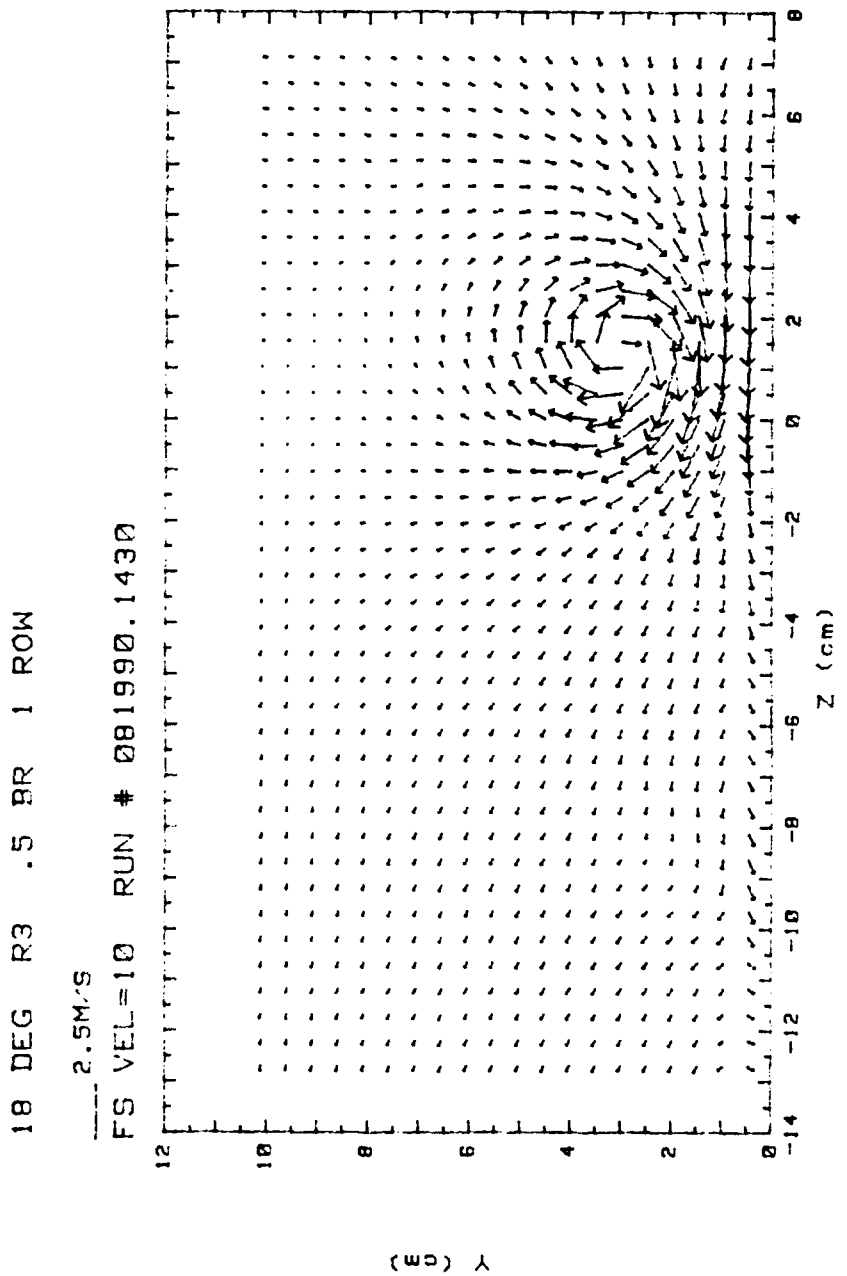

Figure 108. Secondary Flow Vectors, x/d=45.8, 1 Row, Vortex R3

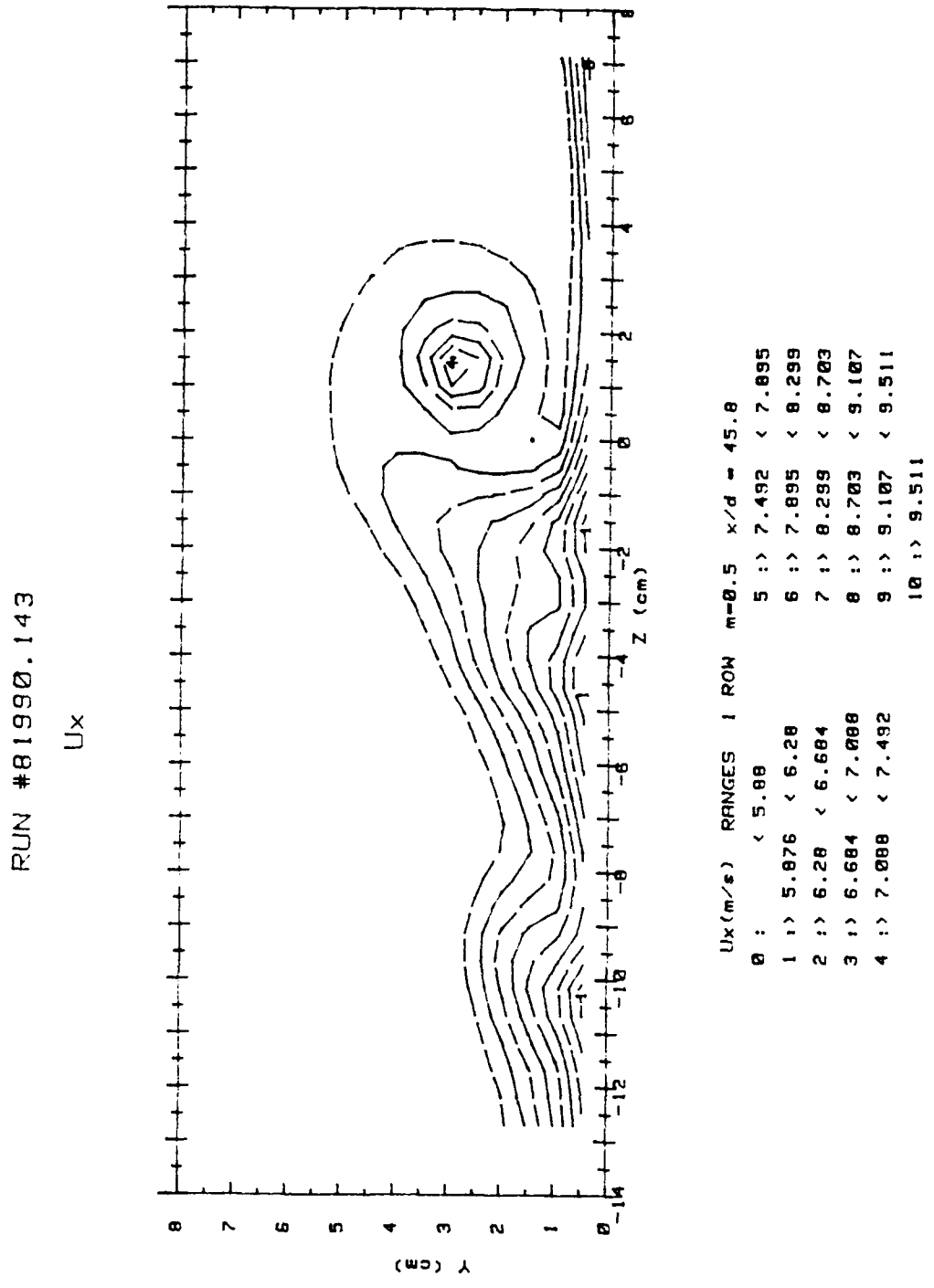

Figure 109. Streamwise Velocity Field, x/d=45.8, 1 Row, Vortex R3

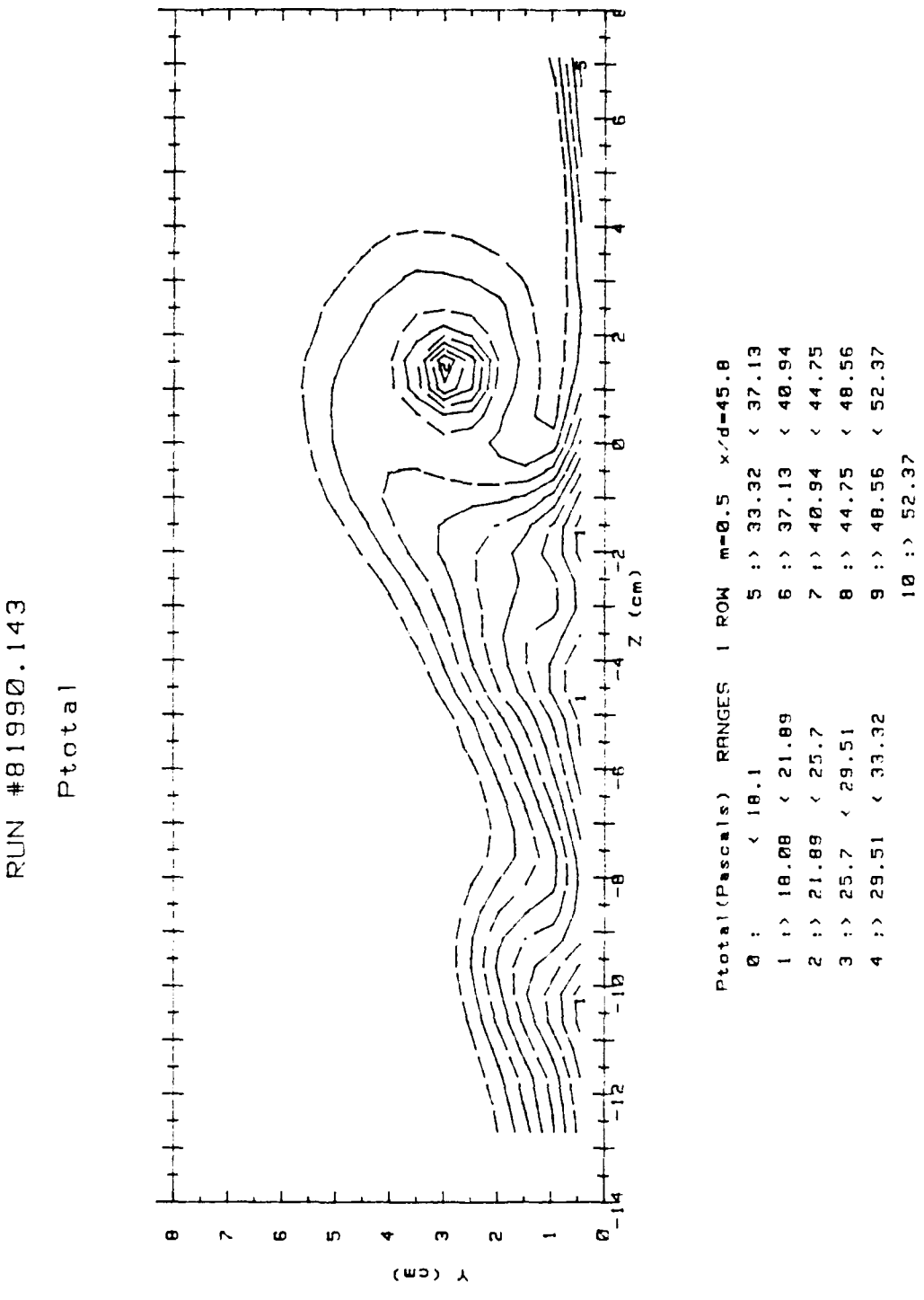

Figure 110. Total Pressure Field, x/d=45.8, 1 Row, Vortex R3

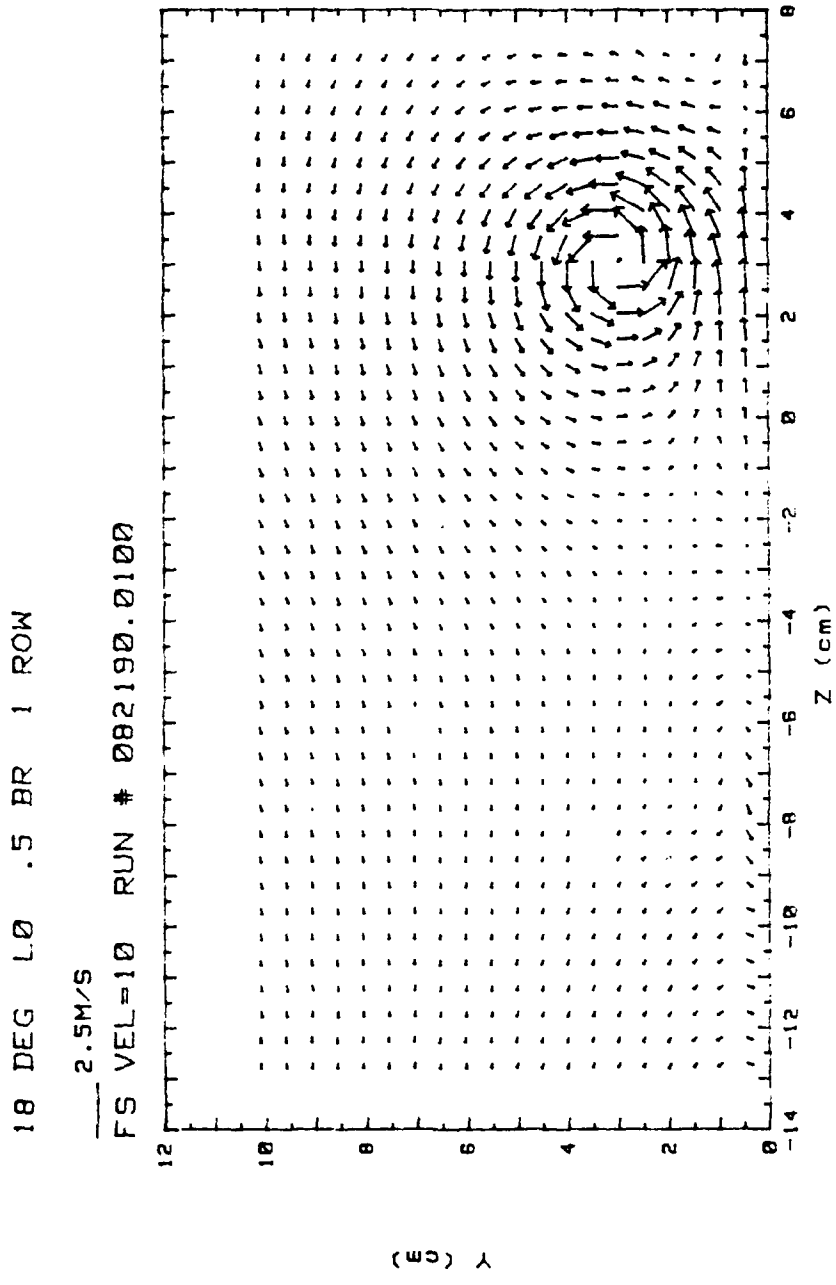

Figure 111. Secondary Flow Vectors, x/d=45.8, 1 Row, Vortex L0

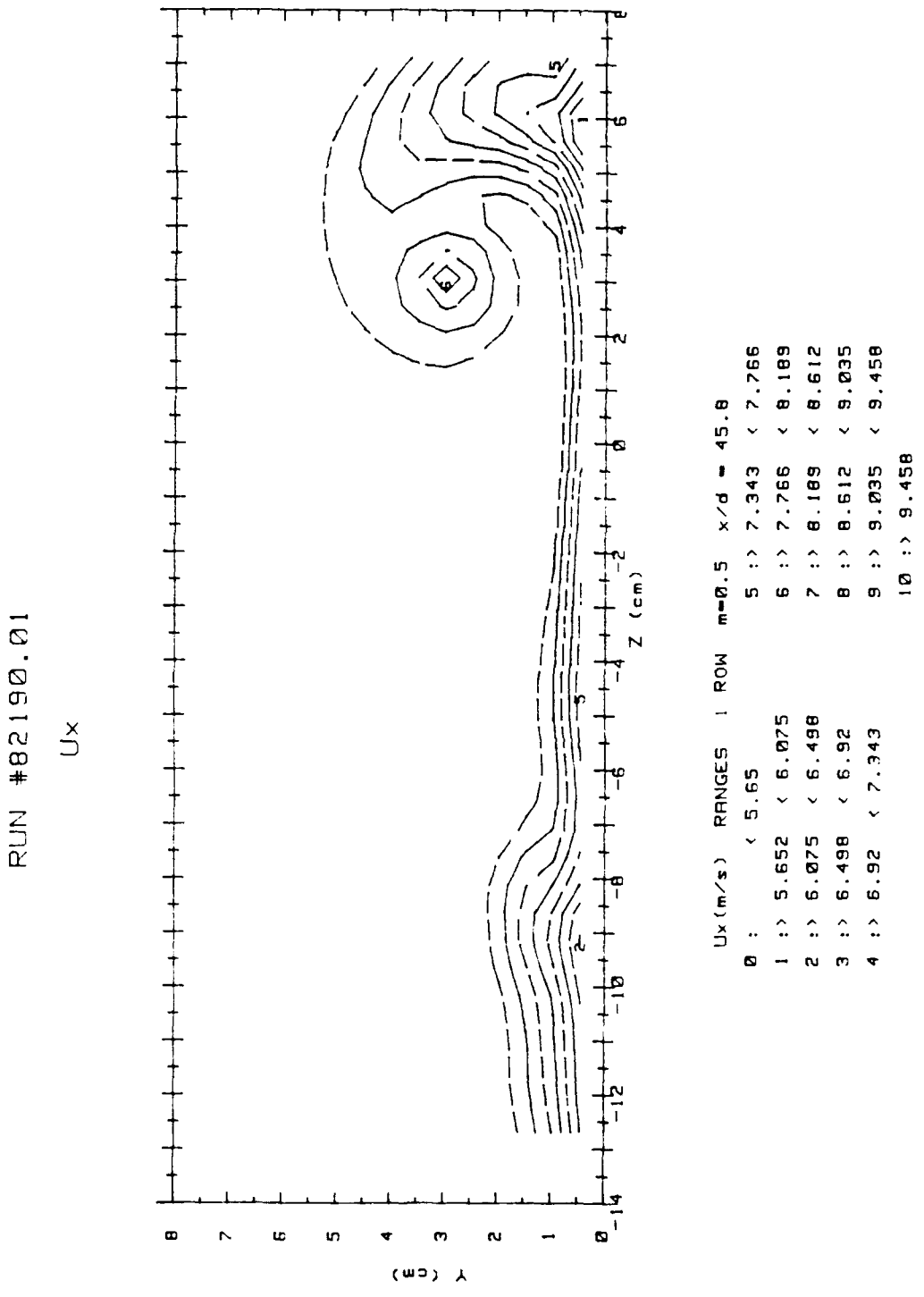

Figure 112. Streamwise Velocity Field, x/d=45.8, 1 Row, Vortex L0

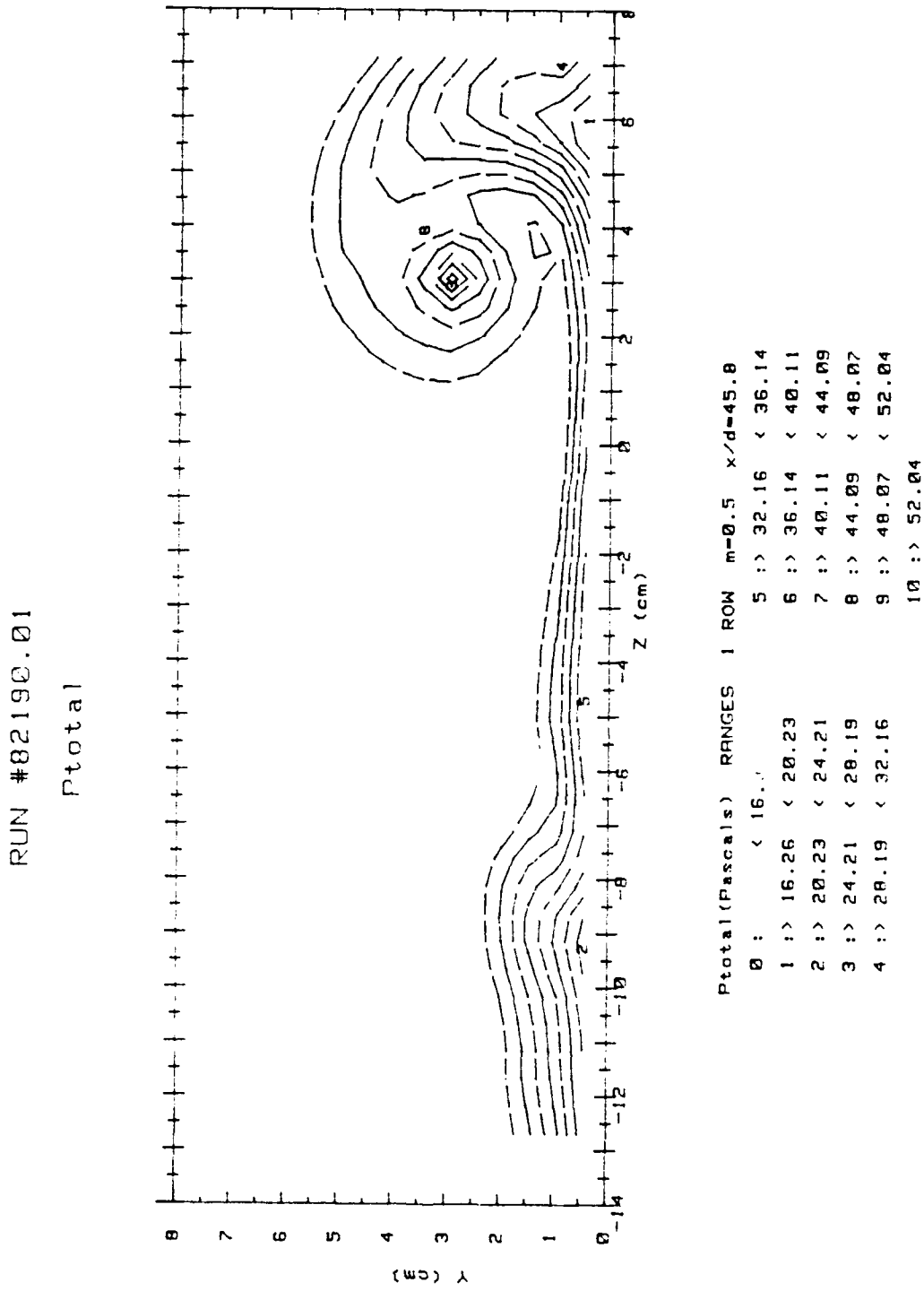

Figure 113. Total Pressure Field, x/d=45.8, 1 Row, Vortex L0

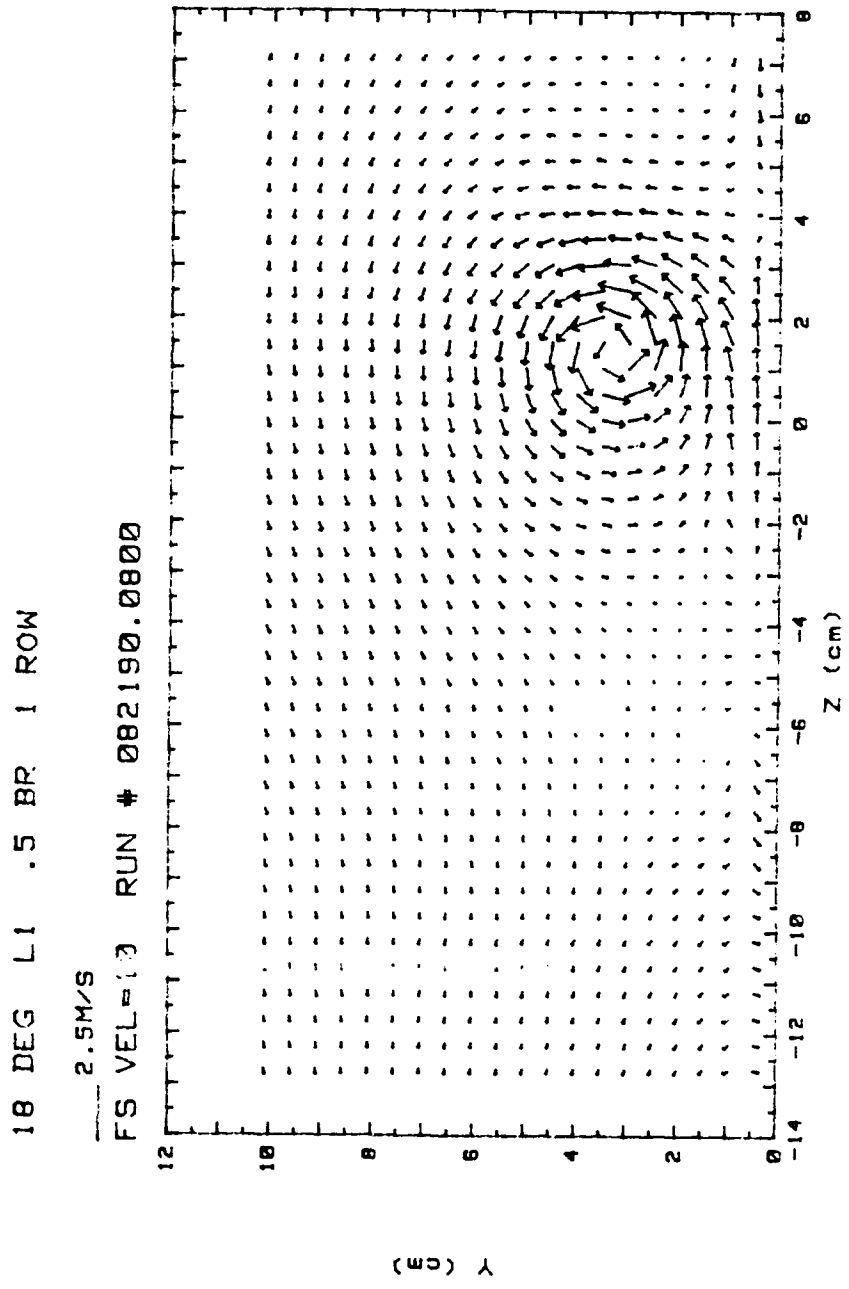

Figure 114. Secondary Flow Vectors, x/d=45.8, 1 Row, Vortex L1

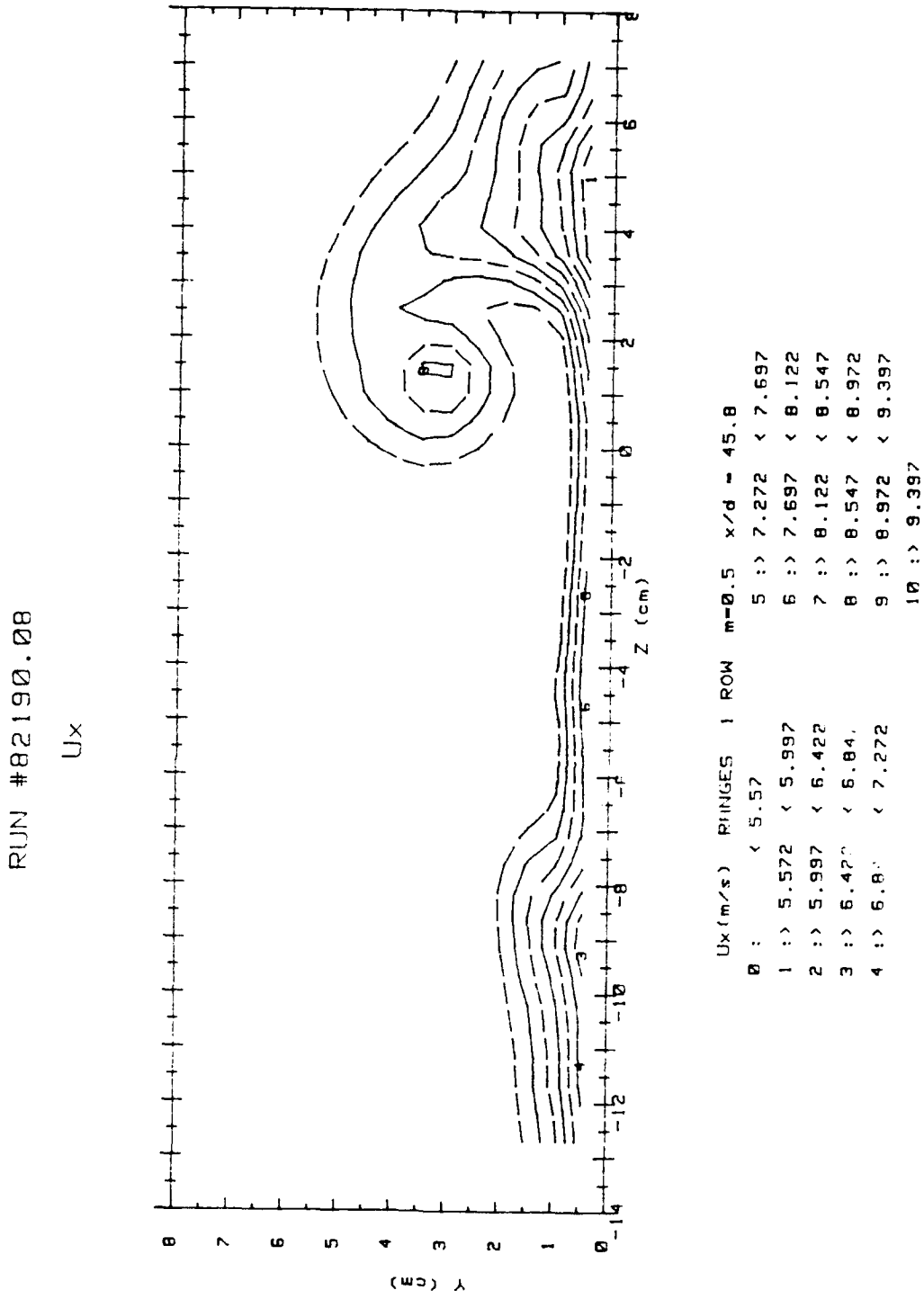

Figure 115. Streamwise Velocity Field, x/d=45.8, 1 Row, Vortex L1

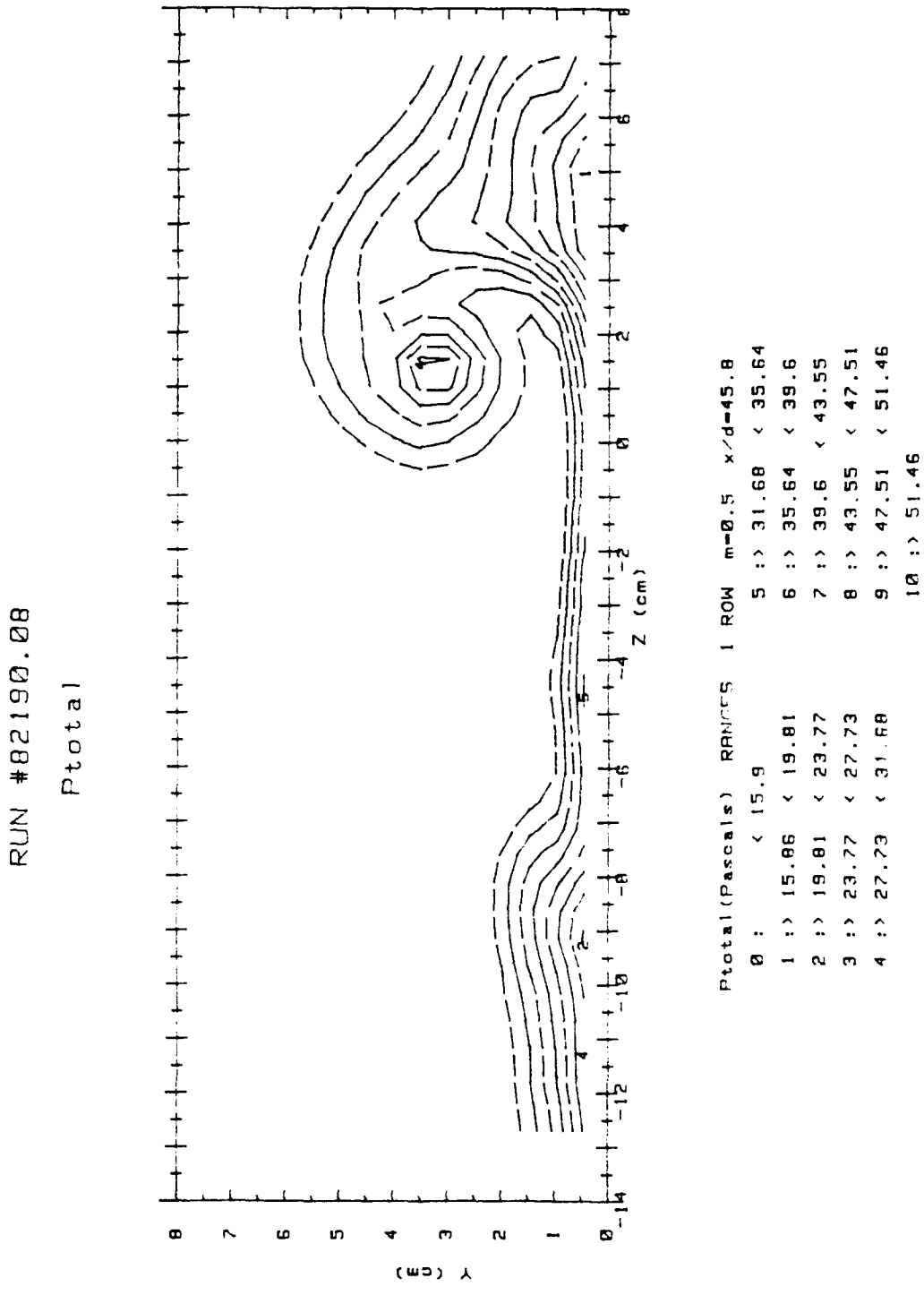

Figure 116. Total Pressure Field, x/d=45.8, 1 Row, Vortex L1

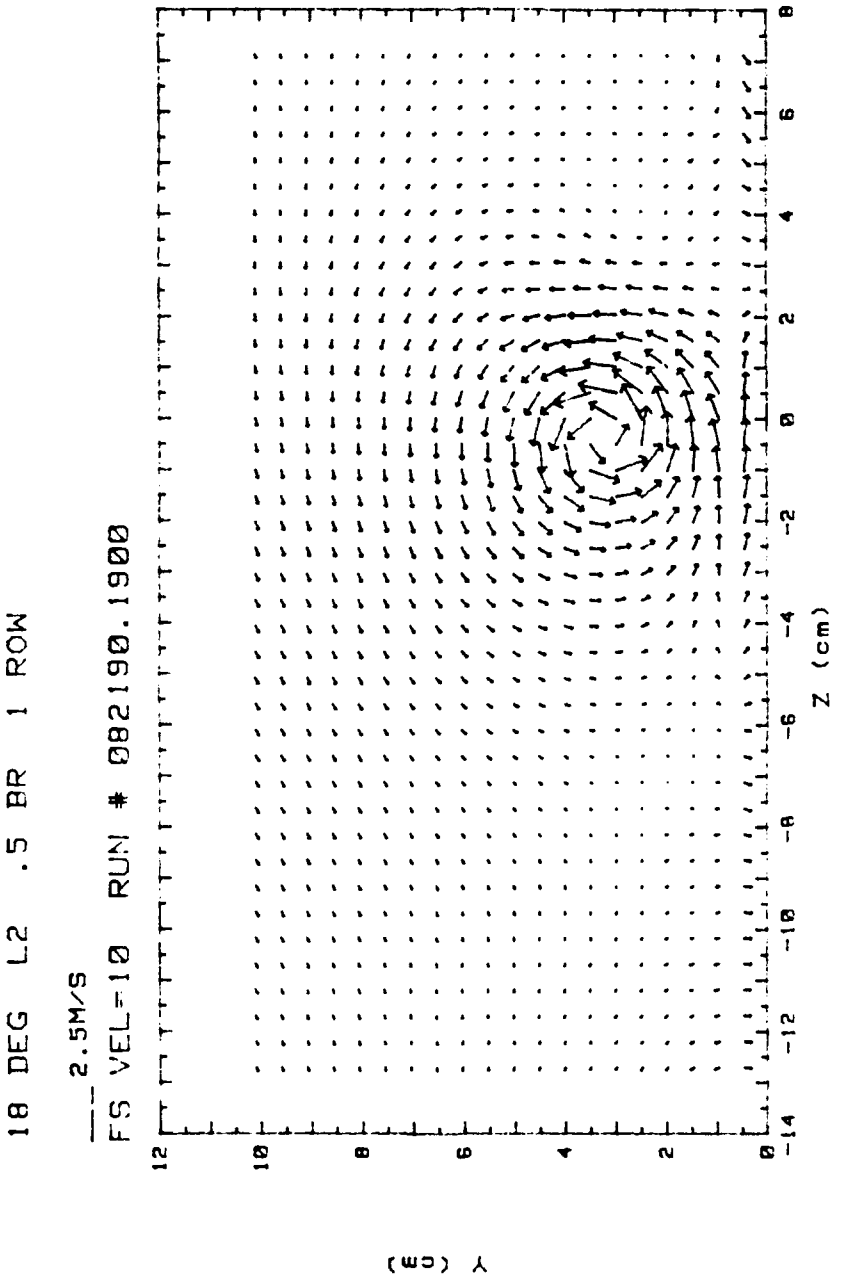

Figure 117. Secondary Flow Vectors, x/d=45.8, 1 Row, Vortex L2

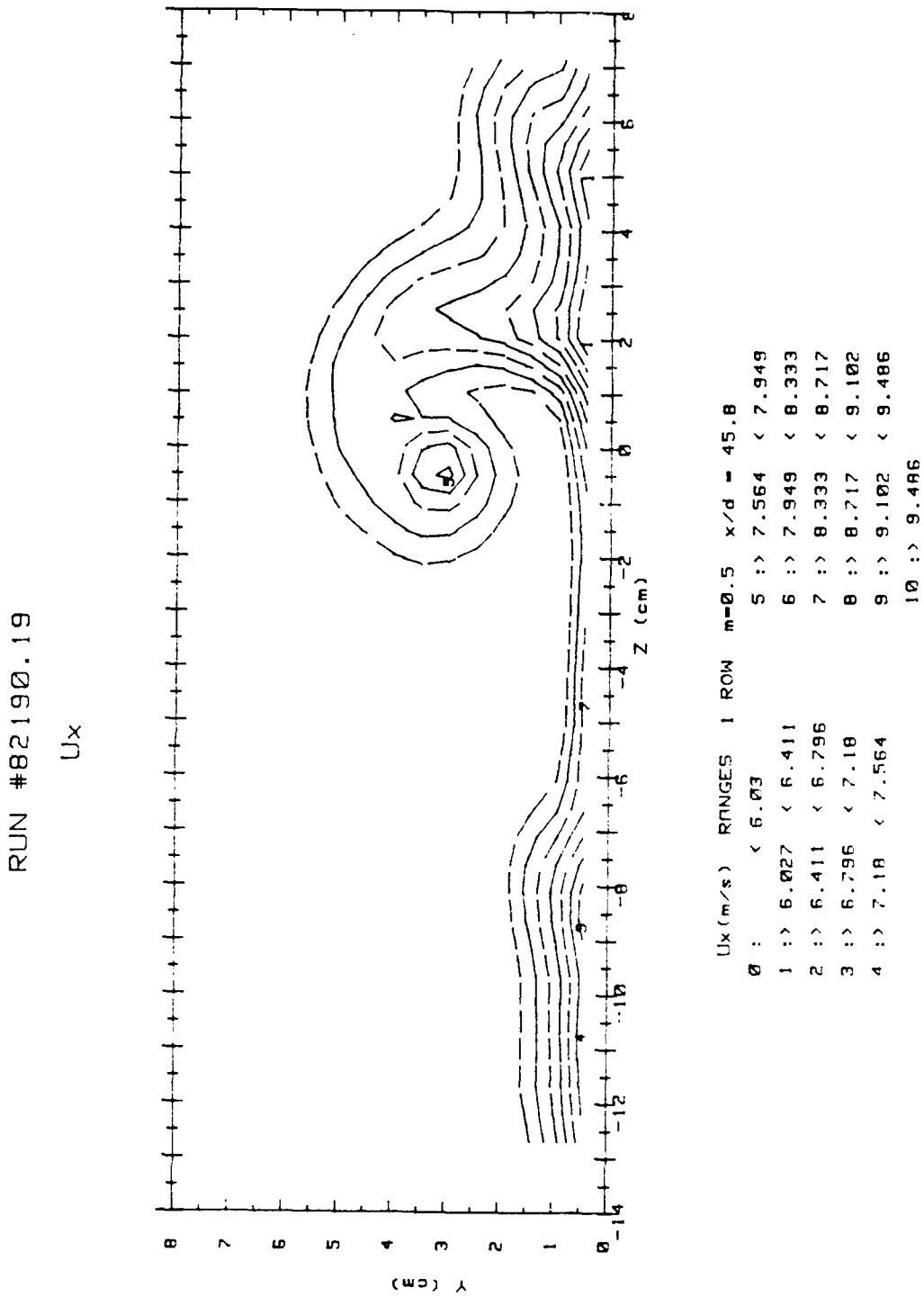

Figure 118. Streamwise Velocity Field, x/d=45.8, 1 Row, Vortex L2

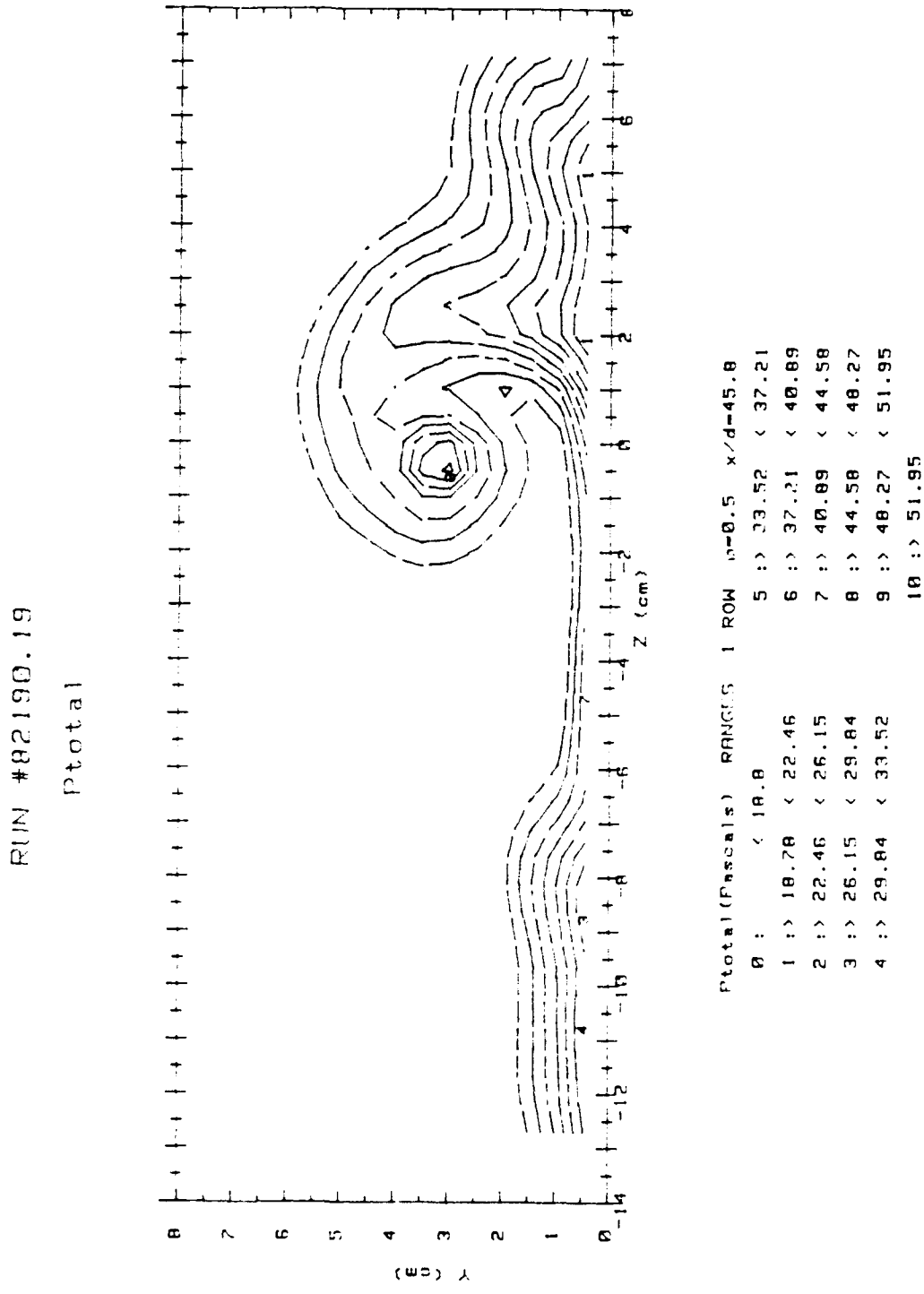

Figure 119. Total Pressure Field, x/d=45.8, 1 Row, Vortex L2

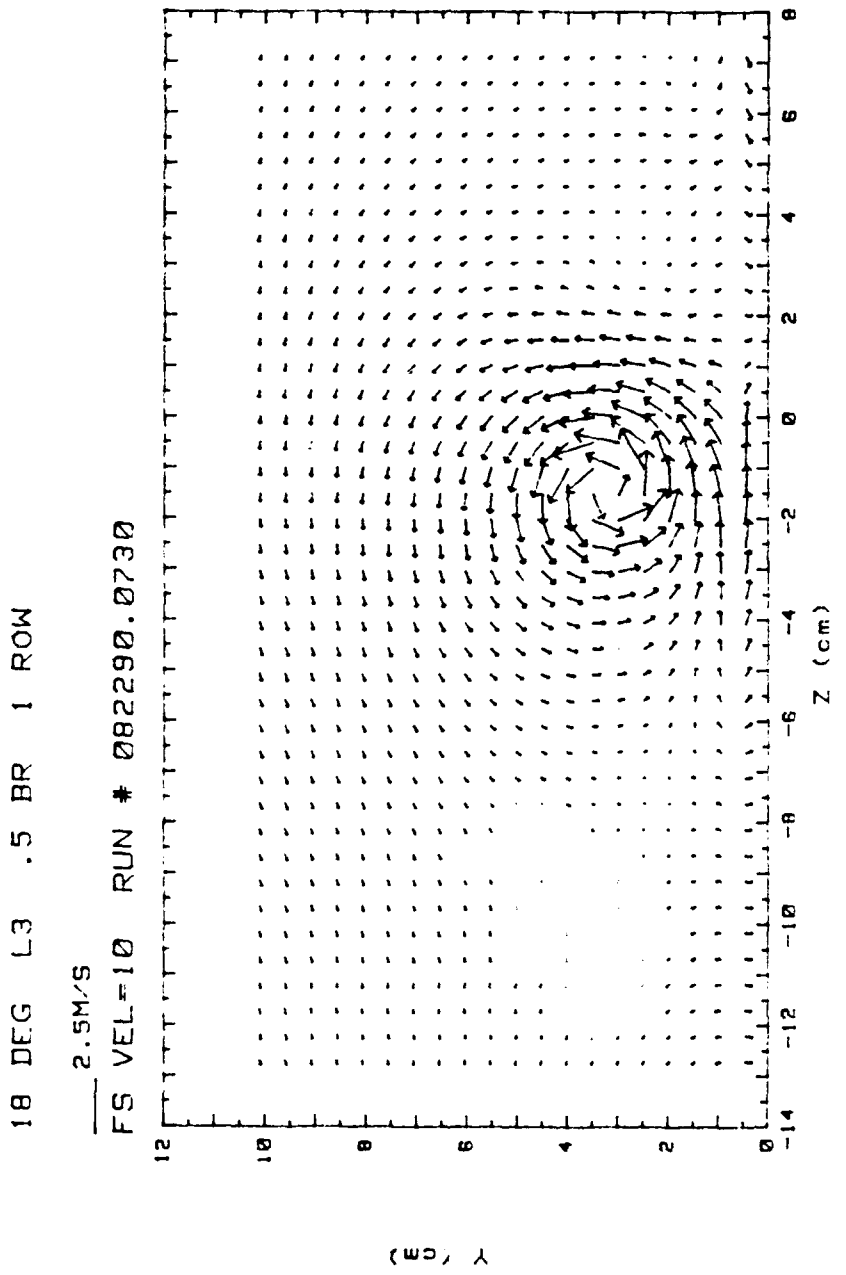

Figure 120. Secondary Flow Vectors, x/d=45.8, 1 Row, Vortex L3

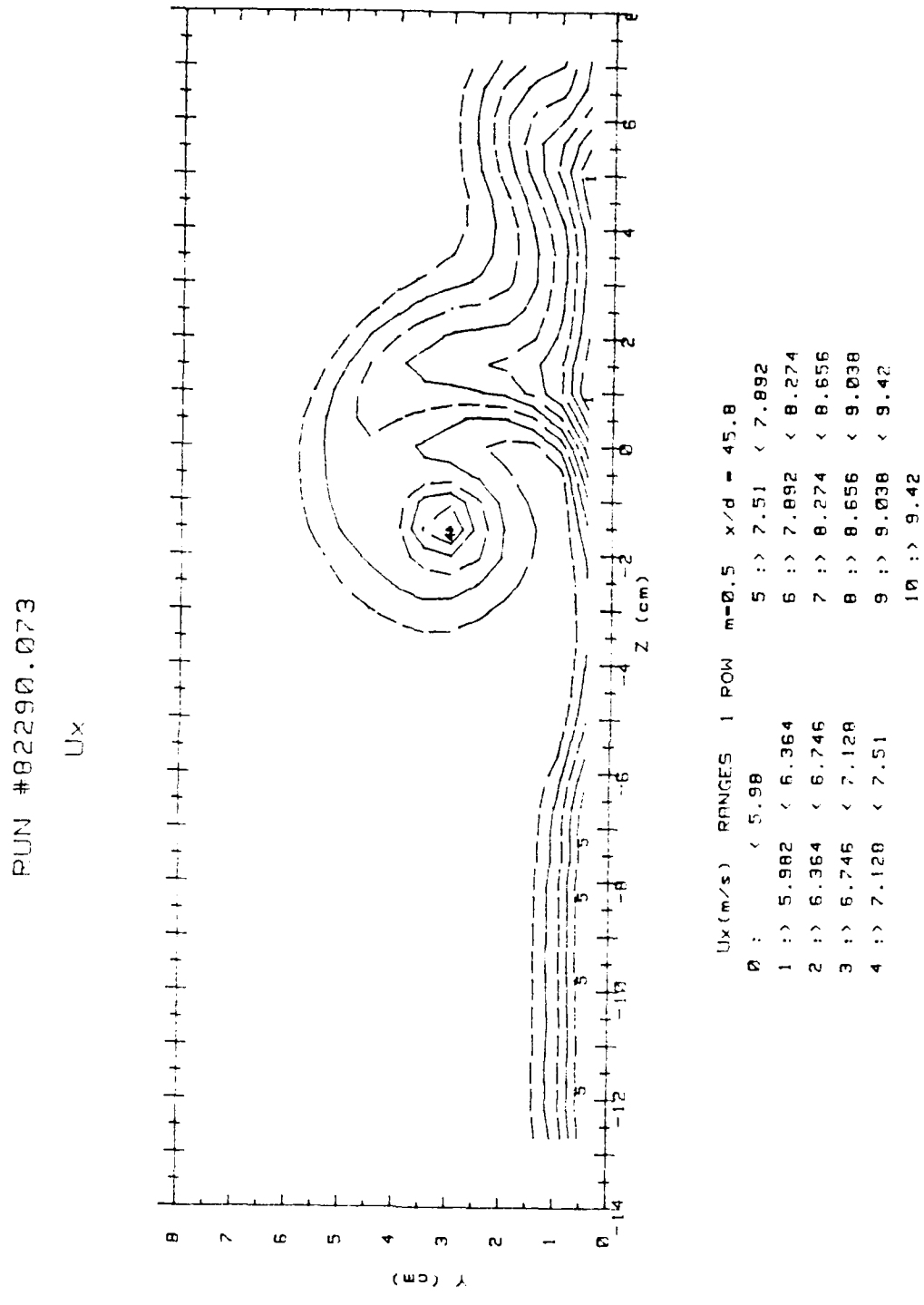

Figure 121. Streamwise Velocity Field, x/d=45.8, 1 Row, Vortex L3

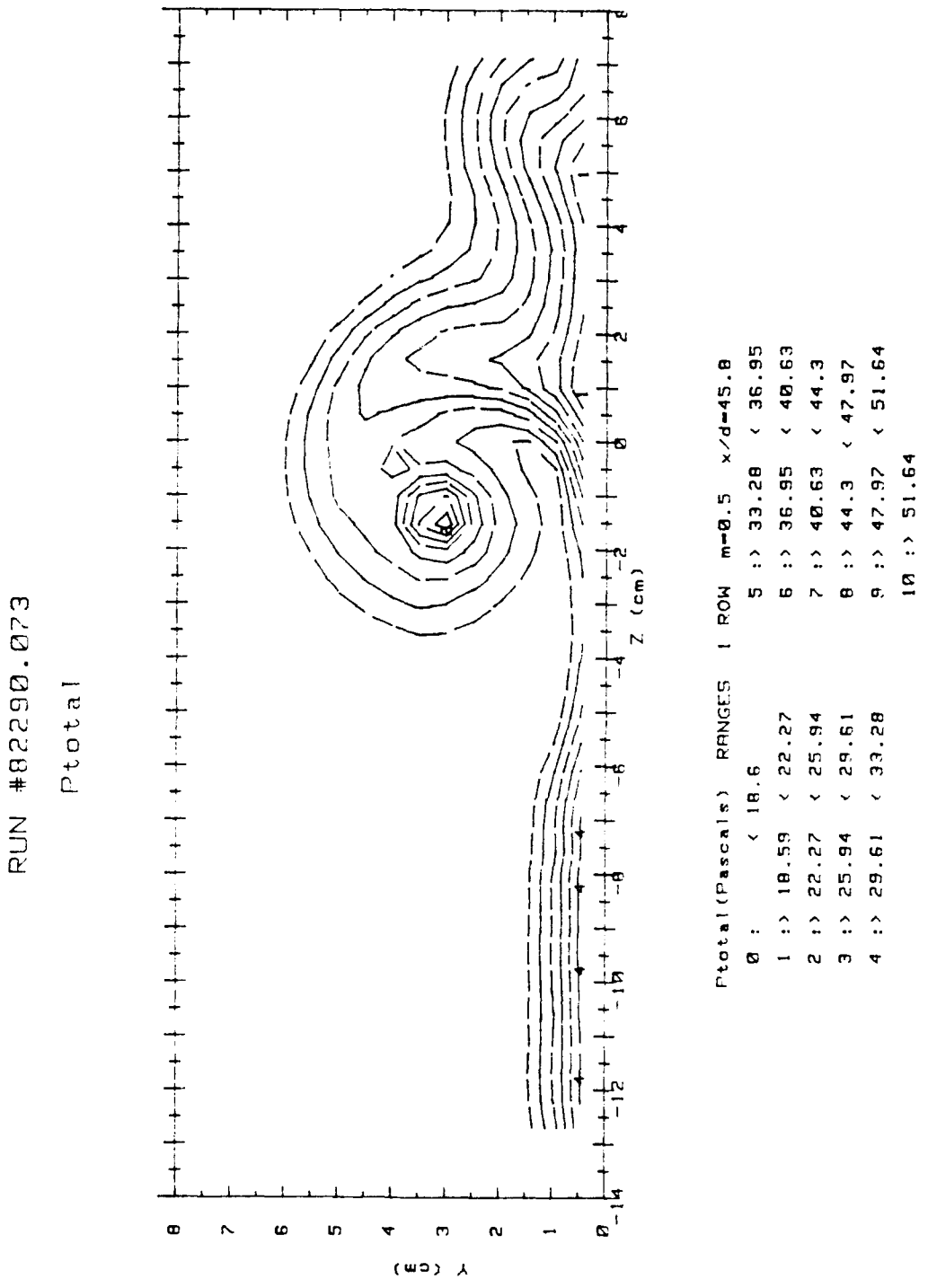

Figure 122. Total Pressure Field, x/d=45.8, 1 Row, Vortex L3

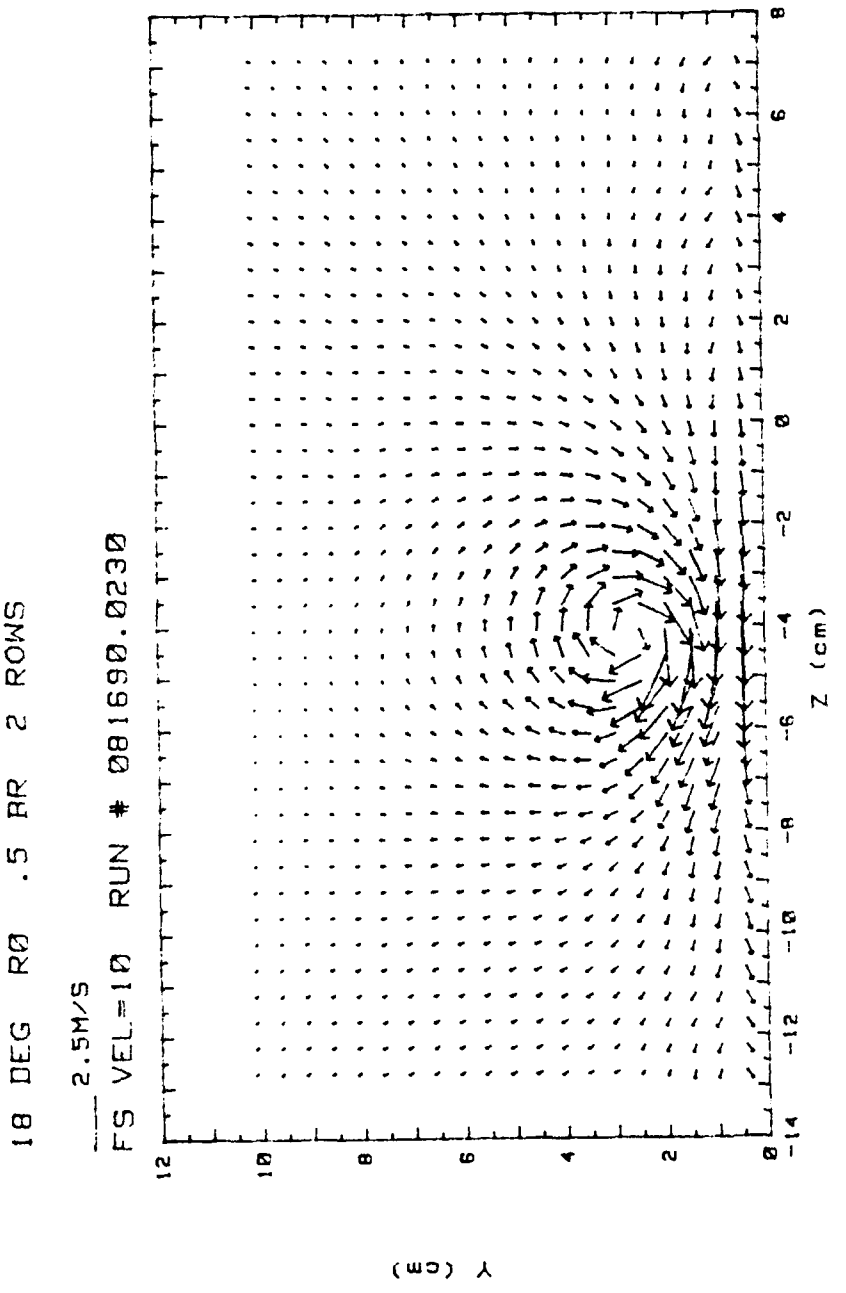

Figure 123. Secondary Flow Vectors, x/d=45.8, 2 Rows, Vortex R0

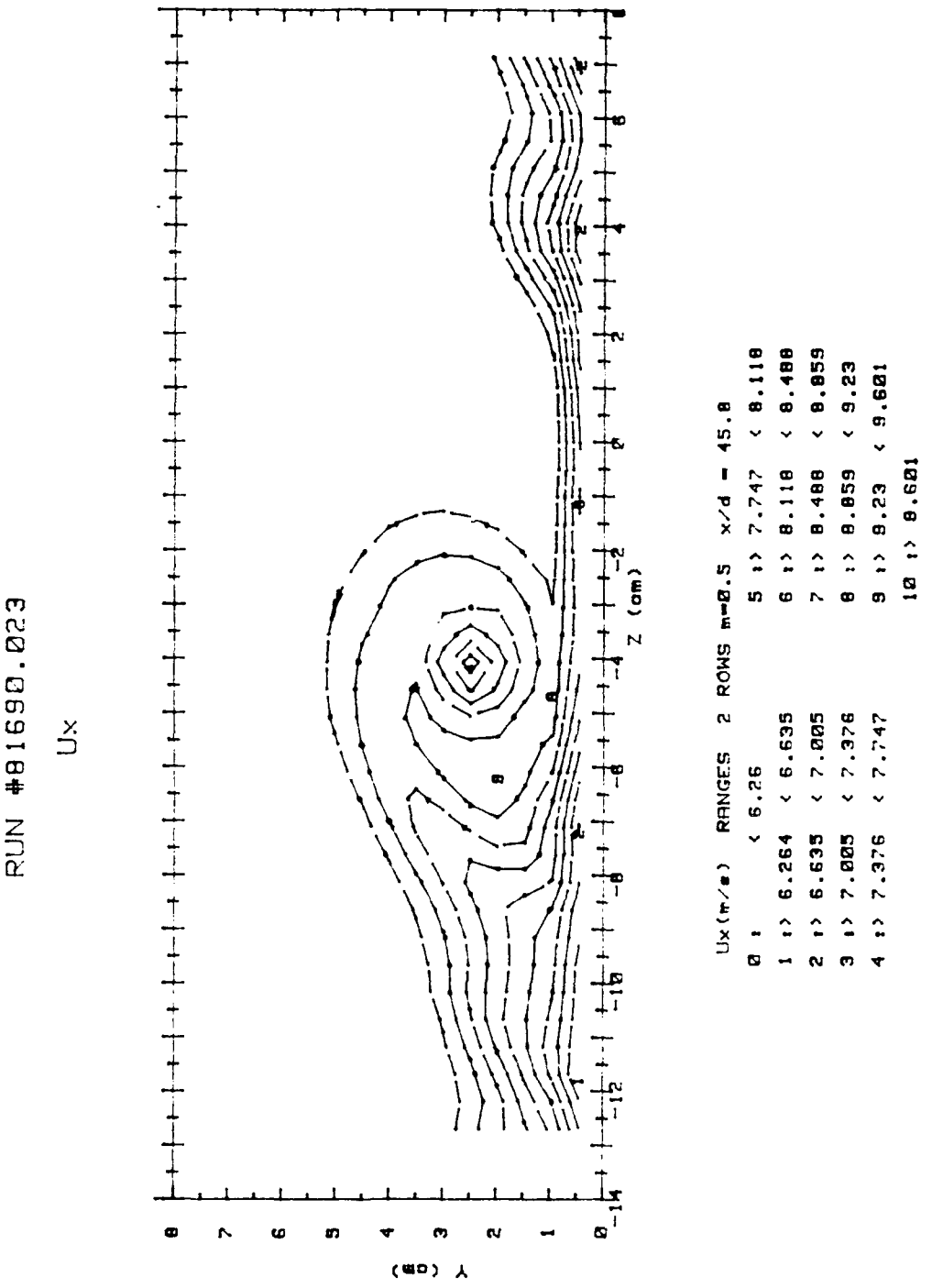

Figure 124. Streamwise Velocity Field, x/d=45.8, 2 Rows, Vortex R0

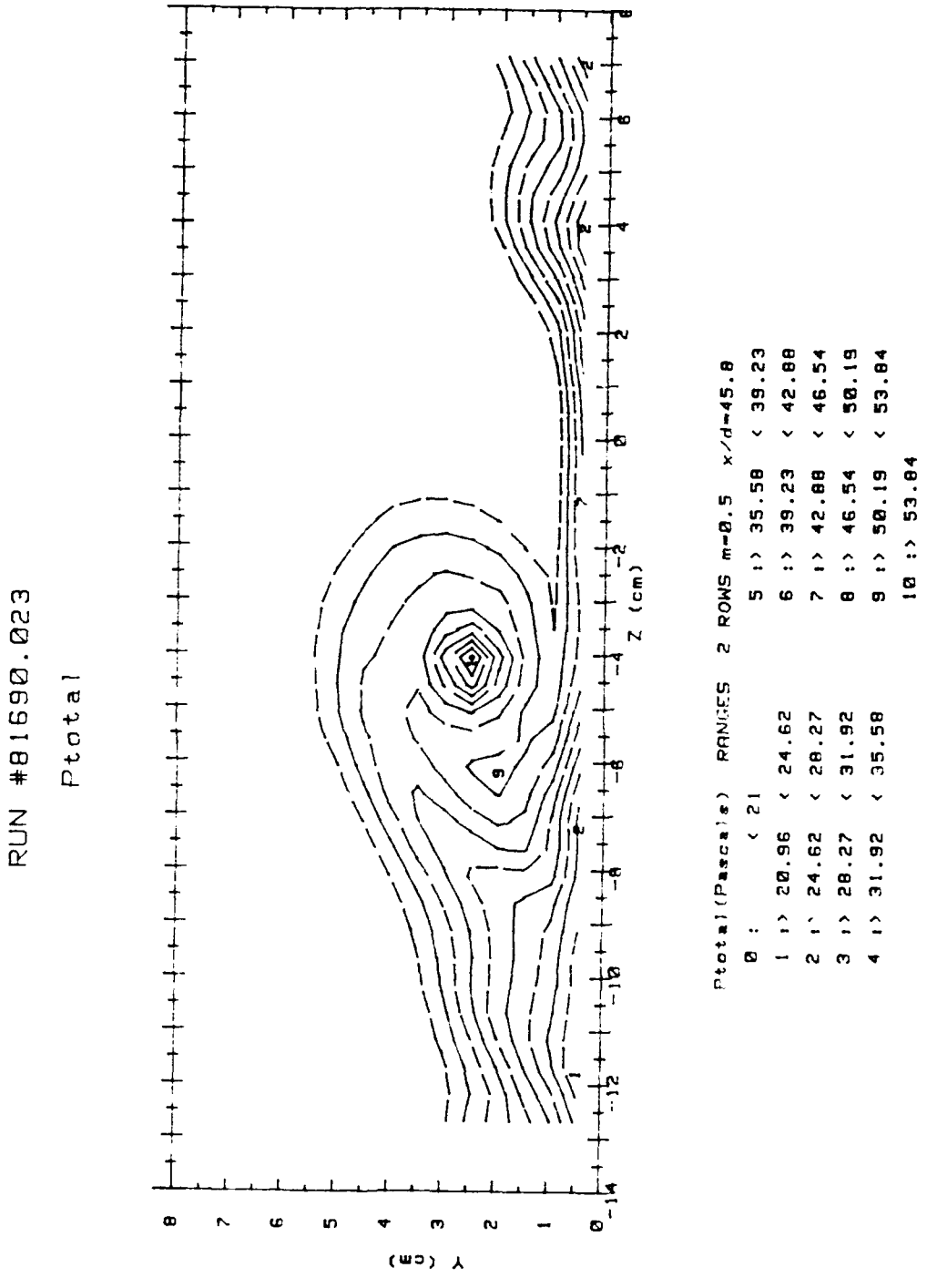

Figure 125. Total Pressure Field, x/d=45.8, 2 Rows, Vortex R0

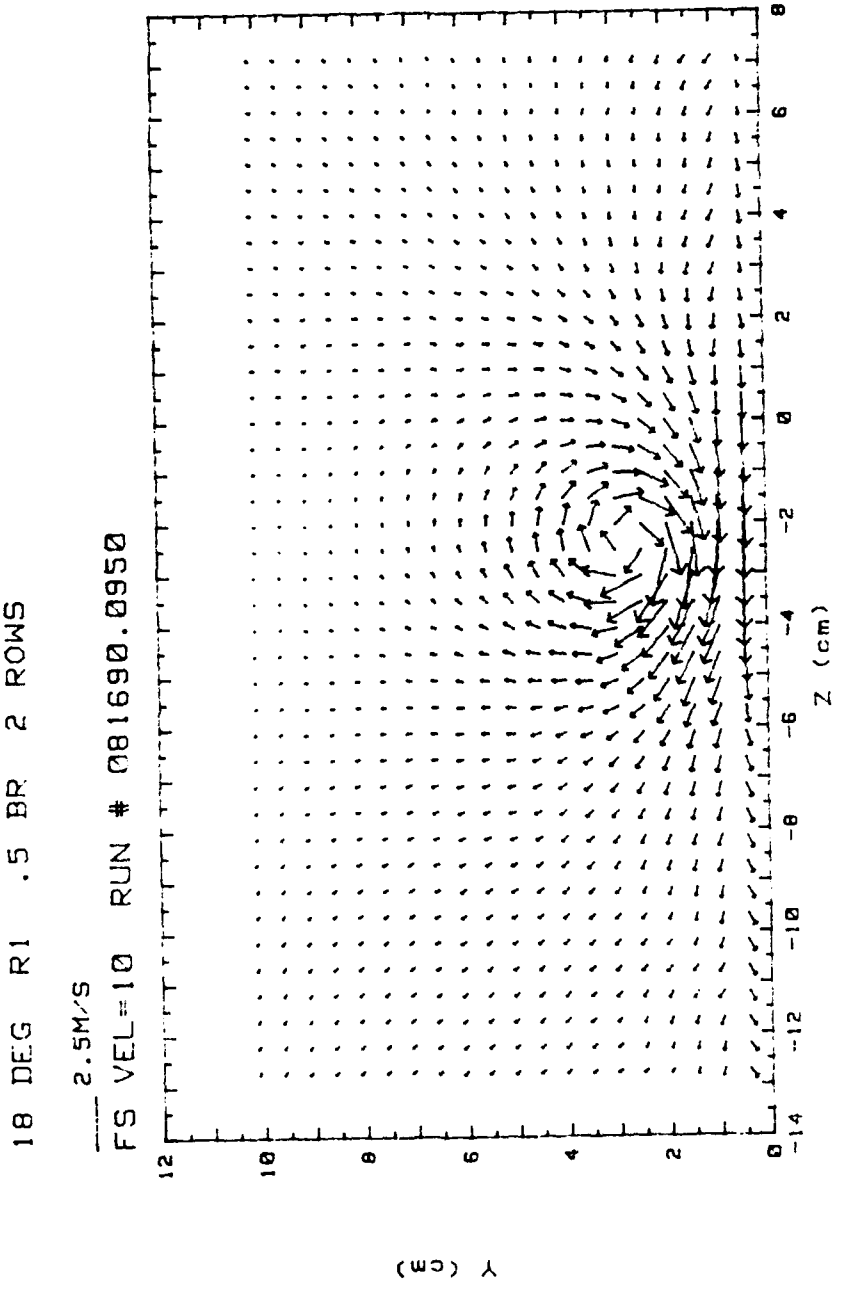

Figure 126. Secondary Flow Vectors, x/d=45.8, 2 Rows, Vortex R1

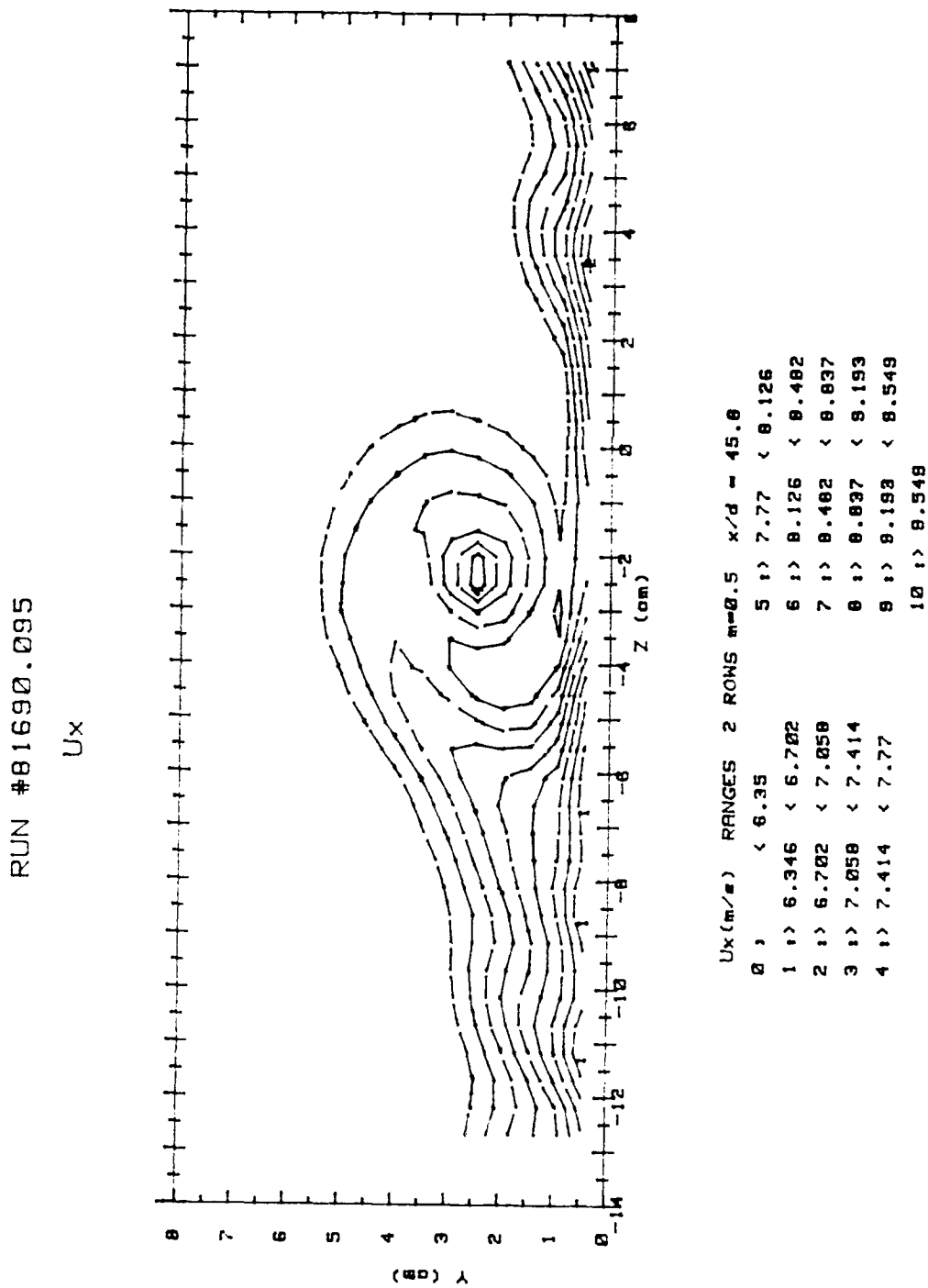

Figure 127. Streamwise Velocity Field, x/d=45.8, 2 Rows, Vortex R1

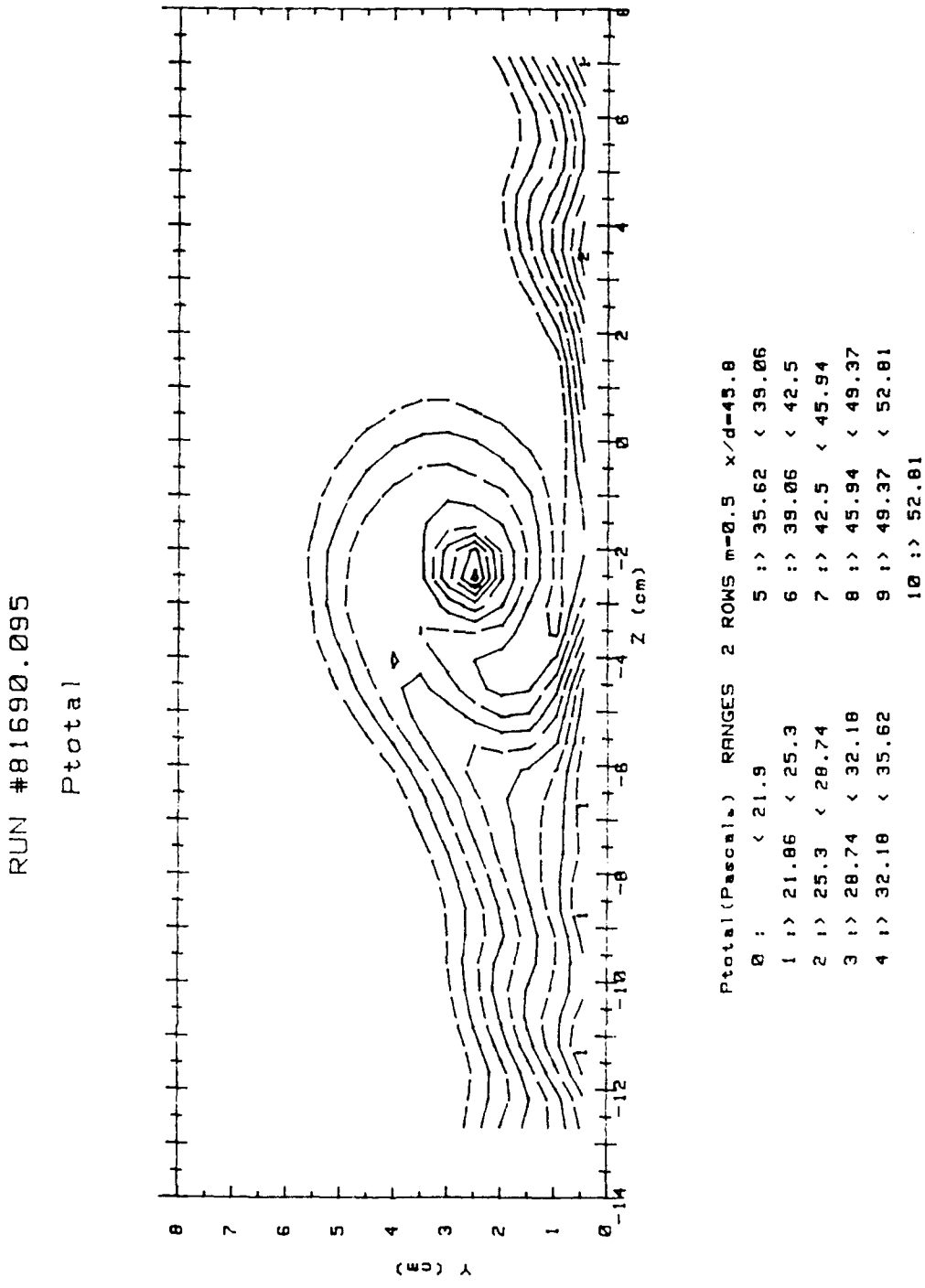

Figure 128. Total Pressure Field, x/d=45.8, 2 Rows, Vortex R1

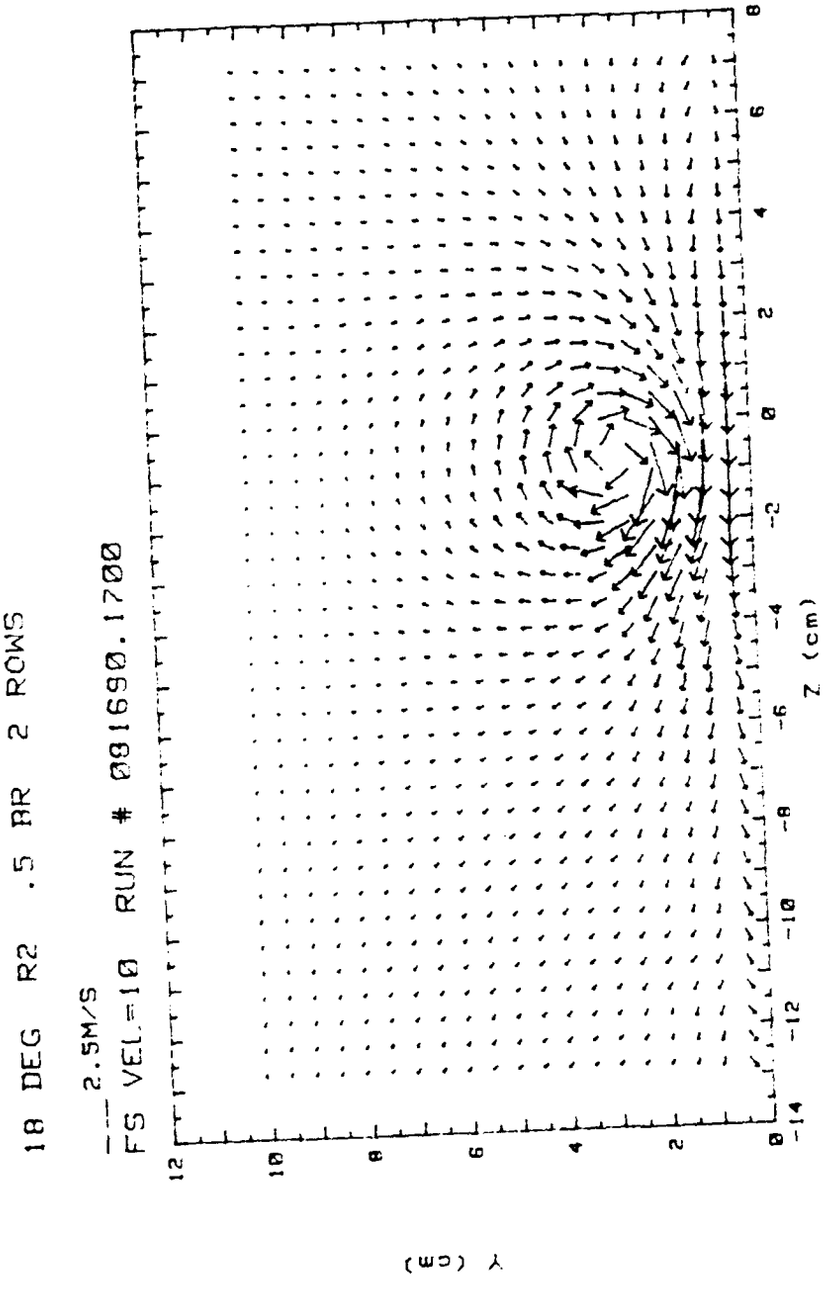

Figure 129. Secondary Flow Vectors, x/d=45.8, 2 Rows, Vortex R2

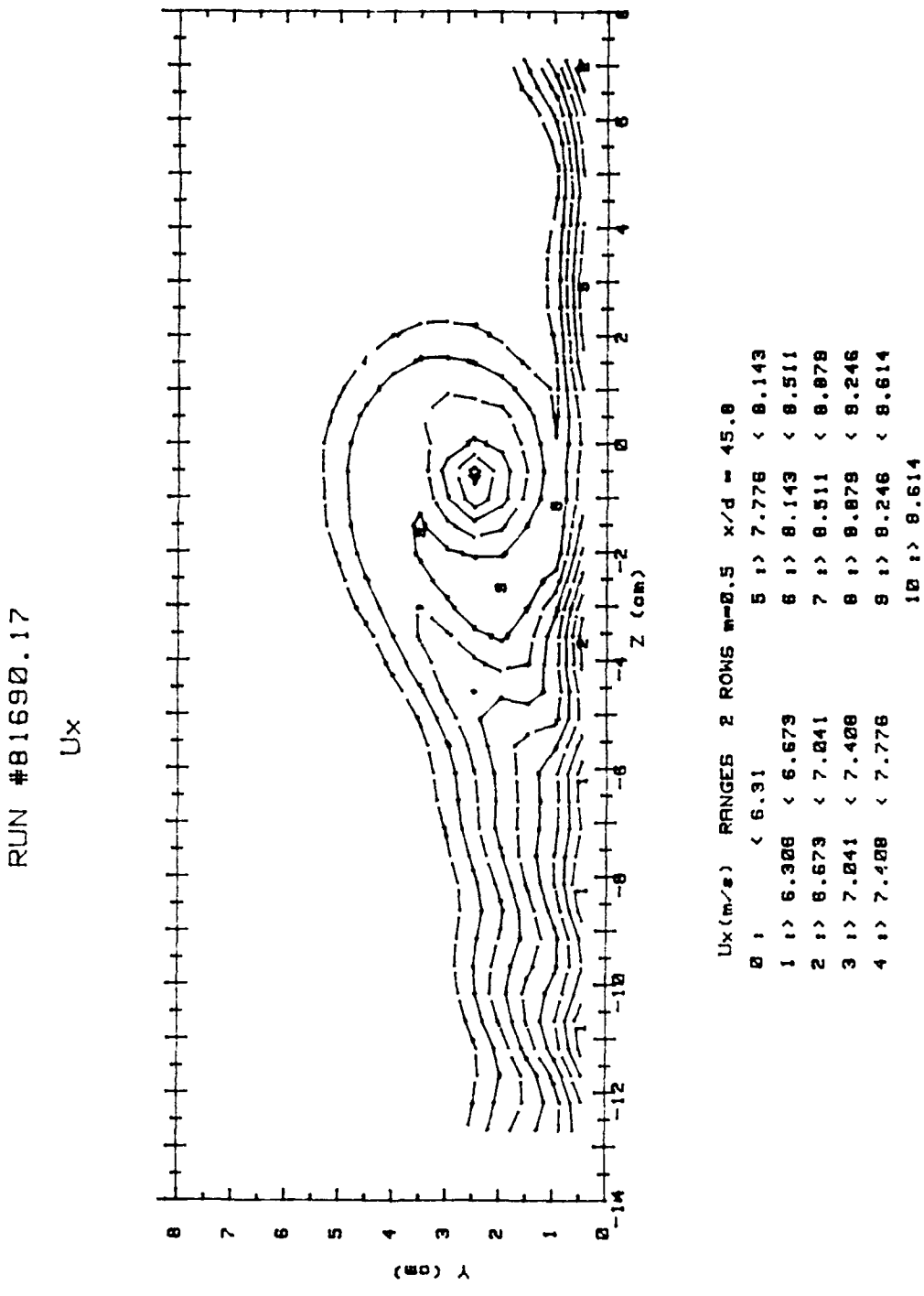

Figure 130. Streamwise Velocity Field, x/d=45.8, 2 Rows, Vortex R2

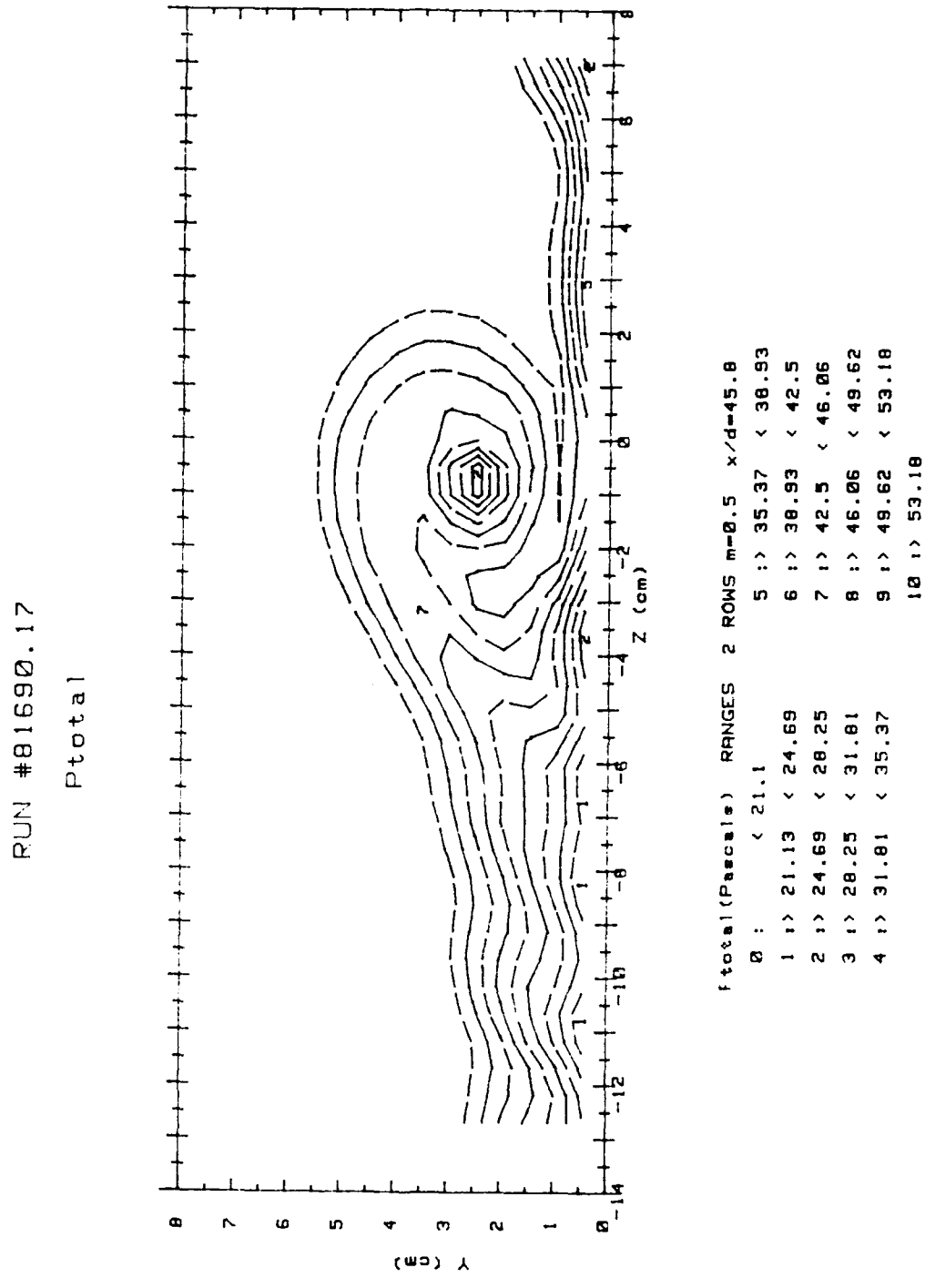

Figure 131. Total Pressure Field, x/d=45.8, 2 Rows, Vortex R2

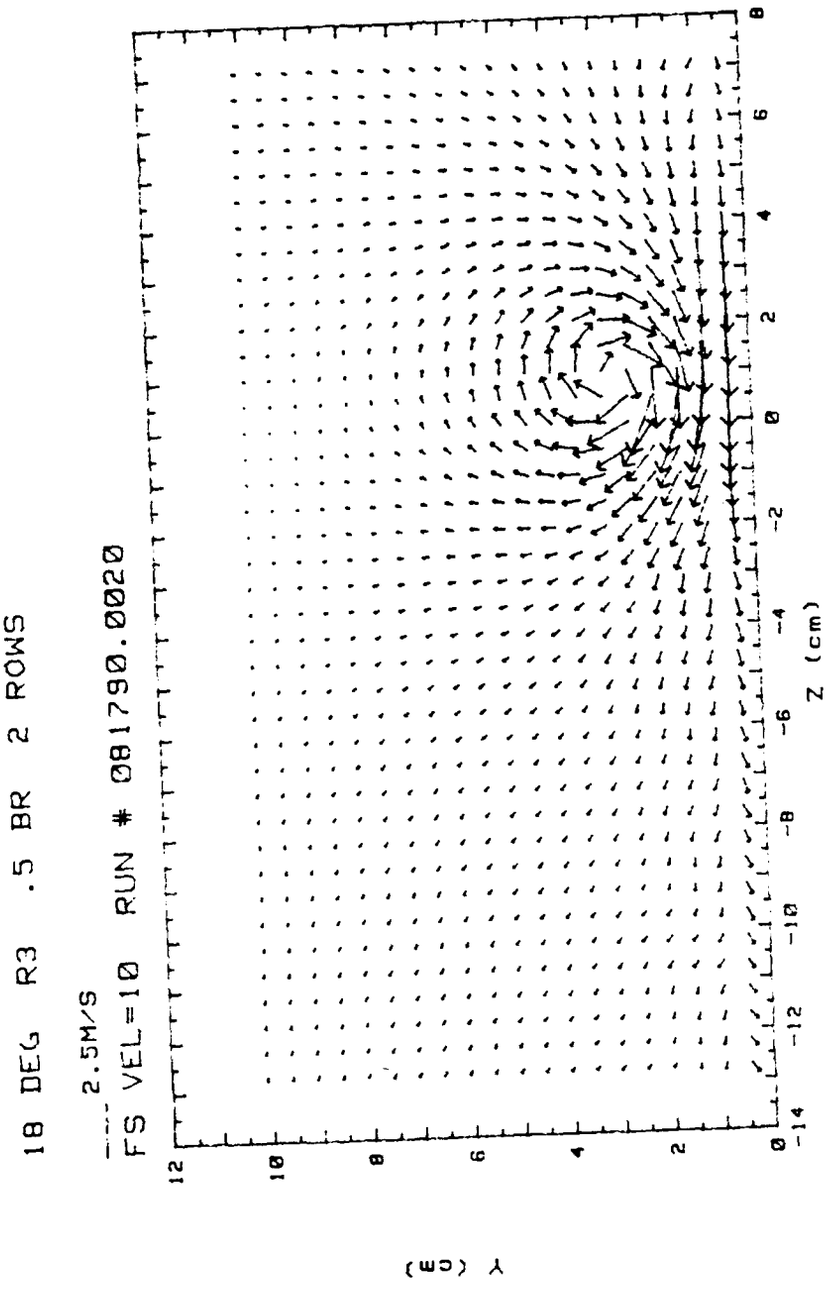

Figure 132. Secondary Flow Vectors, x/d=45.8, 2 Rows, Vortex R3

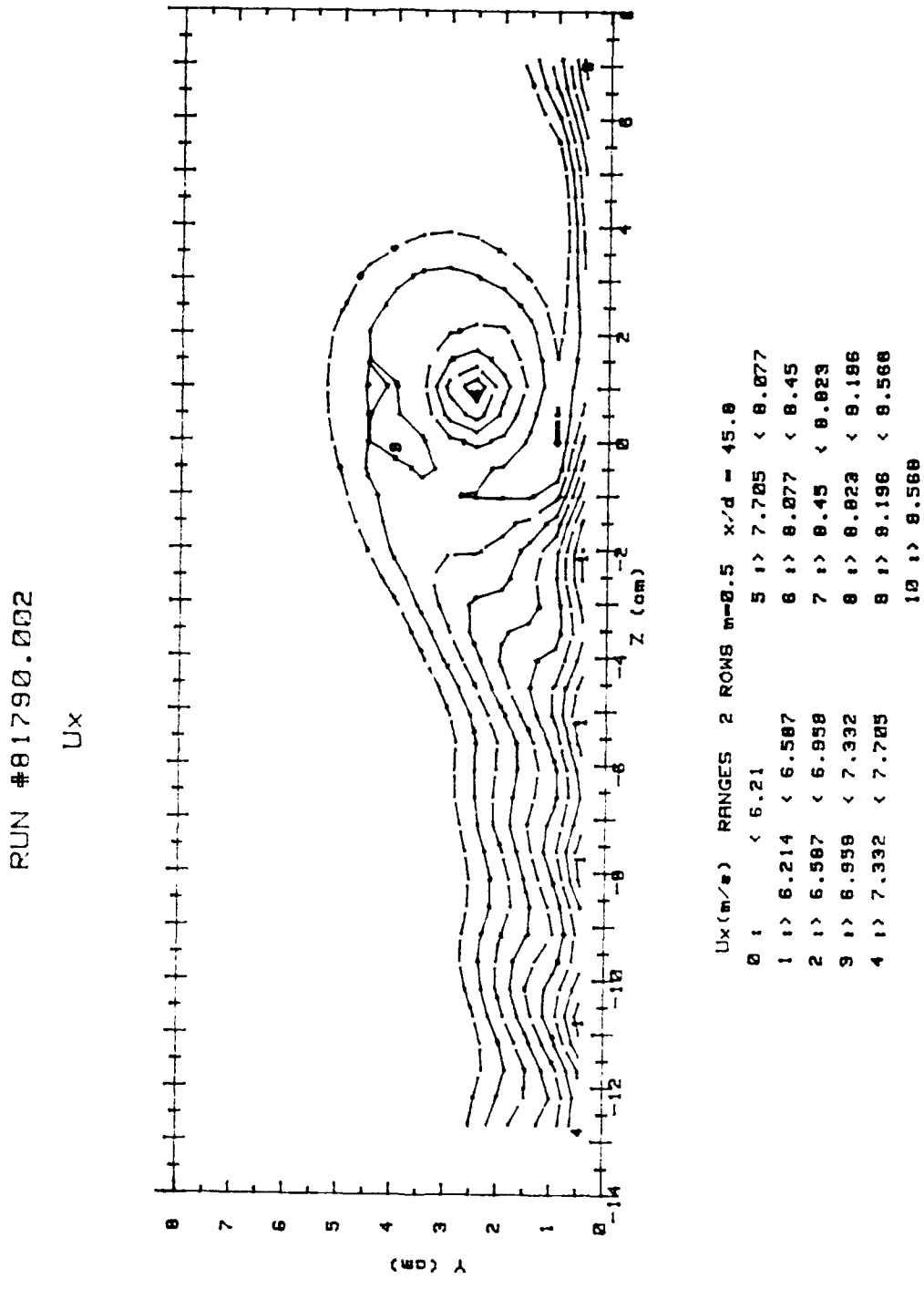

Figure 133. Streamwise Velocity Field, x/d=45.8, 2 Rows, Vortex R3

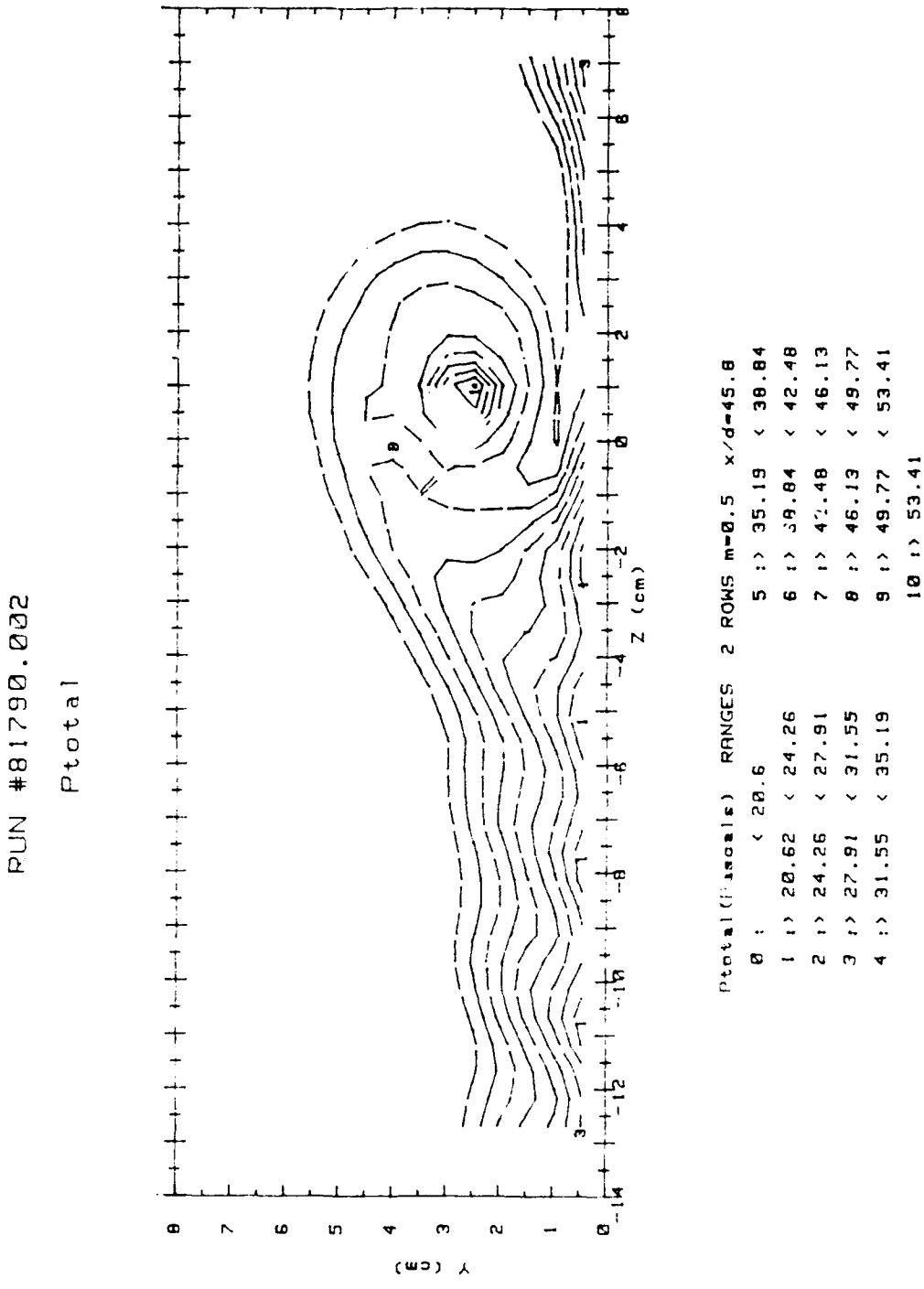

Figure 134. Total Pressure Field, x/d=45 δ, 2 Rows, Vortex R3

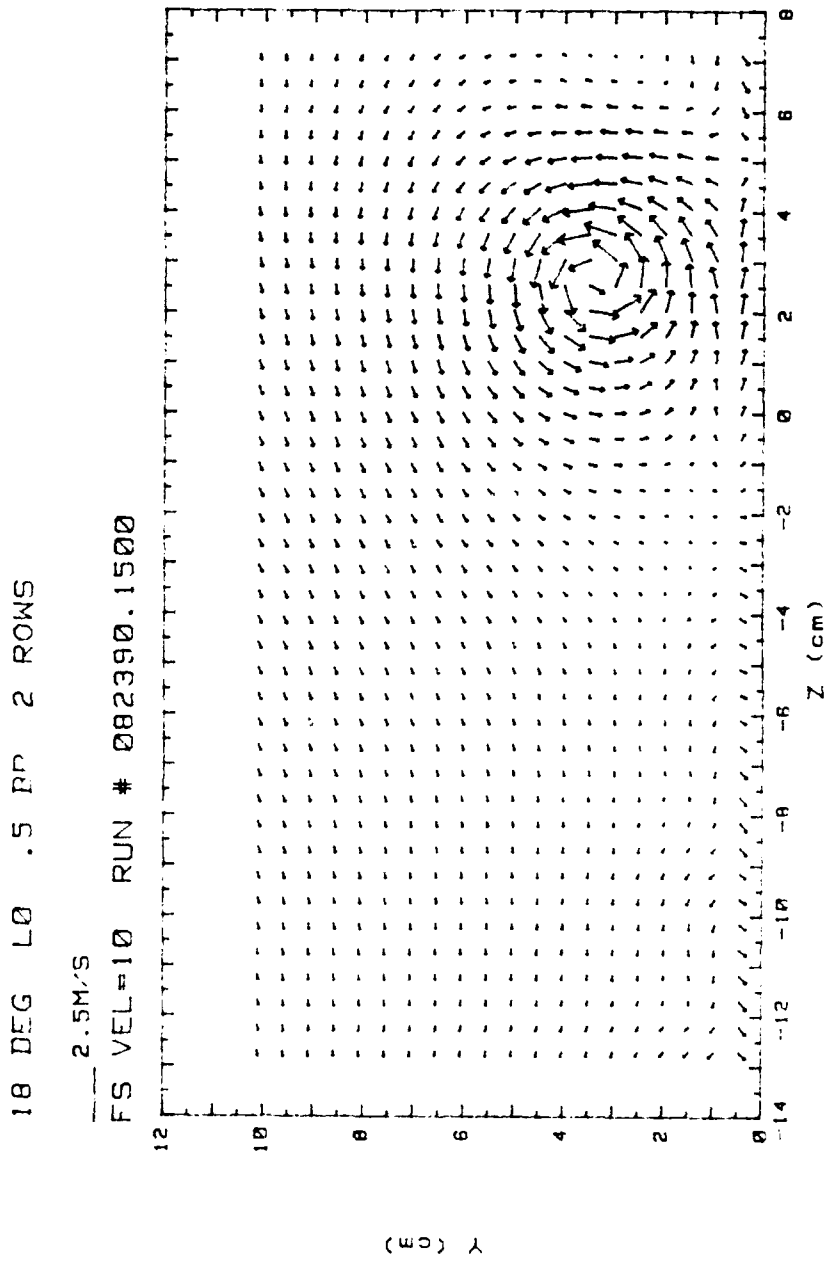

Figure 135. Secondary Flow Vectors, x/d=45.8, 2 Rows, Vortex L0

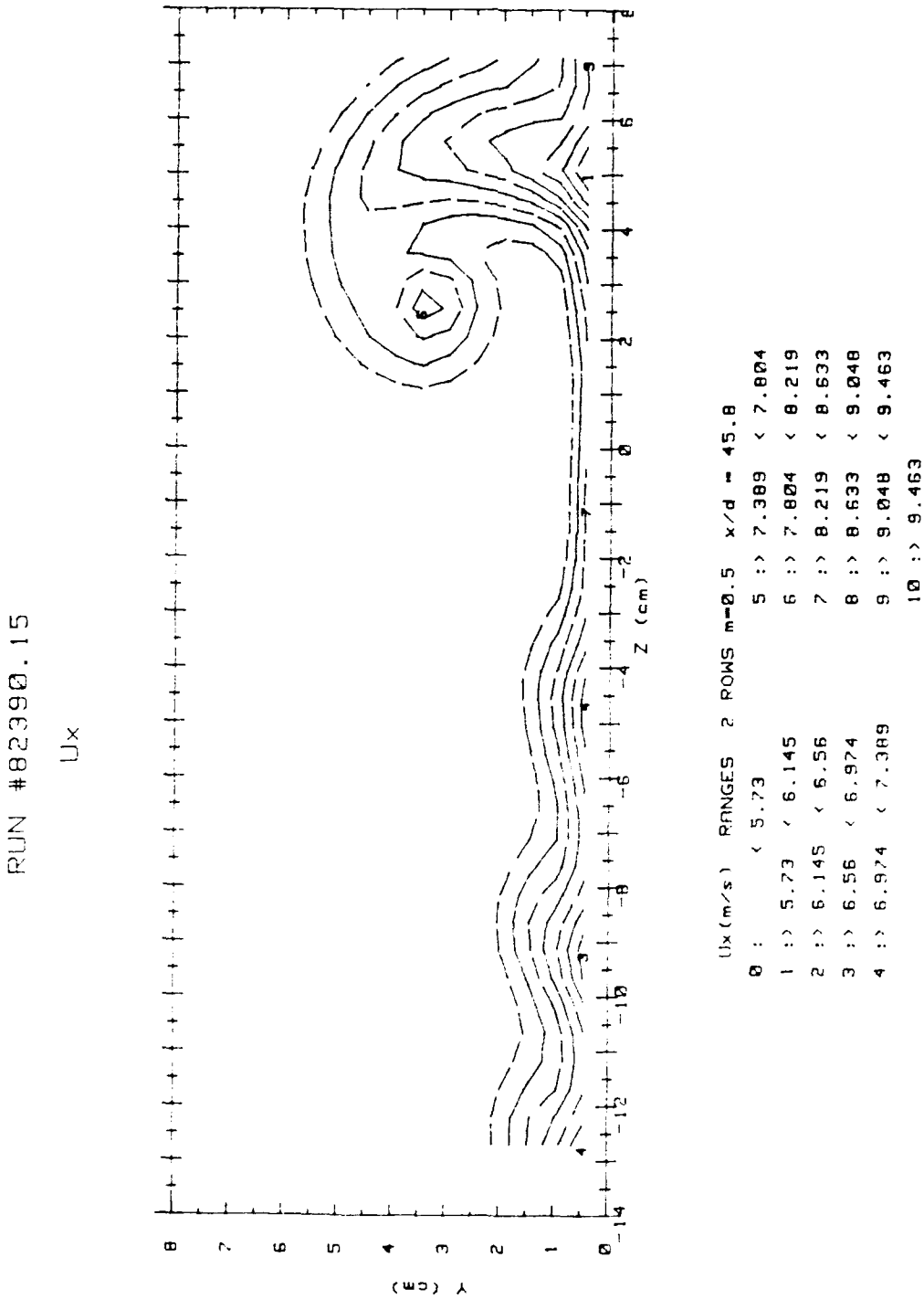

Figure 136. Streamwise Velocity Field, x/d=45.8, 2 Rows, Vortex L0

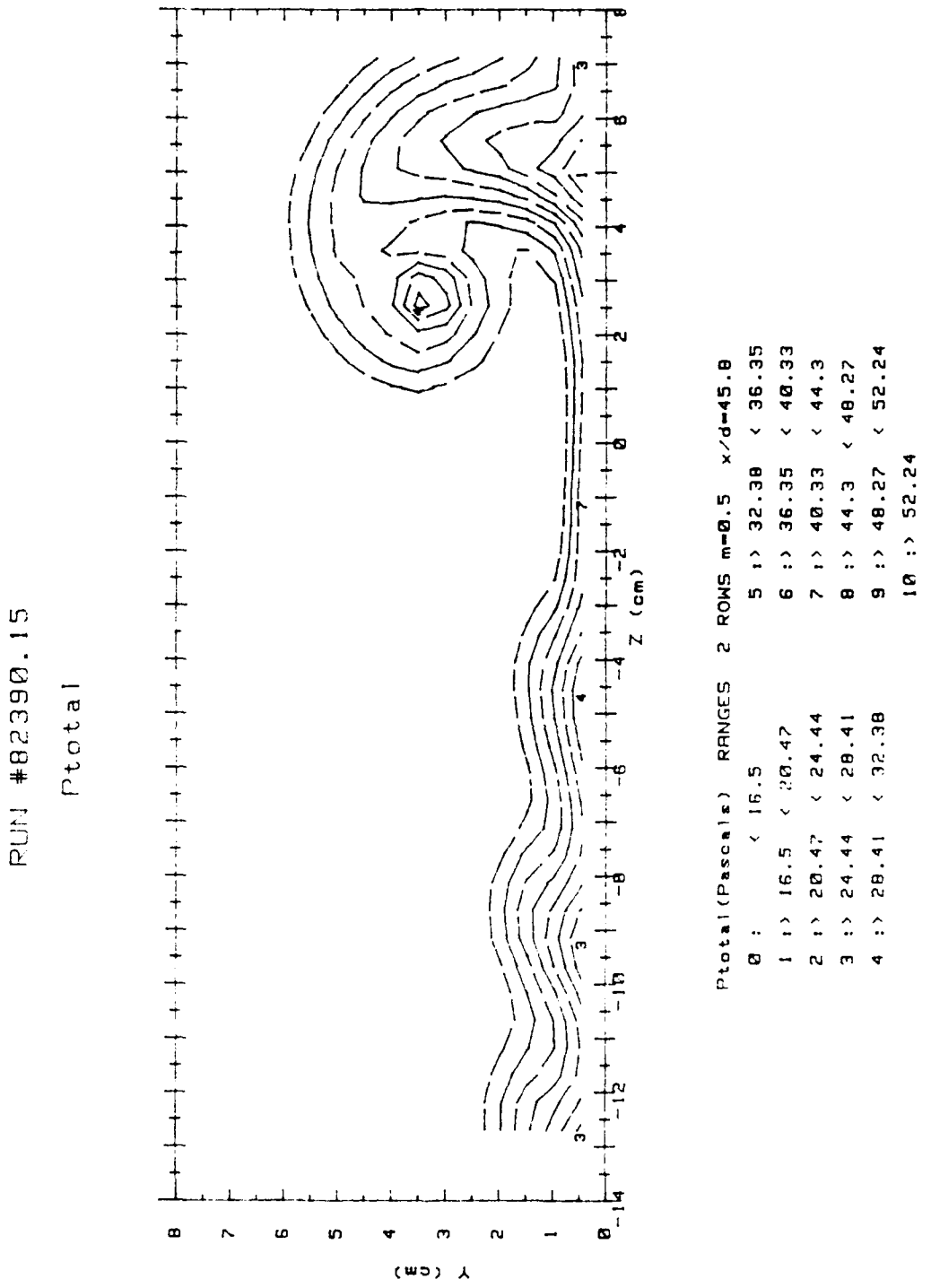

Figure 137. Total Pressure Field, x/d=45.8, 2 Rows, Vortex L0

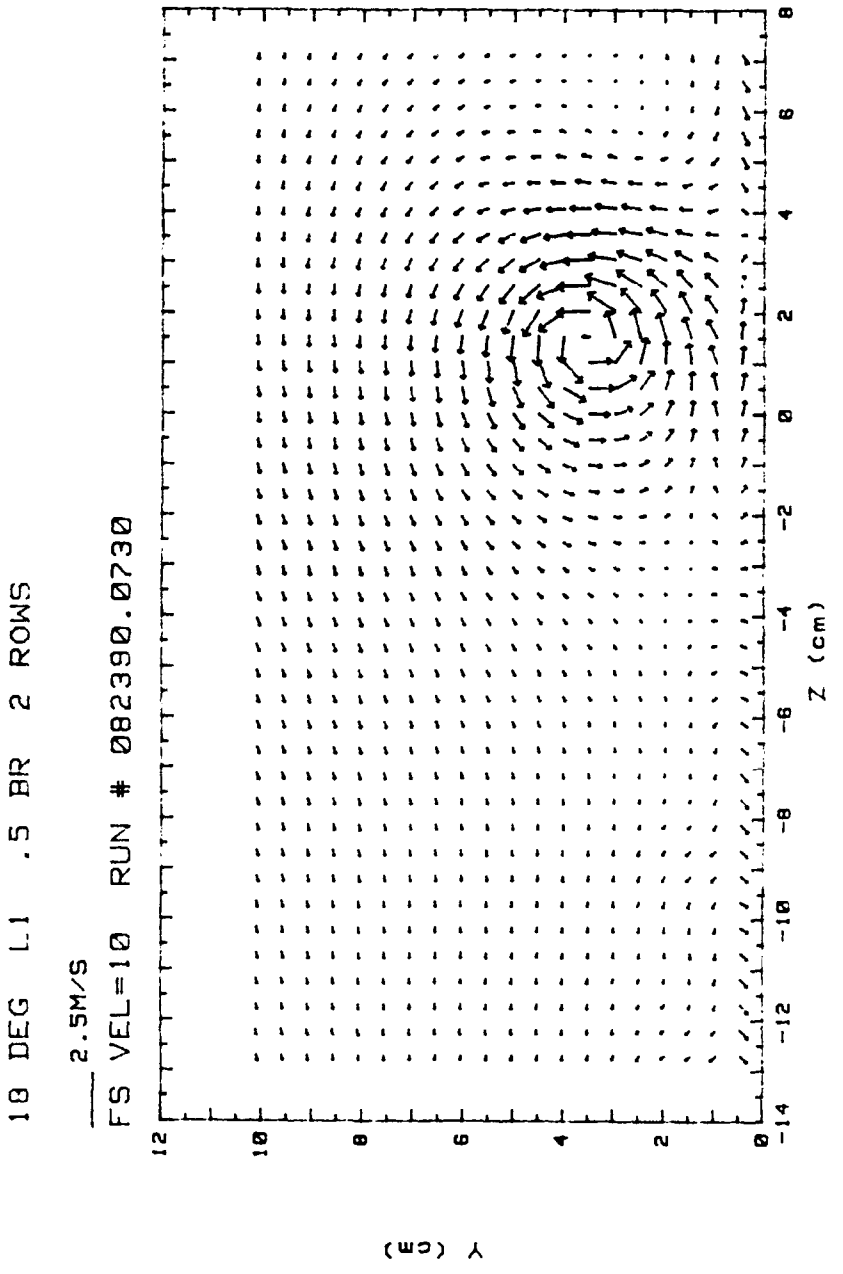

Figure 138. Secondary Flow Vectors, x/d=45.8, 2 Rows, Vortex L1

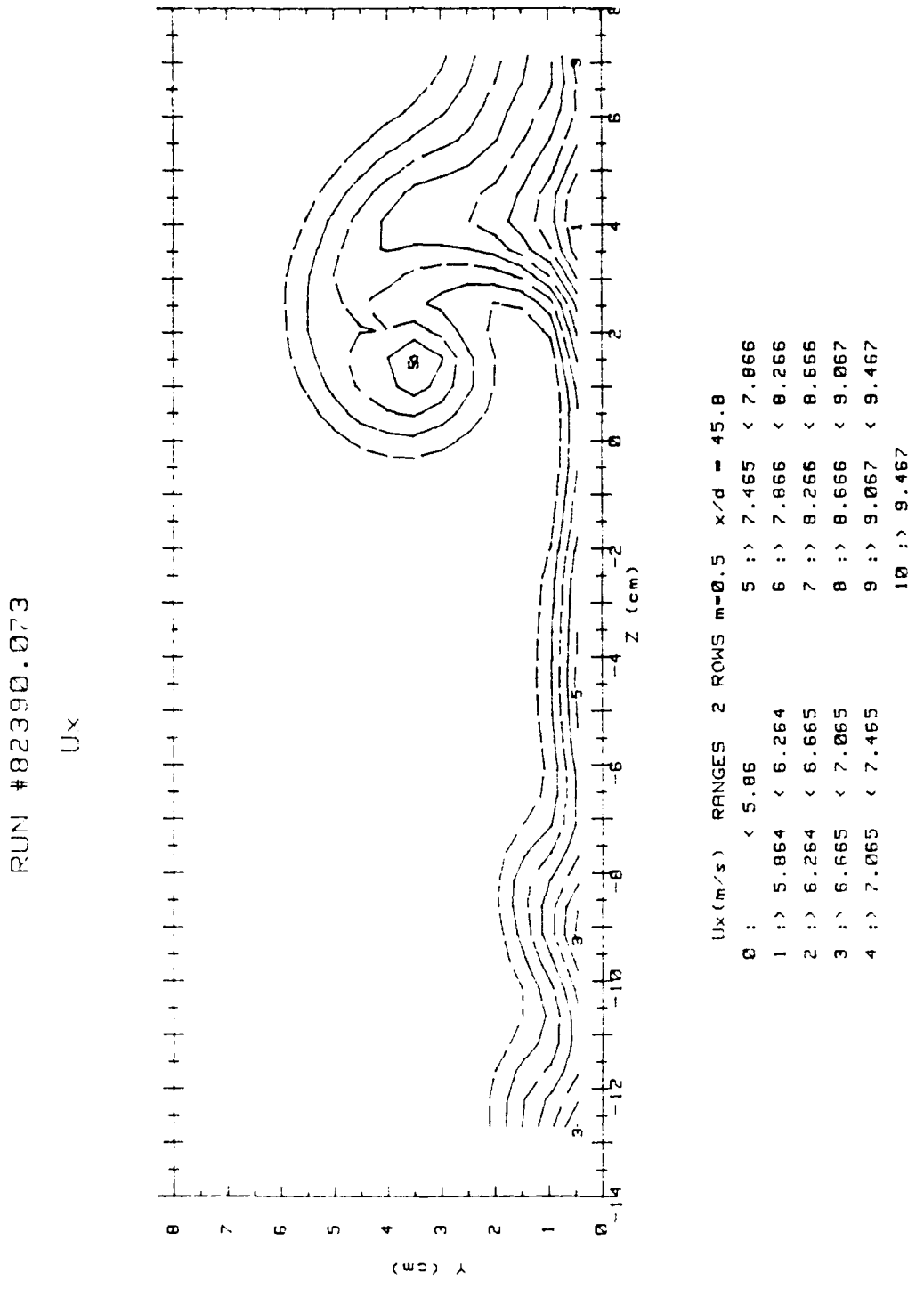

Figure 139. Streamwise Velocity Field, x/d=45.8, 2 Rows, Vortex L1

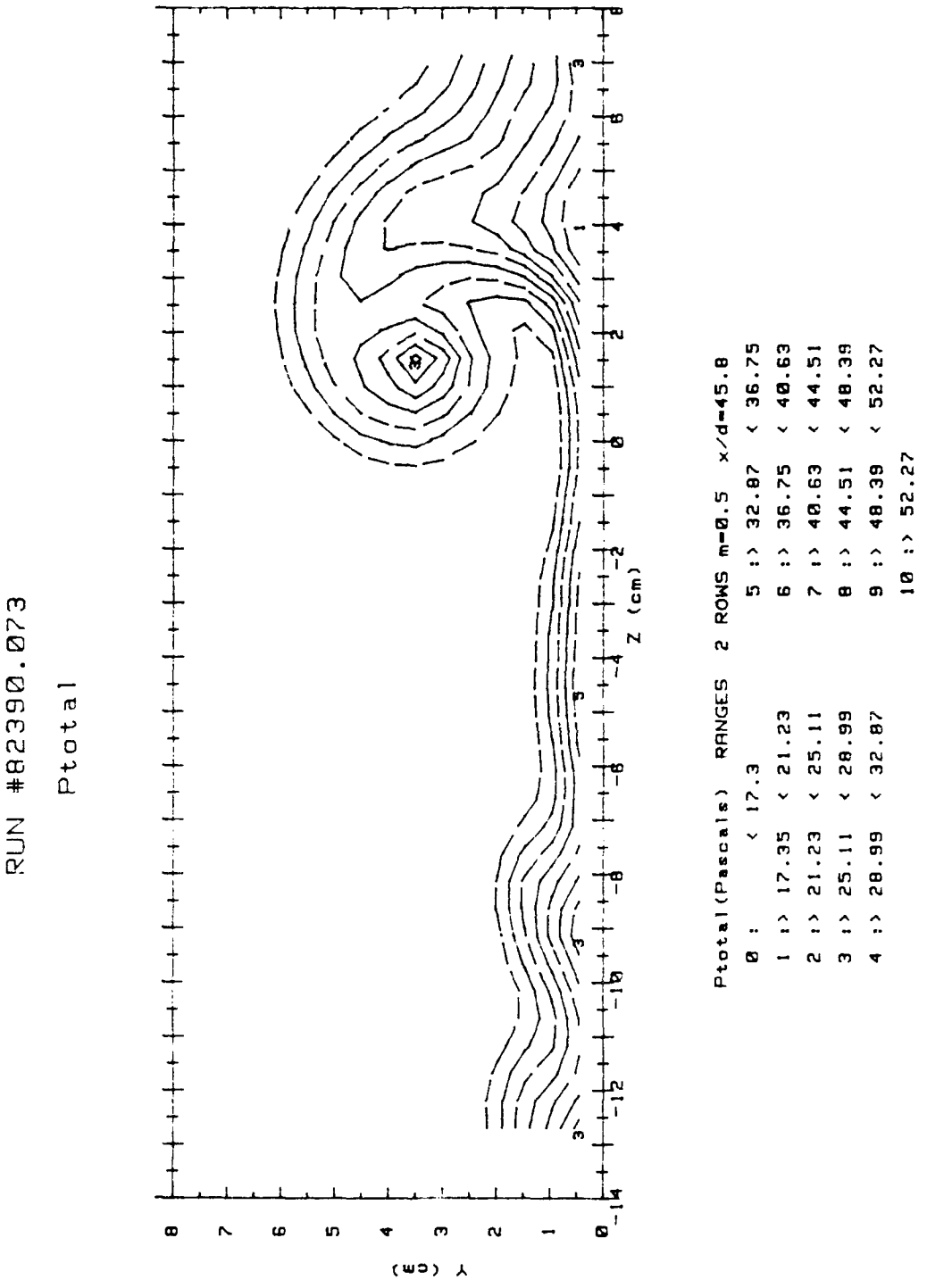

Figure 140. Total Pressure Field, x/d=45.8, 2 Rows, Vortex L1

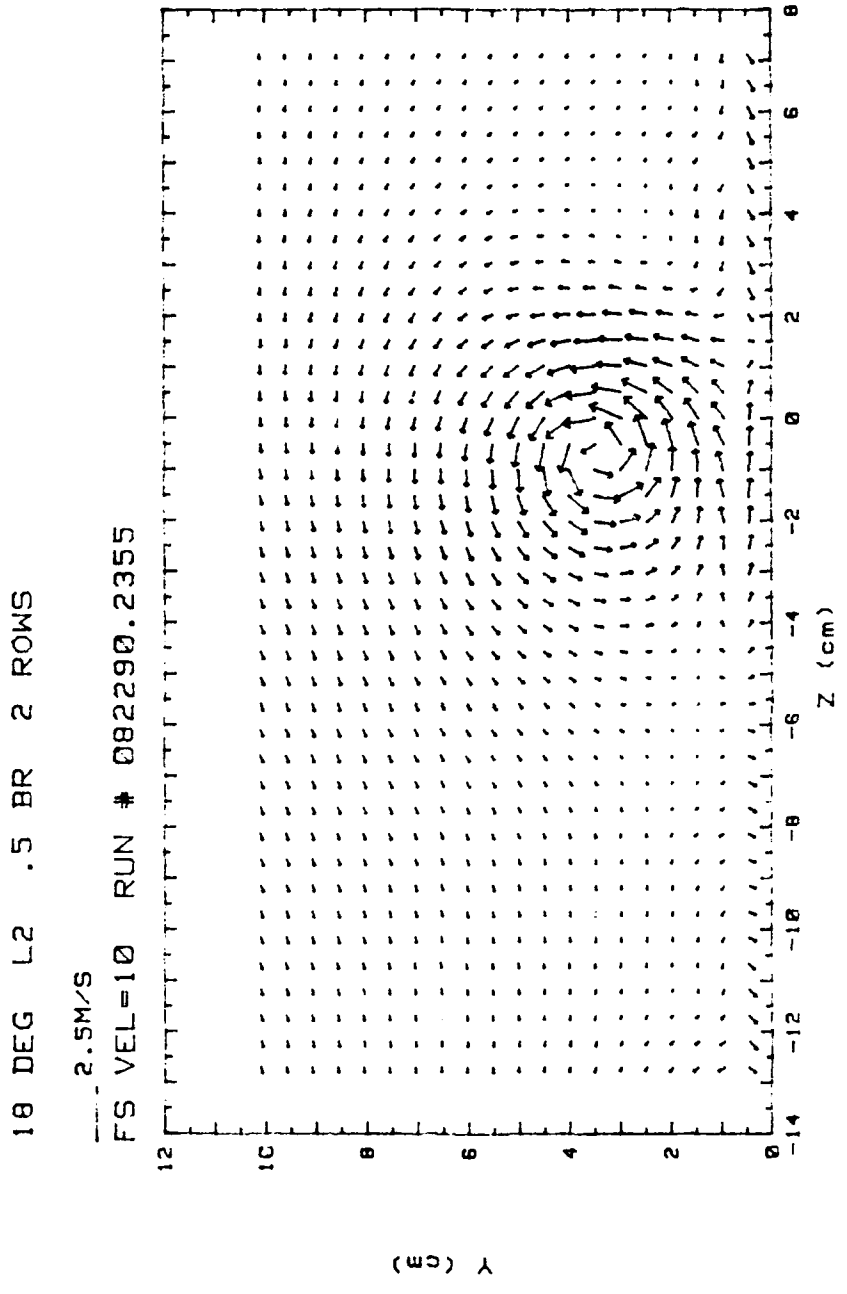

Figure 141. Secondary Flow Vectors, x/d=45.8, 2 Rows, Vortex L2

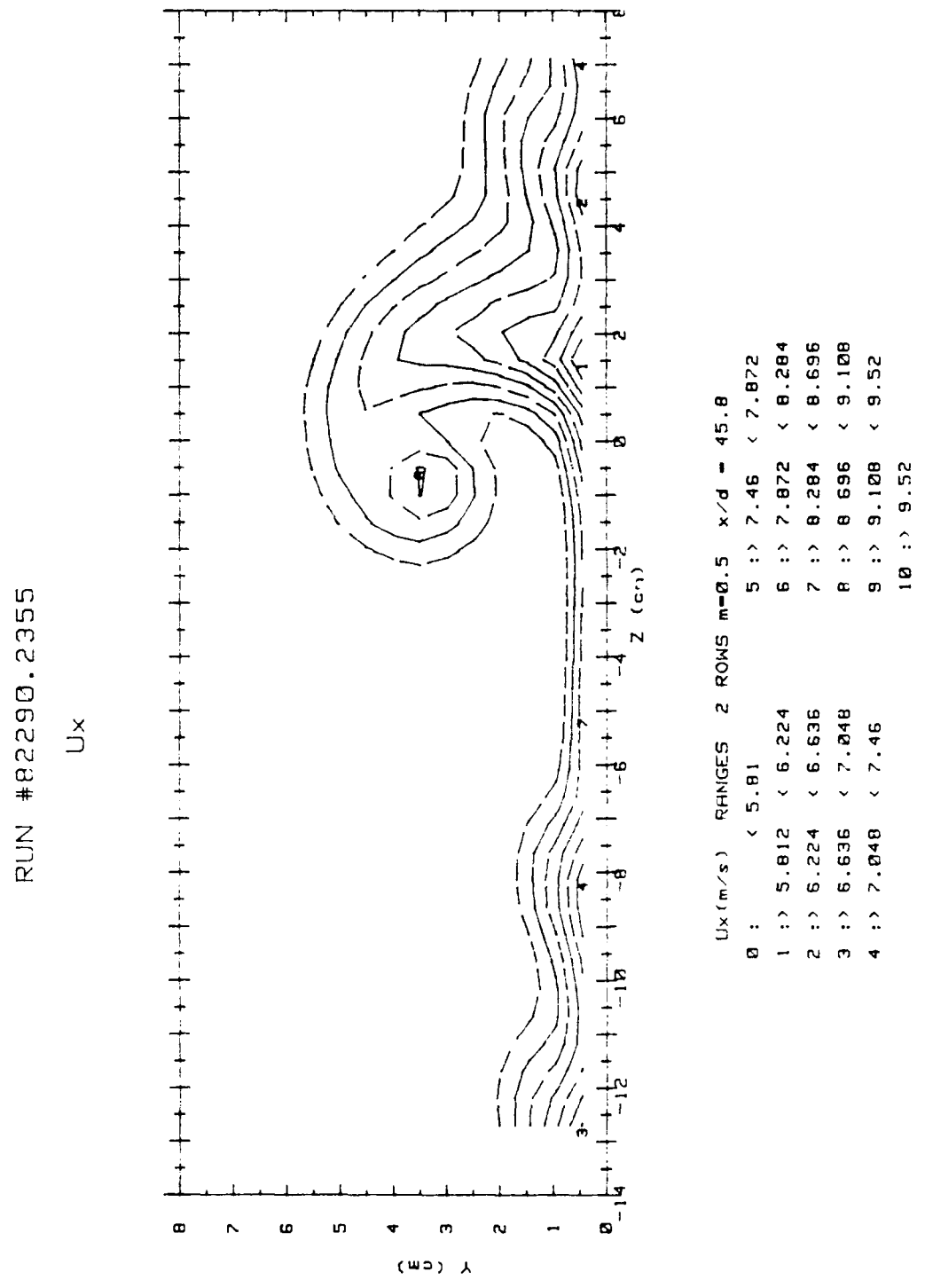

Figure 142. Streamwise Velocity Field, x/d=45.8, 2 Rows, Vortex L2

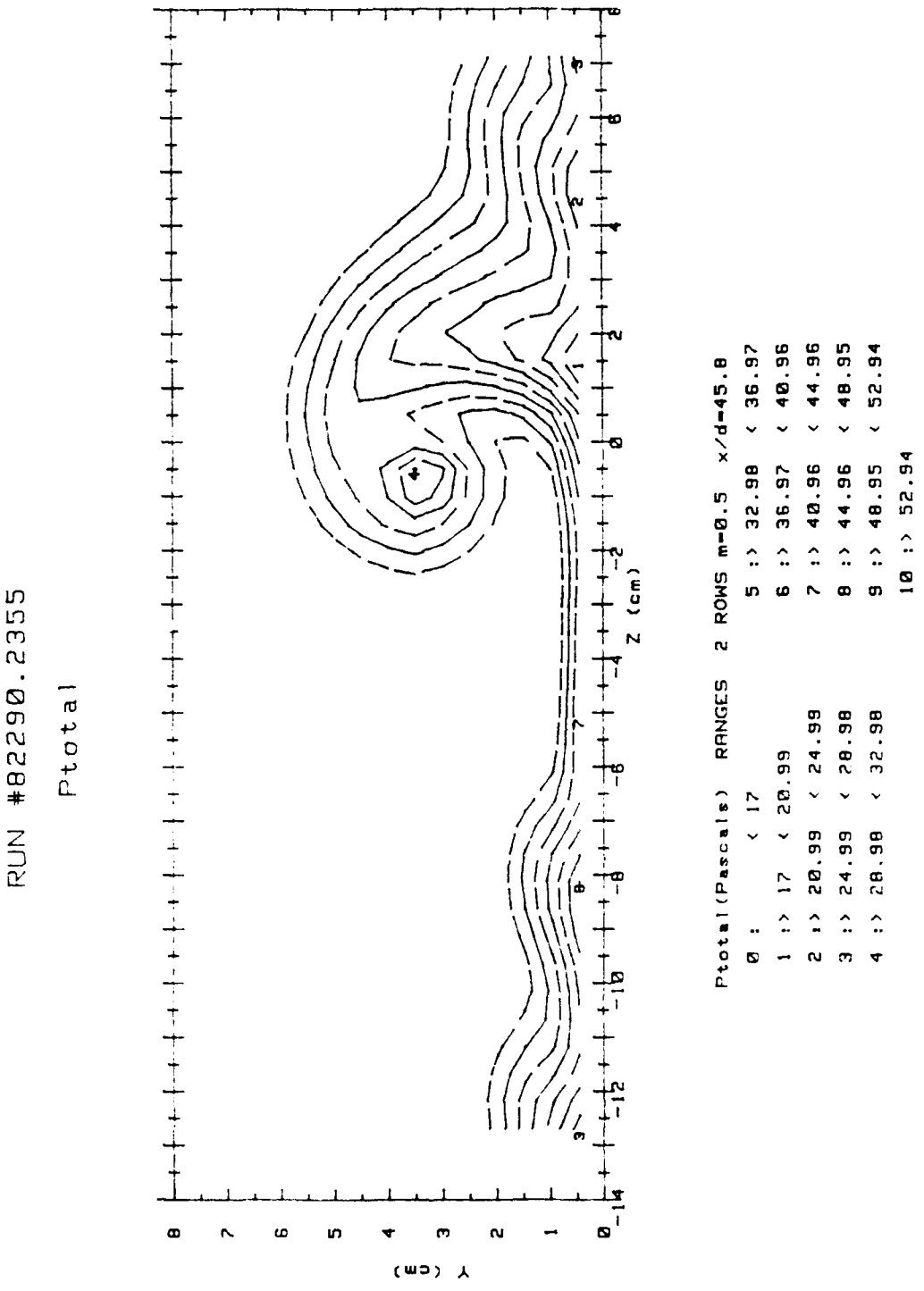

Figure 143. Total Pressure Field, x/d=45.8, 2 Rows, Vortex L2

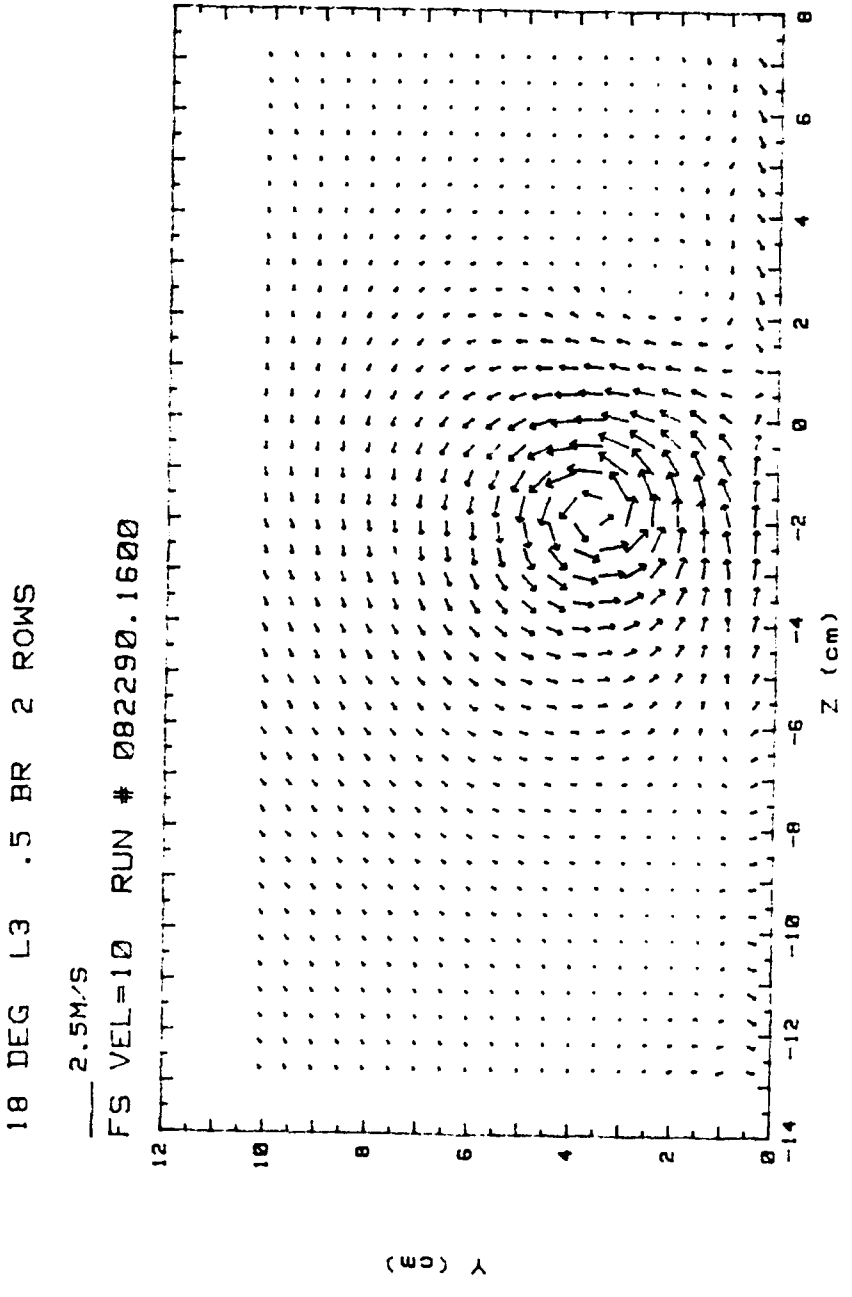

Figure 144. Secondary Flow Vectors, x/d=45.8, 2 Rows, Vortex L3

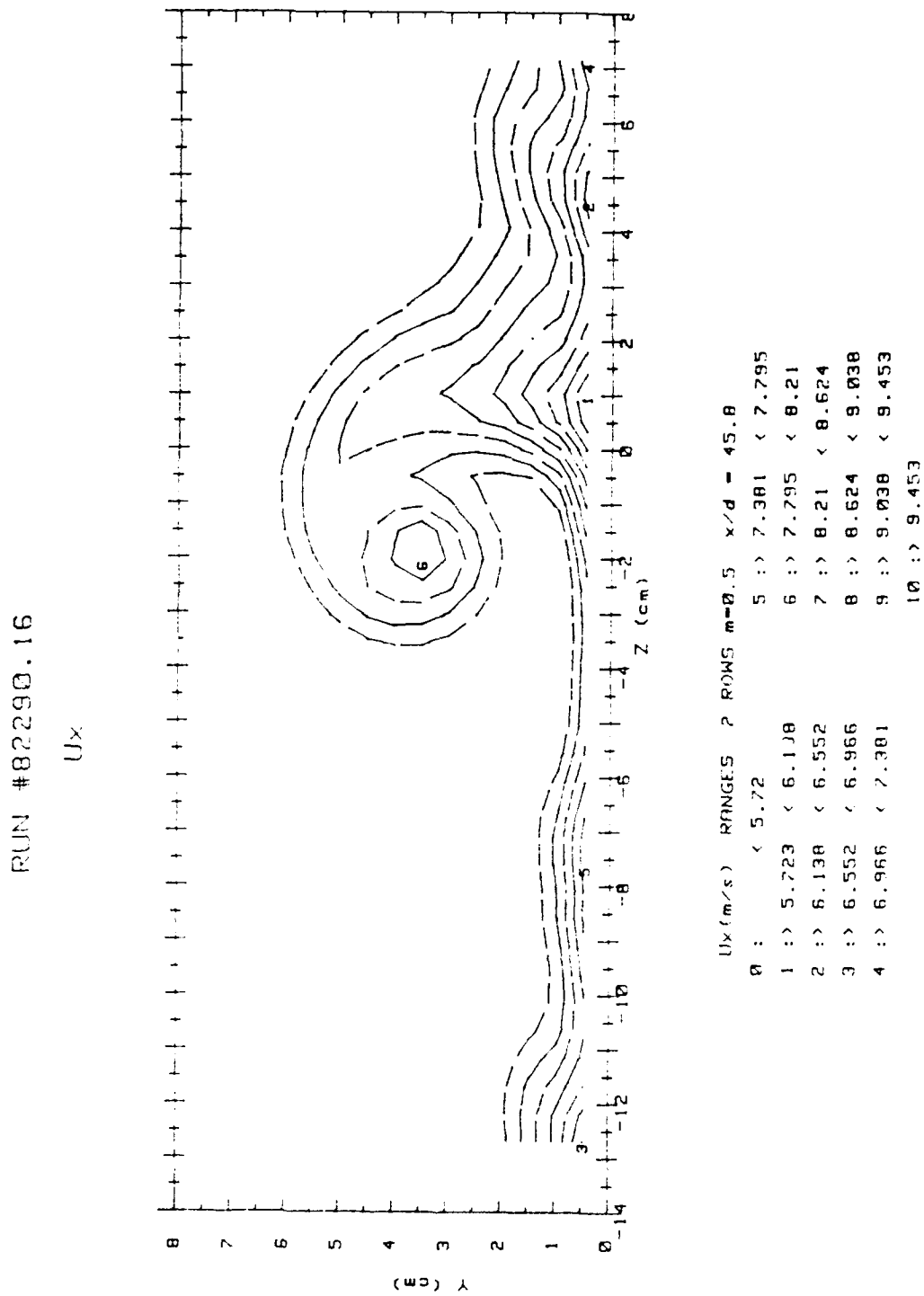

Figure 145. Streamwise Velocity Field, x/d=45.8, 2 Rows, Vortex L3

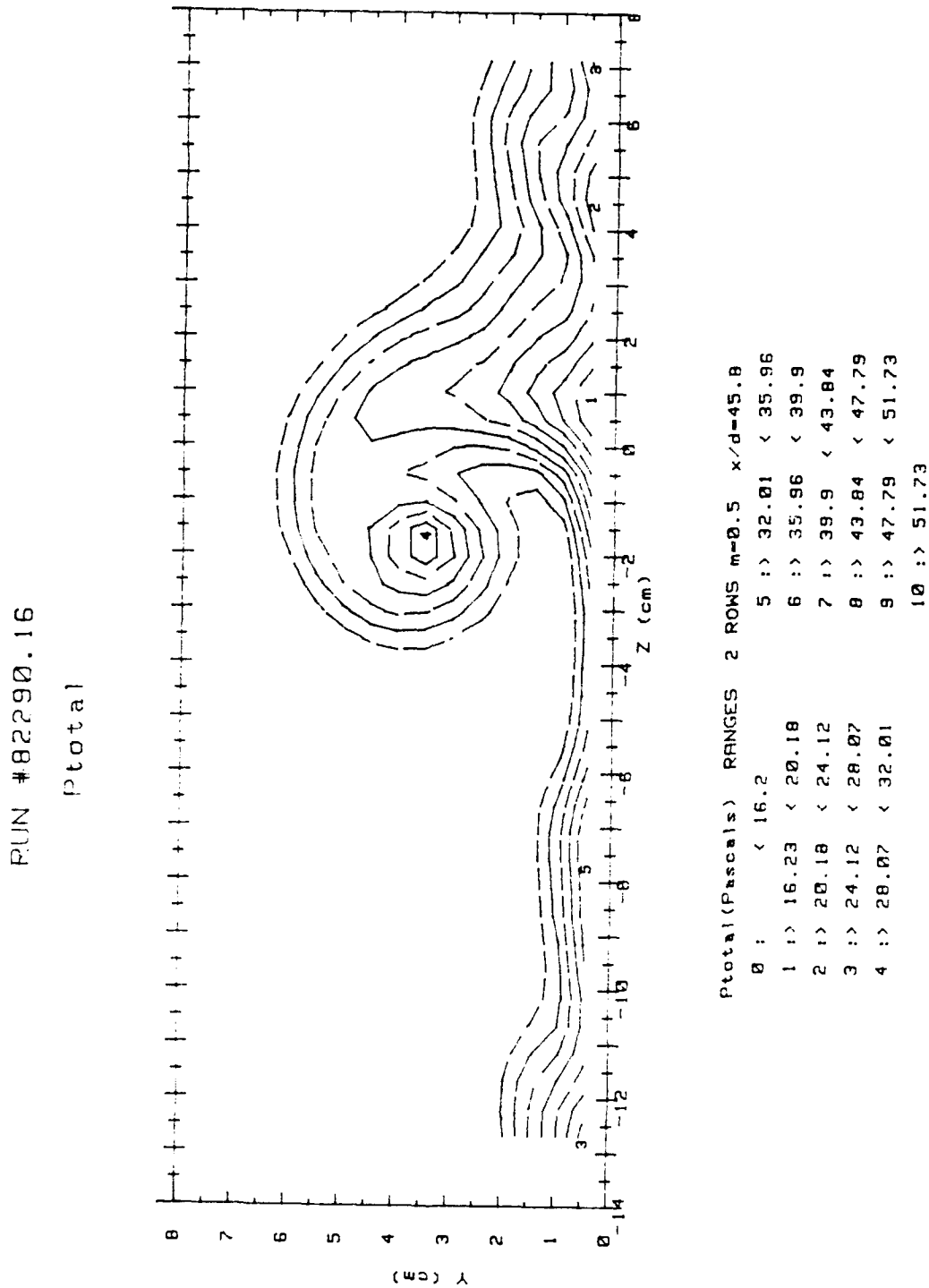

Figure 146. Total Pressure Field, x/d=45.8, 2 Rows, Vortex L3

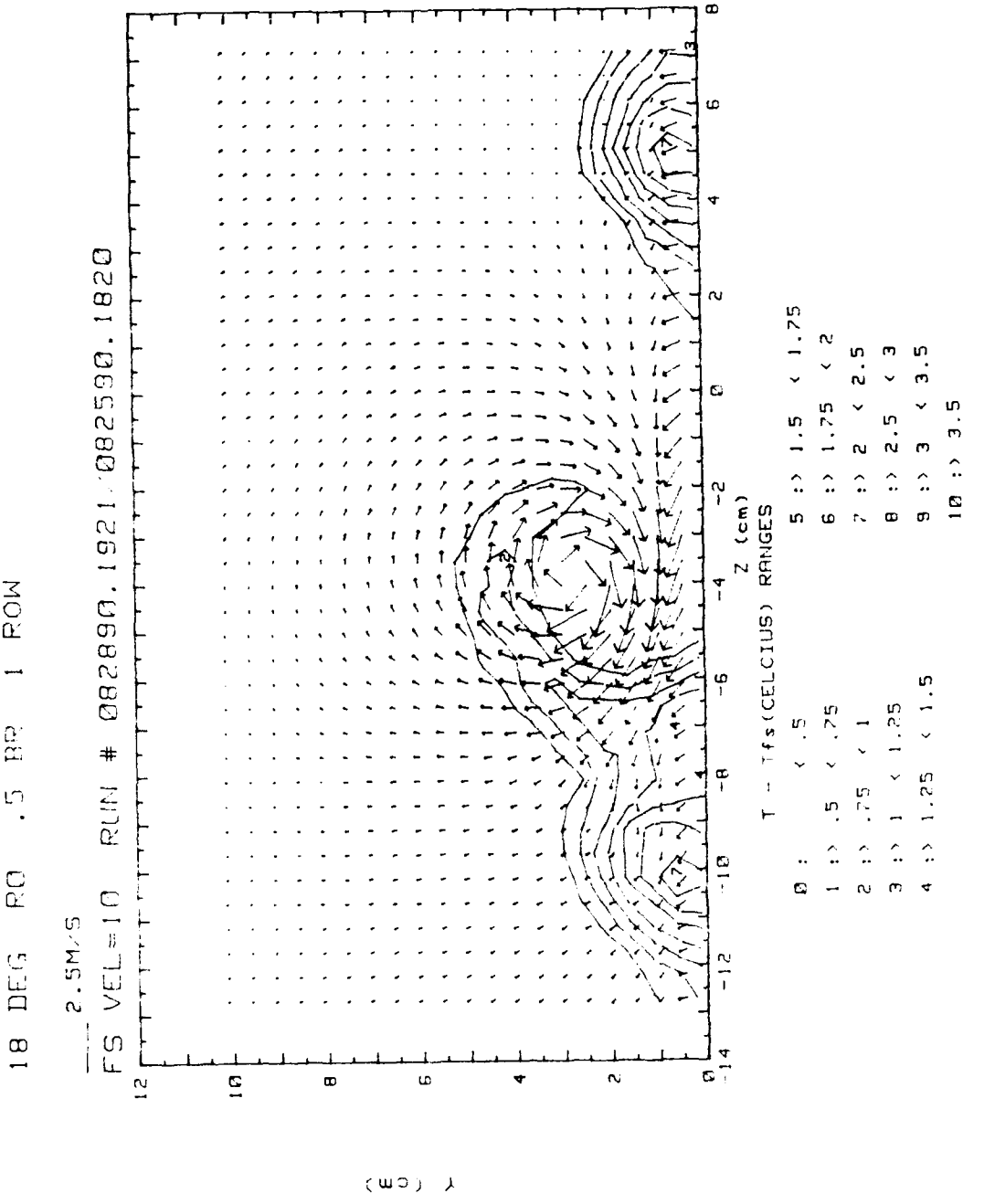

Figure 147. Composite Plot, x/d=45.8, 1 Row, Vortex R0

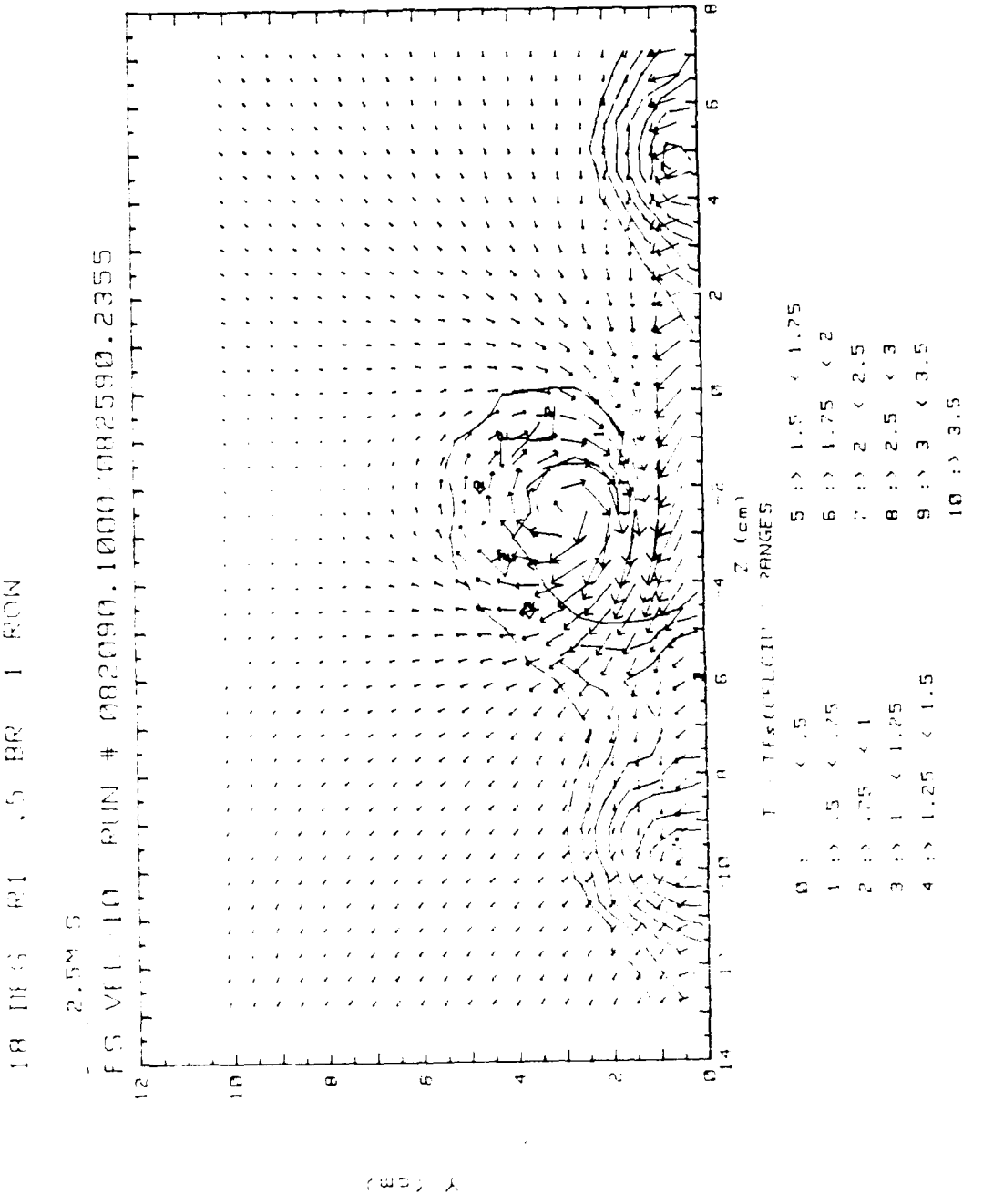

Figure 148. Composite Plot, x/d=45.8, 1 Row, Vortex R1

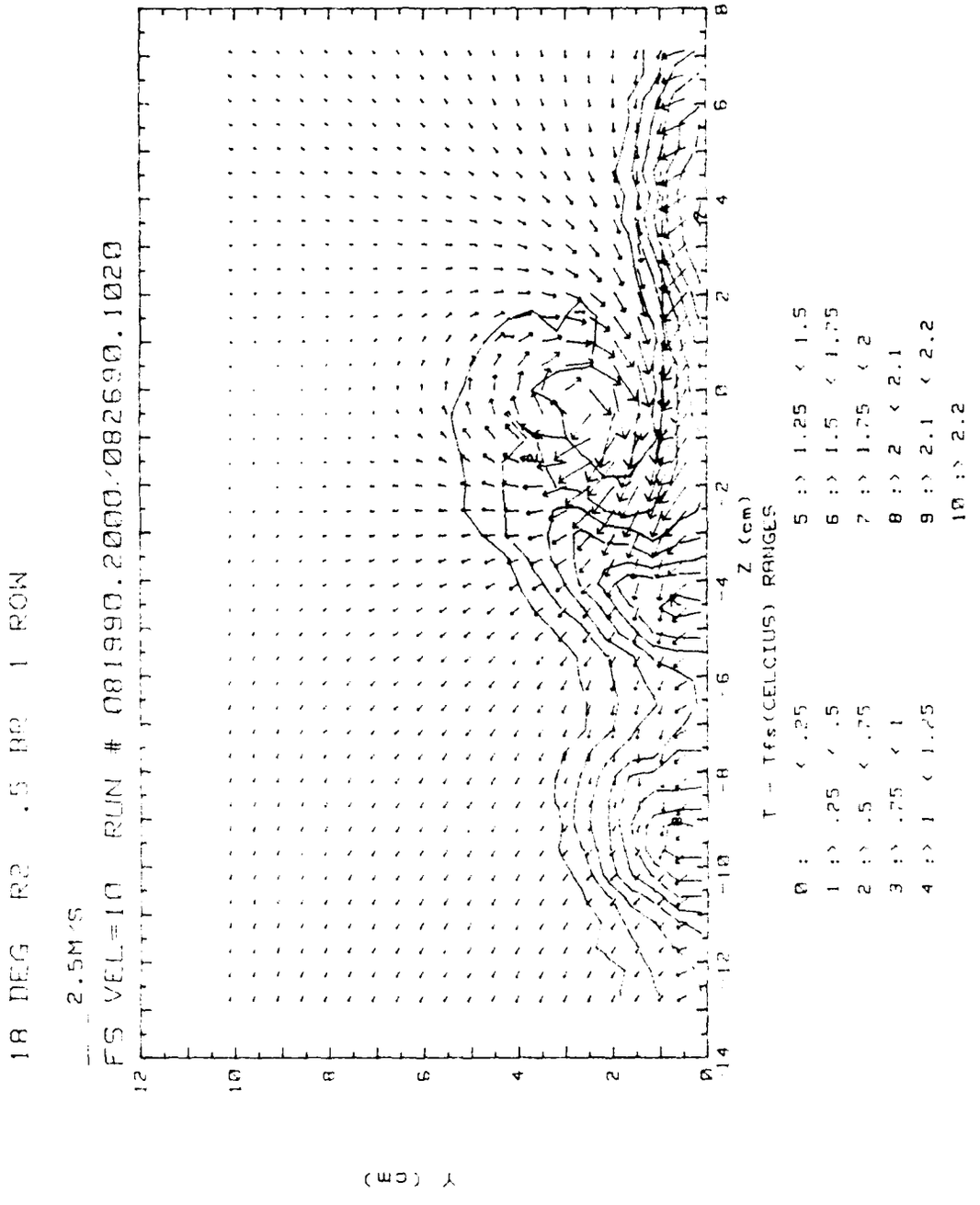

Figure 149. Composite Plot, x/d=45.8, 1 Row, Vortex R2

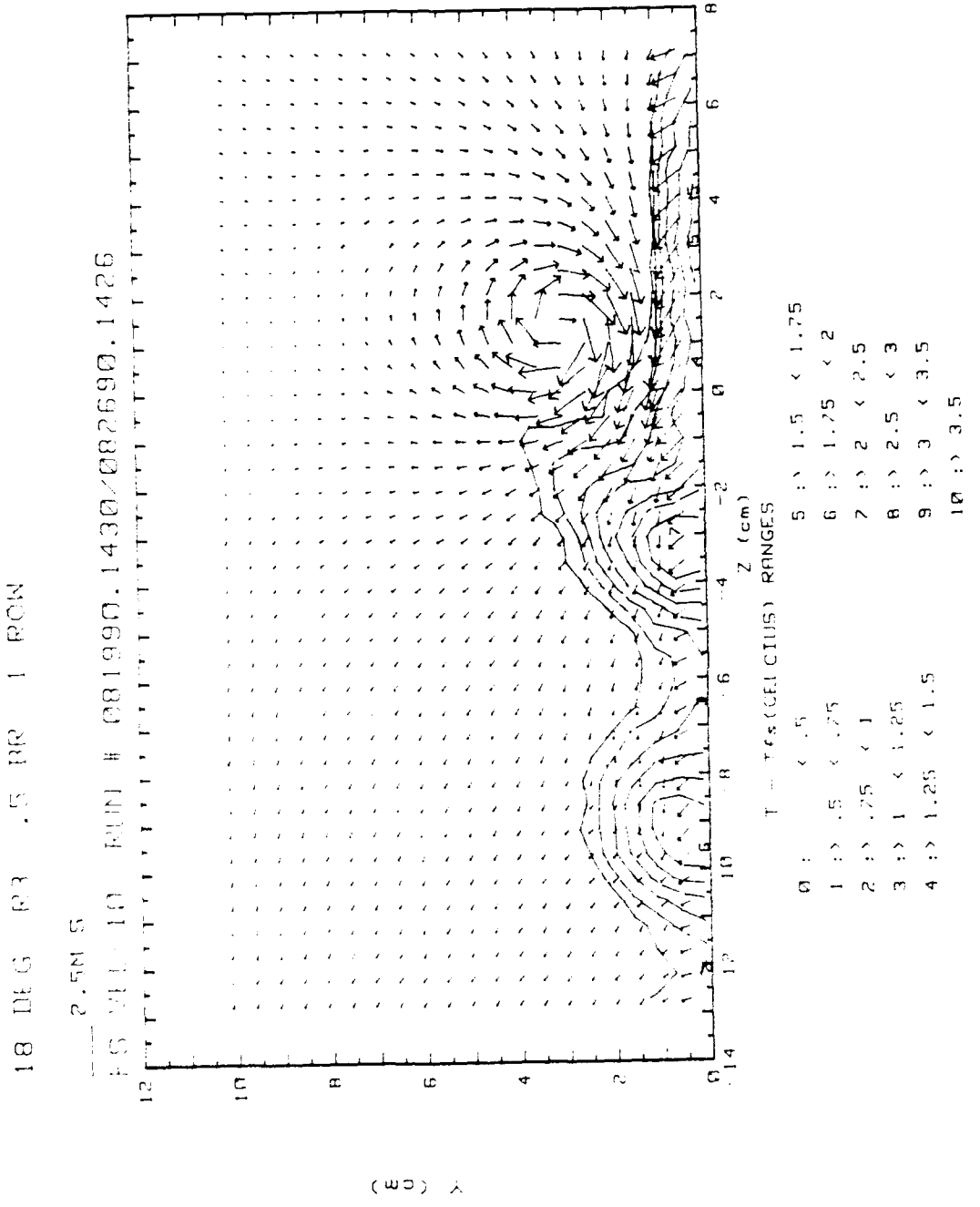

Figure 150. Composite Plot, x/d=45.8, 1 Row, Vortex R3

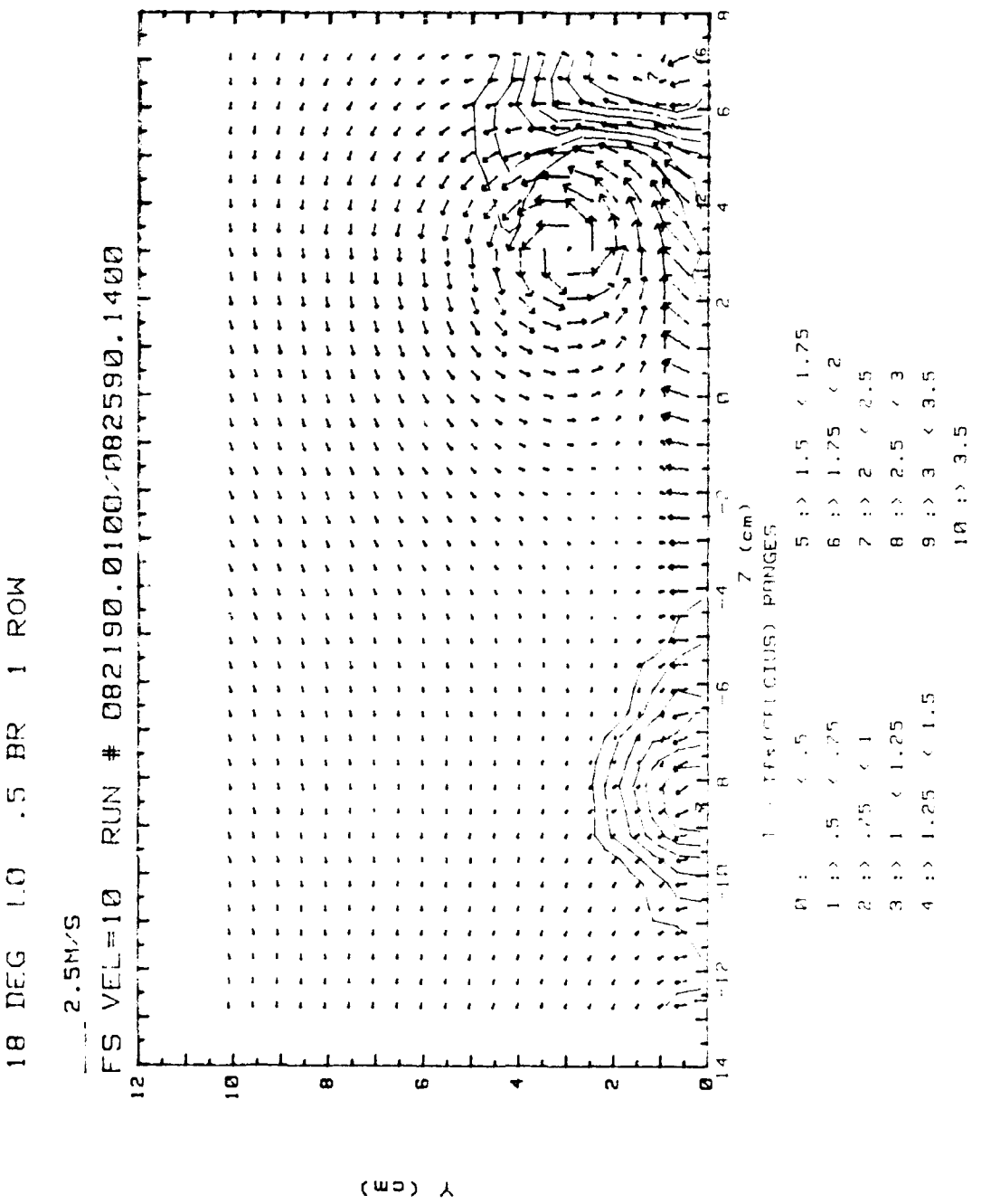

Figure 151. Composite Plot, x/d=45.8, 1 Row, Vortex L0

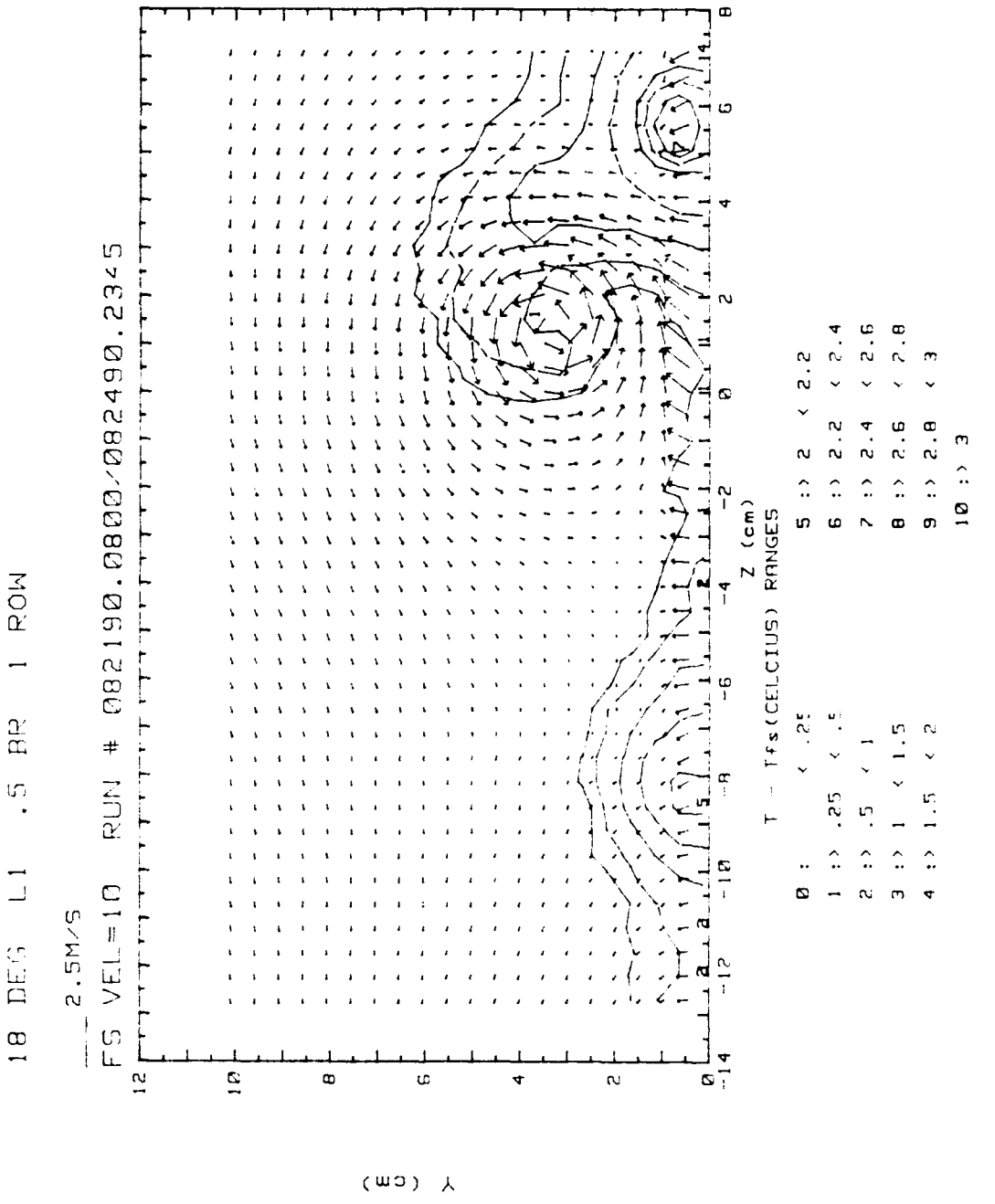

Figure 152. Composite Plot, x/d=45.8, 1 Row, Vortex L1

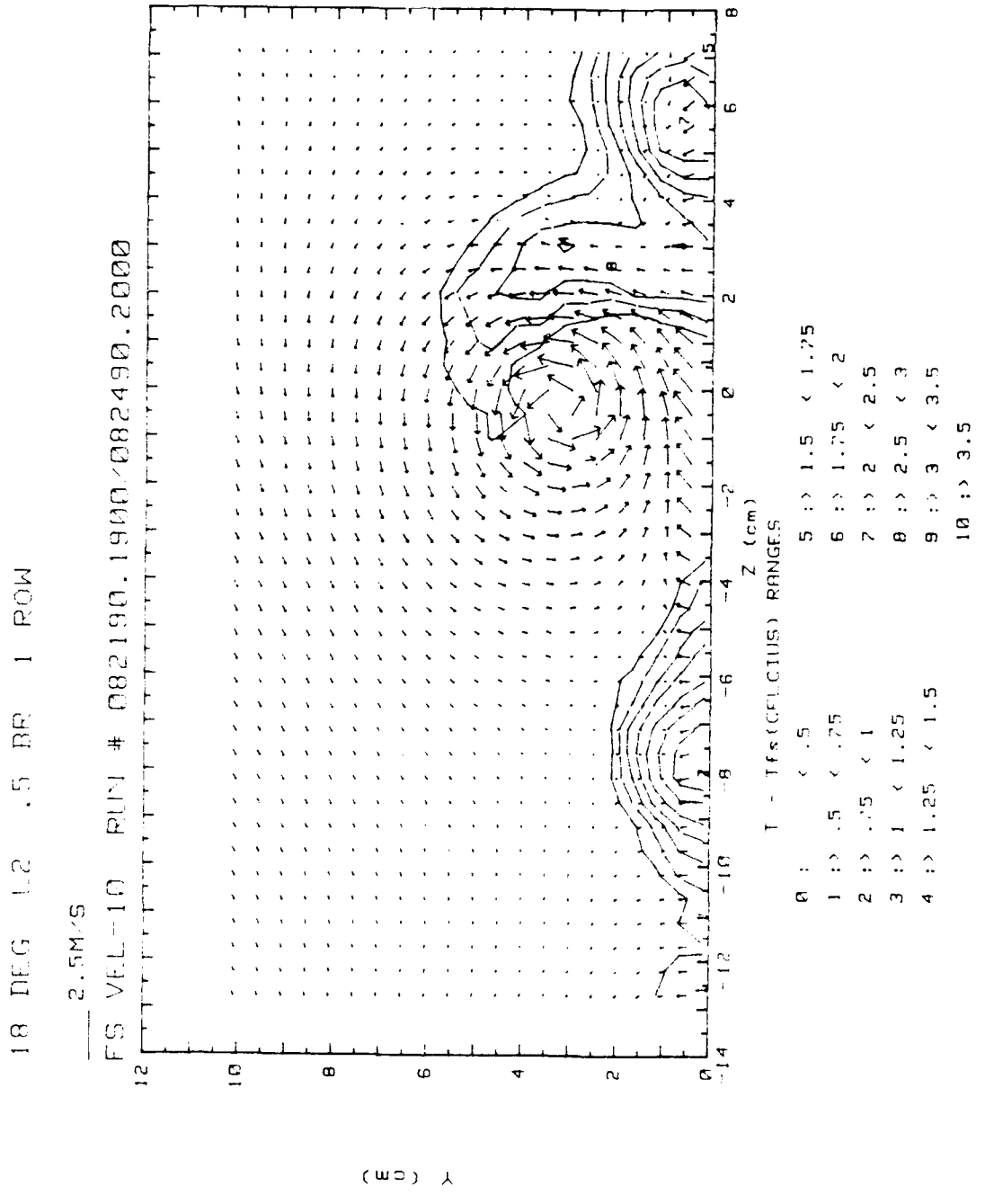

Figure 153. Composite Plot, x/d=45.8, 1 Row, Vortex L2

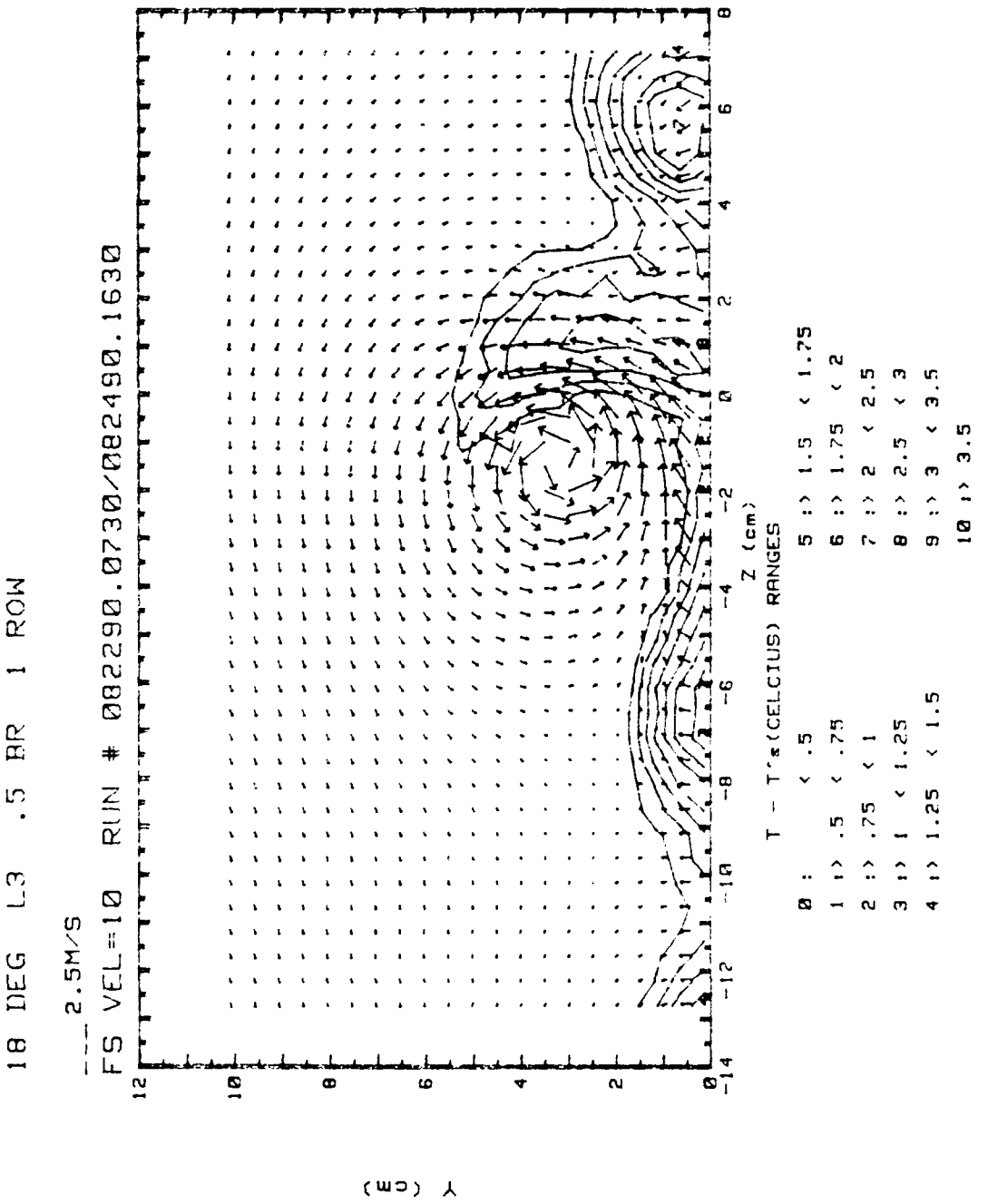

Figure 154. Composite Plot, x/d=45.8, 1 Row, Vortex L3

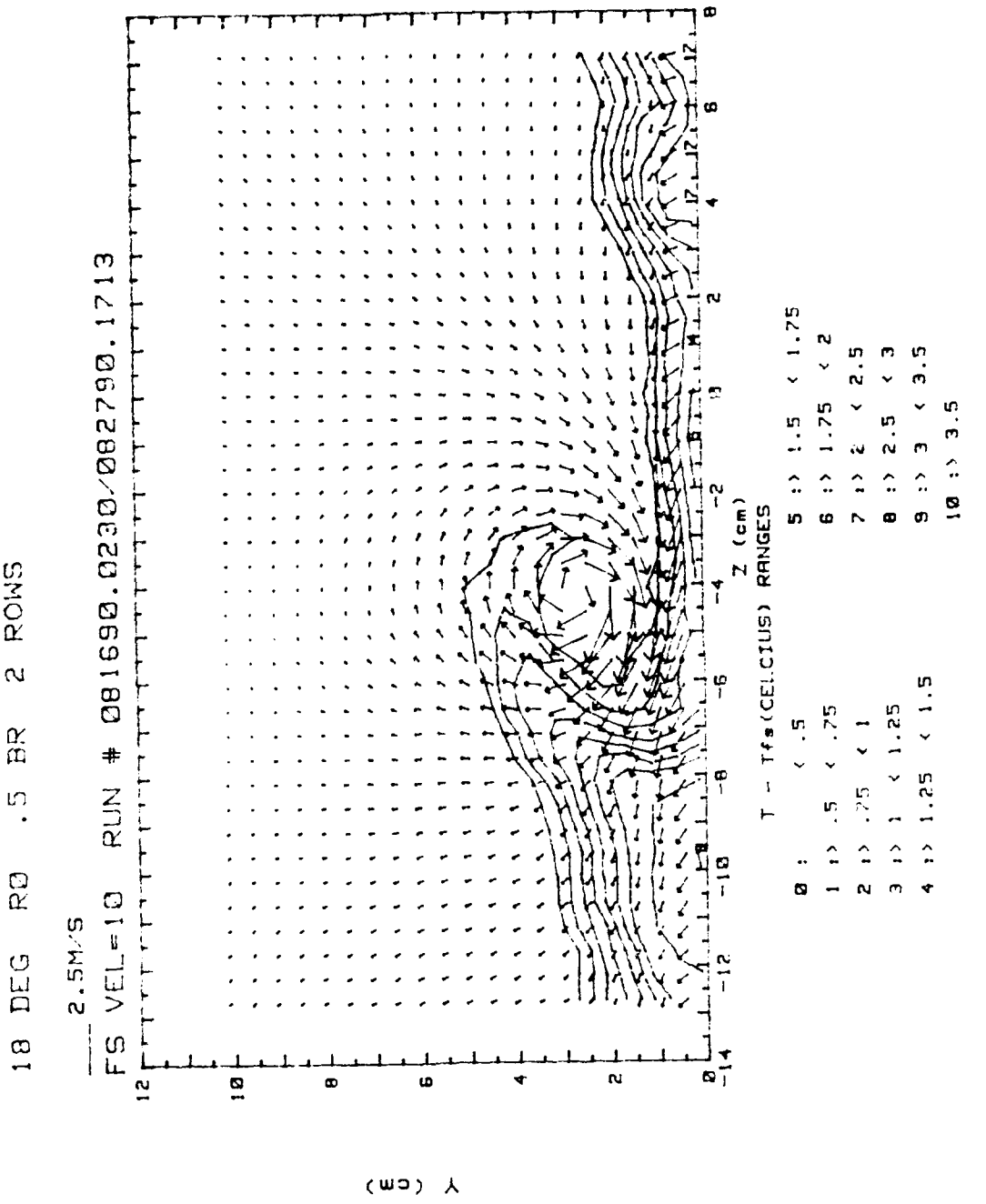

Figure 155. Composite Plot, x/d=45.8, 2 Rows, Vortex R0

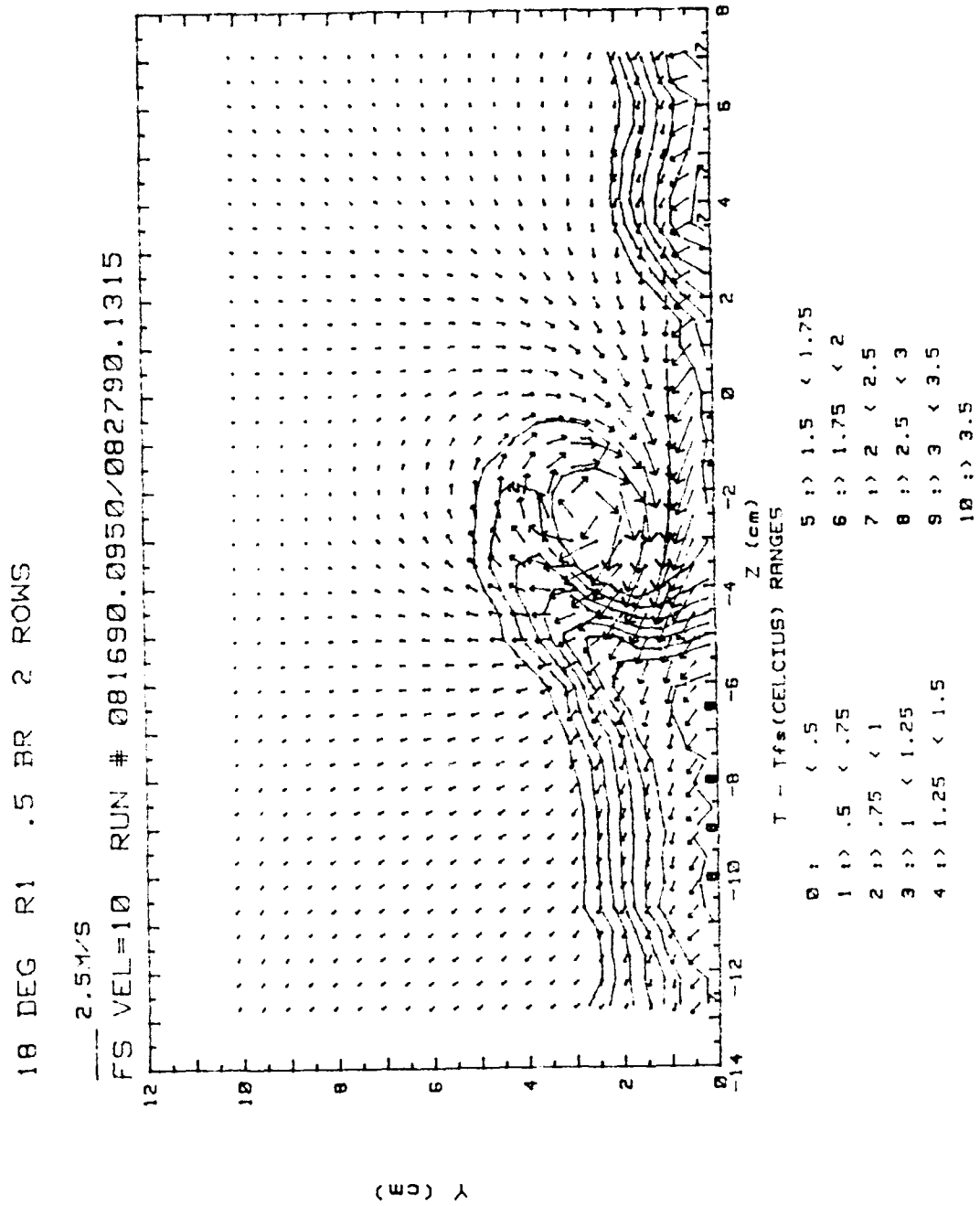

Figure 156. Composite Plot, x/d=45.8, 2 Rows, Vortex R1

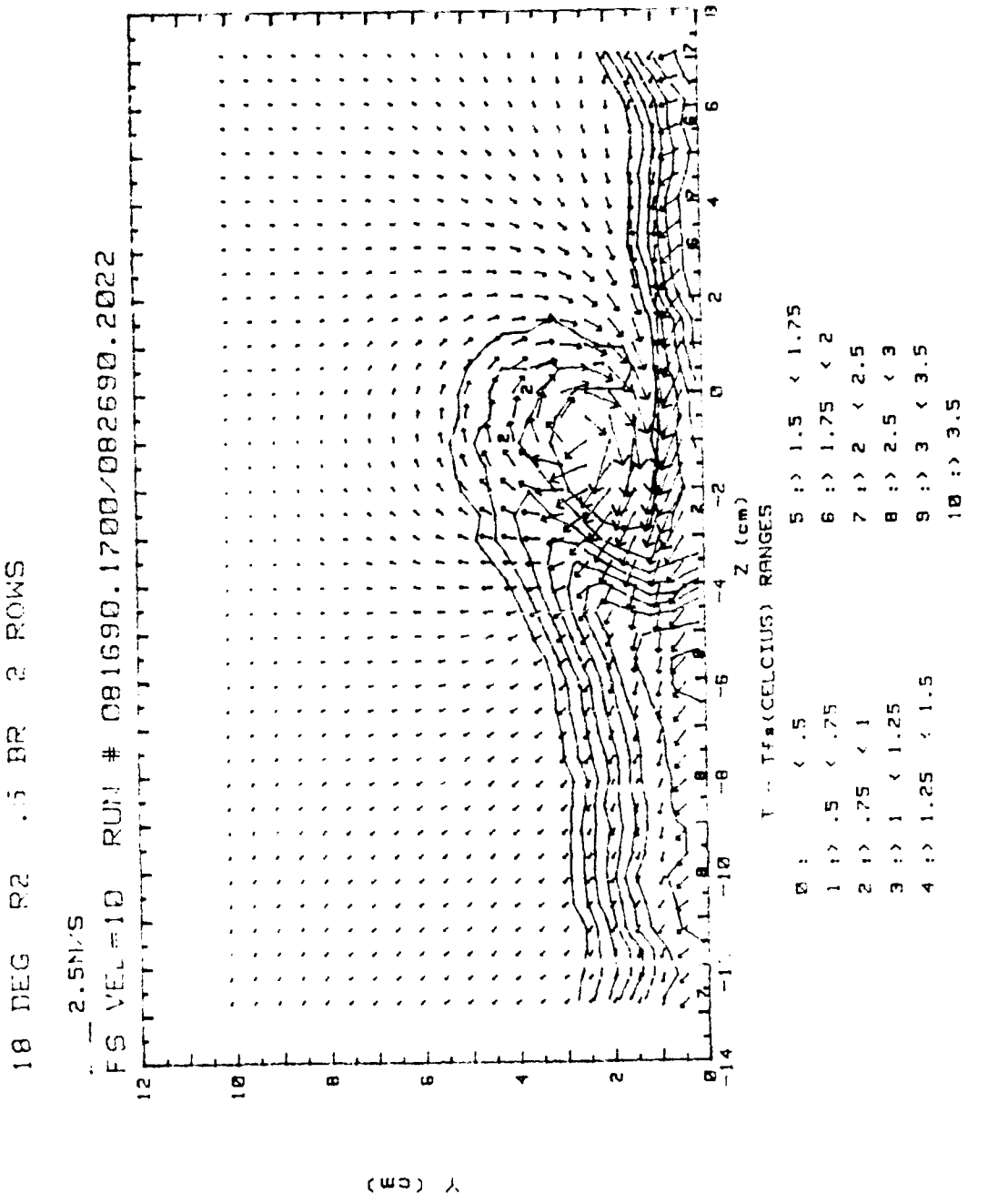

Figure 157. Composite Plot, x/d=45.8, 2 Rows, Vortex R2

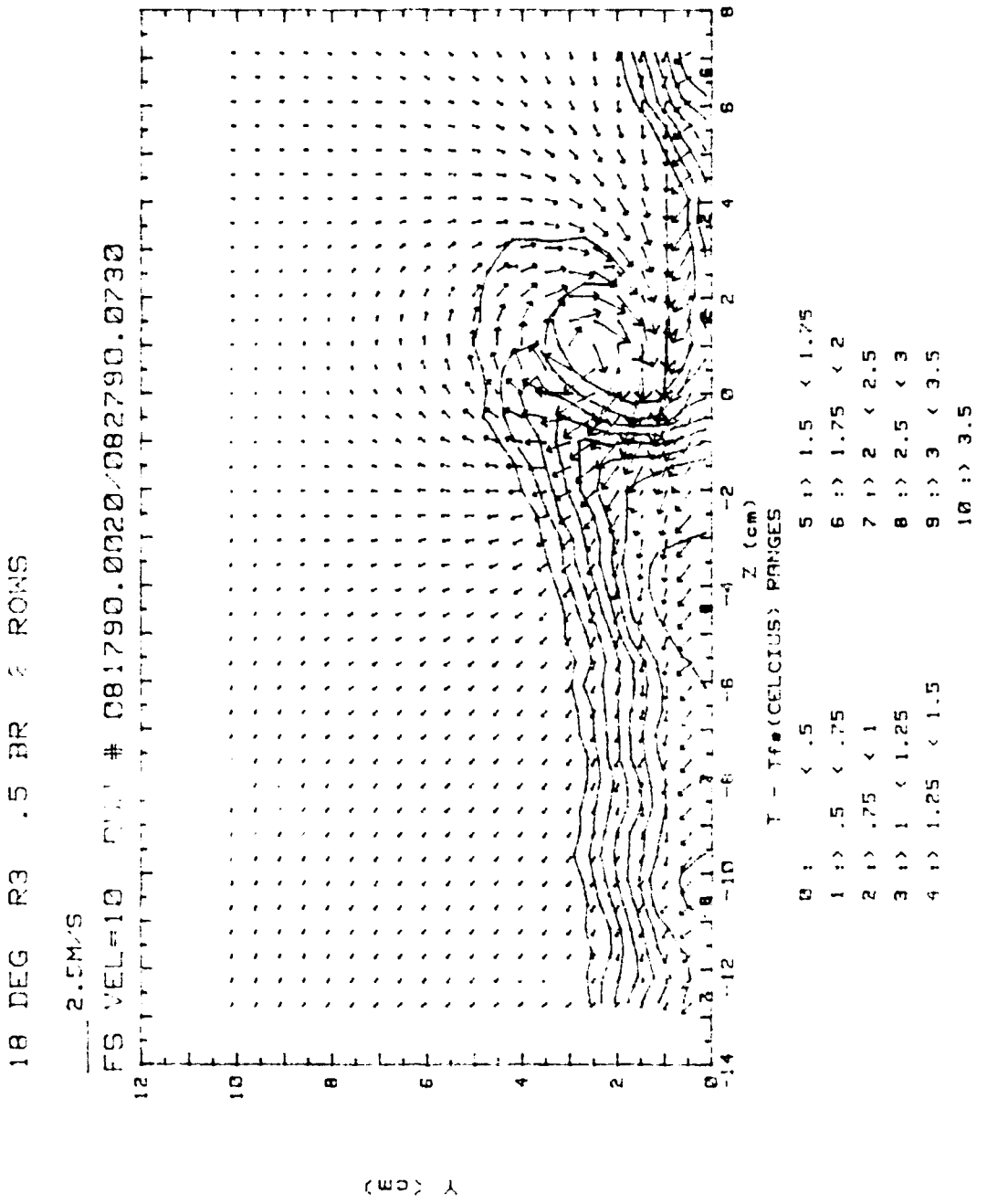

Figure 158. Composite Plot, x/d=45.8, 2 Rows, Vortex R3

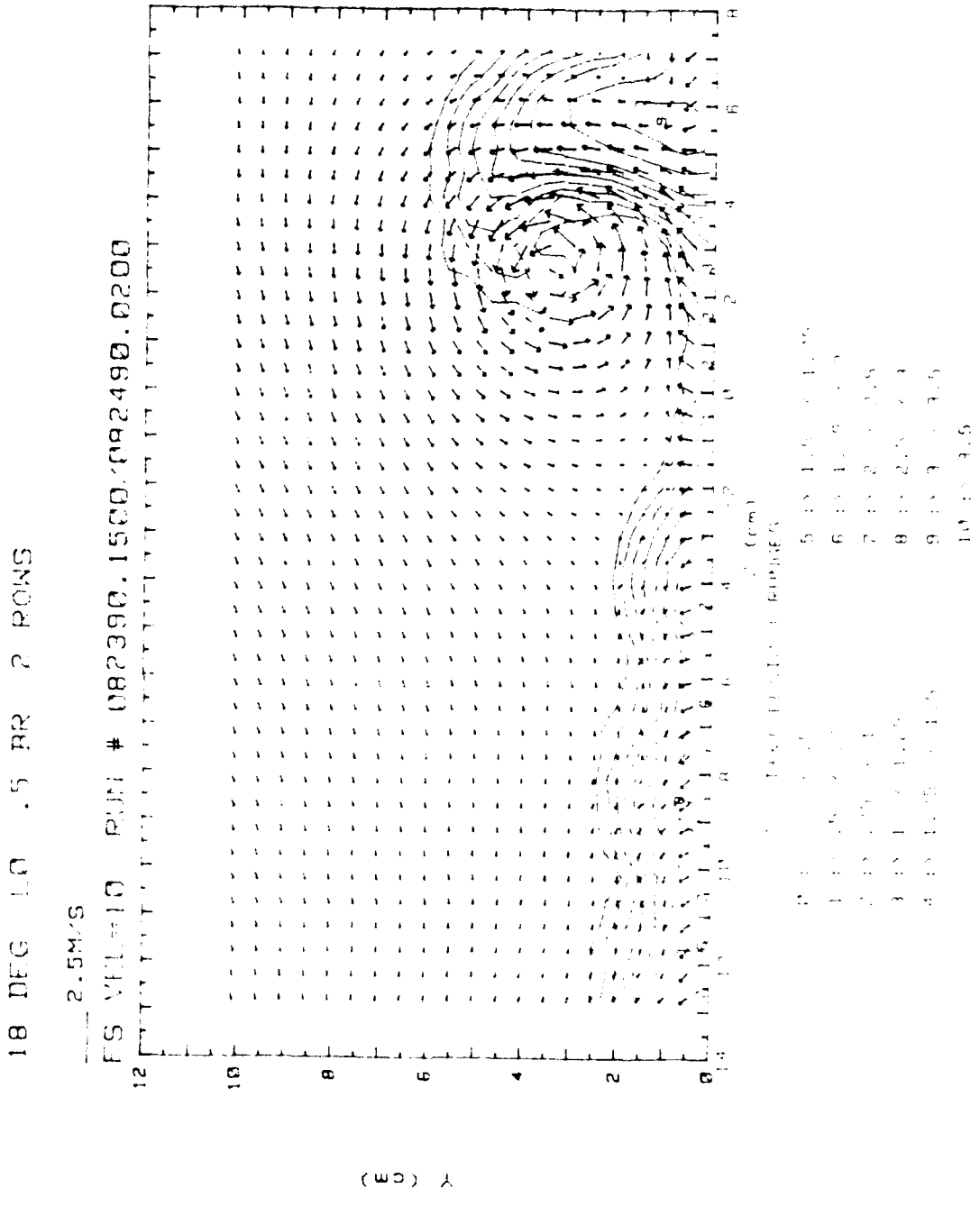

Figure 159. Composite Plot, x/d=45.8, 2 Rows, Vortex LO

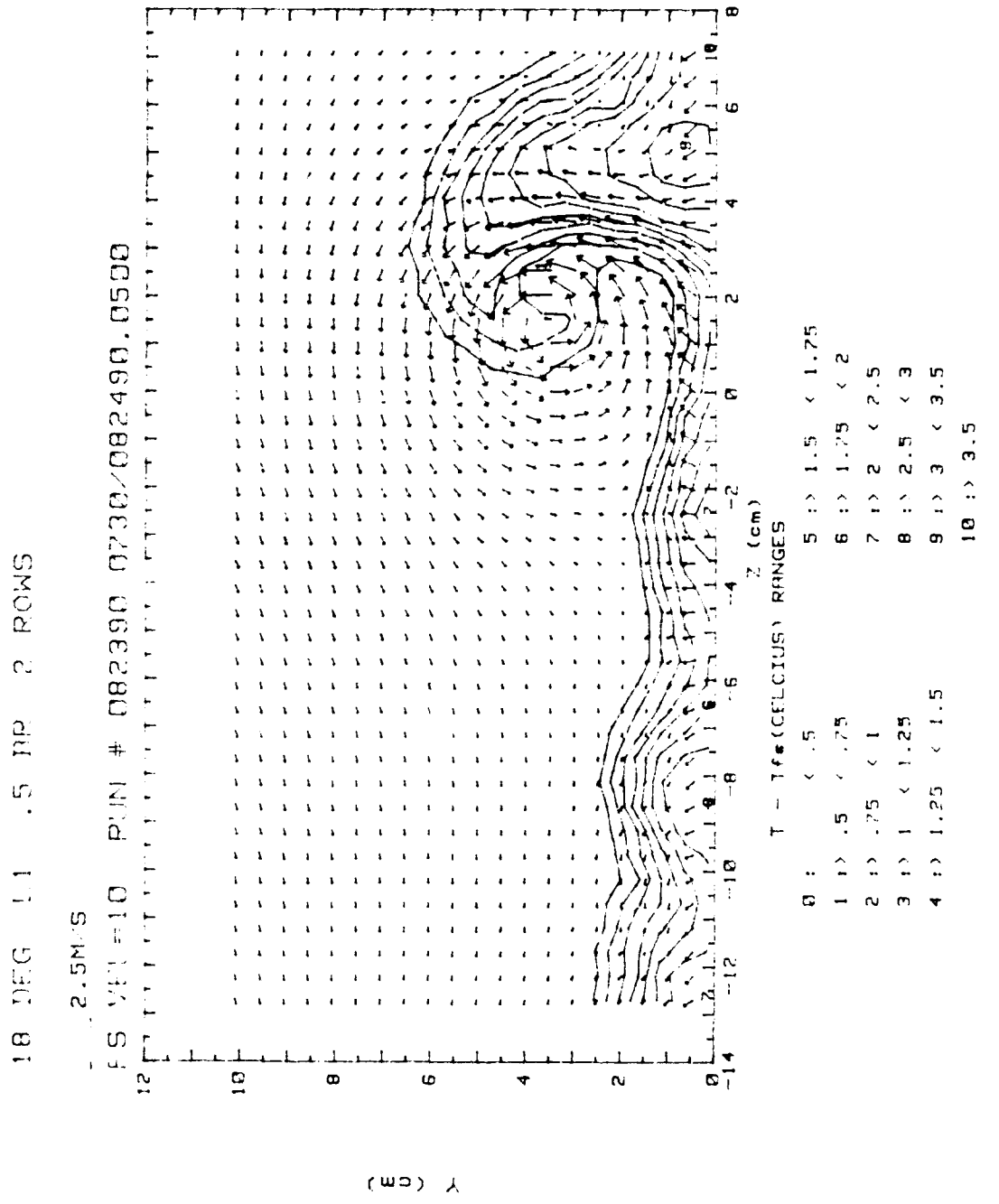

Figure 160. Composite Plot, x/d=45.8, 2 Rows, Vortex L1

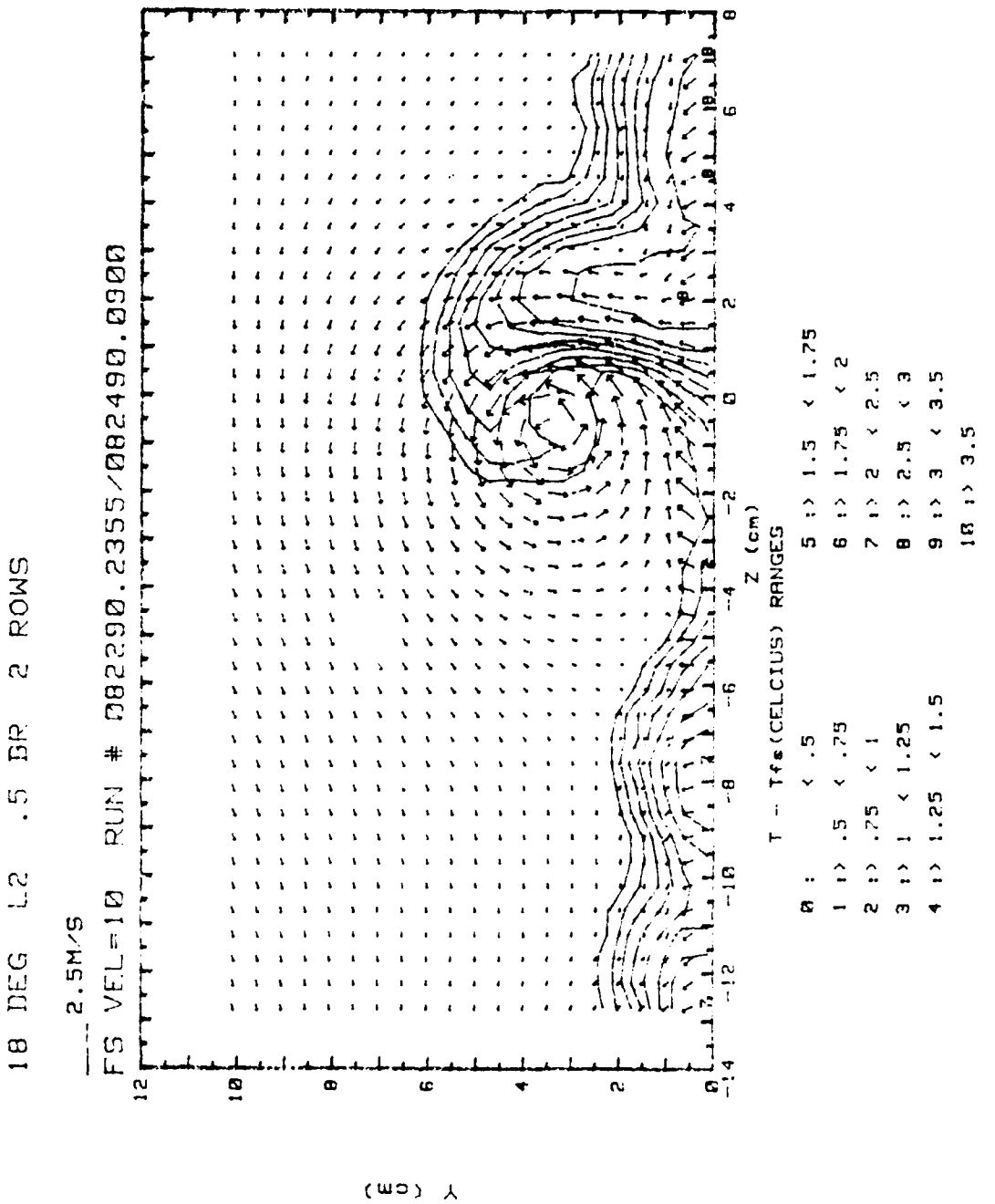

Figure 161. Composite Plot, x/d=45.8, 2 Rows, Vortex L2

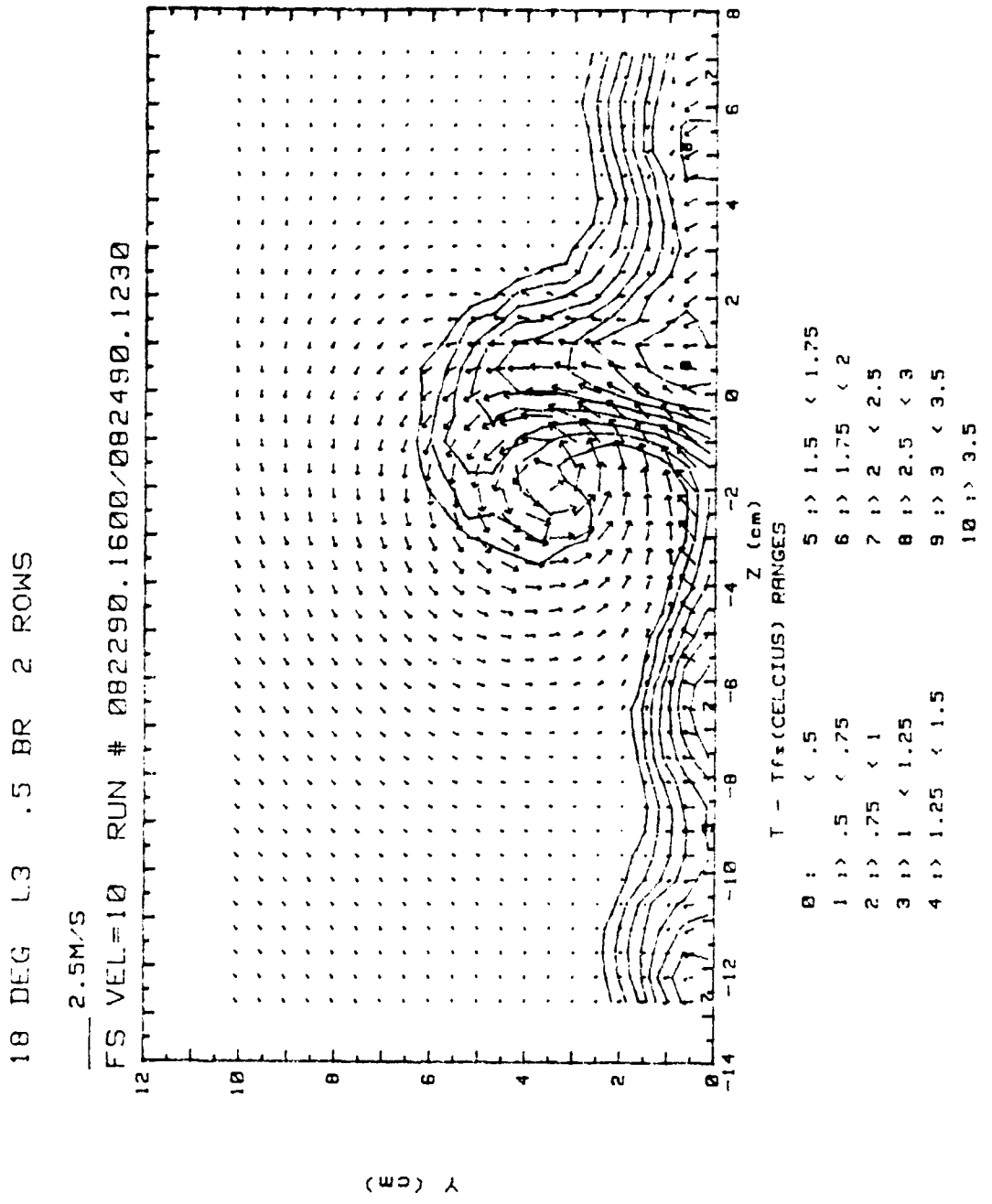

Figure 162. Composite Plot, x/d=45.8, 2 Rows, Vortex L3

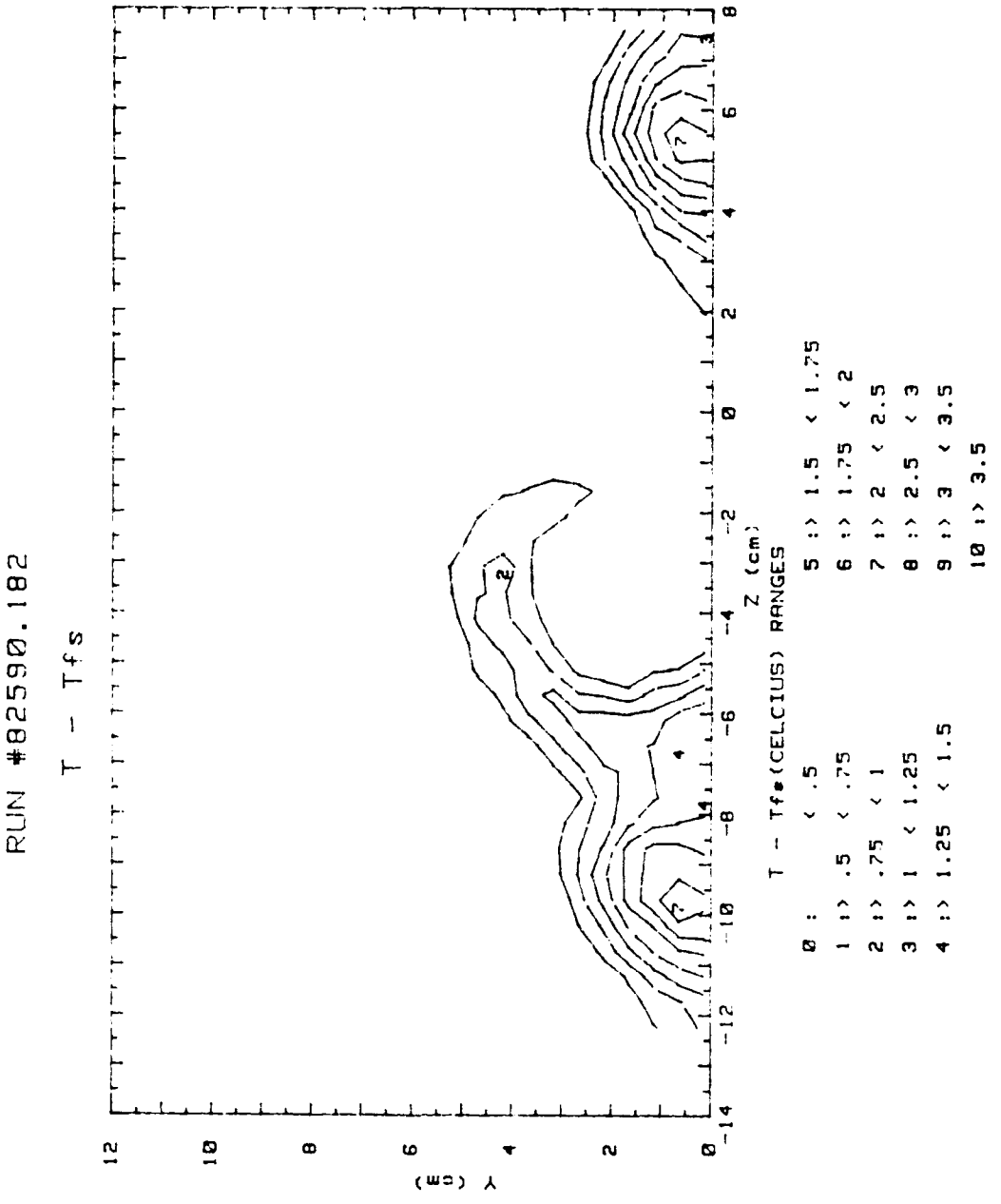

Figure 163. Injectant Distribution, x/d=45.8, 1 Row, Vortex R0

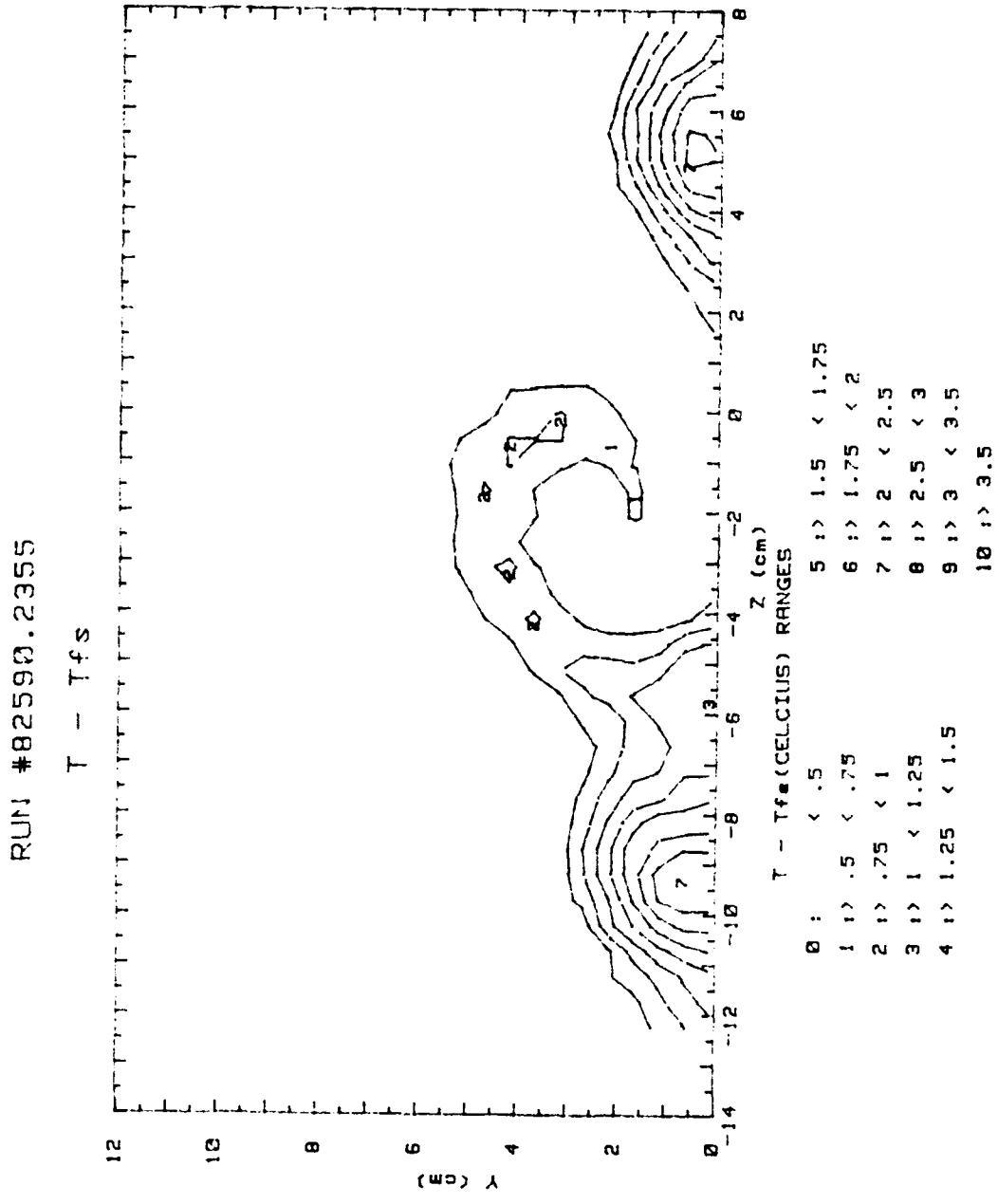

Figure 164. Injectant Distribution, x/d=45.8, 1 Row, Vortex R1

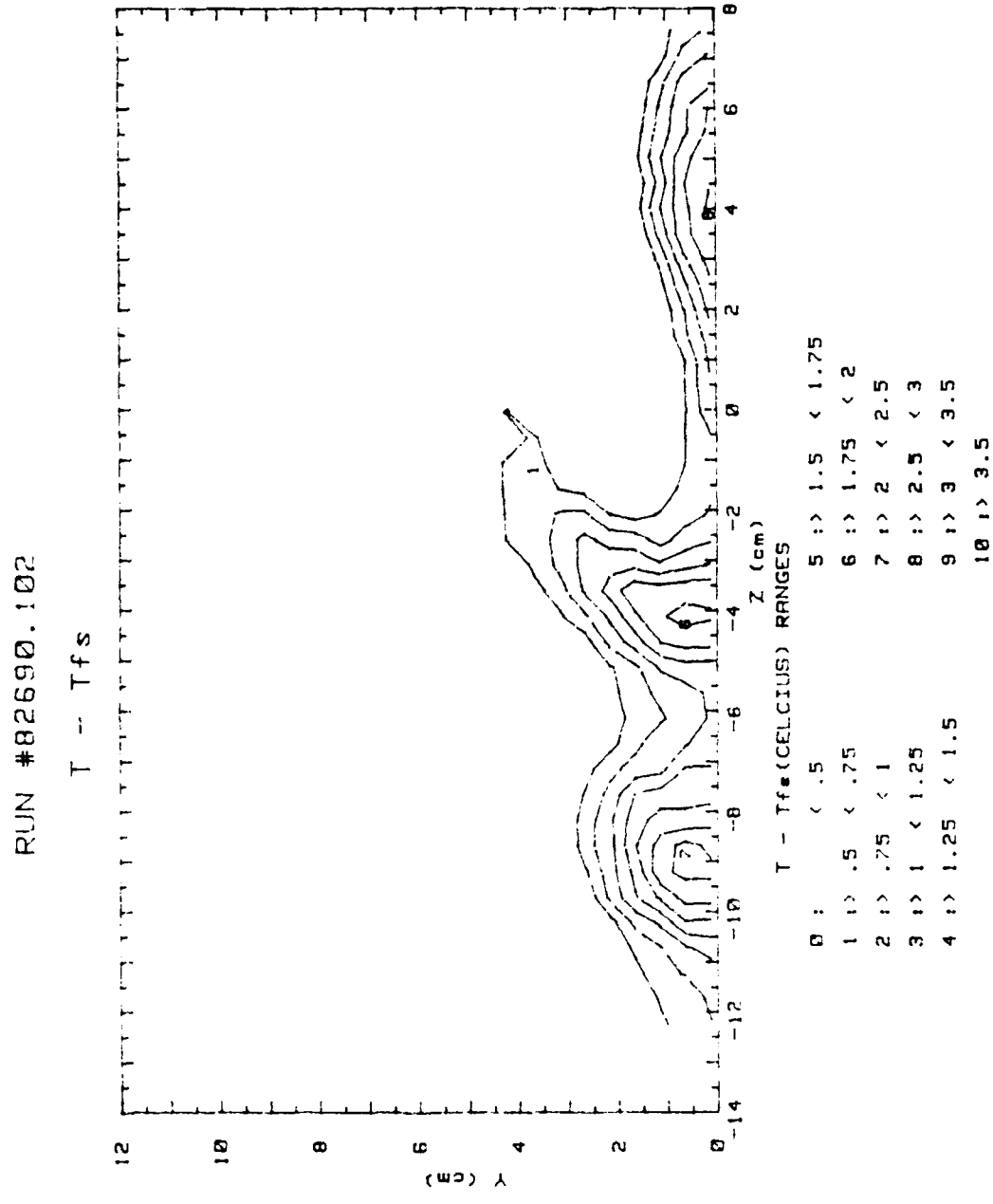

Figure 165. Injectant Distribution, x/d=45.8, 1 Row, Vortex R2

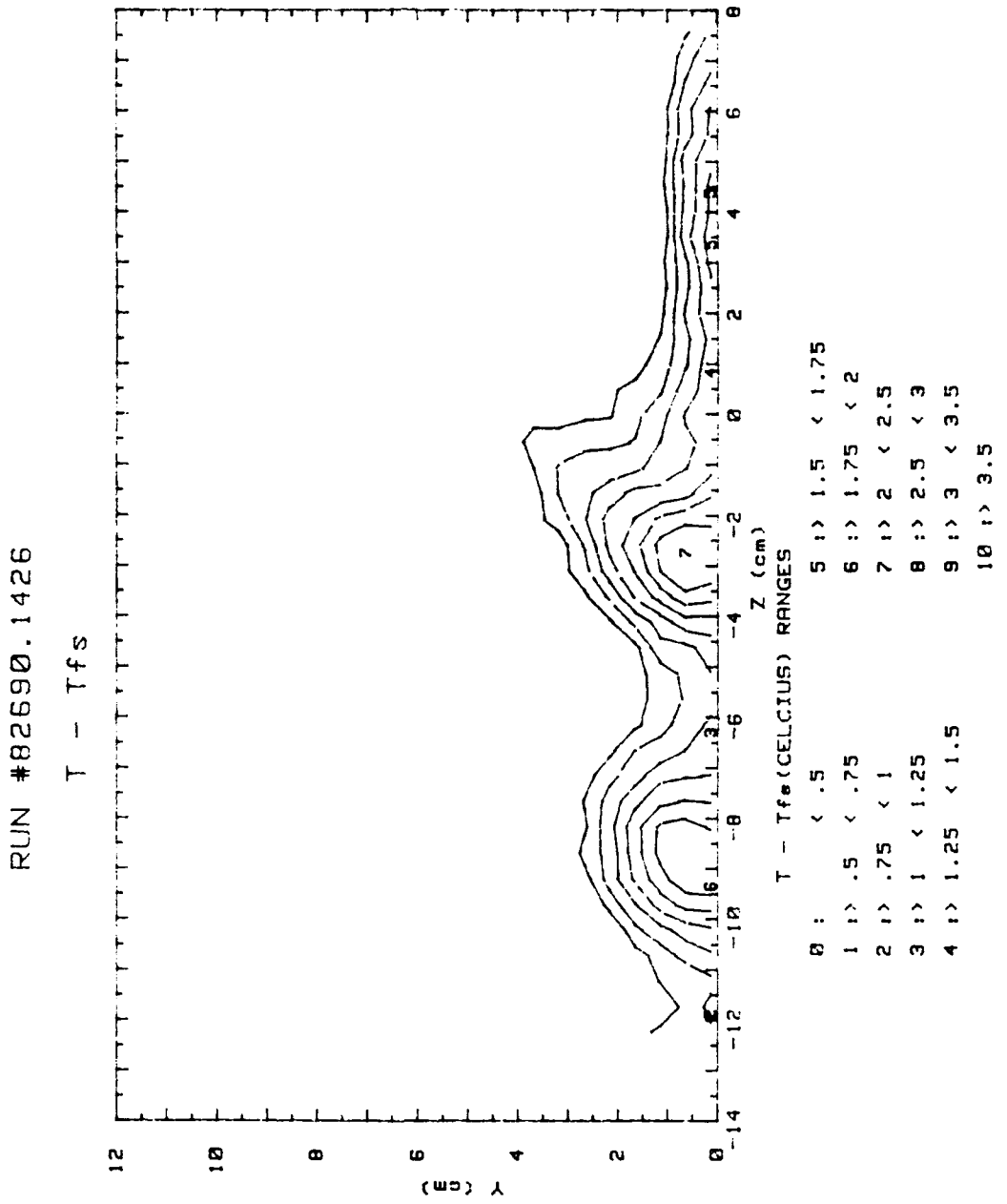

Figure 166. Injectant Distribution, x/d=45.8, 1 Row, Vortex R3

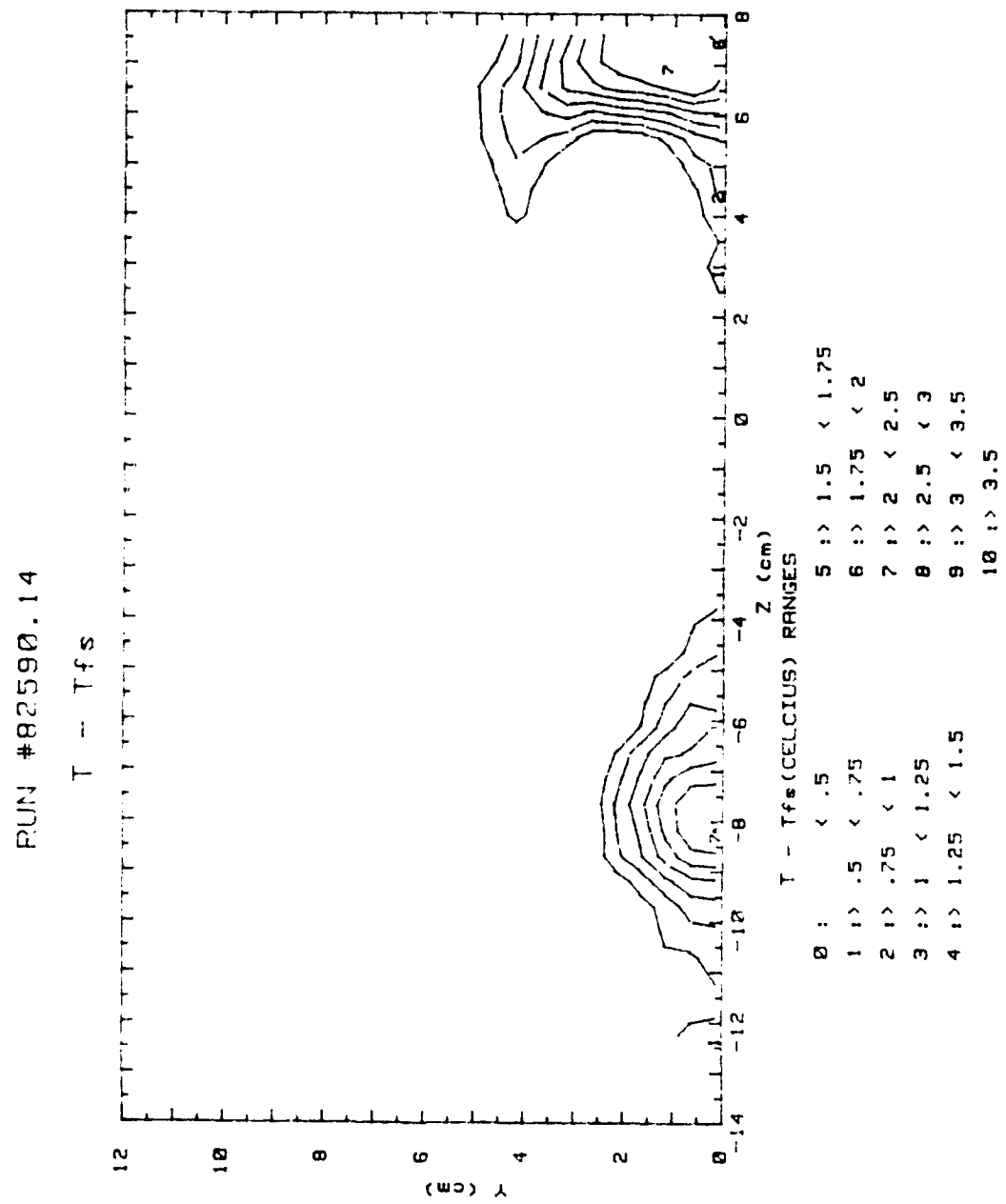

Figure 167. Injectant Distribution, x/d=45.8, 1 Row, Vortex L0

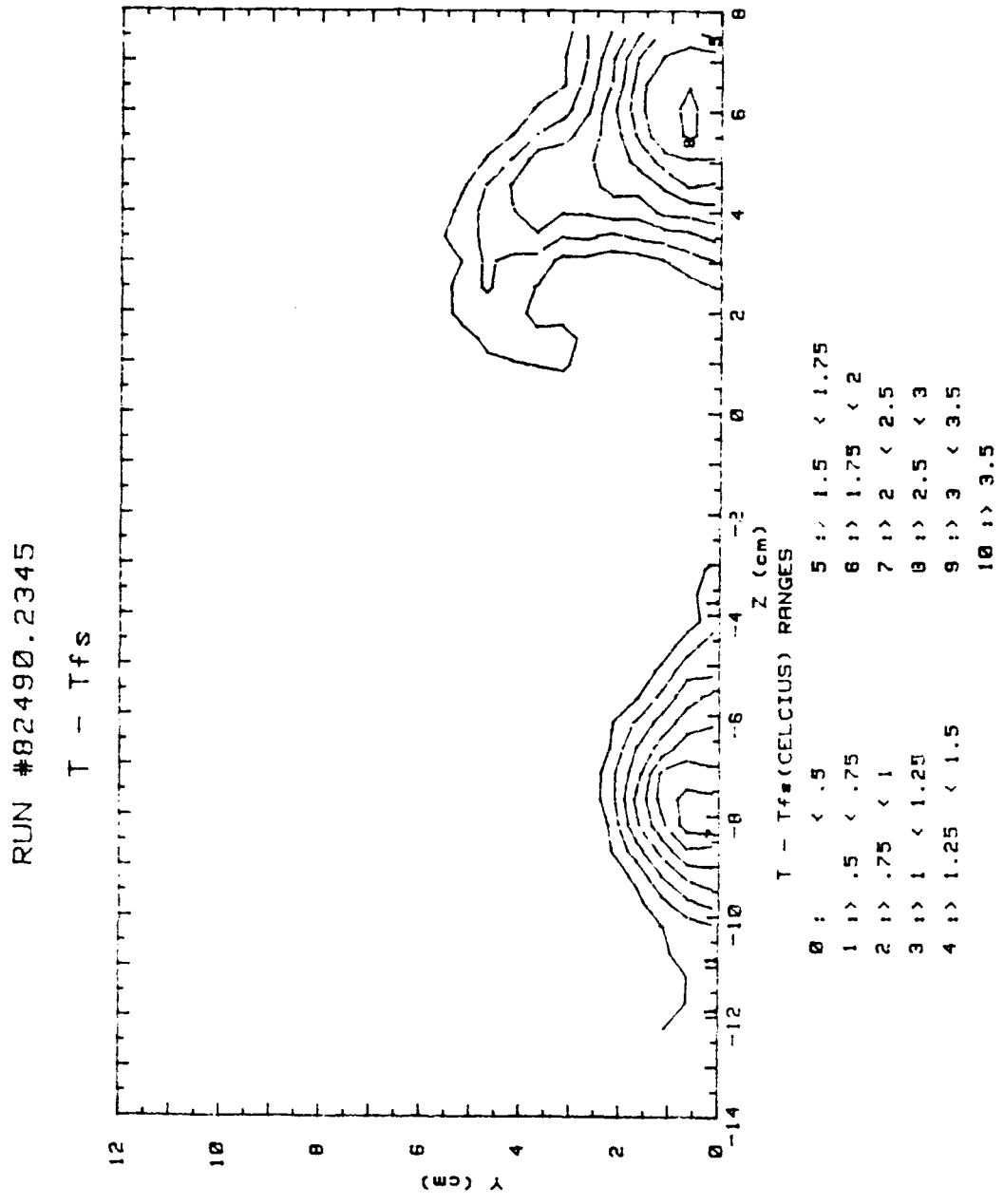

Figure 168. Injectant Distribution, x/d=45.8, 1 Row, Vortex L1

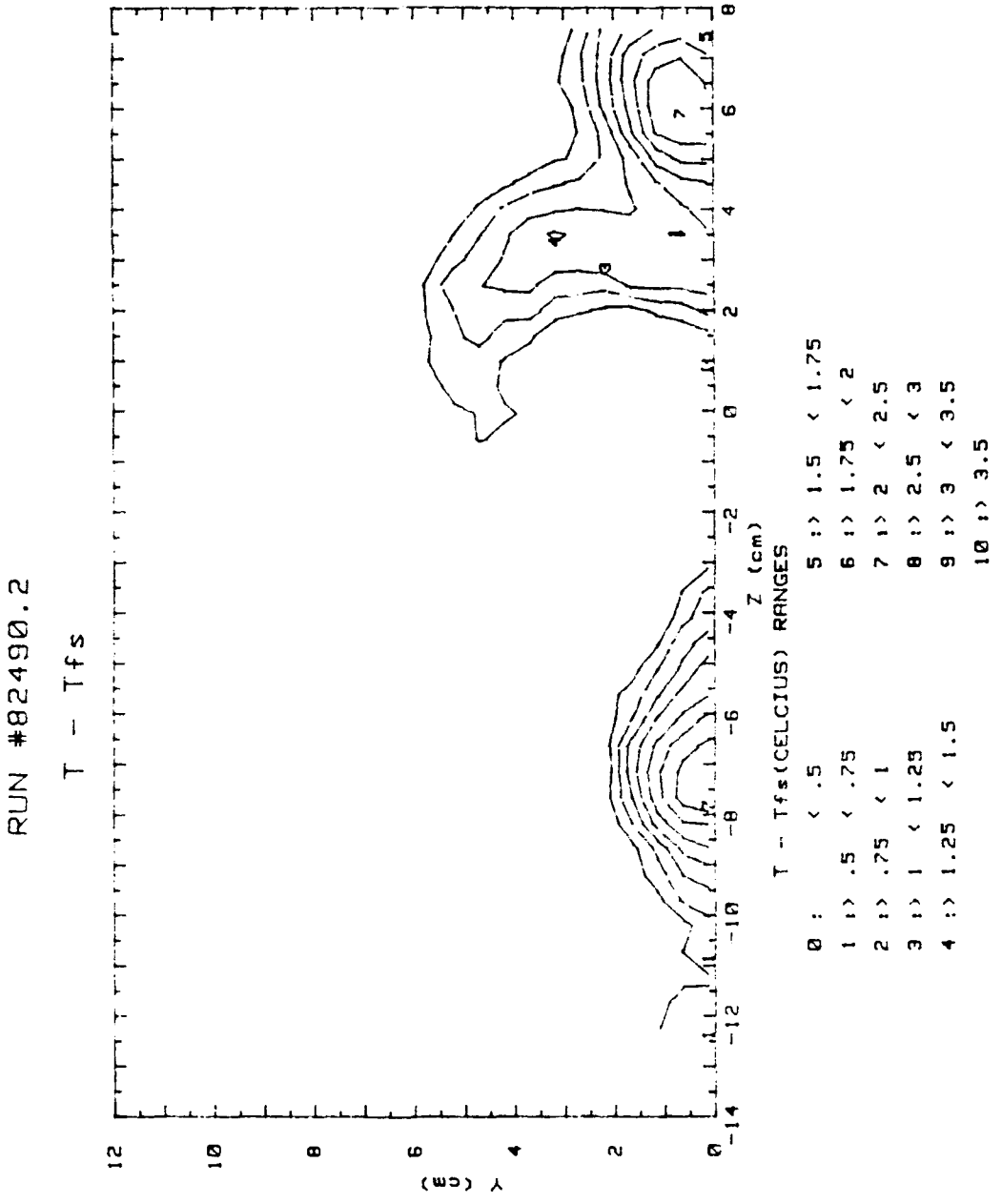

Figure 169. Injectant Distribution, x/d=45.8, 1 Row, Vortex L2

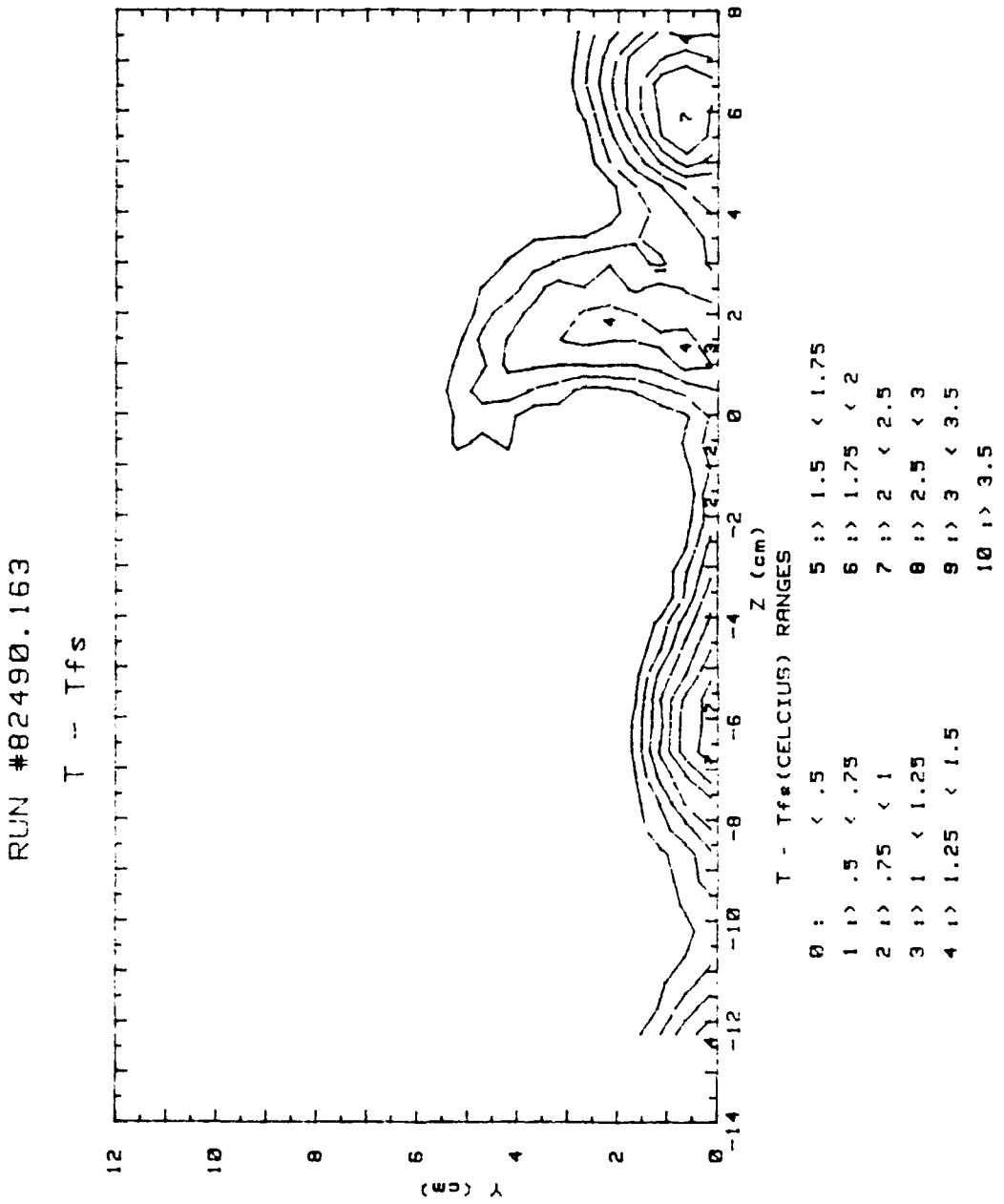

Figure 170. Injectant Distribution, x/d=45.8, 1 Row, Vortex L3

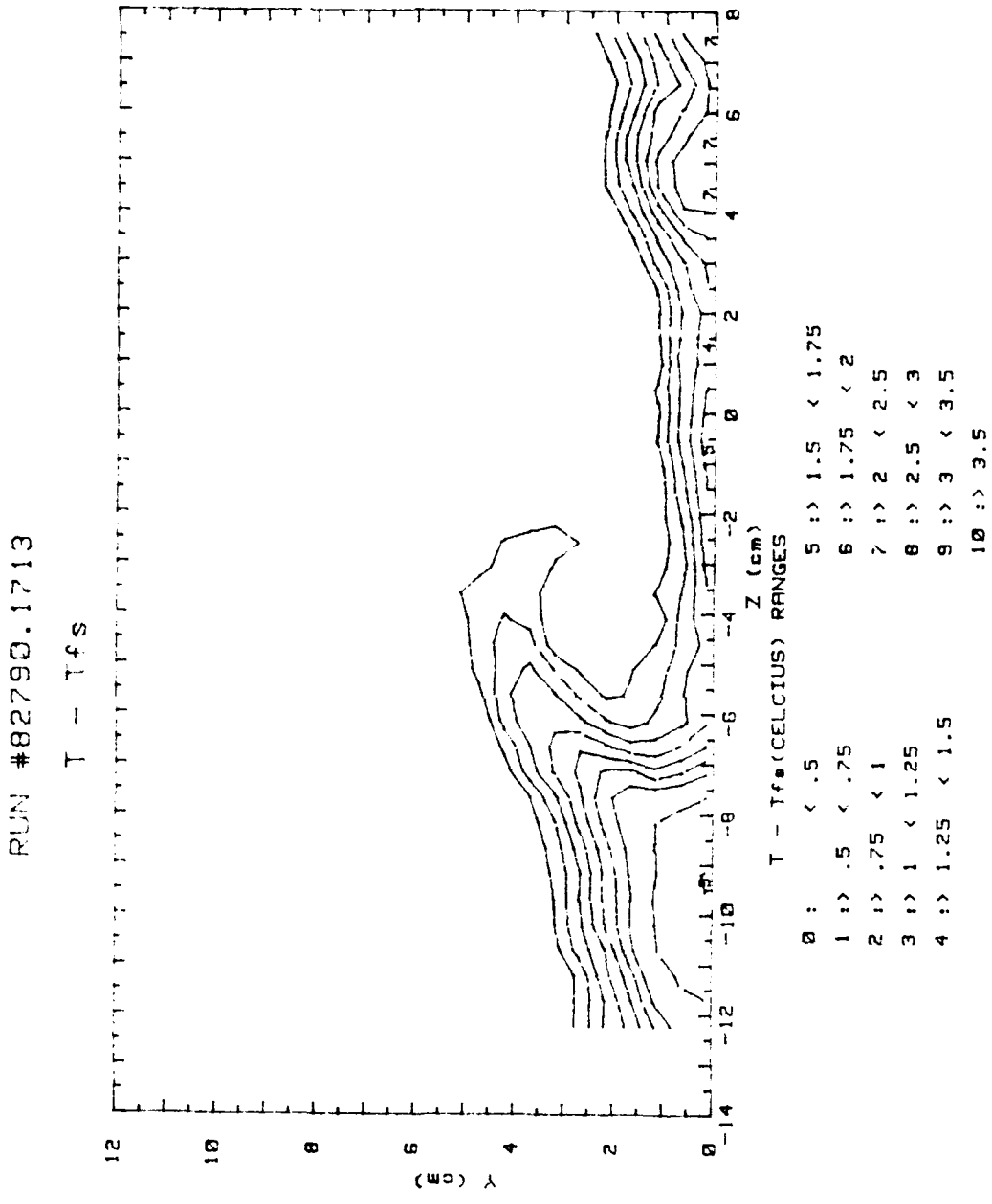

Figure 171. Injectant Distribution, x/d=45.8, 2 Rows, Vortex R0

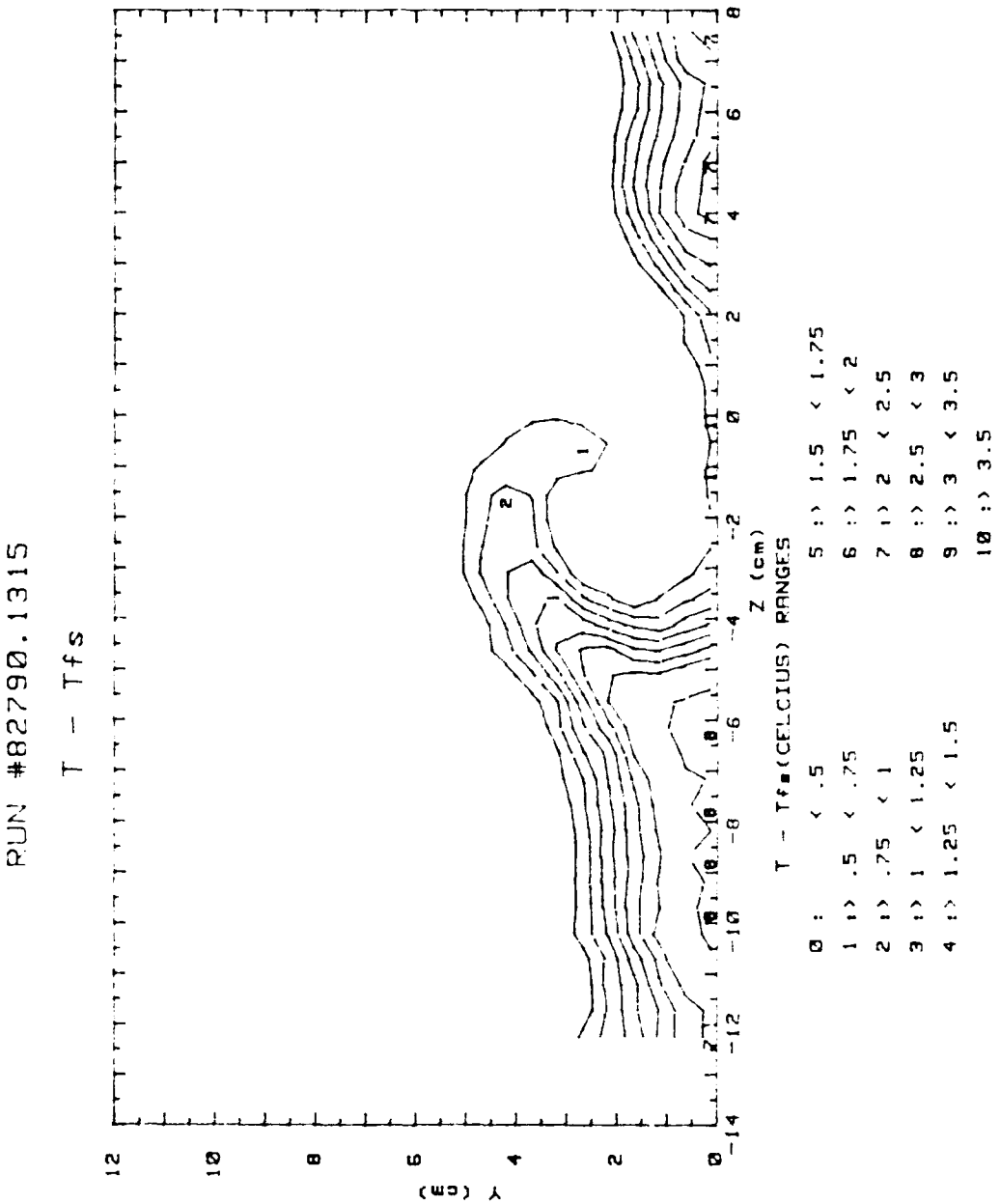

Figure 172. Injectant Distribution, x/d=45.8, 2 Rows, Vortex R1

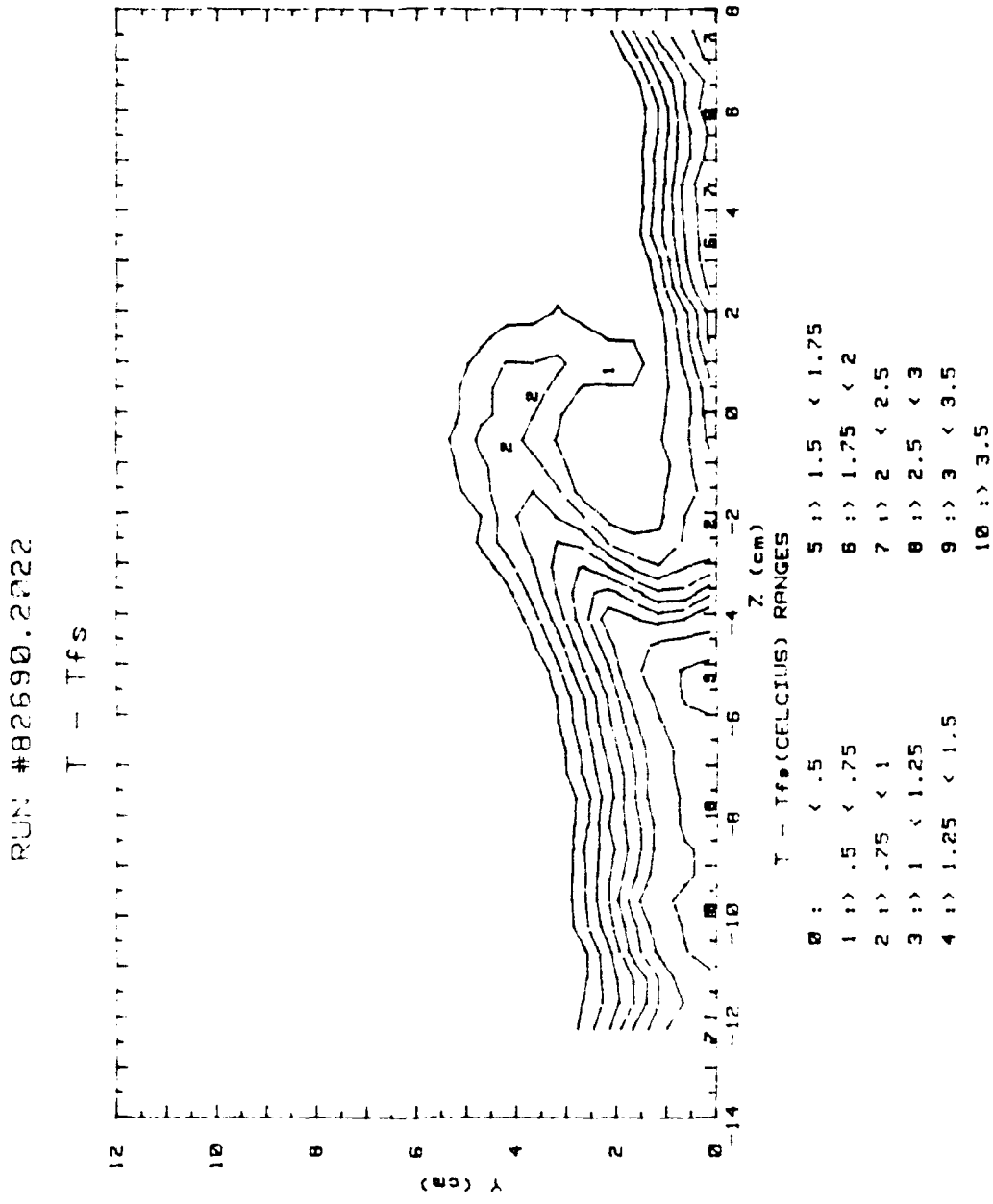

Figure 173. Injectant Distribution, x/d=45.8, 2 Rows, Vortex R2

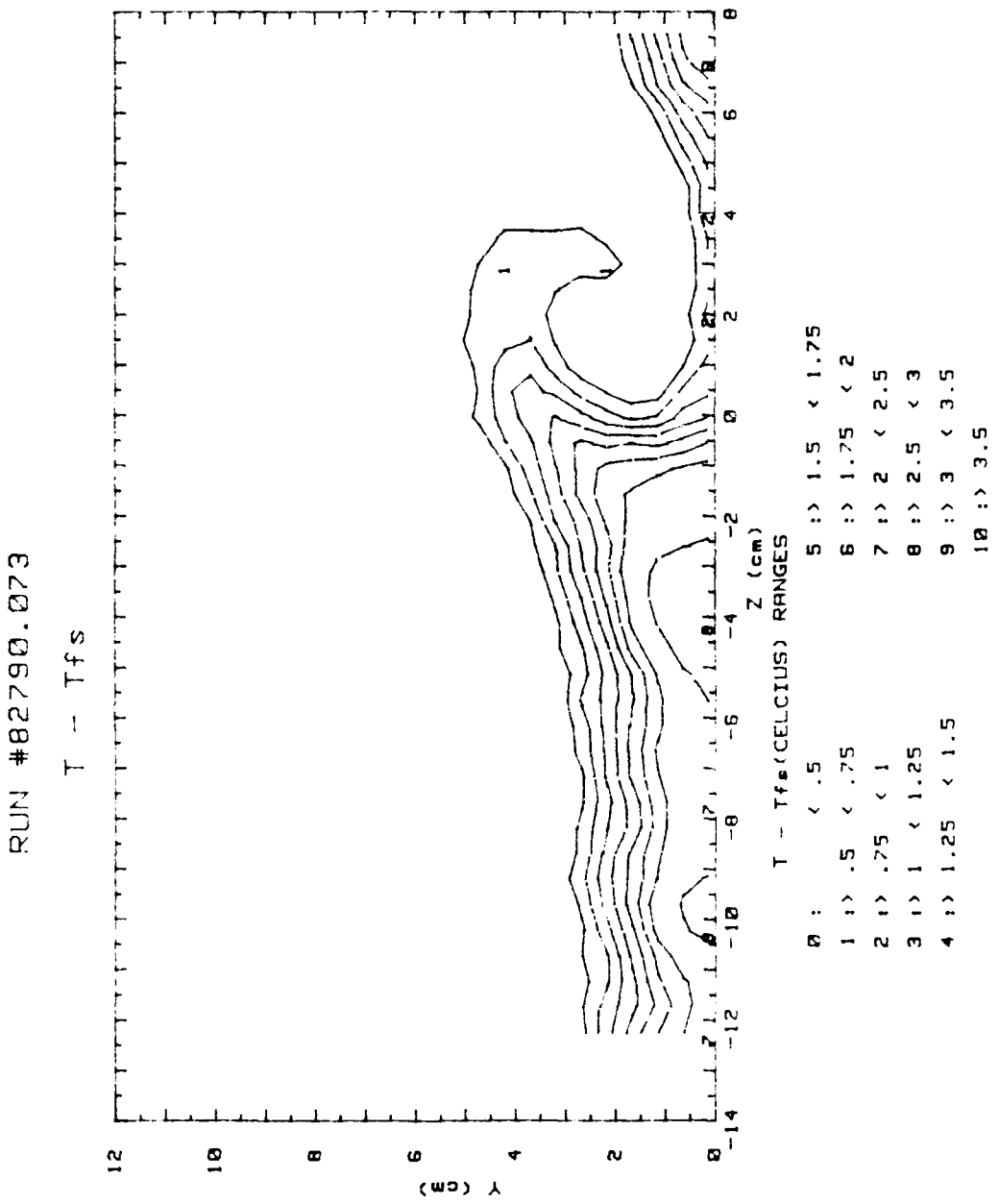

Figure 174. Injectant Distribution, x/d=45.8, 2 Rows, Vortex R3

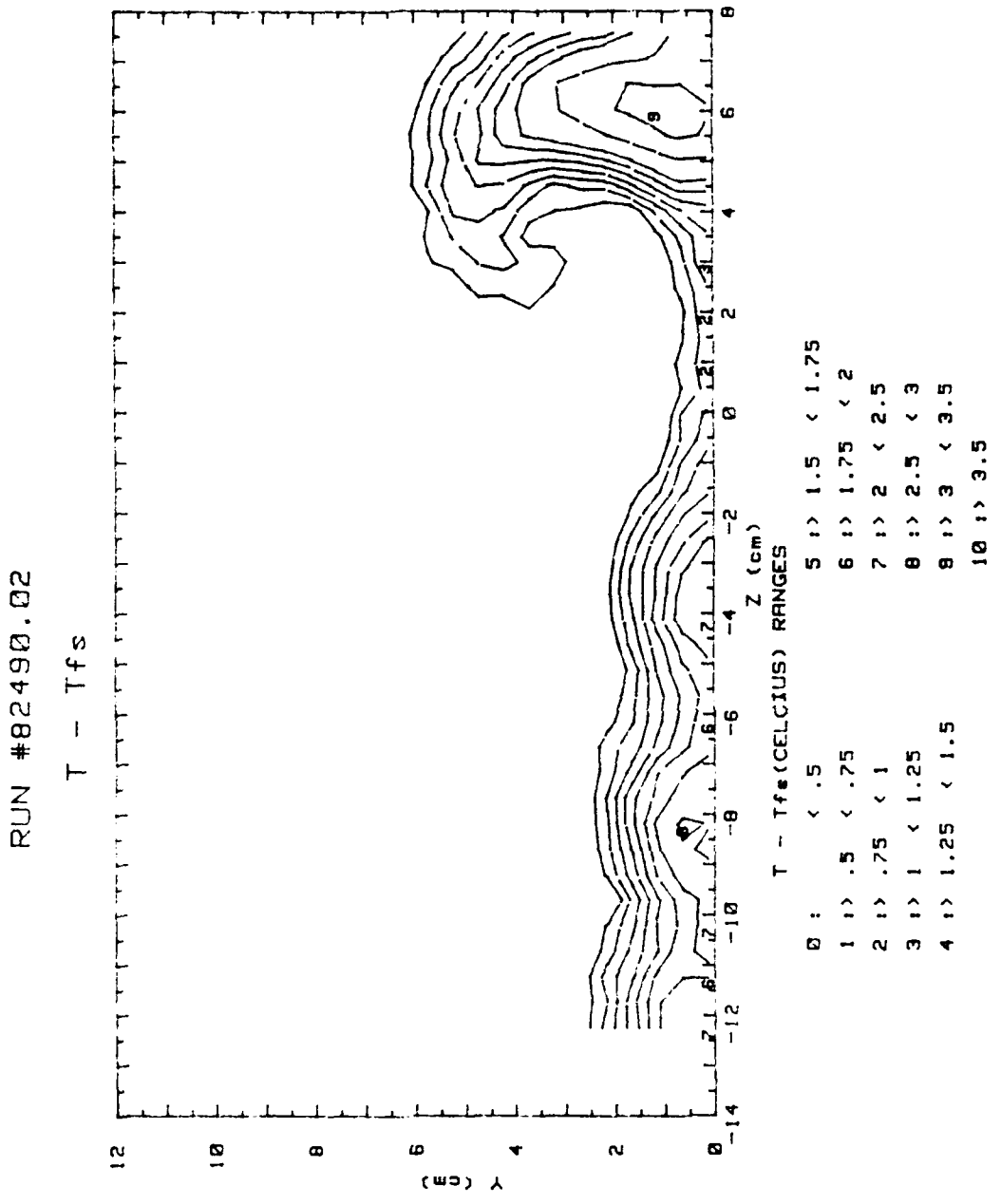

Figure 175. Injectant Distribution, x/d=45.8, 2 Rows, Vortex L0

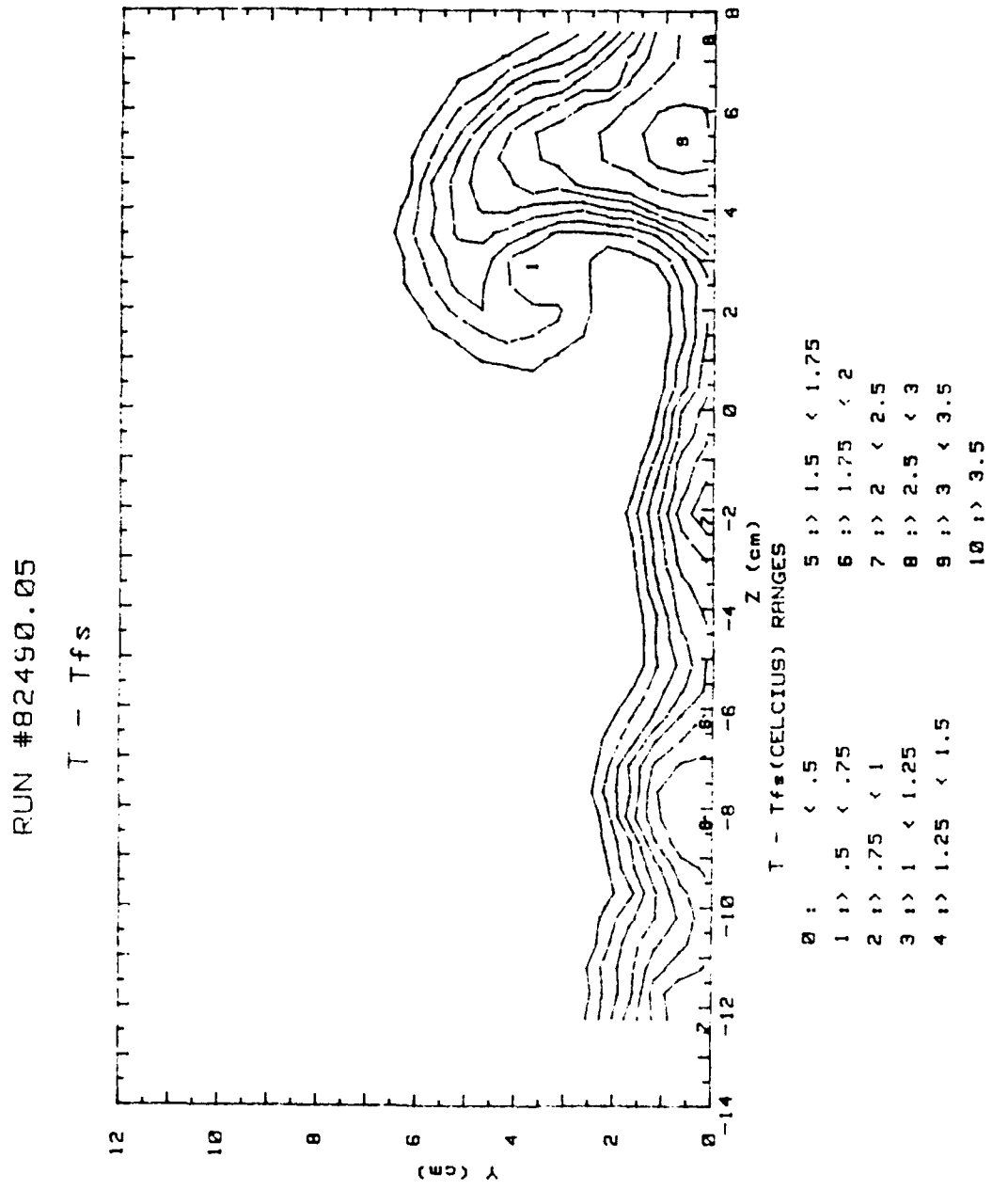

Figure 176. Injectant Distribution, x/d=45.8, 2 Rows, Vortex L1

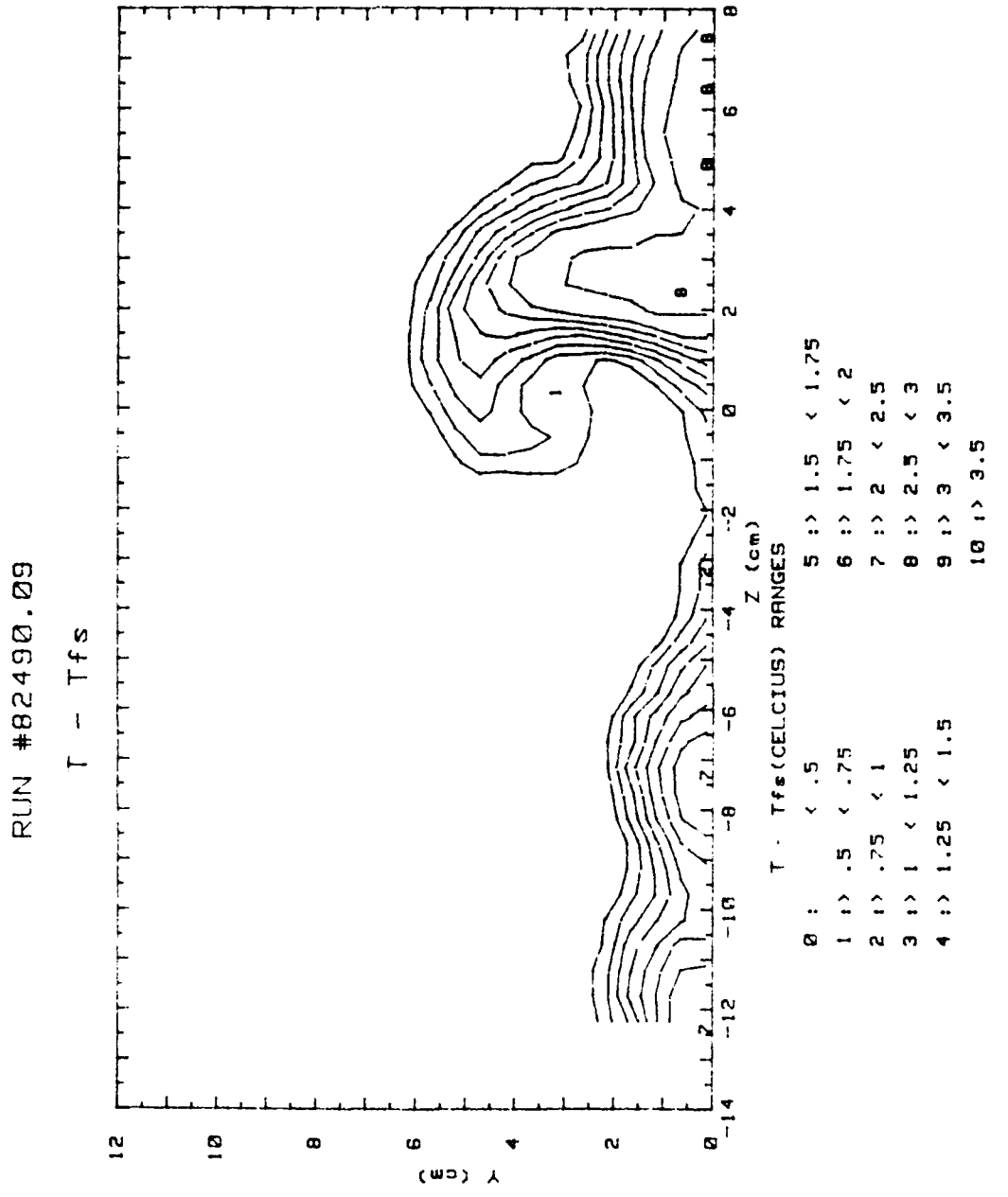

Figure 177. Injectant Distribution, x/d=45.8, 2 Rows, Vortex L2

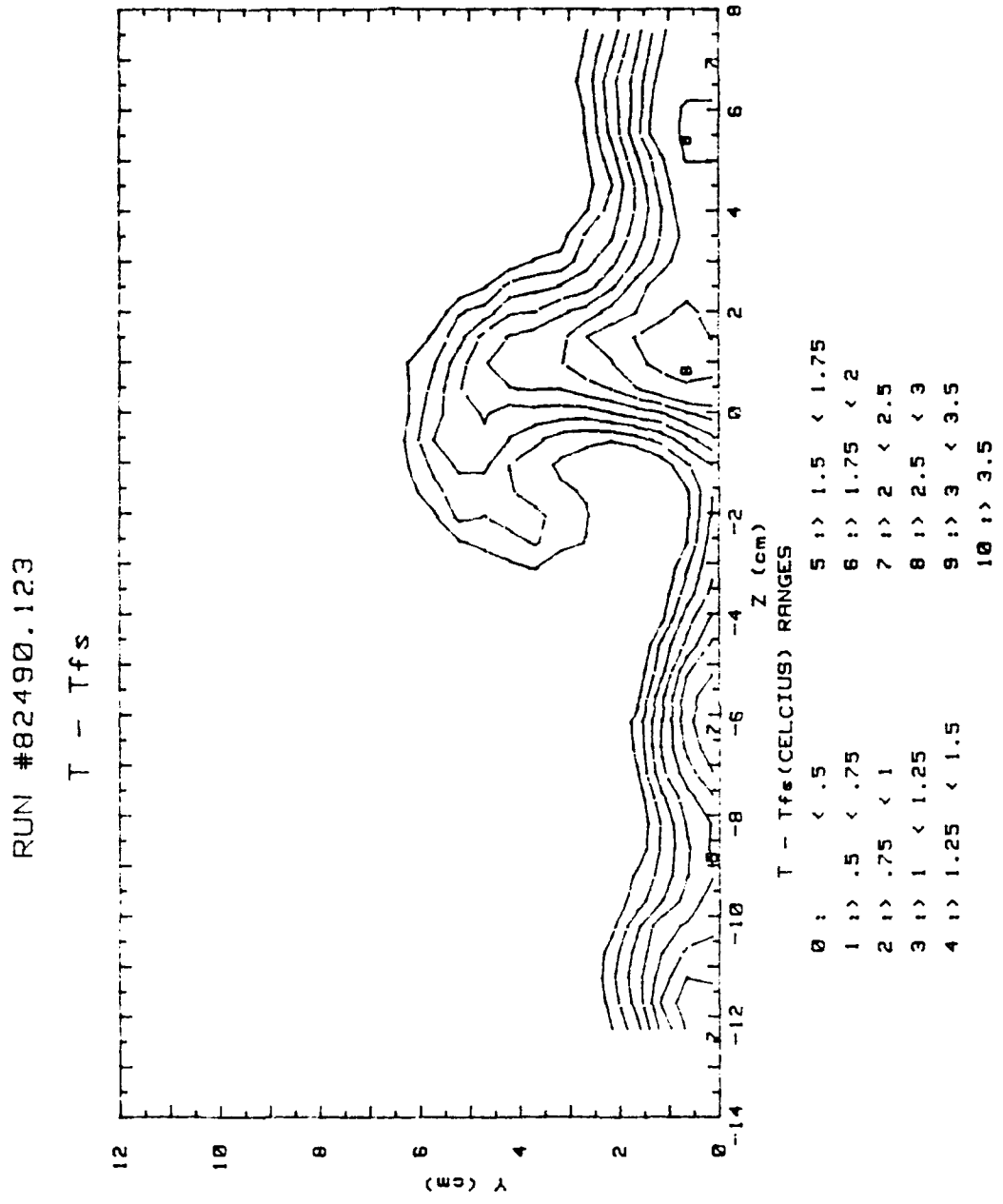

Figure 178. Injectant Distribution, x/d=45.8, 2 Rows, Vortex L3

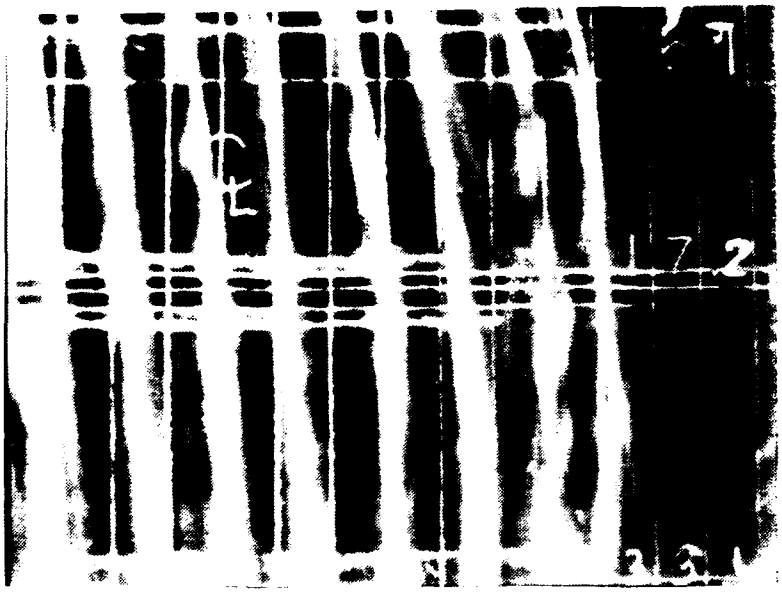

Figure 179. Surface Flow Patterns, x/d=45.8, 2 Rows, No Vortex

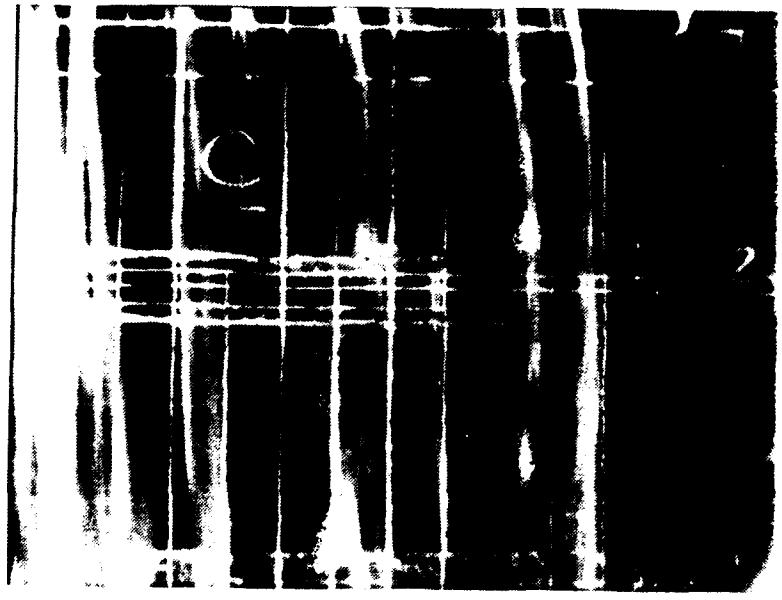

Figure 180. Surface Flow Patterns, x/d=45.8, 2 Rows, Vortex R0

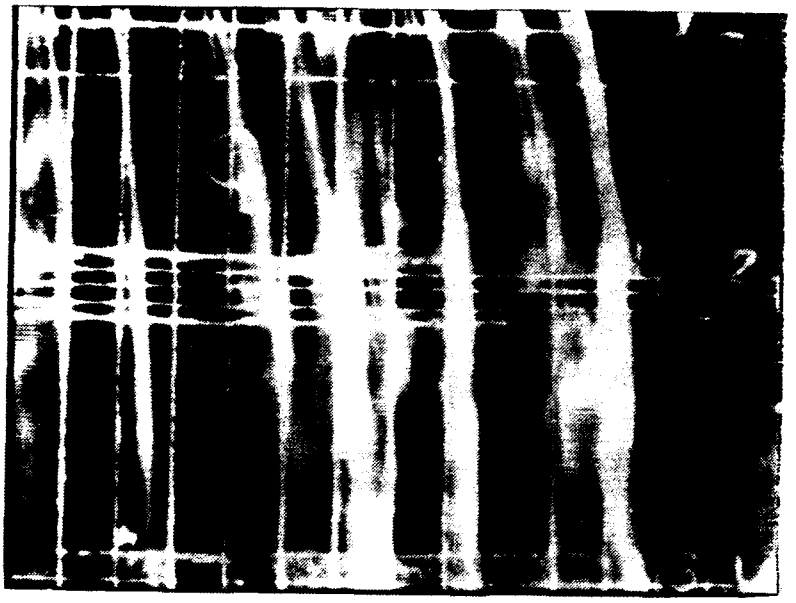

Figure 181. Surface Flow Patterns, x/d=45.8, 2 Rows, Vortex R1

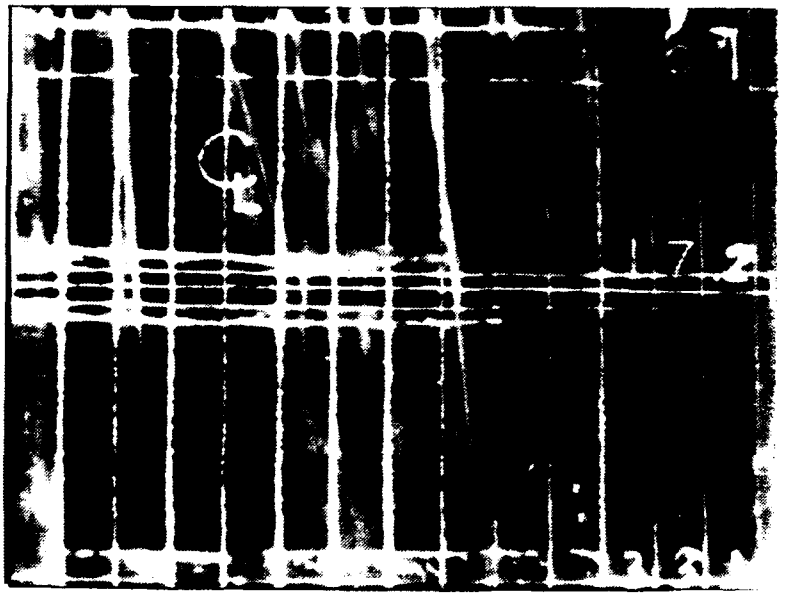

Figure 182. Surface Flow Patterns, x/d=45.8, 2 Rows, Vortex R2

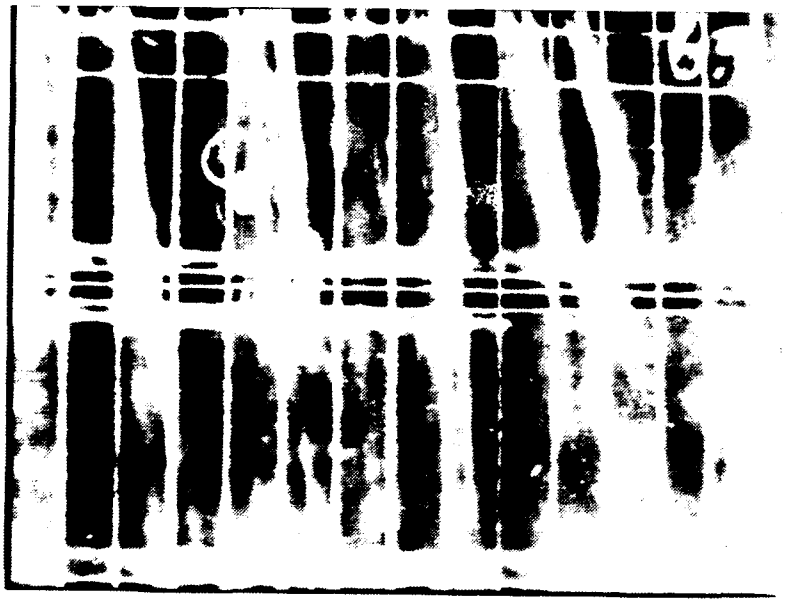

Figure 183. Surface Flow Patterns, x/d=45.8, 2 Rows, Vortex R3

Figure 184. Surface Flow Patterns, x/d=45.8, 2 Rows, Vortex R4

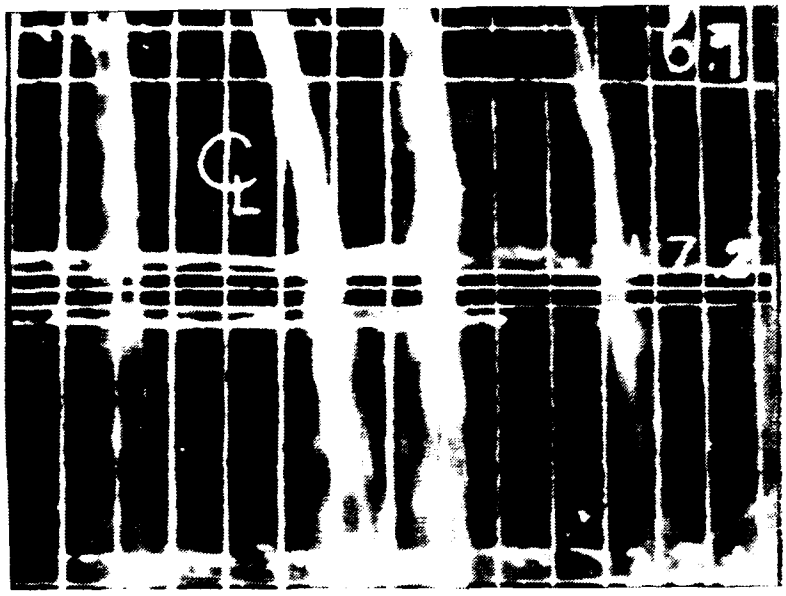

Figure 185. Surface Flow Patterns, x/d=45.8, 1 Row, Vortex R0

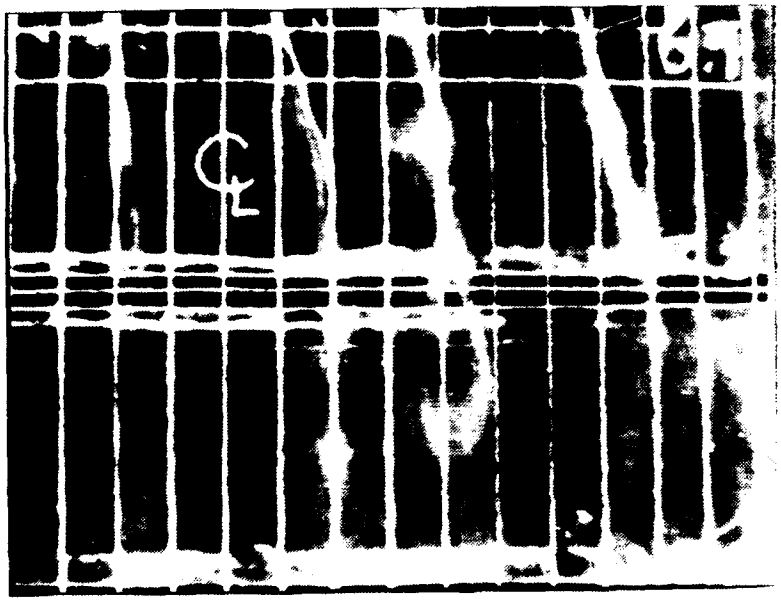

Figu e 186. Surface Flow Patterns, x/d=45.8, 1 Row, Vortex R1

Figure 187. Surface Flow Patterns, x/d=45.8, 1 Row, Vortex R2

Figure 188. Surface Flow Patterns, x/d=45.8, 1 Row, Vortex R3

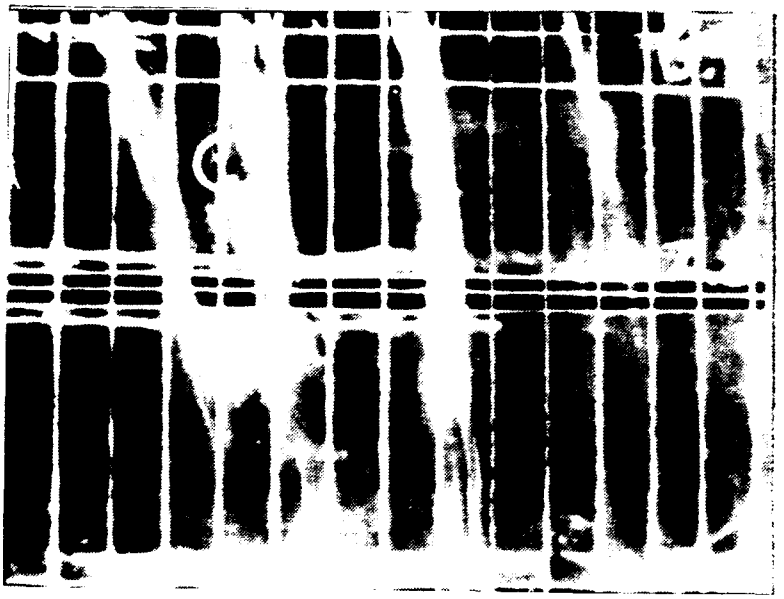

Figure 189. Surface Flow Patterns, x/d=45.8, 1 Row, Vortex R4

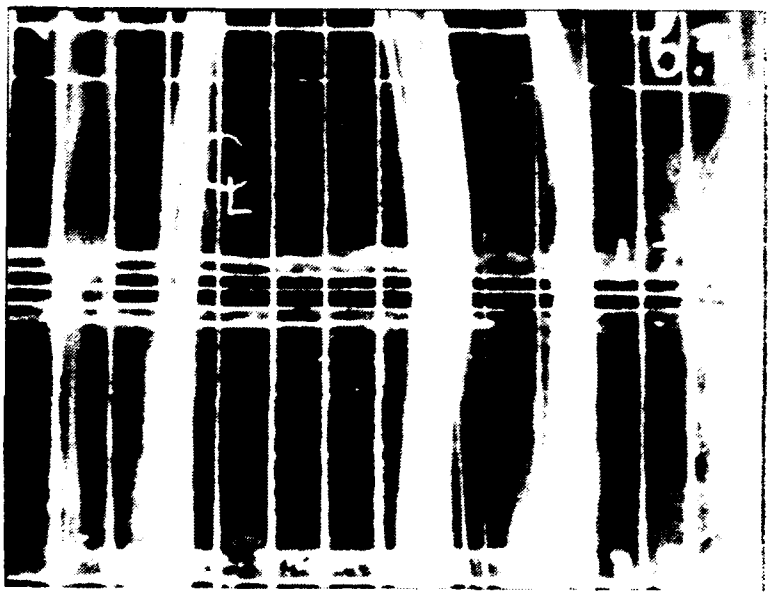

Figure 190. Surface Flow Patterns, x/d=45.8, 1 Row, Vortex L0

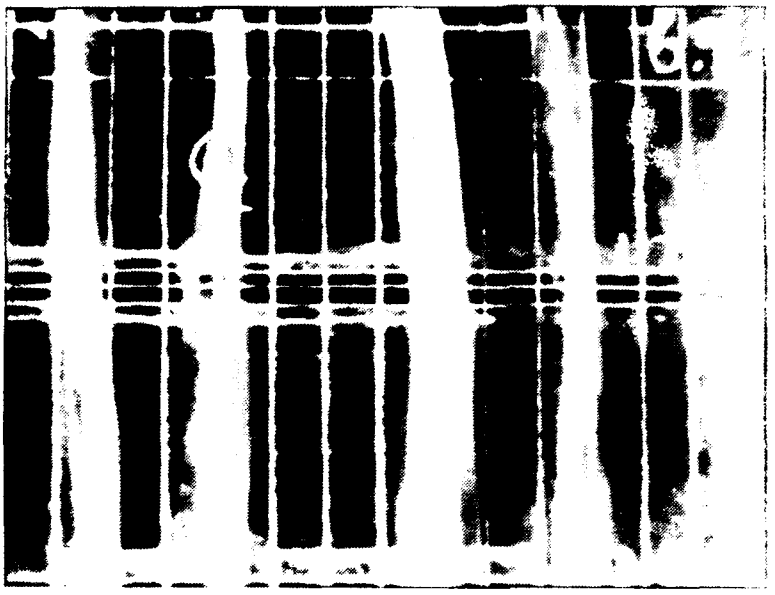

Figure 191. Surface Flow Patterns, x/d=45.8, 1 Row, Vortex L1

Figure 192. Surface Flow Patterns, x/d=45.8, 1 Row, Vortex L2

Figure 193. Surface Flow Patterns, x/d=45.8, 1 Row, Vortex L3

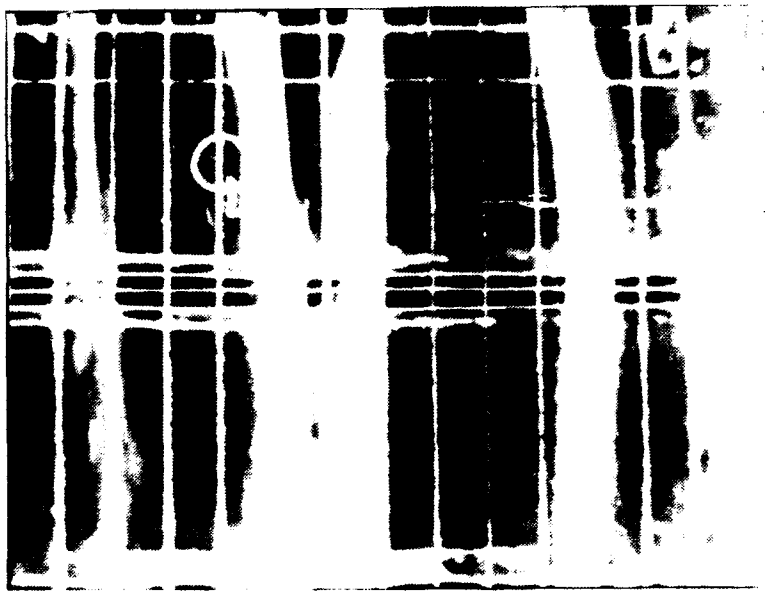

Figure 194. Surface Flow Patterns, x/d=45.8, 1 Row, Vortex L4

APPENDIX B

UNCERTAINTY ANALYSIS

An uncertainty analysis, by Schwartz [Ref. 20], was accomplished on the input parameters and variables used for this study. A 95% confidence interval was utilized. Table II contains a summary of the parameters and their uncertainties :

TABLE II. EXPERIMENTAL UNCERTAINTIES FOR MEASURED QUANTITIES

Quantity (units)	Typical Nominal Value	Experimental Uncertainty
T_∞ (°C)	18.0	0.13
T_W (°C)	40.0	0.21
$P_{ambient}$ (mm Hg)	760	0.71
ρ_∞ (kg/m^3)	1.23	0.009
U_∞ (m/s)	10.0	0.06
C_p [J/(kg K)]	1006	1
$q_W A$ (W)	270	10.5
h [W/(m^2 K)]	24.2	1.03
St	0.00196	0.000086
St/St_o	1.05	0.058
A (m^2)	0.558	0.0065
m	0.98	0.05
x/d	54.6	0.36

APPENDIX C

DATA ACQUISITION, PROCESSING AND PLOTTING PROGRAMS

1. Mean Velocity Survey Software :

ORIENT : This program calculates calibration coefficients for each of the five pressure transducers associated with the five sensing ports of the five hole pressure probe. ORIENT is also used to orient the five hole probe so that at a 0 yaw angle the pressures from the right and left ports are equal.

FIVEHOLE1 : This program acquires pressure data from each of the five transducers associated with the probe. The FIVEHOLE1 program controls the MITAS motor controller which, in turn, controls the automatic traversing device on which the five hole probe is mounted. An 400 point pressure survey is conducted in the Y-Z plane normal to the freestream flow. Two data files, FIV and FIVP, are created. The FIV data file consists of mean velocity, center port pressure, average pressure of the four peripheral ports, and the yaw and pitch coefficients for each of the 400 locations sampled. The FIVP data file consists of the pressures P1 through P5 sensed by each of the five pressure probe sensing ports, the average pressure of the four peripheral ports and the mean velocity, for each of the 400 survey locations.

PADJUST : This program accesses the FIVP data file created by FIVEHOLE1 and adjusts the pressures to account for spatial resolution

problems. Pressure correction is performed using a curve fit to move the measurement location to the center sensing port location.

VELOCITY : This program accesses the data file created by PADJUST and computes Ux, Uy and Uz velocity components.

UX3 : This program accesses the data file created by VELOCITY and plots streamwise velocity (Ux) contours of the Y-Z plane surveyed by the five hole pressure probe.

PTOT3 : PTOT3 accesses the VELOCITY program data file and plots total pressure contours of the surveyed Y-Z plane.

VECTOR2 : This program accesses the VELOCITY program output and plots the secondary flow vectors in the surveyed Y-Z plane.

VORCIRC : This program acquires the velocity component data file created by VELOCITY and plots streamwise vorticity contours of the surveyed Y-Z plane. Vortex parameters calculated by this program include: core center location, core radii, vorticity, vortex circulation, non-dimensional core radii and non-dimensional vortex circulation.

2. Mean Temperature Survey Software :

ROVER1 : This program acquires flow temperature data from the

"roving" thermocouple mounted on the automatic traversing device. The traversing device is controlled by the MITAS controller which is, in turn, controlled by this program. The output data file consists of differential temperatures ($T_{rover} - T_{\infty}$) for each of the 400 survey locations in the Y-Z plane.

PLTMP3 : This program uses the differential temperature data file created by ROVER and plots differential temperature contours of the surveyed Y-Z plane.

3. Heat Transfer Measurement Software (No Film Cooling) :

STANTON3 : This program acquires multiple channel thermocouple data for heat transfer measurements with no film cooling. It creates two output data files, TDATA and IDATA. The TDATA file consists of the 126 test plate thermocouple temperatures. The IDATA file records run number, test plate voltage and current, ambient pressure, pressure differential, ambient temperature, freestream velocity, air density and freestream temperature.

STANTON4 : STANTON4 accesses TDATA and IDATA files created by STANTON3 and calculates heat transfer coefficients and Stanton numbers for each of the 126 thermocouple locations. This program also calculates the average Reynolds number for each thermocouple row. STANTON4 creates three output files. These files are HDATA, SDATA, and STAV. The HDATA file consists of the local heat transfer coefficient, the Stanton number and the X

and Z coordinates for each of the 126 test plate thermocouples. The SDATA file contains only the Stanton number values calculated for each thermocouple location. STAV contains the X location and the average Reynolds and Stanton numbers for each of the six thermocouple rows.

STAVRAT : This program accesses the HDATA files created by STANTON4 and creates an output file which consists of Stanton number ratios and X,Z coordinates for each of the thermocouple locations. STAVRAT is specifically designed to calculate St/Sto ratios for data collected when no film cooling is present. Sto values represent the baseline values, and St values are the Stanton numbers with embedded vortices and no film cooling.

PLOTSTR : This program accesses the Stanton number ratio files created by STAVRAT and plots the spanwise variations of St/Sto for all six thermocouple rows.

4. Heat Transfer Measurement Software (with Film Cooling) :

SETCOND : This program is used to set conditions for heat transfer data acquisition when film cooling is employed. SETCOND determines injection velocity, Reynolds number, blowing ratio (m) and non-dimensional temperature (θ). It requires user input from the terminal of freestream conditions, rotometer percent flow and injection plenum differential pressure.

STANFC1A : This program is used when film cooling is employed to

acquire multiple channel thermocouple data for heat transfer measurements. STANFC1A creates three data files : a temperature data file (T), a terminal input data file (I) and a film cooling data file (FC). The temperature data file consists of the 126 test plate thermocouple temperatures. The terminal input data file records the identical information contained in the IDATA file of STANTON3, as discussed earlier. The film cooling data file contains the injection rotometer percent flow and the injection plenum differential pressure.

STANFC2A : This program accesses the temperature, terminal input and film cooling data files created by STANFC1A. The program calculates Stanton number values for the 126 thermocouple locations and creates a single output file (ST) containing these values.

STANR1 : This program reads three Stanton number data files and creates a single output file containing two Stanton number ratios for each of the 126 thermocouple locations. The required input data files are : SDATA file created by STANTON4 containing baseline Stanton numbers for no film cooling and two ST data files created by STANFC2A containing Stanton numbers with film cooling.

FLMEFF6 : This program processes Stanton number data and calculates the local and spanwise averaged film cooling effectiveness and iso-energetic Stanton number ratios. The program reads several files and creates two output files. The program reads the SDATA file created by STANTON4 which contains the baseline Stanton numbers for no film cooling and up to six ST, TDATA and

IDATA files created by STANFC2A. One of the two output data files contains the local effectiveness and iso-energetic Stanton number ratios and the other output file contains the spanwise averaged effectiveness and iso-energetic Stanton number ratios.

3DSTGETA : This program accesses the files created by FLMEFF6 and plots the spanwise variation of effectiveness in three-dimensional form.

3DSTGSTIRS : This program accesses the files created by FLMEFF6 and plots the spanwise variation of the iso-energetic Stanton number ratio in three-dimensional form.

3DSTRST : This program accesses the Stanton number ratio file created by STANR1 and plots the spanwise variations of the Stanton number ratios in three-dimensional form.

3DSTRAH : This program, which is the three dimensional version of PLSTRVV3H, accesses the Stanton number ratio file created by STANR1. It then plots the spanwise variations of the St/Sto ratios and Stf/Sto ratios for all six thermoncouple rows.

5. Combination Plots Software

VECTCOMBO/TEMPCOMBO : VECTCOMBO and TEMPCOMBO are adapted versions of VECTOR and PLTMP, which plot the differential mean

temperatures superimposed on top of the secondary flow vectors. VECTCOMBO is run first, followed by TEMPCOMBO.

APPENDIX D

DATA FILE DIRECTORY

1. Heat Transfer Data:

A. STANTON3 / STANTON4 data files -- (no film cooling) :

TDATAxx ---- temperature data file

IDATAxx ---- user terminal input data file

HDATAxx ---- heat transfer coefficient data file

SDATAxx ---- local Stanton number data file

Data Run #	Data File	Experimental Conditions
072790.1215	TDATA0 IDATA0 HDATA0 SDATA0	no film cooling
072790.1245	TDATA40 IDATA40 HDATA40 SDATA40	no film cooling Vortex position R0
080390.1800	TDATA43 IDATA43 HDATA43 SDATA43	no film cooling Vortex position L0

B. STANFC1A / STANFC2A data files -- (film-cooling)

Txx ---- temperature data file

Ixx ---- user terminal input data file

FCxx ---- film-cooling parameters data file

STxx ---- local Stanton number data file

Data Run #	Data File	Experimental Conditions
072090.0939	T1A I1A FC1A ST1A	1 row m=1.3 theta=1.27 No vortex
072090.1145	T3A I3A FC3A ST3A	1 row m=1.3 theta=1.06 No vortex
072090.1655	T9A I9A FC9A ST9A	1 row m=1.3 theta=0.57 No vortex
072090.1900	T11A I11A FC11A ST11A	1 row m=1.3 theta=0.10 No vortex
072890.1200	T1 I1 FC1 ST1	1 row m=0.5 theta =1.30 Vortex position R0
072890.1220	T3 I3 FC3 ST3	1 row m=0.5 theta=1.33 Vortex position R1
072890.1240	T5 I5	1 row m=0.5 theta=1.33 Vortex position R2

	FC5 ST5	
072890.1300	T7 I7 FC7 ST7	1 row m=0.5 theta=1.31 Vortex position R3

072890.1320	T9 I9 FC9 ST9	1 row m=0.5 theta=1.33 Vortex position R4
072890.1455	T39 I39 FC39 ST39	1 row m=0.5 theta=1.28 No vortex
072890.1515	T19 I19 FC19 ST19	1 row m=0.5 theta=1.30 Vortex position L0
072890.1535	T21 I21 FC21 ST21	1 row m=0.5 theta=1.30 Vortex position L1
072890.1555	T23 I23 FC23 ST23	1 row m=0.5 theta=1.31 Vortex position L2
072890.1620	T25 I25 FC25 ST25	1 row m=0.5 theta=1.29 Vortex position L3
072890.1640	T27 I27 FC27 ST27	1 row m=0.5 theta=1.30 Vortex position L4

080890.1320	T40 I40 FC40 ST40	2 rows m=0.5 theta=1.35 No vortex
080890.1700	T60 I60 FC60 ST60	2 rows m=0.5 theta=1.37 Vortex position L0
080890.1720	T62 I62 FC62 ST62	2 rows m=0.5 theta=1.38 Vortex position L1
080890.1740	T64 I64 FC64 ST64	2 rows m=0.5 theta=1.38 Vortex position L2
080890.1800	T66 I66 FC66 ST66	2 rows m=0.5 theta=1.38 Vortex position L3
080890.1820	T68 I68 FC68 ST68	2 rows m=0.5 theta=1.38 Vortex position L4
080890.1322	T82 I82 FC82 ST82	2 rows m=0.5 theta=1.31 Vortex position R0

082990.1344	T85 I85 FC85 ST85	2 rows m=0.5 theta=1.30 Vortex position R1
082990.1402	T86 I86 FC86 ST86	2 rows m=0.5 theta=1.32 Vortex position R2
082990.1422	T88 I88 FC88 ST88	2 rows m=0.5 theta=1.30 Vortex position R3
082990.1444	T91 I91 FC91 ST91	2 rows m=0.5 theta=1.30 Vortex position R4

C. FILM EFFECTIVENESS DATA

Generating Program : FLMEFF6

FExx ---- local effectiveness data file

SPAVGxx ---- spanwise average effectiveness data file

Data Run #	Data File	Experimental Conditions
072090.0939	FE00	1 row m=1.3
072090.1145	SPAVG00	4 data sets
072090.1655		
072090.1900		

D. STANTON NUMBER RATIO FILES

Generating Program : STANR1

STRxx ---- Film-coolig data file

Data Run #	Data File	Experimental Conditions
072090.0939	STR1A	1 row m=0.5 No vortex
072090.1145	STR3A	1 row m=0.5 No vortex
072090.1655	STR9A	1 row m=1.0 No vortex
072090.1900	STR11A	1 row m=0.5 No vortex
072890.1200	STR1	1 row m=0.5 R0
072890.1220	STR3	1 row m=0.5 R1
072890.1240	STR5	1 row m=0.5 R2
072890.1300	STR7	1 row m=0.5 R3
072890.1320	STR9	1 row m=0.5 R4
072890.1455	STR39	1 row m=0.5 No vortex
072890.1515	STR19	1 row m=0.5 L0
072890.1535	STR21	1 row m=0.5 L1
072890.1555	STR23	1 row m=0.5 L2
072890.1620	STR25	1 row m=0.5 L3
072890.1640	STR27	1 row m=0.5 L4
080890.1320	STR40	2 rows m=0.5 No vtx
080890.1700	STR60	2 rows m=0.5 L0
080890.1720	STR62	2 rows m=0.5 L1
080890.1740	STR64	2 rows m=0.5 L2
080890.1800	STR66	2 rows m=0.5 L3
080890.1820	STR68	2 rows m=0.5 L4
082990.1322	STR82	2 rows m=0.5 R0
082990.1344	STR85	2 rows m=0.5 R1
082990.1402	STR86	2 rows m=0.5 R2
082990.1422	STR88	2 rows m=0.5 R3
082990.1444	STR91	2 rows m=0.5 R4

E. MEAN VELOCITY DATA :

Data Run #	Data File	Generating Program	Experimental Conditions
081090.1435	FIV01	FIVEHOLE1	Vortex position R0
	FIVP01	FIVEHOLE1	m=0, x/d = 10.2
	FIV0A	PADJUST	
	V1	VELOCITY	
081090.1100	FIV02	FIVEHOLE1	Vortex position R4
	FIVP02	FIVEHOLE1	m=0, x/d = 10.2
	FIV0B	PADJUST	
	V2	VELOCITY	
081190.0900	FIV03	FIVEHOLE1	Vortex position R8
	FIVP03	FIVEHOLE1	m=0, x/d = 10.2
	FIV0C	PADJUST	
	V3	VELOCITY	
081290.1745	FIV04	FIVEHOLE1	Vortex position L0
	FIVP04	FIVEHOLE1	m=0, x/d = 10.2
	FIV0D	PADJUST	
	V4	VELOCITY	
081390.0100	FIV05	FIVEHOLE1	Vortex position L4
	FIVP05	FIVEHOLE1	m=0, x/d = 10.2
	FIV0E	PADJUST	
	V5	VELOCITY	
081390.1110	FIV06	FIVEHOLE1	Vortex position L8
	FIVP06	FIVEHOLE1	m=0, x/d = 10.2
	FIV0F	PADJUST	
	V6	VELOCITY	
081690.0230	FIV07	FIVEHOLE1	Vortex position R0
	FIVP07	FIVEHOLE1	x/d = 45.8
	FIV0G	PADJUST	m=0.5, 2 rows
	V7	VELOCITY	

081690.0950	FIV08	FIVEHOLE1	Vortex position R1
	FIVP08	FIVEHOLE1	x/d = 45.8
	FIV0H	PADJUST	m=0.5, 2 rows
	V8	VELOCITY	
081690.1700	FIV09	FIVEHOLE1	Vortex position R2
	FIVP09	FIVEHOLE1	x/d = 45.8
	FIV0I	PADJUST	m=0.5, 2 rows
	V9	VELOCITY	
081790.0020	FIV10	FIVEHOLE1	Vortex position R3
	FIVP10	FIVEHOLE1	x/d=45.8
	FIV0J	PADJUST	m=0.5, 2 rows
	V10	VELOCITY	
081990.1430	FIV12	FIVEHOLE1	Vortex position R3
	FIVP12	FIVEHOLE1	x/d=45.8
	FIV0K	PADJUST	m=0.5, 1 row
	V12	VELOCITY	
081990.2000	FIV13	FIVEHOLE1	Vortex position R2
	FIVP13	FIVEHOLE1	x/d=45.8
	FIV0L	PADJUST	m=0.5, 1 row
	V13	VELOCITY	
082090.1000	FIV14	FIVEHOLE1	Vortex position R1
	FIVP14	FIVEHOLE1	x/d=45.8
	FIV0M	PADJUST	m=0.5, 1 row
	V14	VELOCITY	
082190.0100	FIV16	FIVEHOLE1	Vortex position L0
	FIVP16	FIVEHOLE1	x/d=45.8
	FIV0N	PADJUST	m=0.5, 1 row
	V16	VELOCITY	
082190.0800	FIV17	FIVEHOLE1	Vortex position L1
	FIVP17	FIVEHOLE1	x/d=45.8
	FIV0O	PADJUST	m=0.5, 1 row
	V17	VELOCITY	
082190.1900	FIV18	FIVEHOLE1	Vortex position L2
	FIVP18	FIVEHOLE1	x/d=45.8

	FIV0P	PADJUST	m=0.5, 1 row
	V18	VELOCITY	
082290.0730	FIV19	FIVEHOLE1	Vortex position L3
	FIVP19	FIVEHOLE1	x/d=45.8
	FIV0Q	PADJUST	m=0.5, 1 row
	V19	VELOCITY	
082290.1600	FIV20	FIVEHOLE1	Vortex position L3
	FIVP20	FIVEHOLE1	x/d=45.8
	FIV0R	PADJUST	m=0.5, 2 rows
	V20	VELOCITY	
082290.2355	FIV21	FIVEHOLE1	Vortex position L2
	FIVP21	FIVEHOLE1	x/d=45.8
	FIV0S	PADJUST	m=0.5, 2 rows
	V21	VELOCITY	
082390.0730	FIV22	FIVEHOLE1	Vortex position L1
	FIVP22	FIVEHOLE1	x/d=45.8
	FIV0T	PADJUST	m=0.5, 2 rows
	V22	VELOCITY	
082390.1500	FIV23	FIVEHOLE1	Vortex position L0
	FIVP23	FIVEHOLE1	x/d=45.8
	FIV0U	PADJUST	m=0.5, 2 rows
	V23	VELOCITY	
082890.1921	FIV24	FIVEHOLE1	Vortex position R0
	FIVP24	FIVEHOLE1	x/d=45.8
	FIV0V	PADJUST	m=0.5, 1 row

F. Mean Temperature Survey Data :

Generating Program : ROVER1

Data Run #	Data File	Experimental Conditions
082490.0200	TEM0	2 rows m=0.5 x/d=45.8

		Vortex position L0
082490.0500	TEM1	2 rows m=0.5 x/d=45.8 Vortex position L1
082490.0900	TEM2	2 rows m=0.5 x/d=45.8 Vortex position L2
082490.1230	TEM3	2 rows m=0.5 x/d=45.8 Vortex position L3
082490.1630	TEM4	1 row m=0.5 x/d=45.8 Vortex position L3
082490.2000	TEM5	1 row m=0.5 x/d=45.8 Vortex position L2
082490.2345	TEM6	1 row m=0.5 x/d=45.8 Vortex position L1
082590.1400	TEM7	1 row m=0.5 x/d=45.8 Vortex position L0
082590.1820	TEM8	1 row m=0.5 x/d=45.8 Vortex position R0
082590.2355	TEM9	1 row m=0.5 x/d=45.8 Vortex position R1
082690.1020	TEM10	1 row m=0.5 x/d=45.8 Vortex position R2
082690.1426	TEM11	1 row m=0.5 x/d=45.8 Vortex position R3
082690.2022	TEM12	2 rows m=0.5 x/d=45.8 Vortex position R2
082790.0730	TEM13	2 rows m=0.5 x/d=45.8 Vortex position R3
082790.1315	TEM14	2 rows m=0.5 x/d=45.8 Vortex position R1

082790.1700	TEM15	2 rows m=0.5 x/d=45.8 Vortex position R0

REFERENCES

1. Bishop, D., Heat Transfer, Adiabatic Effectiveness and Injectant Distributions Downstream of Single and Double Rows of Film Cooling Holes with Compound Angles, M.S. Thesis, Department of Mechanical Engineering, Naval Postgraduate School, Monterey, CA, 1990.

2. Blair, M. E., "An Experimental Study of Heat Transfer and Film Cooling on Large-Scale Turbine Endwalls", *ASME Transactions -- Journal of Heat Transfer,* Vol. 96, pp. 524-529, 1988.

3. Craig, D.W., "Effects of Vortex Circulation on Injectant from a Single Film-Cooling Hole and a Row of Film-Cooling Holes in a Turbulent Boundary Layer, Part 1: Injection Beneath Vortex Downwash", M.S. Thesis, Department of Mechanical Engineering, Naval Postgraduate School, Monterey, CA, 1989.

4. El-Hady, N. M. and Verma, A. K., "Instability of Compressible Boundary Layers Along Curved Walls with Suction or Cooling", *AIAA Journal,* Vol. 22, pp. 206-213, 1984.

5. Evans, D.L., "Study of Vortices Embedded in Boundary Layers With Film Cooling, M.S. Thesis, Naval Postgraduate School, Monterey, California, March, 1987.

6. Goldstein, R.J. and Chen, H.P., "Film-Cooling on a Gas Turbine Blade Near the End Wall", *ASME Transactions - Journal of Engineering for Gas Trubines and Power,* Vol. 107, pp. 117-122, January 1985.

7. Goldstein, R.J. and Chen, H.P., "Film-Cooling of a Turbine Blade with Injection through Two Rows of Holes in the Near-Endwall Region", The American Society of Mechanical Engineers, Paper No. 87-GT-196, pp. 1-7, June 1987.

8. Goldstein, R.J., Eckert, E.R.G. and Ramsey, J.W., "Film Cooling with Injection Through Holes: Adiabatic Wall Temperatures Downstream of a Circular Hole", *ASME Transactions - Journal of Engineering for Power,* Vol. 90, No. 4, pp. 384-395, 1968.

9. Honami, S. and Fukagawa, M., "A Study on Film Cooling Behavior of a Cooling Jet Over a Concave Surface", Paper 87-Tokyo-IGTC-72, Tokyo International Gas Turbine Congress, Tokyo, Japan, 1987.

10. Joseph, S. L., *The Effects of an Embedded Vortex on a Film-Cooled Turbulent Boundary Layer*, M.E. Thesis, Naval Postgraduate School, Monterey, California, December, 1986.

11. Kaisuwan, P., "Effect of Vortex Circulation on Injectant from a Single Film-Cooling Hole and a row of Film Cooling Holes in a Turbulent Boundary Layer, Part 2: Injection Beneath Vortex Upwash", M.S. Thesis, Department of Mechanical Engineering, Naval Postgraduate School, Monterey, CA, 1989.

12. Kays, W. M. and Crawford, M. E., *Convective Heat and Mass Transfer*, Second Edition, p. 216, McGraw-Hill Book Company, 1980.

13. Kobiyashi, R., "Note on the Stability of a Boundary Layer on a Concave Wall with Suction", *Journal of Fluid Mechanics*, Vol. 52, pp. 269-272, 1972.

14. Kobayashi, R., "Taylor Gortler Instability of a Boundary Layer with Suction or Blowing", Report: Institute of High Speed Mechanics, Vol. 32, Series B, pp. 129-148, 1975.

15. Ligrani, P. M.., Joseph, S. L., Ortiz A. and Evans, D. L.,"Heat Transfer in Film-Coolled Turbulent Boundary Layers at Different Blowing Ratios as Affected by Longitudinal Vortices", *Experimental Thermal and Fluid Sciences*, Vol. 1, No. 4, pp. 347-362, 1988.

16. Ligrani, P. M., Ortiz, A., Joseph, S. L. and Evans, D.L., "Effects of Embedded Vortices on Film-Cooled Turbulent Boundary Layers", ASME-88-GT-170, ASME Gas Turbine and Aeroengine Congress and Exposition, Amsterdam, The Netherlands, June, 1988, also *ASME Transactions -- Journal of Turbomachinery*, Vol. 111, pp. 71-77,1989.

17. Ligrani, P. M. and Williams, W., "Effects of an Embedded Vortex on Injectant from a Single Film-Cooling Hole in a Turbulent Boundary Layer", *ASME Transactions -- Journal of Turbomachinery*, Vol. XXX, pp. XX-XX, 1990.

18. Ortiz, A., *The Thermal Behavior of Film Cooled Turbulent Boundary Layers as Affected by Longitudinal Vortices*, M.E. Thesis, Naval Postgraduate School, Monterey, California, September, 1987.

19. Sato, T., Aoki, S., Takeishi, K. and Matsuura, M., "Effect of Three-Dimensional Flow Field on Heat Transfer Problems of a Low Aspect Ratio Turbine Nozzle", Takasago Industries, Ltd., 1987.

20. Schwarz, S.G. and Goldstein, R.J., "The Two-Dimensional Behavior of Film Cooling Jets on Concave Surfaces", Paper 88-GT-161, ASME Gas Turbine and Aeroengine Congress and Exposition, Amsterdam, The Netherlands, 1988.

21. Schwartz, G. E., *Control of Embedded Vortices Using Wall Jets*, M.S. Thesis, Naval Postgraduate School, Monterey, California, September, 1988.

22. Williams, W., *Effects of an Embedded Vortex on a Single Film-Cooling Jet in a Turbulent Boundary Layer*, M.S. Thesis, Naval Postgraduate School, Monterey, California, June, 1988.